

3

Mathematical Modelling Based on Transport Phenomena

The transport phenomena of mass, heat or momentum, are characterized by an assembly of general equations which can be easily particularized. Each particularization of these equations to an actual example defines the mathematical model of the example.

We consider that the notion introduced with the term transfer of property makes reference to the exchange between two fluids, which are separated by a thin wall (interface or membrane). We observe that the transfer includes the motion of the property in each fluid – a process frequently called transport (transport of property) as well as the transfer of the property through the wall.

In the case of momentum transfer, we have a particular situation where the property transport occurs towards the walls and its transformation is controlled by the geometry of the wall.

The problems of mathematical modelling based on transport phenomena always begin with the establishment of equations which are all based on the general equation for the conservation of properties [3.1–3.5].

The general equation of property conservation. For a phase defined by volume V and surface A , we consider a property which crosses the volume in the direction of a vector frequently named the transport flux \vec{J}_t . Inside the volume of control, the property is uniformly generated with a generation rate J_v . On the surface of the volume of control, a second generation of the property occurs due to the surface vector named the surface property flux \vec{J}_{SA} . Figure 3.1 illustrates this and shows a cylindrical microvolume (dV) that penetrates the volume and has a micro-surface dA .

Inside this microvolume and through its microsurface, the property is generated and transported as in the surface A and control volume V .

In volume V and for a small time interval $d\tau$ when the property concentration ($\Gamma = P/V$, where P is the property quantity) changes by accumulation (from Γ to $\Gamma + d\Gamma$), the values of the components that explain the property conservation are defined as follows:

- quantity of the generated property (P_G):

$$P_G = \left(\iiint_V J_v dV \right) d\tau + \left(\iint_A J_{SA} \vec{n} d\bar{A} \right) d\tau \quad (3.1)$$

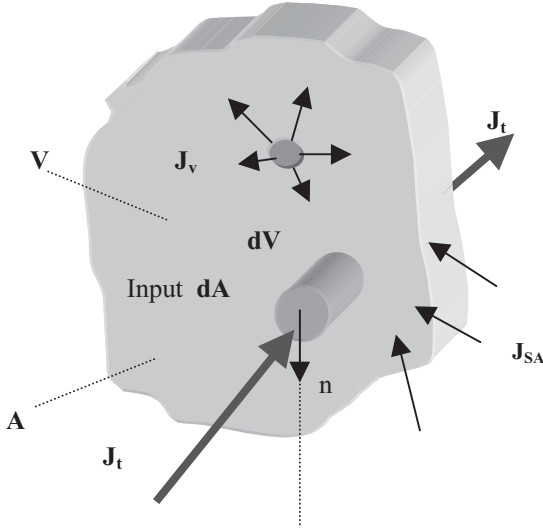


Figure 3.1 Introductory scheme for the equation of a general property balance.

- quantity of the accumulated property (P_A):

$$P_A = \iiint_V \left(\Gamma + \frac{d\Gamma}{d\tau} d\tau - \Gamma \right) dV = \left(\iiint_V \frac{d\Gamma}{d\tau} dV \right) d\tau \quad (3.2)$$

- surplus (excess) P_V of the transported property, output quantity of the property – input quantity of the property):

$$P_V = \left(\iint_A J_t \bar{n} d\vec{A} \right) d\tau \quad (3.3)$$

Based on the law of property conservation that asserts the equality between the difference of the generated and accumulated quantities and the surplus of the transported quantity, we have:

$$P_G - P_A = P_V \quad (3.4)$$

Now we can obtain the relation (3.5) that is recognized as the integral law of the conservation of a property.

$$\iint_A \bar{J}_t d\vec{A} + \iiint_V \frac{\partial \Gamma}{\partial \tau} dV = \iint_A \bar{J}_{SA} d\vec{A} + \iiint_V J_V dV \quad (3.5)$$

This relation can be transformed into its differential form if we make a random selection of the control volume V :

$$\frac{\partial \Gamma}{\partial \tau} + \text{div} \bar{J}_t = \text{div} \bar{J}_{SA} + J_V \quad (3.6)$$

This equation is similar to the relation obtained when making the property balance with respect to the microvolume dV . For a small interval of time we can write the following relations for the different classes of balance of quantity:

- quantity of the generated property (P_G):

$$P_G = (J_V dV) d\tau + (J_{SA} dA)_{srt} d\tau - (J_{SA} dA)_{ent} d\tau \quad (3.7)$$

- quantity of the accumulated property (P_A):

$$P_A = \left(\frac{\partial \Gamma}{\partial \tau} dV \right) d\tau \quad (3.8)$$

- net quantity of the transported property (P_V)

$$P_V = (J_t dA)_{srt} d\tau - (J_t dA)_{ent} d\tau \quad (3.9)$$

By coupling relations (3.7)–(3.9) with (3.4) we obtain:

$$J_V + \frac{[(J_{SA})_{srt} - (J_{SA})_{ent}] dA}{l_n dA} - \frac{\partial \Gamma}{\partial \tau} = \frac{[(J_t)_{srt} - (J_t)_{ent}] dA}{l_n dA} \quad (3.10)$$

where $l_n dA$ is the measure of the microvolume dV and l_n is the normal length of the microcylinder that defines the balance space.

Due to the random selection and random dimension of the control volume, we can assume that it is very small and so l_n approaches zero. Consequently, we can now write relation (3.11). This is identical to Eq. (3.6) that is recognized as the differential form of the property conservation law

$$\frac{\partial \Gamma}{\partial \tau} + \text{div} \vec{J}_t = \text{div} \vec{J}_{SA} + J_V \quad (3.11)$$

All the terms of relations (3.5) and (3.6) are important but special attention must be given to the transport flux vector.

Generally, this vector contains three components, which correspond to the mechanisms characterizing the behavior of the property carriers during their movement. The molecular, convective and turbulent moving mechanisms can together contribute to the vector flux formation [3.6]. In the relation below (3.12), D_Γ is the ordinary diffusion coefficient of the property. D_{Γ_t} represents the diffusion coefficient of the turbulences and \vec{w} is the velocity flow vector, then the general relation of the transport flux of the property is:

$$\vec{J}_t = -D_\Gamma \overrightarrow{\text{grad}} \Gamma + \vec{w} \Gamma - D_{\Gamma_t} \overrightarrow{\text{grad}} \Gamma \quad (3.12)$$

With Eqs. (3.12) and (3.6) we obtain the relation (3.13). It is recognized as the equation field of the property concentration. In fact, it represents the property conservation law for a random point from a homogeneous medium:

$$\frac{\partial \Gamma}{\partial \tau} + \text{div}(\vec{w} \Gamma) = \text{div}[(D_\Gamma + D_{\Gamma_t}) \overrightarrow{\text{grad}} \Gamma] + \text{div} \vec{J}_{SA} + J_V \quad (3.13)$$

Frequently the integral form of the conservation law of the property is particularized as total and partial mass balance and also as energy or thermal balance [3.7]. For each particularization, a control volume must be selected in order to have a form capable of permitting the computation of each integral from the relation (3.5). As an initial condition, we have to declare the property, the transport vector and the property generation rate. Figure 3.2 presents the way to obtain the equations of the differential balance of total mass, mass species and energy (heat). The

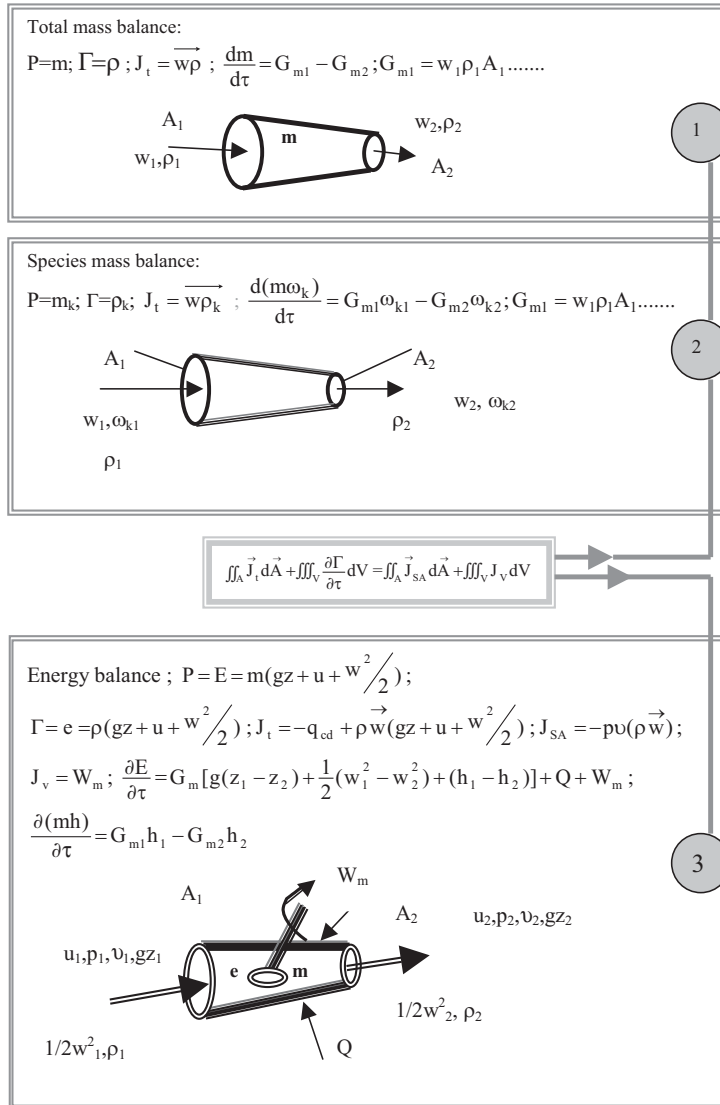


Figure 3.2 Particularization of the integral balance equation of the property (3.5) for mass and energy conservation.

symbols used in Fig. 3.2 have the following meanings: ρ_1, ρ_2 – densities; w_1, w_2 – flow velocity for the flow area A_1, A_2 ; G_{m1}, G_{m2} – mass flow rate; ω_{k1}, ω_{k2} – mass concentrations (fractions) for k species (component); u_1, u_2 – specific internal fluid energy; p_1, p_2 – pressure values; v_1, v_2 – value of the flowing fluid specific volume; z_1, z_2 – positions that characterize the local potential energy; h_1, h_2 – enthalpy for the flowing fluid; g – gravitational acceleration.

We observe from Fig. 3.2 that these transformations of integral equations of the property conservation have been obtained taking into consideration a very simple apparatus, here represented by a frustum conical pipe with flow input at the larger base and output at the smaller base.

Now we can see how the differential form of the property conservation law can generate the equations of the velocity distribution for a flowing fluid (Navier-Stokes equations), the temperature or the enthalpy distribution (Fourier second law) and the species concentration distribution inside the fluid (second Fick's law).

In all these particularization cases, we use the molecular and convective participations in the composition of the vector of transport.

The equation for the momentum transport in vectorial form, gives (by particularization) the famous Navier-Stokes equation. This equation is obtained considering the conservation law of the property of movement quantity in the differential form: $\vec{P} = m\vec{w}$. At the same time, if we consider the expression of the transport vector: $\vec{J}_t = \vec{\tau} + \vec{w}(\rho\vec{w})$ and that the molecular momentum generation rate is given with the help of one external force \vec{F} , which is active in the balance point, the particularization becomes: $\frac{\partial(\rho\vec{w})}{\partial\tau} + \text{div}[\vec{\tau} + \vec{w}(\rho\vec{w})] = \text{div}(-p\vec{n}) + \rho\vec{F}$, where p is defined as the local hydrodynamic pressure. The flux of the momentum quantity can be interpreted as a tension that characterizes the fluid deformation. Indeed, it is a tensor. When the conservable property is the mass from an infinitesimal control volume ($P = m, \Gamma = m/V = \rho$) where the convective flux is dominant, then the particularization of the differential form of the property conservation law becomes the flow continuity equation: $\frac{\partial\rho}{\partial\tau} + \text{div}(\rho\vec{w}) = 0$.

The Navier-Stokes equations and the flow continuity equation together give the general flow model; other cases associate various forms of the energy conservation equation to this model.

For the particularization of the differential conservation law to the heat transport, we consider first that the transported property is the sensible heat ($P = mc_p t, \Gamma = \rho c_p t$) and secondly that it is carried out by molecular and convective mechanisms ($\vec{J}_t = \vec{q}_m + \vec{w}\rho c_p t$).

When the conservable property is represented by the local quantity of the species A ($P = n_{mA}, \Gamma = n_{mA}/V = c_A$) transported by molecular and convective mechanisms, relation (3.6) becomes the equation of field of the species concentration. Figure 3.3 gives the three particularizations of the differential form of the property conservation law. Here we present the basic equations of momentum, heat and mass transport using their vectors and Cartesian expressions. However,

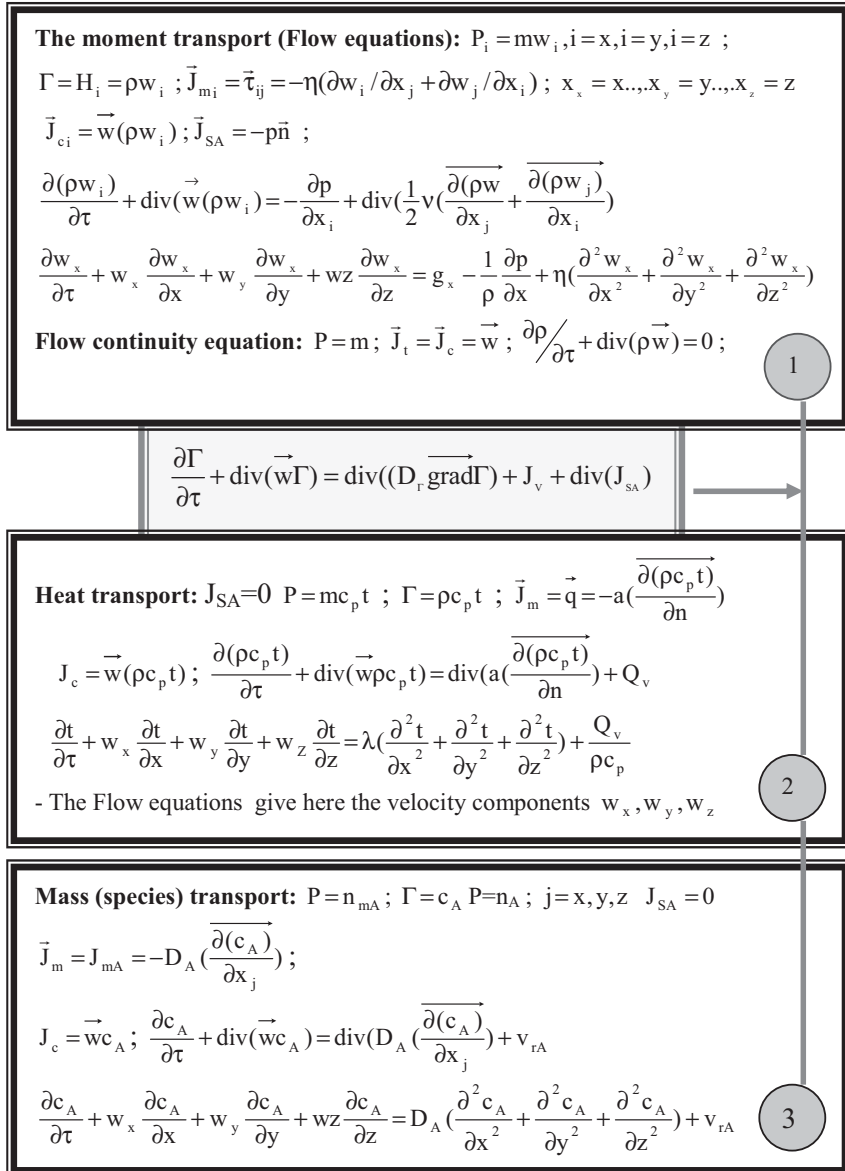


Figure 3.3 Particularization of the differential balance equation of a property (3.6) for momentum, heat and mass transport.

these equations, which characterize the fundamental properties of transport, cannot be used when we have conjugated actions. For example, if in a homogeneous system we simultaneously have gradients of species A concentration, temperature and pressure, then the molecular flux for the species A transport contains all participations and is written as follows:

$\vec{J}_{mA} = -D[\vec{\nabla}c_A + k_t\vec{\nabla}\ln(T) + k_p\vec{\nabla}\ln(p)]$, where D_Ak_t and D_Ak_p are, respectively, the thermal-diffusion coefficient and pressure-diffusion coefficient of species A. When we use the updated transport flux of species in the particularization of the balance of the differential property (Eq. (3.6)) a new expression of the field of the species concentration is obtained. The turbulence has to be considered when we have an important convective transport, which in many cases is the dominant transport mechanism. The contribution of this mechanism to the transport capacity of the medium is introduced in relation (3.3) by the addition of the coefficient of turbulent diffusion of the property.

When the transport is considered without turbulence we have, in general, D_T ; ν is the cinematic viscosity for the momentum transport; $a = \lambda/(\rho c_p)$ is the thermal diffusivity and D_A is the diffusion coefficient of species A. Whereas with turbulence we have, in general, D_{Tt} ; ν_t is the cinematic turbulence viscosity for the momentum transport; $a_t = \lambda_t/(\rho c_p)$ is the thermal turbulence diffusivity and D_{At} is the coefficient of turbulent diffusion of species A; frequently $\nu_t = a_t = D_{At}$ due to the hydrodynamic origin of the turbulence.

Indeed, this is a very simplistic treatment for the general flow mechanism, so, it is important to note here that the turbulence is in fact a vast scientific domain where interdisciplinary characterization methods are frequently needed.

Chemical engineers have developed very powerful methods for the hydrodynamic characterization of flows in different regimes by using specific apparatus; this methodology allows one to model the turbulent flow in industrial or laboratory devices.

We cannot finish this short introduction on the property transport problems without some observations and commentaries about the content of Figs. 3.2 and 3.3. First, we have to note that, for the generalization of the equations, only vectorial expressions can be accepted. Indeed, considering the equations given in the figures above, some particular situations have been omitted. For example, we show the case of the vector of molecular transport of the momentum that in Fig. 3.3 has been used in a simplified form by eliminating the viscous dissipation. So, in order to generalize this vector, we must complete the τ_{ij} expression with consideration of the difference between the molecular and volume viscosities $\eta - \eta_v$:

$$\tau_{ij} = -\frac{1}{2}\nu\left(\frac{\partial(\rho w_i)}{\partial x_j} + \frac{\partial(\rho w_j)}{\partial x_i}\right) + \frac{2}{3}(\eta - \eta_v)\text{div}(\vec{w})\delta_{ij}.$$

However, we remark here that the simplifications of the expressions in the Cartesian coordinates system have been accepted as in the case of an isotropic and non-property dependent diffusion coefficient of a property. Indeed, the independence of the general diffusion coefficient with respect to the all-internal or external solitations of the transport medium appears unrealistic in some situations.

For actual cases, the equations from these tables have to be particularized to the geometry of the device used and to all conditions of the process including the conditions that show the process state at the wall and interphases.

Interphase transfer kinetics. At this point, we need to characterize the process that leads to the transfer of the property through the interphase. The transport of the momentum from one phase to another is spectacular when the contacting phases are deformable. Sometimes in these situations we can neglect the friction and the momentum transfer generates the formation of bubbles, drops, jets, etc. The characterization of these flow cases requires some additions to the momentum equations and energy transfer equations.

Boundary layers appear in flow situations near the walls or other non-deformable structures that exist in the flow field [3.8]. Their formation and development, stability and local thickness are of great interest to engineers and researchers because all the gradients of property concentration are concentrated here. Consequently, we can write a very simple expression for the flux of the property.

In a general case, when a property crosses the interphase, we must consider that the property flux is identical between both contacted phases. Indeed, we consider ideal behaviour of the interphase or, in other words, we must accept the interphase to be not resistive to the transfer. We can criticize this fact but frequently it is accepted as a datum.

So when we accept the ideality of the interphase and when it is positioned to the coordinate x_i we can write:

$$J_{i1} = -D_{\Gamma_1} \left[\frac{d\Gamma}{dx} \right]_{x=x_i} = J_{i2} = -D_{\Gamma_2} \left[\frac{d\Gamma_2}{dx} \right]_{x=x_i} = J_t \quad (3.14)$$

Now we have to take into account the boundary layers at the left and right sides of the interphase where we have already shown the gradient of concentration of the property of the phase. With this last consideration, we can write a set of relations (3.15) that introduce the notion of the partial coefficient of the transfer of property (3.16):

$$\begin{aligned} -D_{\Gamma_1} \left[\frac{d\Gamma_1}{dx} \right]_{x=x_i} &= -D_{\Gamma_2} \left[\frac{d\Gamma_2}{dx} \right]_{x=x_i} = J_t = \\ \frac{-D_{\Gamma_1} \left[\frac{d\Gamma_1}{dx} \right]_{x=x_i}}{(\Gamma_{1\infty} - \Gamma_{x=x_i})} (\Gamma_{1\infty} - \Gamma_{x=x_i}) &= k_{\Gamma_1} (\Gamma_{1\infty} - \Gamma_{x=x_i}) = k_{\Gamma_2} (\Gamma_{x=x_i} - \Gamma_{2\infty}) \end{aligned} \quad (3.15)$$

$$k_{\Gamma_1} = \frac{-D_{\Gamma_1} \left[\frac{d\Gamma_1}{dx} \right]_{x=x_i}}{(\Gamma_{1\infty} - \Gamma_{x=x_i})} \quad ; \quad k_{\Gamma_2} = \frac{-D_{\Gamma_2} \left[\frac{d\Gamma_2}{dx} \right]_{x=x_i}}{(\Gamma_{x=x_i} - \Gamma_{2\infty})} \quad (3.16)$$

It is of interest that, for the computation of the transfer coefficients, various procedures have been advanced and in the past an immense quantity of data and reference materials have been collected on this subject.

3.1

Algorithm for the Development of a Mathematical Model of a Process

The relationships among the variables for a concrete process can be known through the particularization of the processes of transport phenomena. The mathematical model has to describe the state and evolution of the process while knowledge of the previous description of the operating conditions of the studied case is necessary. Indeed, terms such as flow, heat, diffusion and reaction clearly show that the transport phenomena are not absent from the investigated process. The verbal or written description must be clear and decisive with regard to identifying the effect of the independent variables on the exits of the process (dependent variables). At the same time, this description must correctly show how the dominant transport phenomena between all the unitary steps occur while the concrete process takes place. The observation spirit, a good engineering background, a good knowledge of the case and a fluent engineering language must be associated with the researcher's acute sense of responsibility in describing the process.

Indeed, the description of the process is recognized as the *first step* in the building of the mathematical modelling of a process. The result obtained here is recognized as a *descriptive model* or *model by words*. During this step, dependent and independent process variables resulting from the identification of the actions and interactions of the elementary phenomena that compose the state and evolution of the investigated process will be listed. At the same time, the effect of each independent variable on each dependent variable must be described.

The *second step* begins with a verbal or written analysis showing the coupling of the flow phenomena, heat and mass transfer, chemical reaction thermodynamics and kinetics. Here, a fraction of the factors of the process (independent variables of the process) selected by the first step will be eliminated, whereas a new limited number of factors will be added to the list. This step concerns one of the most delicate problems in mathematical modelling: the identification or creation of the mathematical clothes of the process by summation from the elementary models of the phenomena involved in the process. To finish this step, a mathematical form that characterizes the operating process is definitively established. This mathematical form is recognized as the *general mathematical model* of the process. Indeed, if the general descriptive models have been correctly decomposed into parts, then, each one of the parts will be characterized by its own general mathematical model.

The coupling of the general mathematical model with the evolution of the material and spatial conditions is given by its association with the investigated conditions of univocity of the process. This is the basis of the *third step* in the building of the mathematical model of a process. At the end of this step, we will have a *particularized mathematical model*. This step will be specified for each one of the decomposed models of the parts; i.e. for each of the particular devices in a unit. For this particularization, we use the following conditions of univocity:

- *the geometric conditions* establish the dimensions of the apparatus where the process is carried out from the geometric viewpoint.

Indeed, we made the choice of the coordinates system (cartesian, cylindrical or spherical) which will be used for our actual case and the model equation will be transformed for the selected coordinates system.

- *the material conditions* describe the physicochemical properties of the medium where the process takes place as well as the variation of these properties with temperature, pressure and composition using numerical values or analytic relations. Here we select the values or relations for the density, viscosity, thermal coefficient capacity, thermal conductivity, and diffusion coefficient of each component.
- *the dynamic conditions* give the initial spatial distribution and its evolution with time for each transported property. They also give the flux for each geometrical frontier as well as for each line or surface of symmetry of the system. Three major types of frontier have been established for the dynamic conditions:
 - *the boundary conditions of type I:* give the numerical values of the transported property or the function describing the variation of these values with time for each frontier of the system.
 - *the boundary conditions of type II:* give the flux values of the transported property to each frontier and to each symmetry line and surface of the system. Each flux can be described by a constant value or is dependent on time.
 - *the boundary conditions of type III:* give the values of the property state but here these values are out of the frontiers. At the same time, these conditions give the values or calculus relations for the coefficients of transfer at the interphase. With these data and using relation (3.15), we can compute the flux of the property at the frontiers. If we denote by $\Gamma_{1\infty}$ the property concentration for phase 1 and we assume a non-resistive interphase (the phases are in equilibrium with k_d , as distribution coefficient of the property) then, relation (3.15) becomes:

$$k_{\Gamma 1} \left(\Gamma_{1\infty} - \frac{\Gamma_2 \frac{x-x_{\text{int}}}{k_d}}{\Gamma_2} \right) = -D_{\Gamma 2} \left(\frac{d\Gamma_2}{dx} \right)_{x=x_{\text{int}}}$$

For all the situations, the *dynamic conditions for the symmetry lines and surfaces of the system* contain the specification that the property flux is zero. From the viewpoint of the property concentration, this fact shows that here it has a maximal or a minimal value.

- *the tendency conditions* show the state of a dynamic process after a very long time. If a stationary state is possible for the process, then the tendency conditions show the transition from a dynamic process model to a stationary process model (steady state).

In the *fourth step* of the building of a mathematical model of a process the assemblage of the parts (if any) is carried out in order to obtain the *complete mathematical* model of the process. Now the model dimension can be appreciated and a frontal analysis can be made in order to know whether analytical solutions are possible.

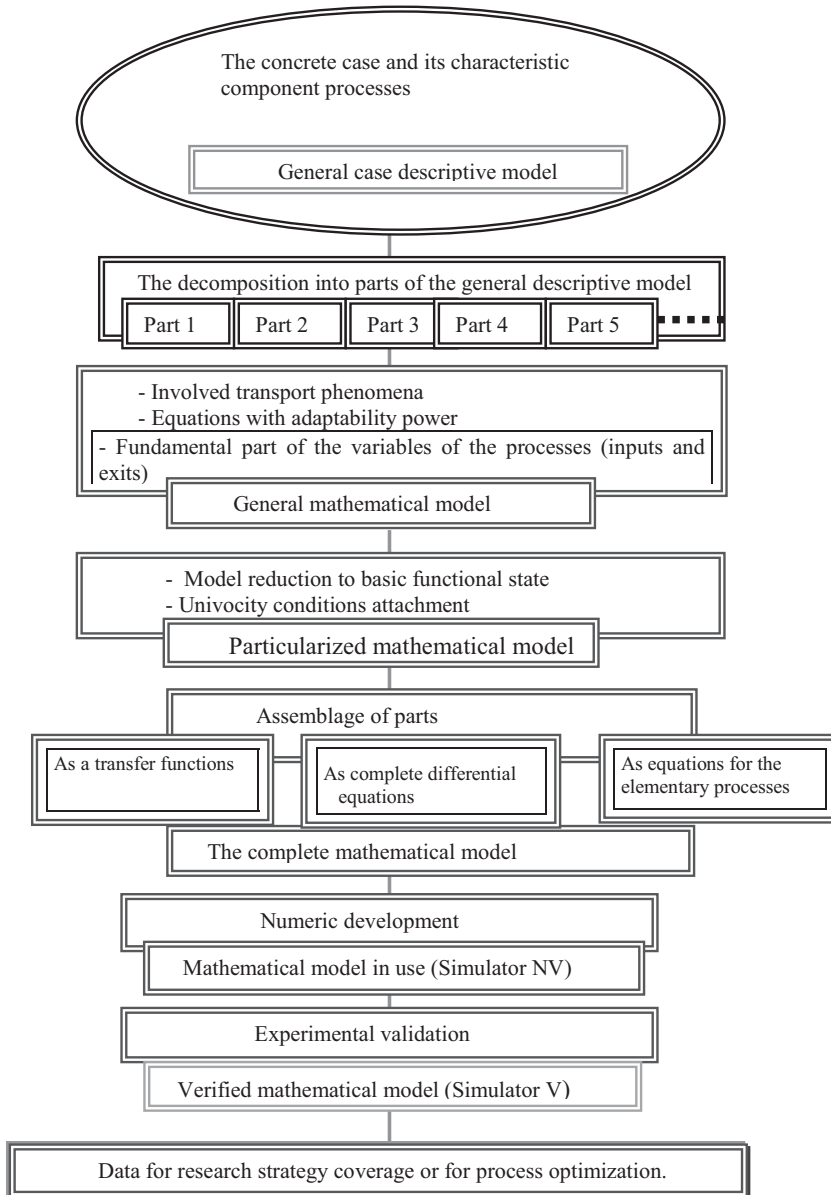


Figure 3.4 Steps in the building of a mathematical model for a concrete case.

Considering that, in this last step, we have a complete mathematical model of the process, we can now think about its valorization, by selecting the most convenient and acceptable possible solution for the model transformation into a numerical state. Indeed, the *fifth step* of this procedure results in a problem of computer software creation. Then, we have to choose the numerical solutions for the model integration as well as to select the input and output data state for the running of the computer program. We also have to select the representation of the solutions obtained with the output data processing. The final output of this step is a non-verified simulator (*Simulator NV*). The degree of sophistication of the simulator obviously depends on the model complexity. When we have some experimental data characterizing the relationship between one or more dependent variables and the independent process variables, then we can verify, after a normal calibration, whether the model produces identical or very similar data. If the model results match the experimental data, then we can affirm that we have a verified process simulator (*Simulator V*). Figure 3.4 shows this gradual development schematically, step by step, from the model establishment to simulator V. Here, we cannot logically separate the model creation part from the software creation part (numeric model transposition). It is also clear that the sense of the presented scheme is to show how we develop the model of one part of the general decomposed model. When we recompose the parts, we use the principle of maximum coupling. So, some parts will be introduced in the global model by their transfer functions, other parts with the help of their governing differential equations assemblies.

This procedure for building a mathematical model for a concrete case has also been mentioned in some scientific papers where the object is mathematical modelling by the use of transport phenomena [3.9–3.13].

3.1.1

Some Observations about the Start of the Research

Young researchers' first finished models are a source of great joy because they show their creative power. Moreover, when the models developed are successfully validated by experimentation, we can claim that the new researchers have actually stepped into real research activity.

Concerning the situation of the models that fail the test of experimental validation, we generally have two cases. The first case concerns a model that is unable to describe the whole project and which, normally, has to be rejected. The second case concerns a model that reproduces the general trends of the process but shows important differences with respect to the experimental data. This model will be again subjected to the building procedure where, with small or large modifications, it will improve its performance.

A special case occurs when some material or transport parameters are still unknown at the starting point and yet, at the same time, we have a lot of experimental data for the model validation. In this situation, we consider both data and model by formulating a *parameter identification* problem. The validation test for

this type of model will be transformed into hypotheses concerning the identified values of parameters.

Another special case occurs when the model is obtained by assembling different parts, and when each part has been successfully validated. In this case, the global validation is in fact a model calibration with the experimental data available.

In an actual research programme carried out with modelling coupled with experimental work, we cannot work randomly, without a research plan. The planning research method, given in this book in Section 5.3.2, has the capacity to be used for solving the most refined requirements. For this purpose, we must accept a model simulation to be as good as an experiment. With this procedure, we can derive an indirect but complex statistical model presenting a high interest for a computer-guided process from a model of transport phenomena. In the same way, we can use the model of transport phenomena as a database for a neural network model. Therefore, the data produced by the real model will be used in the learning procedure by the neural network model. Excellent behaviour of the neural network model is expected because the learning data volume can be very rich. We point out here that in the building of a model for a concrete chemical fabrication in an industrial unit, more aspects may be considered, each requiring qualified knowledge. Indeed, the procedures and methods coming from different scientific branches have to be coupled to the basic process model.

It is evident that, in these situations, problems concerning coupling hierarchy between the different parts can appear. Generally, for a fabrication that involves a chemical reaction, the top of the hierarchy is occupied by the reactor and separator models.

Figure 3.5 shows the most important scientific branches of chemical engineering research, which have to be taken into account for the modelling. Indeed, the

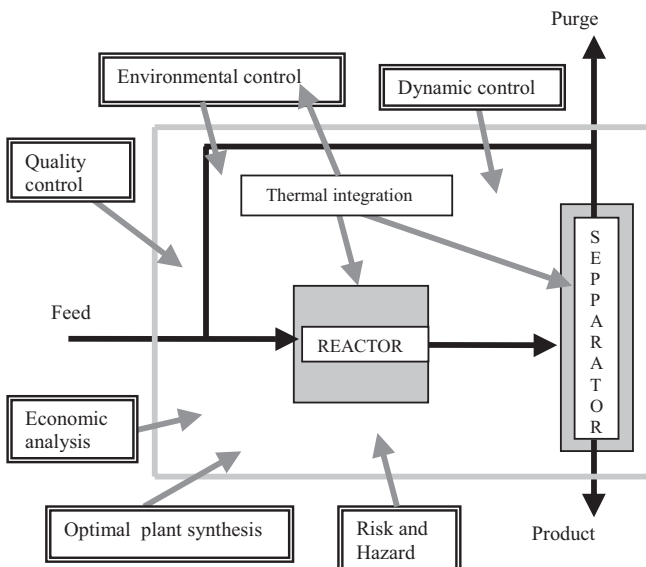


Figure 3.5 Secondary research activities related to chemical processing.

mathematical model of a process must answer the specific questions of each area division. In each case, the response comes as a result of the coupling of the computation procedures characterizing each branch. This is a complex and high-level research that gives consistency to a new scientific activity named *Advanced Processes Simulators*.

3.1.2

The Limits of Modelling Based on Transport Phenomena

Since the start of Section 3.1 we have been presenting how the transport phenomena equations are used for the mathematical modelling of a process and how we transform this model into a process simulator.

Actually, research by modelling is more and more extensively used in many applications because complex devices' models, composed of different elements, can be made by assembling models the solutions of which are frequently available. This behaviour presents an impressive growth and is sustained by the extraordinary developments in numerical calculations and by the implementation of commonly used computers with a high capacity and calculus rate. Nevertheless, modelling based on the equations of transport phenomena cannot be applied to every system, because they can present some limitations, which are summarized here.

The first limit derives from the model construction and can be called the constructive limit. It is explained by the quantity of simplifications accepted for model construction. The flow reduction by use of ideal models and the treatment of the transfer processes in equilibrium by using abstract notions – as for example, theoretical plate in distillation – represent only two of countless similar examples.

The second limit is named the cognition limit and arises from the less controlled assumptions concerning the complicated and ill acquainted phenomena involved in the process. Considering the interface as an equilibrium Gibbs interface and introducing the turbulent flow from the turbulent diffusion coefficient are two famous examples which illustrate this class of cognition limits.

The third limit is represented by the validity limits of the transfer phenomena equation. With respect to this last limitation, Fig. 3.6 shows the fixation of these limits with regard to the process scale evolution.

At this time, only a small number of nanoscale processes are characterized with transport phenomena equations. Therefore, if, for example, a chemical reaction takes place in a nanoscale process, we cannot couple the elementary chemical reaction act with the classical transport phenomena equations. However, researchers have found the keys to attaching the molecular process modelling to the chemical engineering requirements. For example in the liquid–vapor equilibrium, the solid surface adsorption and the properties of very fine porous ceramics computed earlier using molecular modelling have been successfully integrated in modelling based on transport phenomena [4.14]. In the same class of limits we can include the validity limits of the transfer phenomena equations which are based on parameters of the thermodynamic state. It is known [3.15] that the flow equations and, consequently, the heat and mass transport equations, are valid only for the

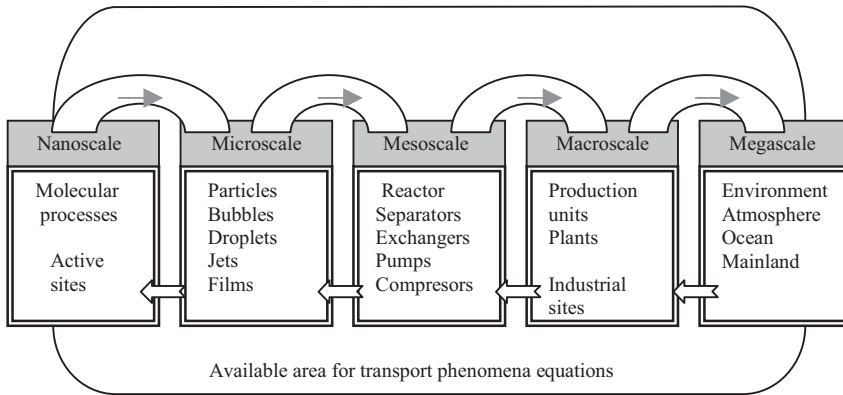


Figure 3.6 Validity domains for the transfer phenomena equations.

domain where the Truesdell criterion stays below unity. The Truesdell number given by $Tr = \frac{2\eta\varepsilon}{p}$, where η is the medium viscosity, ε the molecular oscillation frequency and p the medium pressure, is a combination of the Knudsen (Kd) and Mach (Ma) criteria.

Therefore, gases with very small pressure and some very viscous liquids can have a Truesdell number value over unity.

The fourth limit is the limit of contradiction. It takes place when sophisticated and complex models produced by academic and specialized research are used in industrial applications. Indeed, in industrial production, engineers can expect the current exploitation problems but they do not have any time to face new problems.

In fact, this limit depends on the standard of teaching of modelling research in technical universities. They have a key role in educating engineers capable of working with modelling and simulation as well as in research and development. The work of a process engineer in the future will be more and more concerned with modelling and using computers. Indeed, process engineers must have a considerable knowledge of physics and chemistry, as well as of processes, numerical calculation, modelling, programming and of the use of commercial programs.

The skills of graduating students are generally not very good in the fields of modelling and simulation. The goal of universities should be to produce more modelling-oriented engineers with good engineering, chemistry, physics, programming and mathematical skills.

3.2

An Example: From a Written Description to a Simulator

In this section, we will show the process of the construction of a mathematical model, step by step, in accordance with the procedure shown in Fig. 3.4. The case studied has already been introduced in Figs. 1.1 and 1.2 of Chapter 1. These figures are concerned with a device for filtration with membranes, where the gradient is given by the transmembrane pressure between the tangential flow of the suspension and the downstream flow. The interest here is to obtain data about the critical situations that impose stopping of the filtration. At the same time, it is important to, *a priori*, know the unit behaviour when some of the components of the unit, such as, for example, the type of pump or the membrane surface, are changed.

Descriptive model and its division into parts. The first steps in the model construction are related to Fig. 3.7. The pump PA assures simultaneously the suspension transport and the necessary transmembrane pressure. The excessive accumulation of the solid in the retentate is controlled by its permanent removal as a concentrated suspension from the reservoir RZ. The clear liquid (permeate) flow rate and the solid concentration in the exit suspension are permanently measured and these values are transferred to the control and command computer CE. The instantaneous values of the operation pressure and input rate of fresh suspension are established by the computer (this works with software based on the mathematical model of the process) and corrected with the command execution system CSE.

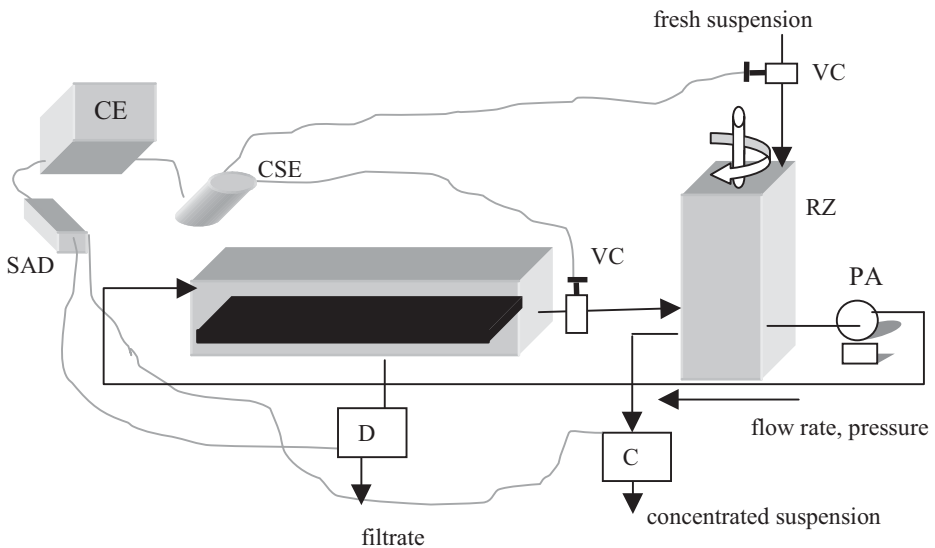


Figure 3.7 Membrane filtration plant.

If in stationary operation conditions, membrane clogging does not occur or is negligible, then the modelling case becomes banal. Nevertheless, when surface clogging cannot be eliminated by the tangential flow rate, we must introduce a continuous increase in the hydrodynamic resistance of the membrane [3.16–3.18]. In this situation, if the pressure filtration stays unchanged, the filtrate rate will decrease with time. When unacceptable values of the filtrate rate are reached, the process must be stopped and the membrane cleaned or replaced. This mode of operation is uneconomical. One solution to this problem is to increase the trans-membrane pressure in order to maintain the flow rate but, in this case, the pumping flow rate has to be reduced because pumps generally present a pre-established and characteristic flow rate–pressure relation which is, *a priori*, unchangeable. Consequently, when the pressure is continuously increased, the clogging rate will increase faster than when a high tangential velocity is used in the unit.

The clogging effect can be considered as a reduction in the value of the surface filtration constant for practical purposes. Indeed, when clogging takes place, the surface filtration constant can be given by its initial value k_0 multiplied by a decreasing time function. This assumption is frequently used when the function is obtained from experiments [3.19, 3.20]. In our example, if we do not consider the friction (and heat transfer) we can note that only a concrete mass transfer problem can be associated with the membrane separation process. The first step before starting to build the general mathematical model, concerns the division of the system into different elementary sections. Indeed, we have a model for the filtration device (i.e. the membrane and its envelope), for the pump (P) and for the reservoir of concentrated suspension (RZ) (Fig. 3.7).

General mathematical model. Considering that all we have is a mass transfer phenomenon, then, in such a system, the solid concentration changes in each plant device. With the considered coordinates system and after the notations given in Fig. 3.8, we can write the mathematical model of the filter unit as a particularization of the flow equations and the solid transport equation:

The Navier-Stokes equation in the x direction:

$$\frac{\partial w_x}{\partial \tau} + w_x \frac{\partial w_x}{\partial x} = -\frac{1}{\rho} \frac{\partial p}{\partial x} + \eta_{sp} \left(\frac{\partial^2 w_x}{\partial x^2} + \frac{\partial^2 w_x}{\partial y^2} + \frac{\partial^2 w_x}{\partial z^2} \right) \quad (3.17)$$

The Bernoulli equation with respect to an elementary local length dx:

$$\frac{\partial p}{\partial x} = -\frac{1}{2} \left(\rho_{susp} \frac{\partial \bar{w}_x}{\partial x} \right)^2 - \frac{\lambda}{d_c} \frac{\bar{w}_x^2}{2} \rho_{susp} \quad (3.18)$$

The formula of the definition of the suspension mean flow velocity:

$$\bar{w}_x = \frac{1}{hl} \int_0^h \int_0^l w_x(z, y) dz dy \quad (3.19)$$

The total mass balance equation with respect to the elementary local length dx:

$$\frac{dG_{pr}}{dx} = \rho_f l h \frac{\partial w_x}{\partial x} \tag{3.20}$$

The transfer equation for the permeate given by the use of its flux expression through the membrane surface:

$$\frac{dG_{pr}}{dx} = k_0 l (p_x - p_0) f(c_s \rho_s, \tau) \tag{3.21}$$

The simplified solid concentration field equation:

$$\frac{\partial c_s}{\partial \tau} + w_x \frac{\partial c_s}{\partial x} = 0 \tag{3.22}$$

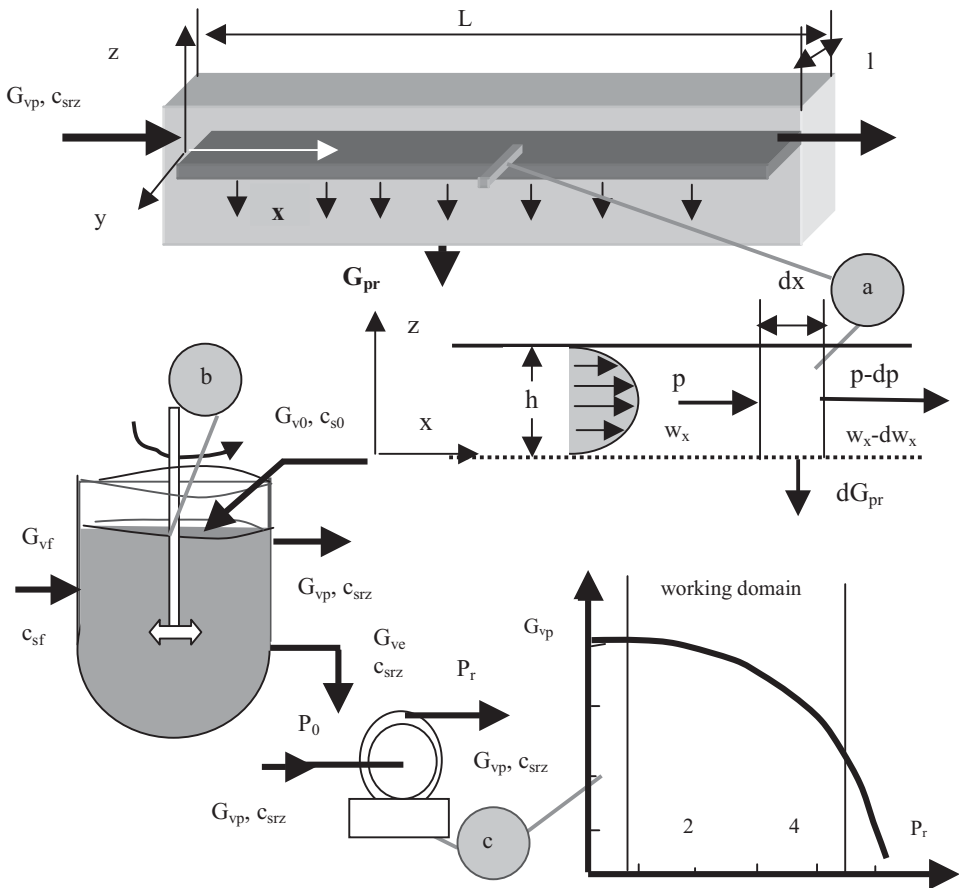


Figure 3.8 Decomposition of the filtration unit into sections and their corresponding description with relationships of the basic variables.

It is important to note that, except for the heat transfer problems, which have not been considered here, the model contains, in a particular form, all the transport phenomena relationships given at the start of this chapter. From the mathematical viewpoint, we have an assembly of differential and partly differential equations, which show the complexity of this example. However, this relative mathematical complexity can be matched with the simplicity of the descriptive model. Indeed, it will be convenient to simplify general mathematical models in order to comply with the descriptive model. Two variants can be selected to simplify the flow characterization in the membrane filtration unit.

The first variant considers that the model suspension flow corresponds to a plug flow model. In this case, the velocity w_x is a function of the coordinate x only. Its value is obtained from the ratio between the local suspension flow rate and the flow section [3.21]. With this assumption, the general mathematical model of the filter becomes:

$$w_0 = \frac{G_{vp}}{lh}, w_x = \frac{G_{vx}}{lh} \quad (3.22)$$

$$P_x = P_{x-dx} - \frac{\lambda}{d_e} \frac{(w_0 + w_x)^2}{8} \rho_{susp} dx \quad (3.23)$$

$$\frac{dG_{pr}}{dx} = k_0 l (p_x - p_a) f(c_s, p_x, \tau) \quad (3.24)$$

$$G_{vx} = G_{vp} - G_{pr} \frac{\rho_f}{\rho_{susp}} \quad (3.25)$$

$$\frac{\partial c_s}{\partial \tau} + w_x \frac{\partial c_s}{\partial x} = 0 \quad (3.26)$$

In *the second variant*, the plug flow model is considered as a series of tanks with perfect mixing flow [3.22, 3.23]. In this case, the real filter will be supposedly replaced by a series of some small filters (three in this analysis) with perfect mixing flow. Figure 3.9 shows the scheme, relations and notations used. The filtrate transfer equation has been used for the mathematical characterization of each small filter for the total material balance equation and non-steady-state solid balance equation:

- *first small filter:*

$$G_{pr1} = k_0 A_1 (p_1 - p_a) f(c_{s1}, p_1, \tau) \quad (3.27)$$

$$G_{v1} = G_{vp} - G_{pr1} \frac{\rho_f}{\rho_{susp}} \quad (3.28)$$

$$\frac{dc_{s1}}{d\tau} = \frac{G_{vp}}{V_1} c_{srz} - \frac{G_{v1}}{V_1} c_{s1} \quad (3.29)$$

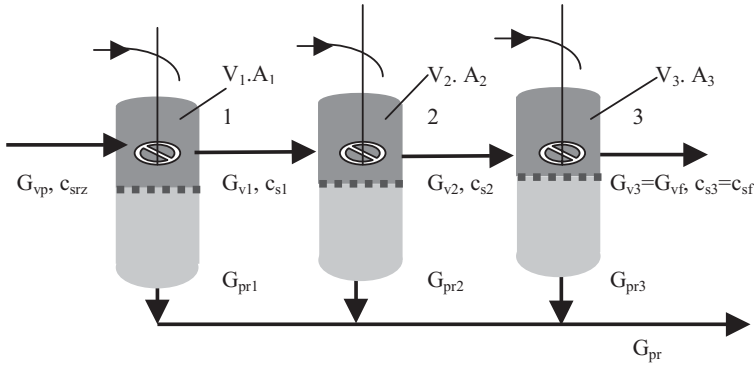


Figure 3.9 Representation of the membrane filtration unit as an ensemble of three small perfect mixing filters.

- *second small filter:*

$$G_{pr2} = k_0 A_2 (p_2 - p_a) f(c_{s2}, p_2, \tau) \quad (3.30)$$

$$G_{v2} = G_{v1} - G_{pr2} \frac{\rho_f}{\rho_{susp}} \quad (3.31)$$

$$\frac{dc_{s2}}{d\tau} = \frac{G_{v1}}{V_2} c_{s1} - \frac{G_{v2}}{V_2} c_{s2} \quad (3.32)$$

- *third small filter:*

$$G_{pr3} = k_0 A_3 (p_3 - p_a) f(c_{s3}, p_3, \tau) \quad (3.33)$$

$$G_{v3} = G_{v2} - G_{pr3} \frac{\rho_f}{\rho_{susp}} \quad (3.34)$$

$$\frac{dc_{s3}}{d\tau} = \frac{G_{v2}}{V_3} c_{s2} - \frac{G_{v3}}{V_3} c_{s3} \quad (3.35)$$

$$G_{v3} = G_{vf} \quad , \quad c_{s3} = c_{sf} \quad (3.36)$$

The general mathematical process model has to be completed with the models for the recycled suspension reservoir and for the pump. The suspension reservoir is a classical perfect mixing unit (see Fig. 3.8) so its model includes the unsteady total and solid balances. These balances are given below by relations (3.37) and (3.38). After Fig. 3.8, the mathematical model of the pump gives the relationship between the pump exit flow rate and its pressure (relation (3.39)):

$$\frac{dV_{rz}}{d\tau} = G_{v0} \frac{\rho_{s0}}{\rho_{susp}} + G_{vf} - G_{vp} - G_{ve} \quad (3.37)$$

$$\frac{dc_{srz}}{d\tau} = \frac{G_{vf}}{V_{rz}} c_{sf} + \frac{G_{v0}}{V_{rz}} - \frac{(G_{vp} + G_{ve})}{V_{rz}} c_{srz} \quad (3.38)$$

$$G_{vp} = a - bp_r^2 \quad (3.39)$$

For the whole unit we have to complete the general mathematical model with constraints that can be given by the device construction and/or operating conditions:

For the correct pump operation, the suspension level in the recycled reservoir must be within a range around a minimal value ($V_{rz\min}$), which is lower than the geometric volume (V_0):

$$V_{rz\min} < V_{rz} < V_0 \quad (3.40)$$

The pump cannot operate under a minimal flow rate value:

$$G_{vp} > G_{vp\min} \quad (3.41)$$

The ratio of solid concentration between the recycled and fresh suspension must be limited in order to reach a good flow in the filter unit and a rational recycling; this constraint can also be applied to flow rates G_{v0} and G_{vf} :

$$1 < \frac{c_{srz}}{c_{s0}} < \beta \quad (3.42)$$

The filtrate rate or the working pressure must be limited to imposed selected constant values. For a two-dimensional model (x, τ) these constraints are given by relations (3.43) and (3.44)

$$G_{pr/x=L} = G_{primp} \quad (3.43)$$

$$P_r = P_{r0} \quad (3.44)$$

In the case of a mono-dimensional model (τ), relations (3.45) and (3.46) comply with the technological requirements

$$G_{pr1} + G_{pr2} + G_{pr3} = G_{primp} \quad (3.45)$$

$$P_r = P_{r0} \quad (3.46)$$

Table 3.1 shows all general mathematical models resulting from the analysis of the filtration plant operation. The equations include the parts assembly in the model (Fig. 3.4) and an overall formula that shows the relationships that compose each model.

Table 3.1 Mathematical models for the filtration plant analysis.

Model		Model	
Two-dimensional x, τ		Monodimensional τ	
Constant filtrate flow rate operation	Constant pressure operation	Constant filtrate flow rate operation	Constant pressure operation
(3.22)–(3.26) + (3.37)–(3.43)	(3.22)–(3.26) + (3.37)–(3.42) and (3.44)	(3.27)–(3.36) + (3.37)–(3.42) and (3.45)	(3.27)–(3.36) + (3.37)–(3.42) and (3.46)

Particularized mathematical model. The univocity conditions given by the system geometry, the material conditions and the initial and frontiers state of the process variables have to be related with the models shown in Table 3.1:

- *geometrical conditions:* for the membrane and the two-dimensional model: $l = 0.15$ m; $L = 10$ m; $h = 0.075$ m; for the membrane and the monodimensional model: $A_1 = A_2 = A_3 = 0.5$ m²; $V_1 = V_2 = V_3 = 0.04$ m³; for the suspension reservoir: $V_0 = 1$ m³, $V_{rz \min} = 0.15$ m³.
- *material conditions:* liquid density $\rho_f = 1000$ kg/m³, solid density $\rho_s = 1500$ kg/m³, liquid viscosity $\eta_f = 10^{-3}$ kg/(m s), initial value of the filtration constant $k_0 = 6 * 10^{-4}$ m³/(m² h Pa), solid concentration of the fresh suspension $C_{s0} = 10$ kg/m³. The remaining values of the material properties will be computed by use of suitable relations (see Fig. 3.10).
- *initial and/or boundary conditions:* for the two-dimensional model, we attach the following initial and boundary conditions to the differential and partly differential equations:

$$\text{Eq. (3.24)} : x = 0, G_{px} = 0 \quad (3.47)$$

$$\text{Eq. (3.26)} : 0 < x < L; \tau = 0; c_s = c_{s0}, x = 0; \tau > 0, c_s = c_{srz} \quad (3.48)$$

$$\text{Eq. (3.37)} : \tau = 0, V_{rz} = 0.5 \quad (3.49)$$

$$\text{Eq. (3.38)} : \tau = 0, c_{sf} = c_{s0} \quad (3.50)$$

For the monodimensional model, only initial conditions are requested. The following data express the initial model conditions and definition functions for relations (3.49) and (3.50):

$$\text{Eq. (3.39)} : G_{vp} = 5 * 10^{-2} - 3 * 10^{-3} p_r^2 \quad (3.51)$$

$$\tau = 0, p_r = p_{r0} = 2 \quad (3.52)$$

$$G_{vp \min} = 6 * 10^{-3} \quad (3.53)$$

$$F(c_s, p, \tau) = \exp \left[-0.5 \left(\frac{c_s}{100} \right) \left(\frac{p}{p_{r0}} \right) \frac{\tau}{3600} \right] \quad (3.54)$$

The complete model. The parts assemblage is already given in Table 3.1. Here the result of the assembly of the models of the devices is an enumeration of the relations contained in each model.

The numerical model-Simulator NV-Simulator V. At this point, we must find the more suitable variant for passing from the differential or partly differential model equations to the numerical state. For the case of the monodimensional model, we can select the simplest numerical method – the Euler method. In order to have a stable integration, an acceptable value of the integration time increment is recommended. In a general case, a differential equations system given by relations (3.55)–(3.56) accepts a simple numerical integration expressed by the recurrent relations (3.57):

$$\left\{ \begin{array}{l} \frac{dy_1}{dx} = F_1(y_1, \dots, y_N, x) \\ \cdot \\ \cdot \end{array} \right.$$

$$\frac{dy_N}{dx} = F_N(y_1, \dots, y_N, x) \quad (3.55)$$

$$y_1(x_0) = y_{10}, y_2(x_0) = y_{20}, \dots, y_N(x_0) = y_{N0} \quad (3.56)$$

$$\left\{ \begin{array}{l} y_{1k} = y_{1k-1} + F_1(y_{1k-1}, y_{2k-1}, \dots, y_{Nk-1}, x_k) \\ \cdot \\ \cdot \end{array} \right.$$

$$y_{Nk} = y_{Nk-1} + F_N(y_{1k-1}, y_{2k-1}, \dots, y_{Nk-1}, x_k) \quad (3.57)$$

Figure 3.10 shows the details of the numerical-solving algorithm for the monodimensional. This numerical transposition has the capacity of being related with any available software. In Fig. 3.10, we can note that only the case of constant filtrate rate has been presented. Otherwise, when we operate at constant pressure, the filtrate rate decreases with the time due to the continuous clogging phenomenon. To simulate a constant pressure filtration, some changes in the computing program of Fig. 3.10 are necessary; these modifications are shown in Fig. 3.11. It is easily observable that here the stop criterion has been completed with the decreasing of the solid concentration in the recycled suspension.

1. **Constants:** $A_1, A_2, A_3, V_1, V_2, V_3, V_0, k_0, p_f, \rho_{s0}, \Delta\tau, G_{vp0}, p_{r0}, G_{vpmin}, V_{rz\ min}, V_{00}, \eta_f, \rho_{solid}, p_a, G_{v0}, G_{primp}, rap$
2. **Values:** $A_1=A_2=A_3=0.5; V_1=V_2=V_3=0.04; k_0=6*10^{-4}; c_{s0}=10; p_f=1000; \rho_{s0}=1005; \Delta\tau=10; G_{vp0}=38*10^{-3}; p_{r0}=2; V_0=1; G_{vpmin}=6*10^{-3}; V_{rzmin}=0.1; V_{00}=0.5; \eta_f=10^{-3}; \rho_{solid}=1500; p_a=1; G_{v0}=3.8*10^{-3}; p_{rmax}=3.7; G_{primp}=3.58*10^{-3}; rap=10$
3. **Functions:** $F(c_s, p, \tau) = \exp\left[0.5\left(\frac{c_s}{100}\right)\left(\frac{p}{p_{r0}}\right)\frac{\tau}{3600}\right]$; $\rho_{susp}(c_s) = \rho_f + c_s\left(1 - \frac{\rho_f}{\rho_{solid}}\right)$; $\eta_{susp}(c_s) = \eta_f\left(1 + 2.5\left(\frac{c_s}{\rho_{solid}}\right)^{0.25}\right)$
4. **Variables:** n, k
5. **Sequences:**

- 5.1 $n=0$
- 5.2 $c_{s10}=c_{s0}; c_{s20}=c_{s0}; c_{s30}=c_{s0}; c_{sr20}=c_{s0}; c_{s30}=c_{sf}; V_{rz0}=V_{00}; p_r=p_{r0}; G_{vp}=G_{vp0}$
- 5.3 $n=1$
- 5.4 $\Delta p_1 = 0.04\left[\frac{\eta_{susp}(c_{s1n-1})}{\eta_f}\right]^{0.25}$
- 5.5 $\Delta p_2 = 0.04\left[\frac{\eta_{susp}(c_{s21n-1})}{\eta_f}\right]^{0.25}$
- 5.6 $\Delta p_3 = 0.04\left[\frac{\eta_{susp}(c_{s3n-1})}{\eta_f}\right]^{0.25}$
- 5.7 $p_1=p_r-\Delta p_1; \tau=n\Delta\tau$
- 5.8 $G_{pr1}=k_0A_1(p_1-p_a)F(c_{s1n-1}, p_1, \tau)$
- 5.9 $G_{v1}=G_{vp}-G_{pr1}/\rho_{susp}(c_{s1n-1})$
- 5.10 $c_{s1n}=c_{s1n-1} + (G_{vp}c_{s\ rz\ n-1}/V_1 - G_{v1}c_{s1n-1}/V_1)\Delta\tau$
- 5.11 $p_2=p_r-\Delta p_2$;
- 5.12 $G_{pr2}=k_0A_2(p_2-p_a)F(c_{s2n-1}, p_2, \tau)$
- 5.13 $G_{v2}=G_{v1}-G_{pr2}/\rho_{susp}(c_{s2n-1})$
- 5.14 $c_{s2n}=c_{s2n-1} + (G_{v1}c_{s\ 1n-1}/V_2 - G_{v2}c_{s2n-1}/V_2)\Delta\tau$
- 5.15 $p_3=p_r-\Delta p_3$;
- 5.16 $G_{pr3}=k_0A_3(p_3-p_a)F(c_{s3n-1}, p_3, \tau)$
- 5.17 $G_{v3}=G_{v2}-G_{pr3}/\rho_{susp}(c_{s3n-1})$
- 5.18 $c_{s3n}=c_{s3n-1} + (G_{v2}c_{s\ 2n-1}/V_3 - G_{v3}c_{s3n-1}/V_3)\Delta\tau$
- 5.19 $G_{vf}=G_{v3}; c_{sf}=c_{s3n}; k=0$
- 5.20 $G_{ve}=G_{v0}/rap$
- 5.21 $V_{rzn}=V_{rz\ n-1} + [G_{v0}\rho_{s0}/\rho_{susp}(c_{sf\ n-1}) + G_{vf} - G_{vp} - G_{ve}]\Delta\tau$
- 5.22 $c_{srzn}=c_{srz\ n-1} + (G_{vf}c_{sf}/V_{rz} + G_{v0}c_{s0}/V_{rz} - (G_{vp} + G_{ve})c_{srz\ n-1}/V_{rz})\Delta\tau$
- 5.23 **Write:** $p_1, p_2, p_3, c_{s1n}, c_{s2n}, c_{s3n}, G_{pr1}, G_{pr2}, G_{pr3}, p_r, G_{ve}, G_{vp}, \tau$
- 5.24 **For** $V_{rz} \leq V_{rz\ min}$ **then** $k=1$ **and** $rap=rap+k$
- 5.25 **For** $V_{rz} \geq V_0$ **then** $k=-1$ **and** $rap=rap+k$
- 5.26 **For** $V_{rz\ min} \leq V_{rz} \leq V_0$ **then** $k=0$ **and** $rap=rap+k$
- 5.27 $G_{pr} = G_{pr1} + G_{pr2} + G_{pr3}$
- 5.28 **For** $p_r \geq p_{rmax}$ **then STOP**
- 5.29 **For** $G_{pr} < G_{pr\ imp}$ **then** $p_r = p_r + p_r/30; G_{vp} = 5*10^{-2} - 3*10^{-3}p_r^2; n=n+1; \text{Jump to 5.4}$

Figure 3.10 Numerical algorithm for the monodimensional model of the membrane filtration unit. Plant operating case: Constant filtrate flow rate $G_{pr} = G_{pr\ imp}$.

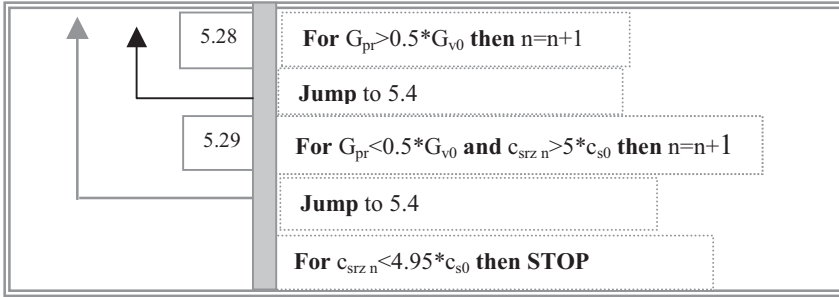


Figure 3.11 Changes to be introduced in the algorithm of Fig. 3.10 for the simulation of a constant pressure filtration (constraint $p_r = p_{r0}$ according to Eq. (3.46)).

It is obvious that the application of the two-dimensional model will introduce a supplementary mathematical diversity and complexity. Indeed, if we change the order of the relations in a given algorithm or the network integration parameters ($\Delta\tau$, Δx), the proposed integration procedure can rapidly produce integration instabilities in this concrete case. The two-dimensional integration can be maintained in the stability area, taking into consideration some observations concerning the physical meaning of the evolution of the solid concentration of the processed suspension (c_s). This model algorithm is presented in Fig. 3.12. When the intention is to use this algorithm for simulation of a constant pressure filtration, the changes given by Fig. 3.11 will be introduced. It is important to specify that the geometric plant dimensions and the flow rate of the fresh suspension are closely related. So, we cannot arbitrarily change any of these parameters independently. Once all the steps of the building of the process model have been successfully completed, the results produced with the models and their associated computer programs (software) can be presented.

Simulations and their results. It is not easy to assign the correct data to start the software running. Some of these data can be measured, others can be selected from practical design and others will be created. However, all these data must comply with the real investigated process.

First, we show that three calculation aspects seem to be interesting and must consequently be mentioned here: initially for the integration a small $\Delta\tau$ value has to be used ($\Delta\tau = 1$ s); secondly we admit that a good stability with the integration network parameters has been observed in the case of the two-dimensional model: $\Delta\tau = 1$ s and $\Delta x = 0.1$ m. Finally, we consider that the clogging rate can be selected by a careful modification of the argument of the exponential function that characterizes this process ($F(c_s, p, \tau)$).

We have selected four examples with different operating conditions: (a) a constant filtration flow rate with rapid clogging of the membrane; (b) a constant filtration flow rate with slow clogging of the membrane; (c) a constant pressure with rapid clogging of the membrane; (d) a constant pressure with slow clogging of the membrane. Each graphic representation of the simulations contains five

1. Constants: $l, h, L, \Delta x, \Delta \tau, \lambda_0, V_0, k_0, \rho_f, \rho_{s0}, \Delta \tau, G_{vp0}, p_{r0}, G_{vpmn}, V_{rzmin}, V_{00}, \eta_f, \rho_{solid}, p_a, G_{v0}, G_{primp}, rap$

2. Values: $l=0.15; h=0.075; L=10; \Delta x=0.1; \Delta \tau=1; \lambda_0=0.024; k_0=6 \cdot 10^{-4}; c_{s0}=10; \rho_f=1000; \rho_{s0}=1005; \Delta \tau=10; G_{vp0}=38 \cdot 10^{-3}; p_{r0}=2; V_0=1; G_{vpmn}=6 \cdot 10^{-3}; V_{rzmin}=0.1; V_{00}=0.5; \eta_f=10^{-3}; \rho_{solid}=1500; p_a=1; G_{v0}=3.8 \cdot 10^{-3}; p_{rmax}=3.7; G_{primp}=3.58 \cdot 10^{-3}; rap=10$

3. Functions: $F(c_s, p, \tau) = \exp[-0.5(c_s/100)(p/p_{r0})\tau/3600]$; $\rho_{susp}(c_s) = \rho_f + c_s(1 - \rho_f/\rho_{solid})$; $\eta_{susp}(c_s) = \eta_f [1 + 2.5(c_s/\rho_{solid})^{0.25}]$

4. Contours: n, k

5. Sequences:

```

5.1  M=L/Δx
5.2  n=0; cs,0=cs,1,0=cs,2,0=cs,3,0=cs,4,0=cs,5,0=cs,6,0=cs,7,0=cs,8,0=cs,9,0=cs,10,0=cs0; cs,rz=cs0
      ; Gvp=Gvp0; pr=pr0; num=25; de=[lh/(l+h)]0.5
5.3  n=1;
      cs,0,1=cs0+0.5; p0=pr; Gpr0=0; τ=nΔτ
5.4  m=1
5.4.1 w0=Gvp/(lh)
5.4.2 Gv,m=Gvp-Gv0/num;
      wm=Gv,m/(lh); λ=λ0[ηsusp(cs,m-1,n)/ηf]0.25;
      pm=pm-1-(λ/de)((w0+wm)2/8)ρsusp(cs,m-1,n)Δx;
      Gpr,m=Gpr,m-1+k0(pm-pa)F(cs,m-1,n,pm,τ)Δx; Gv,m=Gv,m-Gpr,m; Ere=(Gv,m-Gv,m)/Gv,m
      For Ere<0 and ABS(Ere)≥0.01 then : k=-1; num=num+k; Jump to 5.42
      For Ere≥0 and Ere≥0.01 then : k=+1; num=num+k; Jump to 5.42
      cs,m,n=cs,m-1,n/(1-Δx/(wmΔτ)); Write : pm,Gpr,m,Gv,m,cs,m,n
      For m≤M then : m=m+1; Jump to 5.4.1
5.5  csf,n=cs,M,n; Gve=Gv0/rap; Gvf=Gv,M
5.6  Vrz,n=Vrz,n-1+ [Gv0ρs0/ρsusp(csf,n-1)+Gvf-Gvp-Gve]Δτ
5.7  csz,n=csz,n-1+ (Gvfcs/Vrz+Gv0cs0/Vrz-(Gvp+Gve)csz,n-1/Vrz)Δτ
5.8  Write : Gpr,M,pr,cs,M,n,csz,n,Gve,Gvp,τ
5.9  For Vrz≤Vrz,min then : k=1 and rap=rap+k; For Vrz≥V0 then : k=-1 and rap=rap+k
5.10 For Vrz,min≤Vrz≤V0 then : k=0 and rap=rap+k
5.11 For pr≥pr0 then STOP
5.12 For Gpr≤Gprimp then : pr=pr+pr/10; Gvp=5*10-2-3*10-3pr2; Jump to 5.13
5.13 m=0
5.14 n=2
5.15.0 cs,0,n=csz,n; τ=nΔτ; m=1
5.15.1 w0=Gvp/(lh)
5.15.2 Gv,m=Gvp-Gv0/num; wm=Gv,m/(lh); λ=λ0[ηsusp(cs,m-1,n)/ηf]0.25;
      pm=pm-1-(λ/de)((w0+wm)2/8)ρsusp(cs,m-1,n)Δx;
      Gpr,m=Gpr,m-1+k0(pm-pa)F(cs,m-1,n,pm,τ)Δx; Gv,m=Gv,m-Gpr,m; Ere=(Gv,m-Gv,m)/Gv,m
      For Ere<0 and ABS(Ere)≥0.01 then : k=-1; num=num+k; Jump to 5.15.2
      For Ere≥0 and Ere≥0.01 then : k=+1; num=num+k; Jump to 5.15.2
      cs,m,n=cs,m-1,n+Δx/(wmΔτ)(cs,m,n-1-cs,m,n-2); Write : pm,Gpr,m,Gv,m,cs,m,n
      For m≤M then : m=m+1; Jump to 5.15.1
5.16 csf,n=cs,M,n; Gve=Gv0/rap; Gvf=Gv,M; Vrz,n=Vrz,n-1+ [Gv0ρs0/ρsusp(csf,n-1)+Gvf-Gvp-Gve]Δτ
5.17 csz,n=csz,n-1+ (Gvfcs/Vrz+Gv0cs0/Vrz-(Gvp+Gve)csz,n-1/Vrz)Δτ
5.18 Write : Gpr,M,pr,cs,M,n,csz,n,Gve,Gvp,τ; For Vrz≤Vrz,min then k=1 and rap=rap+k
5.19 For Vrz≥V0 then k=-1 and rap=rap+k; For Vrz≤V0 then k=-1 and rap=rap+k
5.20 For pr≥pr0 then STOP
5.21 For Gpr≤Gprimp then pr=pr+pr/10; Gvp=5*10-2-3*10-3pr2; n=n+1
5.22 Jump to 5.15.0

```

Figure 3.12 Numerical algorithm for the two-dimensional model of the membrane filtration plant. Plant operating case: Constant filtrate rate $G_{pr} = G_{primp}$.

operation cases: F1: filtration type **a** where the concentrated suspension evacuation is controlled by the suspension level of the reservoir RZ; F1S: the same filtration as F1 but here the evacuation of the concentrated suspension is controlled by the instantaneous mass balance; F2/2, F2/1.8, F2/1.6: filtration type **c** with the corresponding trans-membrane pressures of 2, 1.8 and 1.6 bar. The curves that show an oscillatory state correspond to the simulations where the process control requires some intervention on the pressure pump and/or on the control of the suspension level in the recycling reservoir. Each intervention that increases and decreases the pressure to maintain the filtrate flow at a fixed value is an oscillatory process. This process is rapidly detected and processed by the model. Table 3.2 gives the oscillations that characterize the filtration with the control of the pressure. These data give the limitations of the simulation cases. At the same time, they do not reproduce reality because it is not possible to change the pressure of the pump each second. This fact imposes a condition which has to be introduced in the computation program: a change in the pressure can be produced after a minimum 30 s time interval. This constraint has been used for the simulations named F1, F1S, LF1 and LF1S.

The simulations shown in Figs. 3.10 and 3.12 were made for the following operating conditions: 1, for the monodimensional model, the filter was considered to be composed of three identical membranes with a 0.5 m^2 surface, the minimum permeate flow was imposed at $3.8 \times 10^{-4} \text{ m}^3/\text{s}$, the initial value of the filtration constant $k_0 = 33 \times 10^{-4} \text{ m}^3/\text{m}^2 \text{ bar}$; 2, in the second case, a 10 m long, 0.075 m high and 0.15 m wide filter was analyzed with a constant permeate flow rate while keeping the initial value of the filtration constant. A concentration of $10 \text{ kg}/\text{m}^3$ was used for the fresh suspension.

It is important to specify here that complete clogging is reached between 3800 and 4200 s only in cases F1 and F1S. For the other cases – F2/2, F2/1.8 and F2/1.6 – the total clogging occurs later, between 6800 and 7300 s. However, after 2500–3000 s the filtrate flow rate becomes too low and unacceptable, as shown in Fig. 3.17 below.

As mentioned above, three factors are considered in the function which characterizes clogging: first, the time factor, which is a consequence of the Poisson distribution of the pore surface that blocks evolution; then the pressure factor, which accelerates the process of pore blocking; and finally the solid concentration factor.

The main difference between the operation at constant filtrate flow rate and at constant pressure can be observed in Fig. 3.13. In the case of a constant filtrate flow rate, the solid concentration inside the unit increases permanently, whereas, at constant pressure, the solid concentration increases very quickly initially (up to 1200 s) and then decreases for all the remaining time. If we look at both Figs. 3.13 and 3.15 we can see that it is not possible to start with the considered conditions with a 2 bar constant pressure because, in these conditions, a negative value of the exit flow rate appears for the concentrated suspension (Fig. 3.15) and the solid concentration increases tremendously from 10 to $120 \text{ kg}/\text{m}^3$.

Tab. 3.2 Data for the exit of some variables of filtration and their evolution with time.

τ (s)	$p_1(\tau)$	$cs_1(\tau)$	$cs_2(\tau)$	$cs_3(\tau)$	$Gpr_1(\tau)$	$Gve(\tau)$	$Gvp(\tau)$
2500	1.806	108.4	111.6	115.3	0.0012857	3.2289e-05	0.039674
2501	1.713	108.0	111.5	115.0	0.0011395	0.00038912	0.039674
2502	1.801	108.4	111.6	115.3	0.0012783	1.1126e-05	0.039725
2503	1.708	108.1	111.6	115.0	0.0011325	0.00040927	0.039725
2504	1.796	108.4	111.6	115.3	0.001271	9.9759e-006	0.039777
2505	1.704	108.1	111.6	115.0	0.0011256	0.00042937	0.039777
2506	1.792	108.5	111.6	115.3	0.0012637	3.1018e-005	0.039828
2507	1.700	108.1	111.6	114.9	0.0011186	0.00044941	0.039828
2508	1.787	108.5	111.6	115.3	0.0012564	5.2e-005	0.039879
2509	1.695	108.2	111.6	114.9	0.0011117	0.00046939	0.039879
2510	1.783	108.6	111.6	115.2	0.0012492	7.2924e-005	0.039929
2511	1.691	108.2	111.6	114.9	0.0011048	0.00048933	0.039929
2500	1.950	107.3	110.4	113.7	0.0010906	0.00056126	0.038
2501	1.950	107.2	110.4	113.7	0.0010906	0.00056133	0.038
2502	1.950	107.2	110.3	113.6	0.0010905	0.00056141	0.038
2503	1.950	107.2	110.3	113.6	0.0010905	0.00056148	0.038
2504	1.950	107.1	110.3	113.6	0.0010905	0.00056155	0.038
2505	1.950	107.1	110.2	113.5	0.0010905	0.00056163	0.038
2506	1.950	107.0	110.2	113.5	0.0010904	0.0005617	0.038
2507	1.950	107.0	110.2	113.4	0.0010904	0.00056177	0.038
2508	1.950	107.0	110.1	113.4	0.0010904	0.00056185	0.038
2509	1.950	106.9	110.1	113.4	0.0010904	0.00056192	0.038
2510	1.950	106.9	110.0	113.3	0.0010904	0.00056199	0.038
2511	1.950	106.9	110.0	113.3	0.0010903	0.00056207	0.038
2500	2.217	95.2	98.5	102.3	0.0012667	0.00038	0.03459
2501	2.104	95.0	98.5	102.1	0.0011692	0.00038	0.03459
2502	2.211	95.2	98.5	102.2	0.0012615	0.00038	0.034667
2503	2.098	95.0	98.5	102.0	0.0011641	0.00038	0.034667
2504	2.206	95.3	98.5	102.2	0.0012563	0.00038	0.034744
2505	2.0933	95.0	98.5	102.0	0.001159	0.00038	0.034744
2506	2.200	95.3	98.5	102.2	0.0012512	0.00038	0.03482
2507	2.088	95.0	98.5	102.0	0.001154	0.00038	0.03482
2508	2.194	95.3	98.5	102.2	0.001246	0.00038	0.034896
2509	2.082	95.1	98.5	102.0	0.001149	0.00038	0.034896
2510	2.189	95.3	98.5	102.1	0.0012409	0.00038	0.034971
2511	2.077	95.1	98.5	101.9	0.0011439	0.00038	0.034971

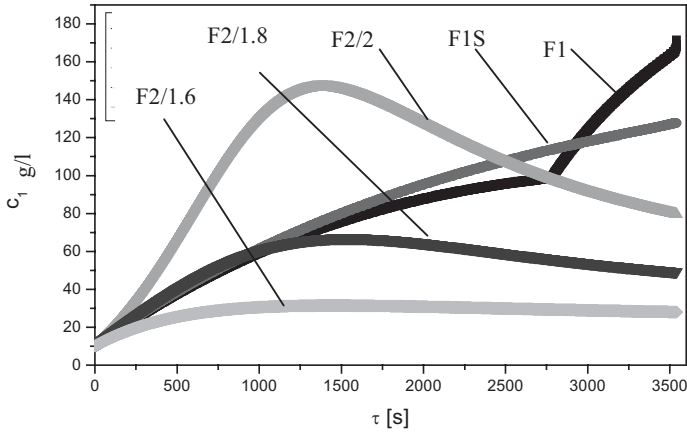


Figure 3.13 Evolution of the solid concentration in the filter unit when the membrane surface is rapidly clogged.

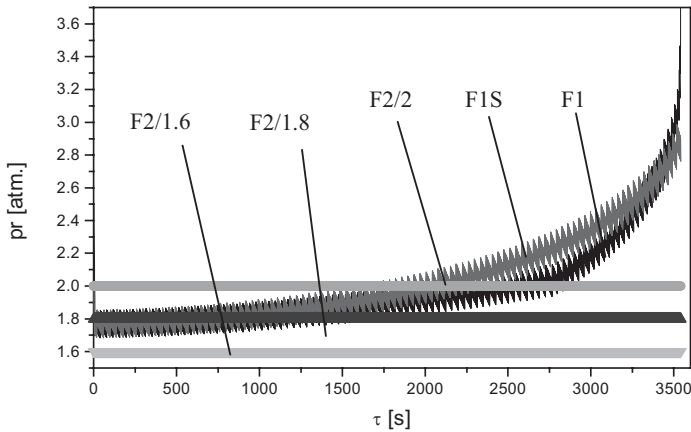


Figure 3.14 Evolution of the pressure of the pump, when a rapid clogging takes place.

When a positive exit rate of the concentrated suspension is obtained in the starting conditions, an important reduction in the filtrate flow rate will be expected, as shown in Fig. 3.17.

From Fig. 3.15 we can note that, by analogy to the 2 bar constant pressure case, example F1S shows a new special case where we have positive and small negative values in the concentrated suspension flow rate at the plant exit. This result can be explained by the background noise in the measurement of the flow of suspension. Nevertheless, the mean value of the flow rate is small but positive. If the efficiency of the filtration at constant pressure is given by the solid concentration ratio between the exit and fresh suspensions, then, as shown in Fig. 3.13, the ratio is always lower than 2 for operation case F2/1.6. For cases F1 and F1S, this ratio increases permanently, non-uniformly and attains values over 12 g/l in the proximity of the complete clogging state.

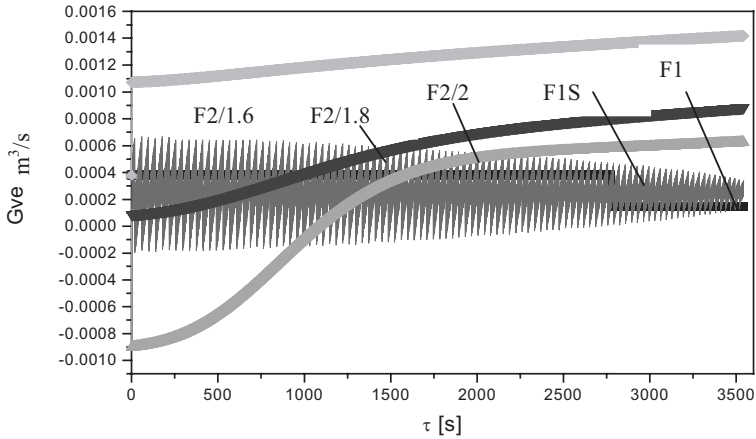


Figure 3.15 Evolution of the flow rate of the concentrated suspension when rapid clogging occurs.

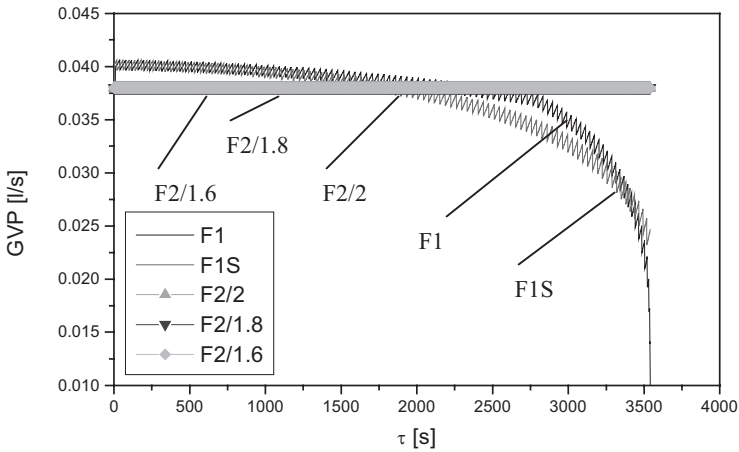


Figure 3.16 Evolution of the pump flow rate when rapid clogging occurs.

Figures 3.14 and 3.16 describe the function of the pump in the unit. When the pressure is constant, we have a constant pump exit flow rate, but, when the pressure increases to maintain the filtrate flow rate, the exit pump flow rate decreases too (see for instance relation (3.52)). In these figures, we can also observe that, for F1 and F1S, more than 110 oscillations are produced by the simulator every 30 s; these large oscillations require a pressure correction.

Figure 3.17 shows the evolution of the permeate flow rate when we work at constant pressure. We can observe (curves F1 and F1S) that controlling the pressure pump with a precision of ± 0.1 bar (for instance see Table 3.2) produces a mean fluctuation of the flow rate that begins with $\pm 20\%$ and progressively decreases to as little as $\pm 5\%$ when we approach the total clogged state. In this case of slow surface clogging, it must be mentioned that the operating time before the total

permeate flow rate decay is very large (40 000 s). Here, the initial filtration coefficient used was the same as that used when fast clogging occurred. Indeed, we can conclude that some properties of the suspension or interaction forces between the suspension and filter have changed and the function that describes the clogging process is not similar in both sets of operating conditions. Also, it may be noticed from Fig. 3.18 that the evolution of the concentration for different operating conditions is spectacular: (a) the solid concentration when the filtration pressure is 2 bar is unacceptable. This increase is correlated with the negative flows of the evacuated suspension (Fig. 3.21) and defines an impossible operating case; (b) the evolution of the solid concentration for the operation at constant permeate flow together with the controlled flow of evacuated concentrated suspension (through the level of the solution at the storage tank (LF1)).

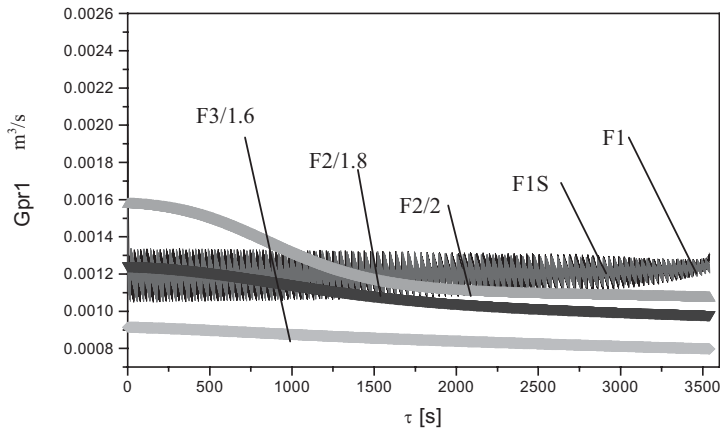


Figure 3.17 Evolution of permeate flow with rapid clogging of the membrane surface.

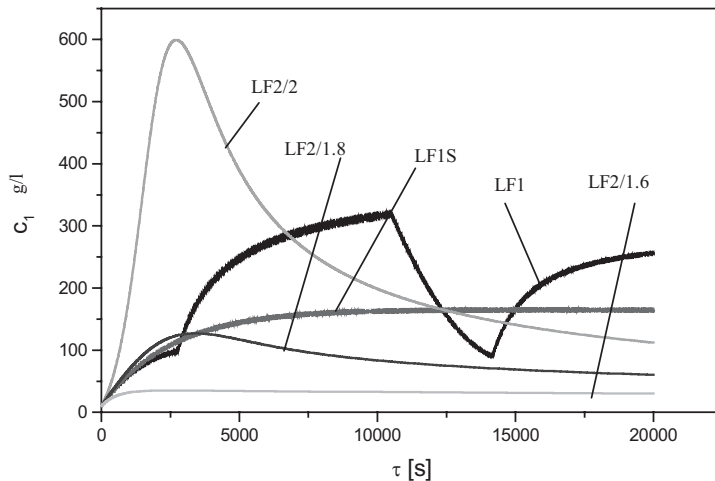


Figure 3.18 Evolution of the solid concentration in the filter unit when the membrane surface is slowly clogged.

It may be noticed that operating at 1.6 bar is not attractive from a technical or from an economic point of view. It is obvious that this state is determined by the increase in the evacuated suspension flow and the slow decrease in the permeate flow (Fig. 3.20).

Concerning Figs. 3.19 and 3.20, if we neglect the changing rate of the pump pressure and exit pump flow rate then we can appreciate that these figures are similar to Figs. 3.14 and 3.16, respectively.

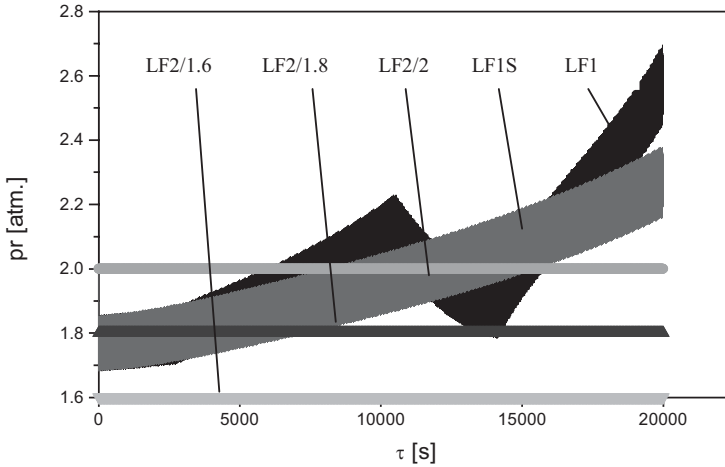


Figure 3.19 Evolution of pressure of the pump when slow clogging occurs.

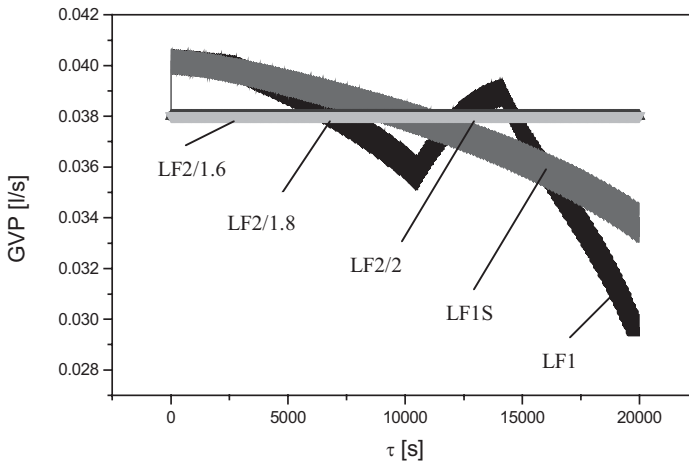


Figure 3.20 Evolution of the pump flow rate when slow clogging occurs.

Referring to the dynamics of the exits of concentrated suspension and filtrate it is interesting to observe (Figs. 3.21 and 3.22) that the cases with slow membrane clogging reproduce almost identically the corresponding cases where a rapid

membrane clogging occur. Otherwise, from these representations we observe that the tendency of the operation case at 1.6 bar is near to the stationary state where all filtration dependent and independent variables stay unchanged with time. However, as explained above with respect to the solid concentration in the exit concentrated suspension (see the above definition of the filtration efficiency) this operation appears to be inefficient.

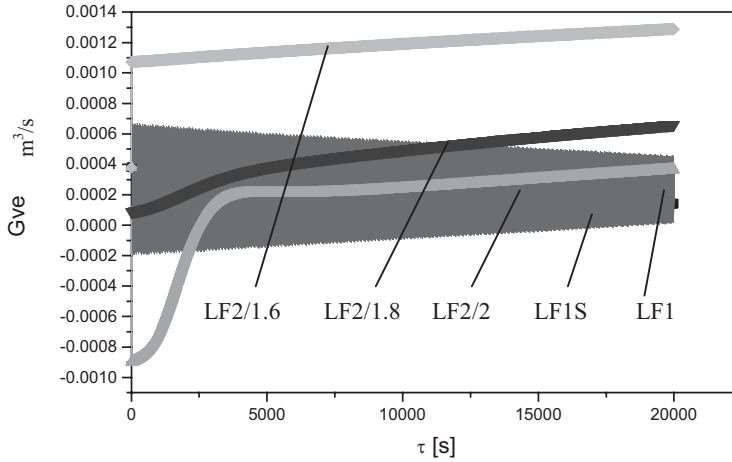


Figure 3.21 Evolution of the flow rate of concentrated suspension when slow clogging occurs during the filtration.

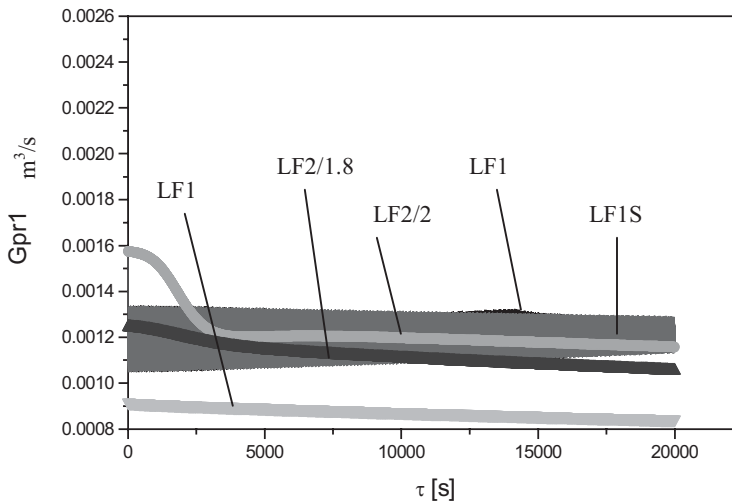


Figure 3.22 Evolution of the permeate flow when slow clogging of the membrane occurs.

To close this analysis, we note the validity of the operation with an increasing oscillatory pressure for a constant filtrate flow rate. The operation on oscillating pressure is very interesting for the enhancement of the performance of the filtration process [3,24].

To conclude this section it is important to give some general conclusions about modelling and how this example helps in the comprehension of the process of construction of a model: (1) to make a mathematical model of a process a good specialized technical knowledge of chemical engineering, software and of the actual case is necessary; (2) the model building has to be realized on a step by step basis with accurate rules for each action; (3) to pass from the complete model to the simulator it is necessary to take into account multiple factors. Among these we can mention the capacity to write a complex program according to the scientific disposable soft; to correctly assign data for the start of the simulator; to integrate the simulator with other simulators when necessary and (4) the choice of the simulation examples is a problem that can be solved only by a specialist who can also interpret the results.

From this example, we can establish some generalities about the modelling of a process:

1. The model of a process is a relation between the “outputs” and “inputs” (feed conditions, design parameters and adjustable parameters of the process) with a view to scaling-up the process from laboratory to industrial scale, predicting the process dynamics (case of this concrete example) and optimizing the operating conditions.
2. In the modelling of an actual case, the chemical engineers apply a methodology which involves establishing:
 - the conservation equations (mass, energy, momentum and electric charge);
 - the equilibrium laws at the interface(s);
 - the constitutive laws (e.g., ideal gas law);
 - the kinetic laws of transport and reaction;
 - the initial and boundary conditions;
 - the optimization criteria.
3. With this methodology, the problem is analyzed from the smallest to the largest scales, as appearing in the process description. As an example, in the case of a catalytic reactor, we consider the process on the following scales:
 - pore scale (catalyst and adsorbent): 1–1000 nm;
 - particle scale: 10 μm –1 cm;
 - reactor/separator scale: 1–10 m.

3.3 Chemical Engineering Flow Models

The modelling example of the previous section shows that to simplify the general mathematical model of the studied process, the real flow in the filter unit has been considered in terms of its own simplified model. Indeed, it is difficult to understand *why we have used a flow model, when in fact, for the flow characterization, we already have the Navier-Stokes equations and their expression for the computational fluid dynamics*. To answer this question some precisions about the general aspects of the computational fluids dynamics have to be given.

Computational fluid dynamics (CFD), is the science of determining a numerical solution to the equations governing the fluid flow. In order to obtain a numerical description of the complete flow field of interest, the solutions are obtained in a dynamic regime (i.e. continuously changing in space or time). CFD obtains solutions for the governing Navier-Stokes fluid flow equations and, depending upon the case under study, it solves additional equations involving multiphase, turbulence, heat transfer and other relevant processes. In CFD, partial differential Navier-Stokes and associated equations are converted into algebraic form (numerically solvable by computing) on a mesh that defines the geometry and flow domain of interest. Appropriate boundary and initial conditions are applied to the mesh, and the distributions of quantities such as velocity, pressure, turbulence, temperature and concentration are determined iteratively at every point in space and time within the domain. CFD analysis typically requires the use of a computer to perform the mathematical calculations. Graphical output shows the results of the analysis. Most of the CFD software available today requires more computing capability than can be obtained from a typical personal computer. CFD has proven its capability in predicting the detailed flow behaviour for a wide-range of engineering applications, typically leading to improved equipment or process design. CFD is used for early conceptual studies of new designs, detailed equipment design; scale-up, troubleshooting and system retrofitting. Examples in chemical and process engineering include separators, mixers, reactors, pumps, pipes, fans, seals, valves, fluidized beds, bubble columns, furnaces, filters and heat exchangers.

Concerning our problem of the modelling of the flow process, even if the CFD seems to be the most complete approach, the use of flow models for its characterization is sustained by the following statements:

1. For the majority of the specific apparatus, the flows present a turbulent compartment and, for such flow, a numerical solution is covered by high uncertainty because some hypotheses have to be accepted *a priori* [3.25]; in all the studied cases, the real apparatus has a complicated geometry that imposes very complex and frequently uncertain univocity conditions in the real CFD-based flow computation.

2. For many cases a flow model is, in fact, the real solution to an equivalent complicated CFD model. Other arguments can be given to recommend the use of the simplest type of flow model: (a) the simple and rapid possibility of these flow models to be qualitatively and quantitatively identified as a result of experimental measurements; (b) the accuracy and suppleness of the data produced by modelling when the flow models are adequately selected and identified; (c) in general, researchers with a large experience of these models, are able to rapidly assign a model after a verbal description of the real flow, in spite of non-identified parameters. The theoretical basis of these flow models is expressed by the possibility to characterize the flow with the residence time distribution of the fluid particles that compose the flow passing through the considered device.

3.3.1

The Distribution Function and the Fundamental Flow Models

The residence time of a signal that passes through a device, is in fact a random variable which is completely characterized by its probability distribution. This probability distribution, known as the residence time distribution, can be found for an actual apparatus after its exit response in the form of an input signal. Generally it is utilized as a signal, a substance (indicator) which is introduced in the input flow as a Dirac's impulse, unitary impulse or harmonic impulse. Figure 3.23 shows the scheme of an experiment dealing with the passing of a signal through a real or a scaled down (laboratory model) device. When a signal impulsion is given to the input flow of the device, the quantity of the substance that is contained in the signal coming out in the exit flow will be:

$$C_m = \int_0^{\infty} c(\tau)E(\tau)d\tau \quad (3.58)$$

where $E(\tau)$ represents the differential function of the residence time distribution and $c(\tau)$ is the instantaneous concentration of the substance (signal) in the exit flow. With respect to the flow, function $E(\tau)$ is in fact the fraction of the signal that comes out from the device after a residence time which ranges between τ and $\tau + d\tau$. The residence time can also be considered from the statistical viewpoint where it is a random variable, then $E(\tau)$ represents its density of probability, which is frequently called distribution function. Indeed, $E(\tau)$ must verify the norma condition:

$$\int_a^{\infty} E(\tau)d\tau = 1 \quad (3.59)$$

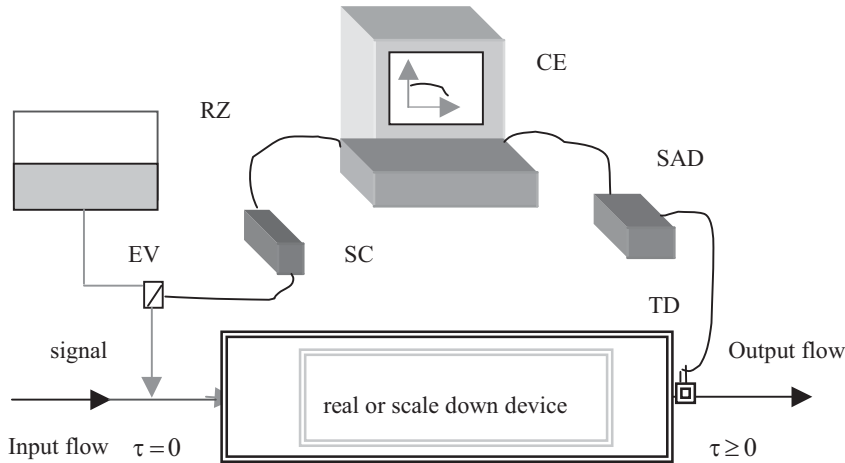


Figure 3.23 Schematic arrangement for a signal introduction in a device. CE: computer, RZ: reservoir with signal solution, SAD: data acquisition system, SC: command system, EV: electric valve, TD: signal concentration transducer.

We can use the experimental data that result from the measuring of the signal concentration in the exit flow, then $E(\tau)$ will be computed with relation (3.60) where N gives the number of experiments necessary for the signal concentration to disappear:

$$E(\tau) = \frac{c(\tau)}{\int_0^{\infty} c(\tau) d\tau} = \frac{c(\tau)}{\sum_{i=1}^N c(\tau_i) \Delta\tau} \quad (3.60)$$

Function $F(\tau)$ is directly connected to the residence time distribution. It is recognized as the repartition function of the residence time random variable. So, $F(\tau)$ shows the fraction of the fluid elements that stayed in the device for a time less than or equal to τ . Between $F(\tau)$ and $E(\tau)$ the following integral and differential link exists:

$$F(\tau) = \int_0^{\tau} E(\tau^{\circ}) d\tau^{\circ} \quad \text{or} \quad E(\tau) = \frac{dF(\tau)}{d\tau} \quad (3.61)$$

Function $F(\tau)$ represents the apparatus response to a unitary impulsion signal where C_0 is the concentration in the input flow. By measuring the signal concentration in the exit flow we can write $F(\tau)$ with the relation (3.62). When the condition of “pure unitary signal” is respected, we can easily observe that $F(0) = 0$ and $F(\infty) = 1$. In this case, function $F(\tau)$ can be written as:

$$F(\tau) = \frac{c(\tau)}{c_0} \quad (3.62)$$

For ideal flow models such as perfect mixing flow, plug flow and all other ideal models, a combination of functions $E(\tau)$ and $F(\tau)$ can be obtained directly or indirectly using the model transfer function $T(p)$. Before obtaining an expression for $E(\tau)$ for the perfect mixing flow, we notice that the transfer function of a flow model is in fact the Laplace's transformation of the associated $E(\tau)$ function:

$$T(p) = L(E(\tau)) = \frac{c_{\text{out}}(p)}{c_{\text{ent}}(p)} \quad (3.63)$$

For the computation of $E(\tau)$ and $T(p)$, in the case of a perfect mixing model, we use the representation and notation given in Fig. 3.24. Including the mass balance of the species in the signal, we derive the following differential equation:

$$\frac{dc}{d\tau} = -\frac{G_v}{V}c \quad (3.64)$$

the characteristic conditions for an impulse δ in the input flow are:

$$c_{\text{inp}} = c_0 \text{ for } \tau = 0 \text{ and } c_{\text{inp}} = 0 \text{ for } \tau \geq 0 \quad (3.65)$$

and then Eq. (3.64) becomes:

$$\frac{c}{c_0} = \exp\left(-\frac{G_v}{V}\tau\right) \quad (3.66)$$

Now, combining relations (3.66) and (3.61), we obtain the expression for the time distribution function of the perfect mixing flow model:

$$E(\tau) = \frac{c(\tau)}{\int_0^{\infty} c(\tau)d\tau} = \frac{c_0 \exp\left(-\frac{G_v}{V}\tau\right)}{\int_0^{\infty} c_0 \exp\left(-\frac{G_v}{V}\tau\right)d\tau} = \frac{G_v}{V} \exp\left(-\frac{G_v}{V}\tau\right) = \frac{1}{\tau_m} \exp(-\tau/\tau_m) \quad (3.67)$$

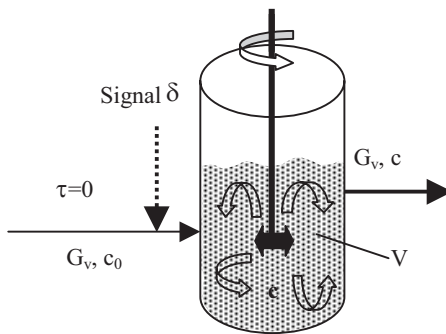


Figure 3.24 Physical model for perfect mixing (PM) flow.

We can obtain the repartition function of the residence time for the model of perfect mixing flow from relations (3.67) and (3.62). This function is:

$$F(\tau) = \int_0^\tau E(\tau) d\tau = \int_0^\tau \tau_m^{-1} \exp\left(-\frac{\tau}{\tau_m}\right) d\tau = 1 - \exp\left(-\frac{\tau}{\tau_m}\right) \quad (3.68)$$

by definition, the transfer function is:

$$T(p) = L(E(\tau)) = \frac{c_{\text{sort}}(p)}{c_{\text{ent}}(p)} = \int_0^\infty \exp(-p\tau) \tau_m^{-1} \exp\left(-\frac{\tau}{\tau_m}\right) d\tau = \frac{1}{\tau_m p + 1} \quad (3.69)$$

In a more general case where the input signal is given by a function $c_{\text{ent}}(\tau)$ the balance of the species characterizing the signal can be written as follows:

$$\frac{dc}{d\tau} = -\frac{G_v}{V}(c - c_{\text{ent}}) \quad (3.70)$$

The Laplace's transformation of the differential equation (3.70) gives relation (3.71) where p is the Laplace's argument:

$$p c_{\text{sort}}(p) - p c(0_-) = \frac{G_v}{V}(c_{\text{sort}}(p) - c_{\text{ent}}(p)) \quad (3.71)$$

In general, we have $c(0) = 0$ for all the signal types; then, we can transform the previous relation to show the transfer model function:

$$\frac{c_{\text{sort}}(p)}{c_{\text{ent}}(p)} = T(p) = \frac{1}{\tau_m p + 1} \quad (3.72)$$

From this last relation we remark that the transfer model function can be obtained from the differential model equation that, in fact, is a particularization of the balance of the concerned species in the actual model.

The species balance in a plug flow (Fig. 3.25) is carried out in an elementary dx length of the control volume; the result is the partial differential equation (3.73) where w is the velocity of the fluid moving with a plug flow pattern. Then, the relation between the flow rate and the section crossed by flow becomes:

$$\frac{\partial c}{\partial \tau} = -w \frac{\partial c}{\partial x} \quad (3.73)$$

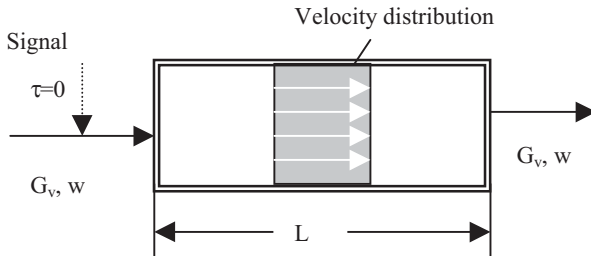


Figure 3.25 Physical model of the plug flow (PF).

The boundary conditions for a δ signal in the input associated to the plug flow model (Eq. (3.73)) are written as follows:

$$\tau = 0_- , \quad 0 < x < L , \quad c = 0 \quad (3.74)$$

$$\tau = 0 , \quad x = 0 , \quad c = c_0 \quad (3.75)$$

$$\tau = 0_+ , \quad x = 0 , \quad c = 0 \quad (3.76)$$

Now, we can write the plug flow model transfer function. With the Laplace's transformation of relation (3.73) and with Eqs. (3.74)–(3.76) we have:

$$pc(p) - pc(0_-) = w \frac{dc(p)}{dx}$$

$$-\frac{dc(p)}{c(p)} = p \frac{dx}{w}$$

$$\frac{c_{\text{sort}}(p)}{c_{\text{ent}}(p)} = T(p) = \exp\left(-p \frac{L}{w}\right) = \exp(-p\tau_m)$$

The residence time distribution $E(\tau)$ and the residence time repartition will be obtained starting with the inverse transformation of the transfer function $T(p)$:

$$E(\tau) = \delta(\tau - \tau_m) \quad (3.77)$$

where the δ impulse function is given by relation (3.78):

$$\delta(\tau - \tau_m) = \begin{cases} 0 & \text{for } x = L , \tau < \tau_m \\ 1 & \text{for } x = L , \tau = \tau_m \\ 0 & \text{for } x = L , \tau > \tau_m \end{cases} \quad (3.78)$$

Here, it is important to notice that, in the case of a combined model composed of PM and PF models, the transfer function is obtained from multiplication of the individual transfer functions:

$$T(p) = T_1(p)T_2(p)T_3(p)\dots T_N(p) \quad (3.79)$$

Table 3.3 shows the transfer functions that characterize the simplest and the combined models which are most commonly obtained by a combination of PM and PF models.

When we have a combination of recycled flow, by-pass connections, the presence of dead regions and a complex series and/or parallel coupling of the basic PM and PF models in a system, we have an important class of flow models recognized as combined flow models (CFM).

Table 3.3 The transfer function and model equation for some flow models

Model name	Model equation	Transfer Function	Symbol
1 Perfect mixing Flow	$\frac{dc}{d\tau} = -\frac{G_v}{V}(c - c_{ent})$	$T(p) = \frac{1}{\tau_m p + 1}$	$\tau_m = \frac{V}{G_v}$
2 Plug flow Model	$\frac{\partial c}{\partial \tau} = -w \frac{\partial c}{\partial x}$	$T(p) = \exp(-p\tau_m)$	$\tau_m = \frac{L}{w}$
3 Cellular perfect mixing Equal N cellules	$\frac{dc_i}{d\tau} = -\frac{G_v}{V}(c_i - c_{i-1})$	$T(p) = \frac{1}{(\tau_m p + 1)^N}$	V – cellule volume
4 Cellular perfect mixing Non-equal N cellules	$\frac{dc_i}{d\tau} = -\frac{G_v}{V_i}(c_i - c_{i-1})$	$T(p) = \prod_{i=1}^N \frac{1}{\tau_{mi} p + 1}$	V_i – cellule i volume
5 Series perfect mixing- Plug flow		$T(p) = \frac{\exp(-p\tau_{md})}{\tau_m p + 1}$	τ_{md} – mean residence time at PFM

3.3.2

Combined Flow Models

The construction of a combined model starts with one image (created, supposed or seeded) where it is accepted that the flow into the device is composed of distinct zones which are coupled in series or parallel and where we have various patterns of flow: flow zones with perfect mixing, flow zones with plug flow, zones with stagnant fluid (dead flow). We can complete this flow image by showing that we can have some by-pass connections, some recycled flow and some slip flow situations in the device.

The occurrence of these different types of flow can be established using the curve that shows the evolution of the species concentration (introduced as a signal at the input) at the device exit. It is important to notice that we can describe a flow process with an arbitrary number of regions and links. This procedure can result in a very complex system which makes it more difficult to identify the parameters of the CFM. In addition, we seriously increase the dimension of the problem, which results in quite a complex process of model building. Table 3.4 presents some simple combined models showing the model response by an analytic expression and by a qualitative graphic representation when we have a signal δ as input. Concerning the relations of Table 3.4, θ represents the dimensionless time τ/τ_m and $C(\theta)$ is the ratio $c(\theta)/c_0$. In fact, $C(\theta)$ is equivalent to $E(\tau)$ and, consequently, the dimensionless repartition function for the residence time $F(\theta)$ will be obtained by the integration of the function $C(\theta)$ from zero to θ . In Table 3.4, the models that result from the simplifications of three general types of combined models presented here below, are shown.

Table 3.4 The response curves to a δ signal for some simple CFM.

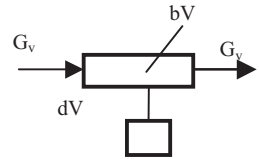
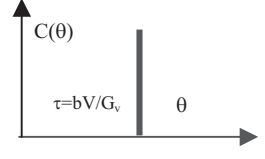
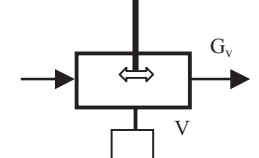
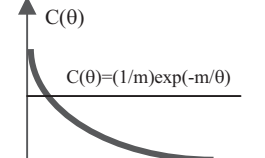
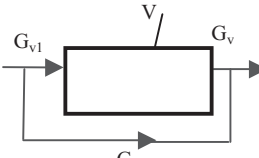
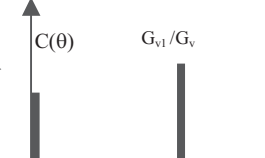
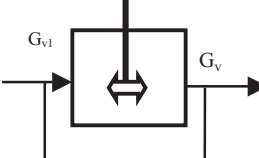
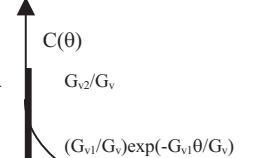
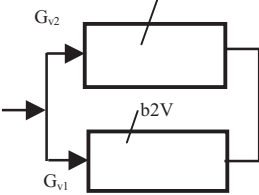
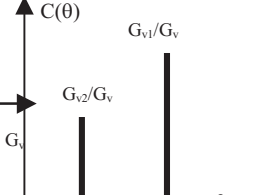
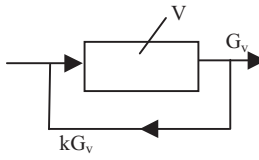
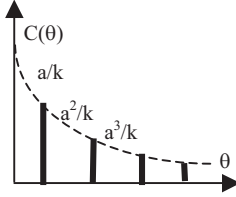
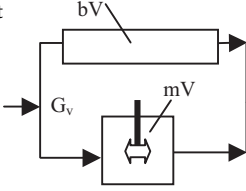
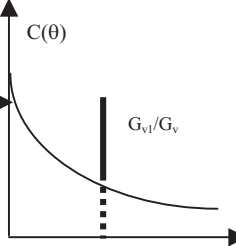
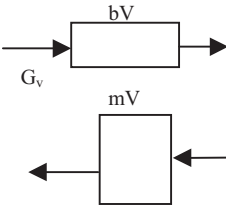
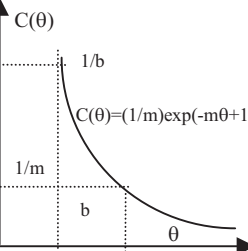
i	Model name	Model schedule	Response $C(\theta)$ vs. θ
1	Plug flow with stagnant zone. Parameters: b, d $b + d = 1$		
2	Perfect mixing flow with stagnant zone Parameters: m, d		
3	Plug Flow with by-pass connection Parameters: G_{v1}, G_{v2} $G_v = G_{v1} + G_{v2}$		
4	Perfect mixing flow with by-pass Parameters: G_{v1}, G_{v2} $G_v = G_{v1} + G_{v2}$		
5	Plug flow with parallel connection Parameters: $G_{v1}, G_{v2}, b1, b2$ $G_v = G_{v1} + G_{v2}$ $b1 + b2 = 1$		

Table 3.4 Continued

i	Model name	Model schedule	Response $C(\theta)$ vs. θ
6	Plug flow with recycling Parameters: k $a = k/(k + 1)$		
7	Plug flow with parallel perfect mixing Parameters: m, b, G_{v1}, G_{v2} $m + b = 1$		
8	Plug flow with series perfect mixing Parameters: b, m $b + m = 1$		

The first kind of CFM is characterized by Eqs. (3.80)–(3.82) and is shown in Fig. 3.26. For this CFM configuration, we can notice a lack of recycled flow or by-pass connections. The second type of CFM is introduced by Fig. 3.27 and is quantitatively characterized by relations (3.83)–(3.85) which show the dimensionless evolution of $C(\theta)$ and $F(\theta)$. Here we observe that we do not have any PF participants and recycled flow. The third CFM class is given in Fig. 3.28 and described by relations (3.86)–(3.88). Here the by-pass connections and PM participants are missing.

$$b_1 + b_2 + b_3 + d_1 + d_2 + m = 1$$

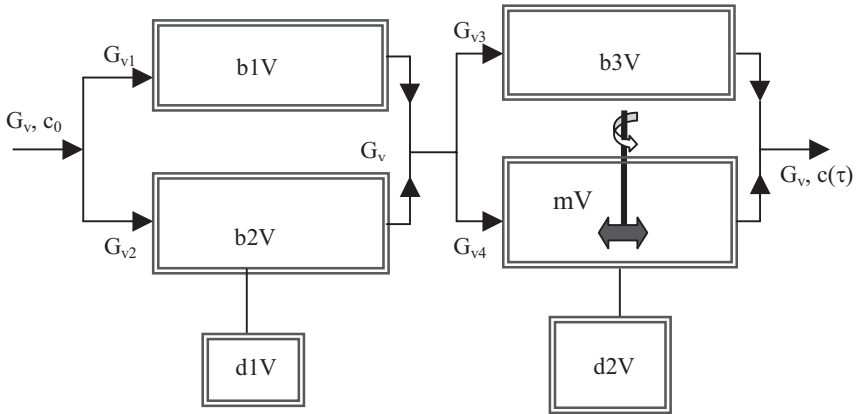


Figure 3.26 Block-scheme for the general mixing CFM.

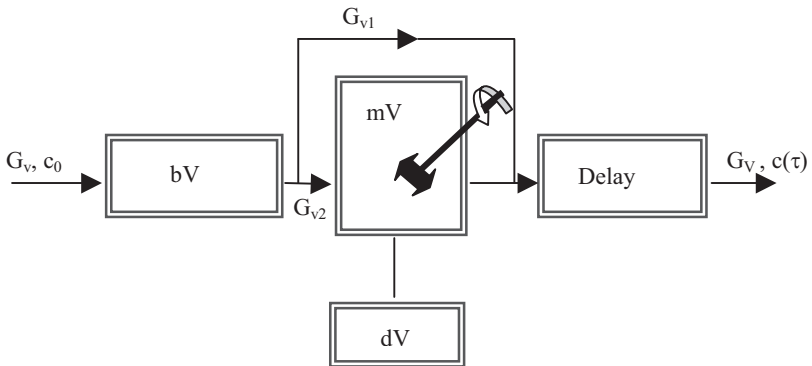


Figure 3.27 Block-scheme for the general by-passing CFM.

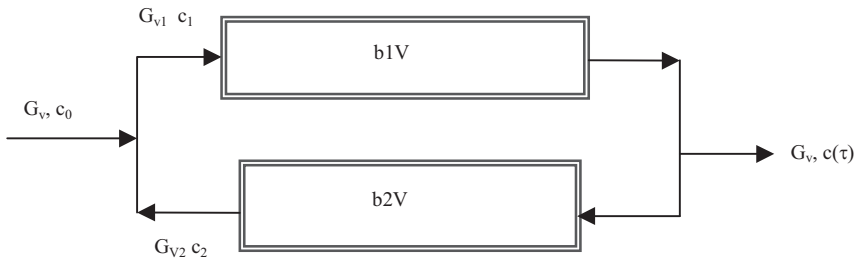


Figure 3.28 Block-scheme for the general recycling CFM.

$$T(p) = \sum_{i=1}^2 \left\{ \frac{\frac{G_{v1}G_{v3}}{G_v^2} \exp\left[-\frac{G_v}{G_{v1}} b_i(p+k)\tau_m\right]}{1 + \frac{mG_v}{G_{v4}}(p+k)} + \frac{G_{v1}G_{v3}}{G_v^2} \exp\left[-\frac{G_v}{G_{v1}} b_1(p+k)\tau_m - \frac{G_v}{G_{v3}} b_3(p+k)\tau_m\right] \right\} \quad (3.80)$$

$$C(\theta) = \sum_{i=1}^2 \left\{ \frac{G_{vi}G_{v3}}{G_v^2} \exp\left(-\frac{G_v}{G_{vi}} b_1 k \tau_m - \frac{G_v}{G_{v3}} b_3 k \tau_m\right) * \delta\left(\theta - \frac{G_v}{G_{v1}} b_1 - \frac{G_v}{G_{v3}} b_3 + \frac{G_{v1}G_{v3}}{mG_v^2}\right) \exp\left[-\frac{G_v}{G_{vi}} b_1 k \tau_m - \left(k\tau_m + \frac{G_{v4}}{mG_v}\right)\left(\theta - \frac{G_v}{G_{vi}} b_i\right) * v\left(\theta - \frac{G_v}{G_{v1}} b_1\right)\right] \right\} \quad (3.81)$$

$$F(\theta) = \sum_{i=1}^2 \left\{ \frac{G_{vi}G_{v3}}{mG_v^2} \frac{\exp\left(-\frac{G_v}{G_{vi}} b_1 \tau_m\right)}{\left(k\tau_m + \frac{G_{v4}}{mG_v}\right)} * \left[1 - \exp\left(-k\tau_m + \frac{G_{v4}}{mG_v}\right)\left(\theta - \frac{G_v}{G_{vi}} b_i\right)\right] * v\left(\theta - \frac{G_v}{G_{vi}} b_i\right) + \frac{G_{vi}G_{v3}}{G_v^2} \exp\left(-\frac{G_v}{G_{vi}} b_i k \tau_m - \frac{G_v}{G_{v3}} b_3 k \tau_m\right) * g\left(\theta - \frac{G_v}{G_{v1}} b_i - \frac{G_v}{G_{v3}} b_3\right) \right\} \quad (3.82)$$

$$T(p) = \frac{\exp(-p\varepsilon - k(\varepsilon - \tau_{rt}))}{\frac{\tau_m}{\eta}(p+k) + 1} \quad (3.83)$$

$$C(\theta) = \eta \exp\left(-k(\varepsilon - \tau_{rt}) - (k\tau_m + \eta)\left(\theta - \frac{\varepsilon}{\tau_m}\right)\right) * \delta\left(\theta - \frac{\varepsilon}{\tau_m}\right) \quad (3.84)$$

$$F(\theta) = \frac{\exp(-k(\varepsilon - \tau_{rt}))}{k\tau + \eta} \left[1 - \exp\left(-k\tau_m + \eta\right)\left(\theta - \frac{\varepsilon}{\tau_m}\right)\right] * g\left(\theta - \frac{\varepsilon}{\tau_m}\right) \quad (3.85)$$

It is important to notice that all the relations characterizing these three CFMs have been established by considering that a first order chemical reaction takes place in volume V and according to the accepted structure of the flow. So, here, k represents the kinetic reaction constant. When the reaction is not taken into account, we consider $k = 0$. In relations (3.83)–(3.85), τ_{rt} is the time delay expressed in a natural value, ε describes the system phase difference in time units and η is the mixing coefficient. This last parameter equals one for a perfect mixing flow and zero for plug flow. In other cases, η can be estimated with $m/(m + b + d)$ as shown in Fig. 3.27.

$$T(p) = \frac{\frac{G_v}{G_{v1}} \exp\left(- (p+k)\tau_m \frac{b1G_v}{G_{v1}}\right)}{1 + \frac{G_{v2}}{G_{v1}} \exp\left(- (p+k)\tau_m \left(\frac{b1G_v}{G_{v1}} + \frac{b1G_v}{G_{v2}}\right)\right)} \quad (3.86)$$

$$C(\theta) = \frac{G_v}{G_{v1}} \exp\left(-k\tau_m \frac{b1G_v}{G_{v1}}\right) * \sum_{N=1}^N \left[\frac{G_{v2}}{G_{v1}} \exp\left(-k\tau_m \left(\frac{b1G_v}{G_{v1}} + \frac{b2G_v}{G_{v2}}\right)\right) \right]^{N-1} \delta\left(\theta - \frac{Nb1G_v}{G_{v1}} + \frac{(N-1)b2G_v}{G_{v2}}\right) \quad (3.87)$$

$$F(\theta) = \frac{G_v}{G_{v1}} \exp\left(-k\tau_m \frac{b1G_v}{G_{v1}}\right) * \sum_{N=1}^N \left[\frac{G_{v2}}{G_{v1}} \exp\left(-k\tau_m \left(\frac{b1G_v}{G_{v1}} + \frac{b2G_v}{G_{v2}}\right)\right) \right]^{N-1} \delta\left(\theta - \frac{Nb1G_v}{G_{v1}} + \frac{(N-1)b2G_v}{G_{v2}}\right) \quad (3.88)$$

The general problem of building a model for an actual process begins with a flow description where we qualitatively appreciate the number of flow regions, the zones of interconnection and the different volumes which compose the total volume of the device. We frequently obtain a relatively simple CFM, consequently, before beginning any computing, it is recommended to look for an equivalent model in Table 3.4. If the result of the identification is not satisfactory then we can try to assimilate the case with one of the examples shown in Figs. 3.26–3.28. If any of these previous steps is not satisfactory, we have three other possibilities: (i) we can compute the transfer function of the created flow model as explained above; (ii) if a new case of combination is not identified, then we seek where the slip flow can be coupled with the CFM example, (iii) we can compare the created model with the different dispersion flow models.

The CFM can be completed with a recycling model (the trajectory of which can be considered as a CFM, such as a PF with PM, series of PM, etc.), or with models with slip flows and models with multiple closed currents.

The next section will first show the importance of flow in a concrete modelling problem such as the slip flow effect on the efficiency of a permanent mechanically mixed reactor. Then the characterization of the combined flow models where the slip flow occurs will be presented.

3.3.3

The Slip Flow Effect on the Efficiency of a Mechanically Mixed Reactor in a Permanent Regime

In this section, we consider a permanent and mechanically mixed reactor, where a chemical transformation occurs and the consumption rate of one reactant is given

by a formal kinetics of n order: $v_r = kc^n$. The flow conditions expressed by the geometric position and rotation speed of the stirrer and by the position on the reactor of the input and exit flow, define an internal flow structure with three regions: the surface region, named slip flow, where the reactants come rapidly to the exit without an important conversion; the middle region, where a perfectly mixing flow exists and consequently an important reactant conversion takes place; the bottom region, where we have a small flow intensity and which can be recognized as a stagnant region. Figure 3.29 gives a graphic presentation of the description of the reactor operation as well as the notation of the variables. The performances of this simplified and actual reactor (SPMR) example will be compared with those of a permanent perfect mixing reactor (PMR) having the same volume.

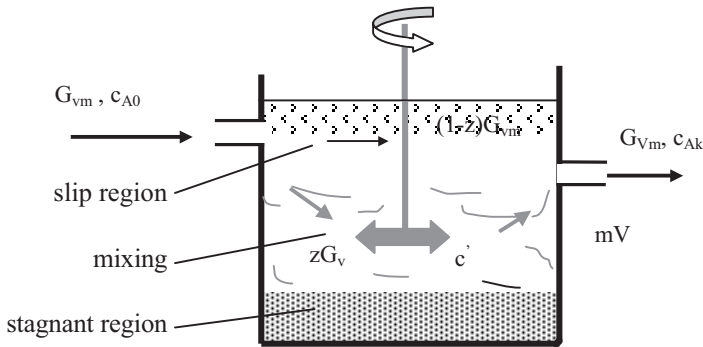


Figure 3.29 Stirred reactor with slip and stagnant flow zones.

The reactant A balance equations for these reactors (PMR and SPMR) can be written as follows:

$$V_{r \max} = G_{vm}(c_{A0} - c_{A \min}) \quad (3.89)$$

$$mV_r = G_{vm}(c_{A0} - c_{Ak}) \quad (3.90)$$

If we compute the ratio between Eqs. (3.89) and (3.90) we have:

$$m = \frac{c_{A0} - c_{Ak}}{c_{A0} - c_{A \min}} \frac{V_{r \max}}{V_r} \quad (3.91)$$

Here the reaction rate will be $v_{r \max} = k(c_{A \min})^n$ and $v_r = k(c')^n$ respectively. The value of the reactant concentration for the mixing zone of the SPMR will be obtained as a result of its comparative mass balance. If we consider that the slip flow is not present (PMR case) or when it is present but the reactant flow rate is identical, then we can write:

$$zG_{vm}c' = G_{vm}c_{Ak} - (1 - z)G_{vm}c_{A0} \quad (3.92)$$

So, for the reactant concentration in the mixing zone of the SPMR we establish the relation:

$$c' = \frac{c_{Ak} - (1-z)c_{A0}}{z} \quad (3.93)$$

Rearranging the five previous equations (3.89) to (3.93), in order to introduce and replace the relation between v_r and $v_{r\max}$, we have:

$$m = \left[\frac{\frac{c_{A0}}{c_{Ak}}}{\frac{c_{A0}}{c_{A\min}}} \right]^{n-1} \left[\frac{\frac{c_{A0}/c_{Ak} - 1}{c_{A0}/c_{A\min} - 1}}{\left[\frac{z}{1 - (1-z) - c_{A0}/c_{Ak}} \right]^n} \right] \quad (3.94)$$

If we introduce $1 - c_{Ak}/c_{A0} = X$ and $1 - c_{A\min}/c_{A0} = X_m$ where X and X_m represent the reactant transformation degree for SPMR and PMR operation modes, then relation (3.94) becomes:

$$m = \frac{X}{X_m} \left[\frac{z(1 - X_m)}{z - X} \right]^n \quad (3.95)$$

Figure 3.30 shows clearly the effect of m and z on the reactant transformation degree for a SPMR. Only for a zero-order kinetics process, does the slip flow not affect the degree of the reactant transformation. For other X_m values, each graphic construction based on Fig. 3.30 shows the same rules of evolution (at $m < 0.5$, z and X increase simultaneously, and, when n increases, X increases slowly; for $m > 0.5$, X keeps a constant value determined by z). When the PM core of SPMR is exchanged with a CFM model, we obtain a special SPMR type in which the performances can be appreciated by the model developed above.

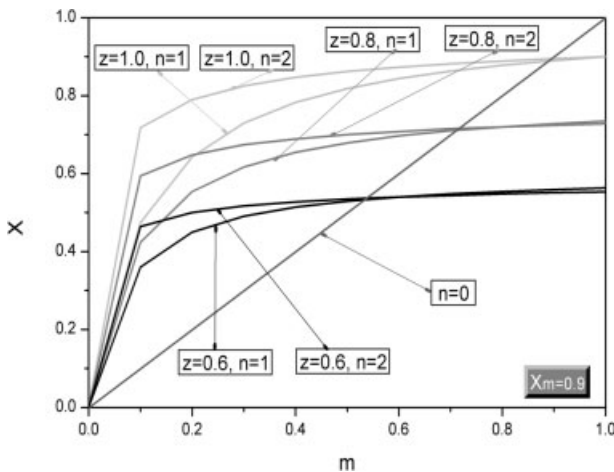


Figure 3.30 The effect of the perfect mixing region dimension and of the slip flow degree on the SPMR conversion (reaction order $n = 0, 0.5, 1, 1.5, 2$; $X_m = 0.9$).

3.3.4

Dispersion Flow Model

The models of flow dispersion are based on the plug flow model. However, in comparison with the PF model, the dispersion flow model considers various perturbation modes of the piston distribution in the flow velocity. If the forward and backward perturbations present random components with respect to the global flow direction, then we have the case of an axial dispersion flow (ADF). In addition, the axial and radial dispersion flow is introduced when the axial flow perturbations are coupled with other perturbations that induce the random fluid movement in the normal direction with respect to the global flow.

With reference to these different types of flow, there is often confusion associated with the terms: “dispersion”, “diffusion” and “turbulence”. When we talk about a *species in a fluid*, diffusion and turbulence produce the molecular or turbulent jumps in the existing flowing area. However, concerning dispersion, it is not conditioned by the concentration gradient (as diffusion can be) nor even by a characteristic level of the global flow velocity (as turbulence can be). The dispersion flow is a result of the effects of the basic flow interaction with various discrete fixed or mobile forms that exist or appear along the flow trajectory [3.26]. The drops moving downward or upward in a flowing or stationary fluid, the bubbles flowing within a liquid, as well as an important roughness of the pipe walls, are some of the phenomena responsible for the dispersion flow. Another case is in a fluid flowing through a packed bed. In these examples, dispersion occurs because we have a microflow situation with a completely different intensity with respect to the basic flow. It is not difficult to observe that, for all the devices where a differential contact solid–fluid or solid–fluid–fluid or fluid–fluid occurs, the dispersion flow is the characteristic flow type. As for turbulence, the dispersion characterization associates a coefficient called *dispersion coefficient* to these microflows responsible for the dispersion phenomenon. When the dispersion participation is very important, the turbulence and molecular components of the vector of total property transport can be neglected. Consequently, we can write the following expression for the vector of the property transport:

$$\vec{J}_{tA} = \vec{w}\Gamma_A - D_l \vec{\text{grad}}\Gamma_A \quad (3.96)$$

The equation of the ADF model flow can be obtained by making a particular species mass balance, as in the case of a plug flow model. In this case, for the beginning of species balance we must consider the axial dispersion perturbations superposed over the plug flow as shown in Fig. 3.31. In the description given below, the transport vector has been divided into its convective and dispersion components.

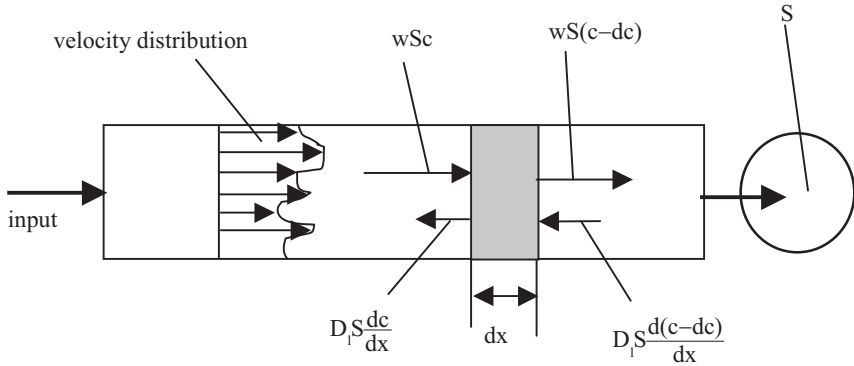


Figure 3.31 Scheme of the axial dispersion flow description.

After the particularization of the species balance in the control volume with section flow S and elementary length dx , as shown in Fig. 3.31, we obtain relation (3.97), which corresponds to the ADF model equation:

$$\frac{\partial c}{\partial \tau} = -w \frac{\partial c}{\partial x} + D_1 \frac{\partial^2 c}{\partial x^2} \quad (3.97)$$

The axial dispersion flow model can be valid when we do not have the gradient of the property with respect to the normal flow direction. In other words, for this direction, we have a perfect mixing state. When this last condition is not met, we have to consider a flow model with two dispersion coefficients: a coefficient for the axial dispersion and another one for the radial dispersion. In this case, the flow model equation becomes:

$$\frac{\partial c}{\partial \tau} = -w \frac{\partial c}{\partial x} + D_1 \frac{\partial^2 c}{\partial x^2} + \frac{D_r}{r} \frac{\partial}{\partial r} \left(r \frac{\partial c}{\partial r} \right) \quad (3.98)$$

The values of the dispersion coefficients will be established for most actual cases by experiments, which pursue the registration and interpretation of the exit time distribution of a signal that passes through a physical reduced model of the real device. However, in some cases, the actual device can be used. The method for identifying the dispersion coefficient [3.27, 3.28] is, in fact, the classical method of flow identification based on the introduction in the device input of a signal; (frequently as a δ impulsion or a unitary impulsion) the exit response is then recorded from its start until it disappears. It is evident that this experimental part of the method has to be completed by calculation of the dispersion model flow and by identification of the value of the dispersion coefficient. For this last objective, the sum of the square differences between the measured and computed values of the exit signal, are minimized.

For the mathematical solution of the dispersion model flow, we add the univocity conditions that include the signal input description for the initial conditions to Eq. (3.97) or (3.98). A more complete description of this mathematical model

can be given with the example of the axial dispersion flow. In this case, we assign the dispersion flow conditions to the input and the exit of the apparatus Eq. (3.99) and to the model equation (3.97). The initial signal input conditions are given by relation (3.100) for the case of a δ signal and by relation (3.101) when a unitary impulse signal is used.

$$\begin{aligned} \bar{w}_1 c - D_1 \frac{\partial c}{\partial z} &= 0, \quad z = 0, \quad \tau > 0 \\ D_1 \frac{\partial c}{\partial z} &= 0, \quad z = H_d, \quad \tau > 0 \end{aligned} \quad (3.99)$$

$$\begin{aligned} c &= 0, \quad 0 < z < H_d, \quad \tau = 0 \\ c &= c_0, \quad z = 0, \quad \tau = 0 \end{aligned} \quad (3.100)$$

$$\begin{aligned} c &= c_0, \quad z = 0, \quad \tau > 0 \\ c &= 0, \quad 0 < z < H_d, \quad \tau = 0 \end{aligned} \quad (3.101)$$

For the unitary impulse signal (relation (3.100)) the axial dispersion flow model has an analytical solution:

$$\left(\frac{c}{c_0} \right)_{z=H_d} = 2 \sum_{n=1}^{\infty} \frac{\lambda_n \sin \lambda_n}{\lambda_n^2 + \left(\frac{Pe}{2} \right)^2 + \frac{Pe}{2}} \exp \left[\frac{Pe}{2} - \left(\frac{\lambda_n^2 + \left(\frac{Pe}{2} \right)^2}{Pe} \right) \theta \right] \quad (3.102)$$

where θ is the dimensionless time ($\theta = \tau/\tau_m$) and the proper values of λ_n are the solutions of Eqs. (3.103) and (3.104):

$$2\lambda_n \operatorname{tg} \frac{\lambda_n}{2} = Pe \quad ; \quad n = 1, 3, 5, \dots, 2k + 1, \dots \quad (3.103)$$

$$2\lambda_n \operatorname{ctg} \frac{\lambda_n}{2} = Pe \quad ; \quad n = 2, 4, 6, \dots, 2k, \dots \quad (3.104)$$

This solution can be used to set up the value of the Peclet criterion ($Pe = wH_d/D_1 = H_d^2/(D_1\tau_m)$) if we only consider the first term of Eq. (3.102). In this situation we obtain relations (3.105) and (3.106). It is not difficult to observe that, from the slope of relation (3.105), we can easily obtain the Pe value:

$$\ln \left(\frac{c}{c_0} \right)_{z=H_d} = \left[\frac{Pe}{2} - \frac{\lambda_1 + \left(\frac{Pe}{2} \right)^2}{Pe} \right] \theta + \left(\ln \frac{2\lambda_1 \sin \lambda_1}{\left(\frac{Pe}{2} \right)^2 + \frac{Pe}{2} + \lambda_1^2} \right) \quad (3.105)$$

$$2\lambda_1 \operatorname{tg} \frac{\lambda_1}{2} = Pe \quad (3.106)$$

When the value of the mean flow velocity cannot be correctly estimated, as in the case of two or three phases contacting, the Pe number will be estimated considering the mean residence time (τ_m), the transport trajectory length (H_d) and the dispersion coefficient (D_1). For the case of a unitary signal impulse Eq. (3.100), the mean residence time will be estimated using relation (3.107):

$$\tau_m = \int_0^{\infty} \left(1 - \frac{c(\tau)}{c_0}\right) d\tau = \frac{\sum_{i=1}^N (c_0 - c(\tau_i))\tau_i}{\sum_{i=1}^N (c_0 - c(\tau_i))} \quad (3.107)$$

where N represents the number of the last appearance of $c_0 - c(\tau_i) > 0$ in the discrete data obtained.

Relation (3.108) gives the analytical solution of the axial dispersion model which contains relations (3.97), (3.99) and (3.100). Here the proper values of λ_k are the solutions of the transcendent equation (3.109):

$$\left(\frac{c}{c_0}\right)_{z=Hd} = \sum_{k=1}^{\infty} \frac{2\lambda_k \exp\left(\frac{Pe}{2} - \frac{Pe}{4}\theta - \frac{4}{Pe}\lambda_k^2\theta\right)}{\left(1 + \frac{Pe}{2}\right) + \frac{Pe}{2}\lambda_k \sin 2\lambda_k - \left(\frac{Pe}{4} - \left(\frac{Pe}{4}\right)^2\theta - \lambda_k^2\right) \cos 2\lambda_k} \quad (3.108)$$

$$\operatorname{tg} 2\lambda_k = \frac{\frac{Pe}{2}\lambda_k}{\lambda_k^2 - \left(\frac{Pe}{4}\right)^2} \quad (3.109)$$

If we consider the random variable theory, this solution represents the residence time distribution for a fluid particle flowing in a trajectory, which characterizes the investigated device. When we have the probability distribution of the random variable, then we can complete more characteristics of the random variable such as the non-centred and centred moments. Relations (3.110)–(3.114) give the expressions of the moments obtained using relation (3.108) as a residence time distribution. Relation (3.114) gives the two order centred moment, which is called random variable variance:

$$v_1 = 1 \quad (3.110)$$

$$v_2 = 1 + \frac{2}{Pe} + \frac{2}{Pe^2}e^{-Pe} - \frac{2}{Pe^2} \quad (3.111)$$

$$v_3 = 1 + \frac{6}{Pe} + \frac{6}{Pe^2} - \frac{24}{Pe^3} + \frac{18e^{-Pe}}{Pe^2} + \frac{24e^{-Pe}}{Pe^3} \quad (3.112)$$

$$v_4 = 1 + \frac{12}{Pe} + \frac{48}{Pe^2} - \frac{336}{Pe^4} - \frac{108e^{-Pe}}{Pe^2} + \frac{360e^{-Pe}}{Pe^3} + \frac{312e^{-Pe}}{Pe^4} + \frac{24e^{-Pe}}{Pe^4} \quad (3.113)$$

$$\sigma^2 = v_2 - v_1 = \frac{2}{Pe} - \frac{2}{Pe^2} + \frac{2}{Pe^2} e^{-Pe} \quad (3.114)$$

Because the device response to the signal input is given by the discrete coupled data $c_i - \tau_i$, the mentioned moment, can be numerically computed as follows:

$$\tau_m = \frac{\sum_i \tau_i c_i}{\sum_i c_i} \quad (3.115)$$

$$v_1 = \frac{\tau_m}{\tau_m} = 1 \quad (3.116)$$

$$v_2 = \frac{\sum_i \tau_i^2 c_i}{\tau_m^2 \sum_i c_i} \quad (3.117)$$

$$v_3 = \frac{\sum_i \tau_i^3 c_i}{\tau_m^3 \sum_i c_i} \quad (3.118)$$

$$v_4 = \frac{\sum_i \tau_i^4 c_i}{\tau_m^4 \sum_i c_i} \quad (3.119)$$

$$\sigma^2 = v_2 - v_1 = \frac{\sum_i \tau_i^2 c_i}{\tau_m^2 \sum_i c_i} - 1 \quad (3.120)$$

The coupling of relations (3.110)–(3.114) with (3.115)–(3.120) shows four possibilities for the identification of the Pe number. With the same data, each possibility must produce an identical result for the Pe criterion.

3.3.5

Examples

Actually, it is acknowledged that all the main chemical engineering devices are well described by known equations and procedures to compute axial and radial mixing coefficients. As an example, we can remember the famous Levenspiel's equation to compute the axial mixing of a mono-phase flow in a packed bed ($Pe = wd_p/D_1 = 2$), an equation verified by experiments. Undeniably, the problem of identifying a flow model can be developed using a laboratory model of the real device if the experiments can be carried out easily. For the construction of such a physical model, we must meet all the requirements imposed by the similitude laws. It is important to note that we assume that the laboratory model undergoes one or more changes in order to produce a flow model in accordance with the mathematical process simulation. Indeed, it contains a selected flow model, which produces the best results for the investigated process. Consequently, the most acceptable flow model has been indirectly established by this procedure.

In order to show how a chemical device can be scaled-up and how a solution to the problem of identifying the best flow model can be given, we suggest the following protocol:

(i) for an actual case (reaction, separation, heating, coupled transport, etc.), we can establish the best flow model (that guarantees the best exits for the fixed inputs in the modeled process) by using the mathematical modelling and simulation of a process; (ii) we design and build a laboratory device, that can easily be modified according to the results obtained from the experiments carried out to identify the flow model; (iii) with the final physical model of the device, we examine the performance of the process and, if necessary, we start the experimental research all over again to validate the model of the process; (iv) when the final physical model of the device is made, the scaled-up analysis is then started, the result of this step being the first image of the future industrial device. It is important to notice that the tricky points of an actual experimental research have to be discussed: (i) the input point of the signal and the exit point of the response must be carefully selected; (ii) the quality of the input signal must respect some requirements: indeed, if we use the expressions from Table 3.4 or those given by the assembly of Eqs. (3.80)–(3.88) to interpret the data, then the signal must be a δ or a unitary impulse; other signal types induce important difficulties for solving the flow model and for identifying the parameters; (iii) the response recording must be carried out with transducers and magnification systems which do not introduce unknown retardation times. This methodology will be illustrated in the next sections with some examples.

3.3.5.1 Mechanically Mixed Reactor for Reactions in Liquid Media

The physical model of the reactor is a 350 mm high cylindrical vessel, with a diameter of 200 mm and an elliptical bottom. The operation volume is: $V = 12 * 10^{-3} \text{ m}^3$. The entrance of the reactants is placed near the middle of the reactor, more exactly at 130 mm from the bottom. The reactor's exit is positioned on the top of the vessel but below the liquid level. At the vessel centre is placed a mixer with three helicoidal paddles with $d/D = 0.33$. It operates with a rotation speed of 150 min^{-1} . In order to establish the reactor flow model, this is filled with pure water which continuously flushes through the reactor at a flow rate of $6.6 * 10^{-5} \text{ m}^3/\text{s}$ (similar to the reactants' flow rate). At time $\tau = 0$, a unitary impulse of an NaCl solution with a $c_0 = 3.6 \text{ kg}/\text{m}^3$ is introduced into the reactor input. The time evolution of the NaCl concentration at the exit flow of the reactor is measured by the conductivity. Table 3.5 gives the data that show the evolution of this concentration at the reactor exit.

The proposal of an adequate flow model of the reactor and the identification of the parameters are the main requirements of this application. Solving this type of problem involves two distinct actions: first the selection of the flow model and second the computations involved in identifying the parameters.

Table 3.5 Evolution of the NaCl concentration at the reactor's exit.

i	1	2	3	4	5	6	7	8	9	10	11	12
τ_i (s)	0	1.8	3.6	4.8	18	36	72	108	144	180	216	252
$c_i = c(\tau_i)$	0	0	0	0.18	0.342	0.651	1.281	1.828	2.142	2.405	2.556	2.772

The selection of the flow model. In accordance with the description given above, we expect a flow model in which a small plug-flow region is associated with an important perfect mixing flow region, whereas a stagnant region is considered at the bottom of the reactor. If this proposal is correct, then, in the general CFM shown in Table 3.4 we must consider:

$G_{v1} = G_{v4} = G_v$; $G_{v2} = G_{v3} = 0$; $b3 = b1 = d1 = 0$; $b1 = b$; $d2 = d$ and $b + m + d = 1$. With $k = 0$ (because, here, the chemical reaction does not occur), the logarithmic transformation of relation (3.82), which gives the response $F(\theta) = c(\theta)/c_0$ for an unitary impulse, can be written as follows:

$$\ln\left(1 - \frac{c(\theta)}{c_0}\right) = -\frac{1}{m}(\theta - b) * \mathcal{I}(\theta - b) \quad (3.121)$$

The computations to identify the parameters are given algorithmically, step by step, by the procedure below:

- We start with the computation of the value of the mean residence time: $\tau_m = V/G_v = 12 * 10^{-3}/6.66 * 10^{-5} = 180$ s.
- Using the data given in Table 3.5 we build the dependence relation $c_i = c(\theta_i)/c_0$ vs θ_i where $\theta_i = \tau_i/\tau_m$ and $C(\theta_i) = c(\theta_i)/c_0$. Table 3.6 presents this dependence. Here d_i values are also computed as $\ln(1 - c(\theta_i)/c_0)$ because they are needed for the flow model equation (3.121).

Table 3.6 Dimensionless NaCl concentration at the reactor's exit.

i	1	2	3	4	5	6	7	8	9	10	11	12
θ_i	0	0.01	0.02	0.03	0.1	0.2	0.4	0.6	0.8	1.0	1.2	1.4
$c(\theta_i)/c_0$	0	0	0	0.05	0.095	0.181	0.356	0.508	0.596	0.668	0.713	0.775
d_i	0	0	0	-0.05	-0.1	-0.2	-0.44	-0.71	-0.91	-1.1	-1.23	-1.45

- the graphic representation of $d_i = \ln(1 - C(\theta_i))$ vs θ_i in Fig. 3.32, shows that all the data do match a line with a slope equal to $-1/m$ and with the origin intersect at b/m . At the same time, function $\mathcal{I}(\theta - b)$ shows its b value.

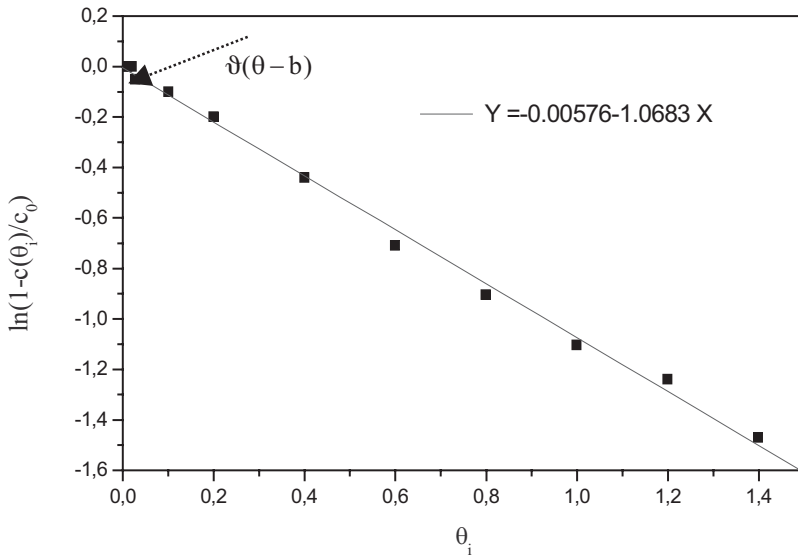


Figure 3.32 Evolution of the $\ln(1 - C(\theta_i))$ vs θ_i .

- the values of m , b and d can be calculated from Fig. 3.32 above, giving respectively $m = 0.936$, $b = 0.00054$, $d = 0.06345$. These results show that 6.34% of the reactor is a stagnant region and 0.054% is a plug-flow region, the remainder being a perfect mixing region.

3.3.5.2 Gas Flow in a Fluidized Bed Reactor

Catalytic butane dehydrogenation can be successfully carried out in a laboratory scale fluidized bed reactor operating at 310 °C and at atmospheric pressure. The catalytic particles have diameter 310 μm and density 2060 kg/m^3 . Such a reactor is 150 mm in diameter and has a fixed 500 mm long catalytic bed. When the catalyst bed is fluidized with butane blown at a velocity of 0.1 m/s, it becomes 750 mm thick.

The establishment of the flow model or a cold model of the reactor is carried out using air instead of butane and working at the same gas velocity as implemented to fluidize the catalytic bed. In these conditions, a slow motion of the solid, without any important bubbling phenomena, is observed at the bottom of the fluidized bed, while a bubbling phenomenon associated with violent solid motion occurs in the middle and upper parts of the fluidized bed. At time $\tau = 0$, a unitary signal, which consists of replacing the air flow by an identical flow of pure nitrogen, is generated at the reactor input. Table 3.7 presents the evolution of the nitrogen concentrations at the bed exit.

Table 3.7 Evolution of the nitrogen concentration at the exit of the fluidized bed reactor.

i	1	2	3	4	5	6	7	8	9	10	11	12
τ_i sec	0	1	2	3	4	5	6	7	8	9	10	11
$c_i = c(\tau_i)$	0.79	0.79	0.79	0.79	0.874	0.924	0.947	0.973	0.981	0.984	0.994	0.996

To solve this example we use the same methodology as applied in the previous section: we begin with the flow model selection and finish by identifying the parameters.

The model selection. According to the description of the fluidization conditions given above, we can suggest a combined flow model of a plug-flow linked in series with a perfect mixing. We obtain the mathematical description of this CFM from the general CFM presented in Table 3.4 by: $G_{v1} = G_{v4} = G_v$; $G_{v2} = G_{v4} = 0$; $b_3 = b_1 = d_1 = 0$; $d_2 = d$ and $b + m + d = 1$. With this consideration, we have the simplified model characterized by relation (3.121). If the figure obtained from the graphical representation of $d_i = \ln(1 - C(\theta_i))$ vs θ_i is linear then, the proposed model can be considered as acceptable.

With *the computation* of the algorithm identifying the parameters of the model we obtain:

- The gas fraction of the bed:
 $\varepsilon = \varepsilon_0 + (H - H_0^o)/H = 0.4 + 0.25/0.75 = 0.66 \text{ m}^3 \text{ gas/m}^3 \text{ bed}$.
- The mean residence time: $\tau_m = \varepsilon H/w_f = 0.66 * 0.75/0.1 = 5 \text{ s}$.
- The relation: $c(\theta_i)/c_0$ vs θ_i is computed in Table 3.8 and plotted.
 Here $c_{00} = 0.79 \text{ kmol N}_2/\text{kmol gas}$ and $c_0 = 1 \text{ kmol N}_2/\text{kmol gas}$. Table 3.8 also contains the computed line that shows the dependence of the $\ln(1 - C(\theta_i))$ vs θ_i .

Table 3.8 Evolution of the dimensionless nitrogen concentration at the reactor's output.

i	1	2	3	4	5	6	7	8	9	10	11	12
θ_i	0	0.2	0.4	0.6	0.8	1.0	1.2	1.4	1.6	1.8	2.0	2.2
$\frac{c(\tau_i) - c_{00}}{c_0 - c_{00}}$	0	0	0	0	0.399	0.643	0.747	0.874	0.924	0.954	0.975	0.983
$\ln(1 - C(\theta_i))$	0	0	0	0	-0.51	-1.03	-1.55	-2.07	-2.58	-3.09	-3.56	-4.03

- Figure 3.33 shows that the hypothesis of a CFM composed of a series of PF and PM is acceptable because the experimental dependence of $\ln(1 - C(\theta_i))$ vs θ_i is linear and we clearly observe the function $\mathcal{Y}(\theta - b)$.

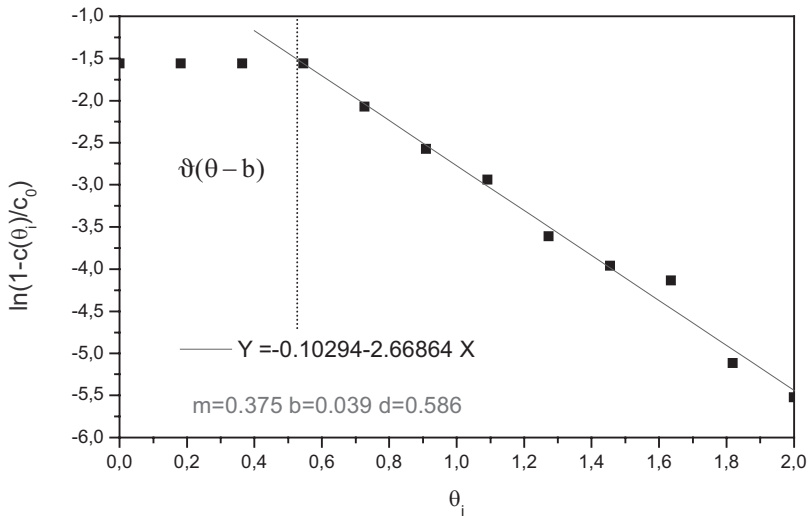


Figure 3.33 The evolution of $\ln(1 - C(\theta_i))$ vs θ_i .

- As in the case of application 3.3.5.1, we identify $m = 0.375$ and $d = 0.586$. The value $b = 0.039$, shown in Fig. 3.33, comes from the origin intersect of the line $Y = -2.66864X - 0.10294$, this value does not have a special significance. The d value can be increased with the b value. So it will become $d = 0.625$.

3.3.5.3 Flow in a Fixed Bed Catalytic Reactor

The laboratory scale physical model of the catalytic sulfur dioxide oxidation is a 0.05 m-diameter reactor containing 3 mm-diameter pellets of catalyst over a height of 0.15 m. The bed is flushed through at 430 °C by a gas flow that contains 0.07 kmol SO_2/kmol total gas, 0.11 kmol O_2/kmol total gas and 0.82 kmol N_2/kmol total gas. The gas spatial velocity is 0.01 m/s.

In order to obtain a reactor model flow that characterizes the gas movement around the catalyst grains, a current of pure nitrogen is blown through the fixed catalyst bed at the same temperature and pressure as in the reaction. At $\tau = 0$ we apply a signal (unitary impulse) to the reactor input introducing a gas mixture containing nitrogen and sulfur dioxide with a concentration of $c_0 = 0.1$ kmol SO_2/kmol gas. Then, we measure the evolution of the sulfur dioxide concentration at the reactor exit. Table 3.9 gives these measured concentrations. In this case, it is necessary to validate if the collected data verify a PF model. If they do not, we have to identify the parameters of the axial mixing model to correct the PF model.

Table 3.9 Evolution of the sulfur dioxide concentration at the exit of the reactor.

i	1	2	3	4	5	6	7	8	9	10	11	12	13	14
τ_i (s)	0	1.2	2.4	3.0	3.6	4.8	6	7.2	8.4	9.6	10.8	12	13.2	14.4
$c_i = c(\tau_i)$	0	0	0	0	0.01	0.03	0.06	0.08	0.085	0.09	0.095	0.097	0.099	0.1

Then, for this application, we directly start with the computations that serve to identify the parameters.

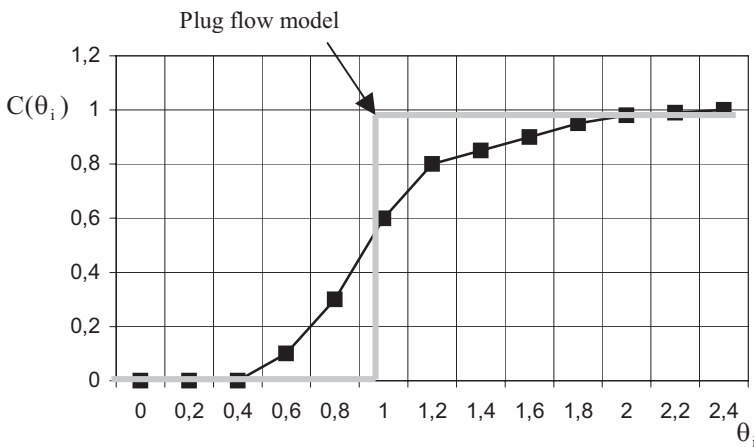
The computation of the values of the following parameters and relations are needed to solve the problem:

- the mean residence time of an elementary fluid particle in the catalyst bed $\tau_m = (\varepsilon_0 H)/w_1 = 0.4 * .015/0.01 = 6$ s;
- the dimensionless dependence $C(\theta_i) = c(\theta_i)/c_0$ vs θ_i is computed and reported in Table 3.10;

Table 3.10 Evolution of the dimensionless signal at the exit of the reactor.

i	1	2	3	4	5	6	7	8	9	10	11	12	13	14
θ_i	0	0.2	0.4	0.5	0.6	0.8	1.0	1.2	1.4	1.6	1.8	2.0	2.2	2.4
$\frac{c(\theta_i)}{c_0}$	0	0	0	0	0.1	0.3	0.6	0.8	0.85	0.90	0.95	0.98	0.99	1.00

- the graphic representation of the dependence $C(\theta_i) = c(\theta_i)/c_0$ vs θ_i is needed to appreciate whether we have a PF or ADF flow type. Figure 3.34 clearly shows that here, an ADF flow model type can be adequate;

**Figure 3.34** Evolution of the dimensionless concentration at the exit of the reactor.

- for the computation of the axial dispersion coefficient, we use an approximate calculation introduced by Eqs. (3.105) and (3.106). These relations are coupled with the numerical data reported in Table 3.10 and then we form the function here given by relation (3.122). It minimizes the sum of the squares of the differences between the computed and experimental values of $C(\theta_i)$. We further show that this problem of axial dispersion coefficient identification is transformed into a variant of a least squares method for parameter identification.

$$F(\lambda_1) = \sum_{i=1}^{14} \left[\sum_{i=1}^{14} \left(\frac{\lambda_1 \operatorname{tg}^2 \frac{\lambda_1}{2} - 1}{2 \operatorname{tg} \frac{\lambda_1}{2}} \right) \theta_i + \ln \frac{2 \sin \lambda_1}{\lambda_1 \operatorname{tg}^2 \frac{\lambda_1}{2} + \operatorname{tg} \frac{\lambda_1}{2} + \lambda_1} - \ln \left(\frac{c(\theta_i)}{c_0} \right)_{\text{exp}} \right]^2$$

$$= \min \tag{3.122}$$

With $a = \frac{\lambda_1 \operatorname{tg}^2 \frac{\lambda_1}{2} - 1}{2 \operatorname{tg} \frac{\lambda_1}{2}}$, $b = \ln \frac{2 \sin \lambda_1}{\lambda_1 \operatorname{tg}^2 \frac{\lambda_1}{2} + \operatorname{tg} \frac{\lambda_1}{2} + \lambda_1}$ and $y_i = \ln \left(\frac{c(\theta_i)}{c_0} \right)_{\text{exp}}$ the

minimization requested by the problem (3.122) takes the common form $F(a, b) = \sum_{i=1}^{14} (a\theta_i + b - y_i)^2 = \min$, which has the quality to accept a very simple solution. So, in order to obtain “a” and “b”, we must solve the equation system (3.123). From these values, we obtain the value of λ_1 . Now, using relation (3.106) we can calculate the Peclet dispersion number.

$$\begin{cases} Nb + a \sum_{i=1}^{N=14} \theta_i = \sum_{i=1}^{N=14} y_i \\ b \sum_{i=1}^{N=14} \theta_i + a \sum_{i=1}^{N=14} \theta_i^2 = \sum_{i=1}^{N=14} y_i \theta_i \end{cases} \tag{3.123}$$

Table 3.11 shows the computation of the Pe number and of the axial dispersion coefficient by the direct minimization of relations (3.122) and (3.106). It is easily observable that this table contains in fact a MathCAD transposition of the λ_1 , Pe and D_1 identification.

Table 3.11 MathCAD computation of Pe, λ_1 , D_1 parameters.

$$\theta_i = \begin{bmatrix} 0 \\ 0.2 \\ 0.4 \\ 0.5 \\ 0.6 \\ 0.8 \\ 1.0 \\ 1.2 \\ 1.4 \\ 1.6 \\ 1.8 \\ 2.0 \\ 2.2 \\ 2.4 \end{bmatrix} \quad \frac{c_i}{c_0} = \begin{bmatrix} 0 \\ 0 \\ 0 \\ 0 \\ 0.1 \\ 0.3 \\ 0.6 \\ 0.8 \\ 0.85 \\ 0.9 \\ 0.95 \\ 0.98 \\ 0.99 \\ 1.0 \end{bmatrix} = \frac{\text{Pe} := 1 \quad \lambda_1 := 19 \quad i := 5..14 \quad H := 0.16 \quad \tau_m = 6}{G}$$

$$\left[\sum_{i=5}^{14} \left[\frac{\lambda_1 \cdot \left(\tan \left(\frac{\lambda_1}{2} \right) \right)^2 - 1}{2 \cdot \tan \left(\frac{\lambda_1}{2} \right)} \theta_i + \ln \left[2 \frac{\sin(\lambda_1)}{\lambda_1 \left(\tan \left(\frac{\lambda_1}{2} \right) \right)^2 + \tan \left(\frac{\lambda_1}{2} \right) + \lambda_1} \right] - \ln \left(\frac{c_i}{c_0} \right) \right]^2 \right] \equiv 0$$

$$2\lambda_1 \tan \left(\frac{\lambda_1}{2} \right) \equiv \text{Pe} \quad \left(\frac{\lambda_1}{\text{Pe}} \right) := \text{Find}(\lambda_1, \text{Pe}) \quad \left(\frac{\lambda_1}{\text{Pe}} \right) = \begin{pmatrix} 19.48 \\ 12.7 \end{pmatrix}$$

$$D_1 = \frac{H^2}{\text{Pe}\tau_m} \quad D_1 = 2.953 \cdot 10^{-4} \text{ m}^2/\text{s}$$

3.3.6

Flow Modelling using Computational Fluid Dynamics

As has been shown at the beginning of this chapter, researchers have been expecting important progress on the modelling of flows in chemical reactors with the development of computational fluid dynamics (CFD). The principle of CFD is to integrate the flow equations for one particular case after dividing the flow volume into a very high number of differential elements. This volume-of-fluid technique can be used for the “*a priori*” determination of the morphology and characteristics of various kinds of flow.

Chemical engineers were not the pioneers in this field because chemical engineering flow problems can be very complex. Some of the first users of CFD were car, plane and boat designers. One of the reasons for this was that CFD could tell the designers exactly what they wanted to know, that is the flow patterns obtained while their new designs moved. Indeed, the possibility to use Euler’s equations for flow description has been one of the major contributions to the development of these applications. These kinds of CFD techniques have also been projected and have been successfully used to analyze heat flow from a body immersed into the flowing fluid [3.29, 3.30].

As far as chemical engineers are concerned, we must notice that there is a considerable academic and industrial interest in the use of CFD to model two-phase flows in process equipment. The problem of the single bubble rising in the fluid [3.31, 3.32] has been resolved using some simplification in the description of bubble–liquid momentum transfer. Considerable progress has been made in the CFD modelling of bubbling gas–fluidized beds and bubble columns. The CFD modelling of fluidized beds usually adopts the Eulerian framework for both dilute (bubble) and dense phases and makes use of the granular theory to calculate the rheological parameters of the dense phase [3.33–3.37].

The use of CFD models for gas–liquid bubble columns has also raised considerable interest; only Euler–Euler and Euler–Lagrange frameworks have been employed for the description of the gas and liquid phase states [3.38–3.42]. Bubble trays, considered as particular kinds of bubble columns, have lately presented enormous interest for the flow description by CFD. The flow patterns on a sieve tray have been analyzed in the liquid phase, solving the time-averaged equations of continuity and momentum [3.43].

The jump to the fully two-phase flow on a sieve tray requires the acceptance of some conditions [3.44]:

- the lift forces for the bubble must be neglected;
- the added mass forces do not have an important participation in the flow processes;
- the interphase momentum exchange must be expressed using the drag coefficient.

Then the simulation of real chemical engineering flows concerns a number of important difficulties beyond the pattern of turbulent flows. One of these complex problems concerns the description of viscosity; however, this can be resolved using rheological equations. Another difficulty is the so-called micromixing problem, which must be characterized at the level considering the integration of a very little unit.

In the case of one homogeneous reactor, where two reactants are continuously fed, mixed, reacted, and flushed out through an outlet, CFD can calculate the concentrations in each fluid element, just as it can calculate the temperature. Nevertheless, CFD cannot consider the reaction of both components as a function of the local mixing

Theoretically, CFD could quantify everything. It could predict the effect of adding reagents quickly or slowly. To achieve a specified yield, we would find out exactly how slow the addition has to be, how intense the mixing is, and what equipment would achieve that mixing. But to get a good prediction, as always, you need good input data. These data include the initial conditions, rate flows and kinetics of the reactions as well as the physical properties of the solutions. In order to get good inputs, of course, it is necessary to come back to laboratory activity.

3.4 Complex Models and Their Simulators

During a process modelling, the development of the model and the simulation of the process using a simulator, as shown in Section 2.2, represent two apparently indivisible operations. Both activities have rapidly evolved with time as a consequence of the development of basic technical sciences. Three main phases can be kept in mind with respect to this vigorous evolution:

In *the first phase*, the modelling and simulation of the apparatus was carried out considering each as independent units in the whole installation. Indeed, here, modelling was assisted by the efforts made in the high technological design of each of the specific apparatuses found in chemical plants. All types of models have been used for this purpose and the current huge computation capacities of universities and of research-design centres have sustained these scientific efforts. At present, the theoretical basis and algorithmic implementation of process modelling based on transport phenomena have been established. The general theory of computer programming has given the fundamentals of the development of easily usable means for the transposition of the models into process simulators and as guidelines for designers. Various utilitarian software languages have backed this new scientific branch and, among them, FORTRAN (FORmula TRANslation) can be considered as the most notorious. It is estimated that the full start of this phase began around 1968, when the series production of high power computers started.

The second phase began with the start of commercial activities in the modelling and simulation of processes. These commercial activities were born in the USA in 1980–1985 when the first simulators for oil distillation appeared. DistillR™, Maxstill™, and Hysim™ are some of these scientific software packages, which reach the level of the interactive simulation of a complex process model. During these years, modelling and simulation succeeded in automatically assembling the parts of a complex model according to the formal description of each part and their links. At the same time, an important data base began to be fed with the description of the different unitary operations of processes in terms of physical and chemical properties, consumption kinetics or appearance and equilibrium distribution at interphases.

The modelling tools in current commercial simulators may roughly be classified into two groups depending on their approach: block-oriented (or modular) and equation-oriented.

Block-oriented approaches mainly address the modelling at the level of flow-sheets. Every process is abstracted in a block diagram consisting of standardized blocks, which model the behaviour of a process unit or a part of it. All the blocks are linked by signal-like connections representing the flow of information, material and energy, employing standardized interface and stream formats. Models of process units are pre-coded by a modelling expert and incorporated into a model library for later use. The modelling at the level of the flow-sheet is either supported by a modelling or by a graphical language. In both cases, the end user selects

the models from the library, provides the model parameters and connects them to the plant model. However, the chemical engineering knowledge accumulated up to now, as well as the structure of the models, are easily accessible. Common exceptions include the models of physical properties, which can be selected in the literature independently from the process unit model.

Equation-oriented modelling tools support the implementation of the unit models and their incorporation into a model library by means of declarative modelling languages or by providing a set of subroutine templates. In this case, the tools for the modelling expert or for the end user are similar. Hence, modelling at the unit level requires a profound knowledge in such diverse areas as chemical engineering modelling and simulation, numerical mathematics, and computer science. The development of new process models is therefore often restricted to a small group of experts.

Figure 3.35 presents the page of a modern commercial simulator (Hysim™ 1995) where we can identify the different elements of the process specified in this block-oriented simulator.

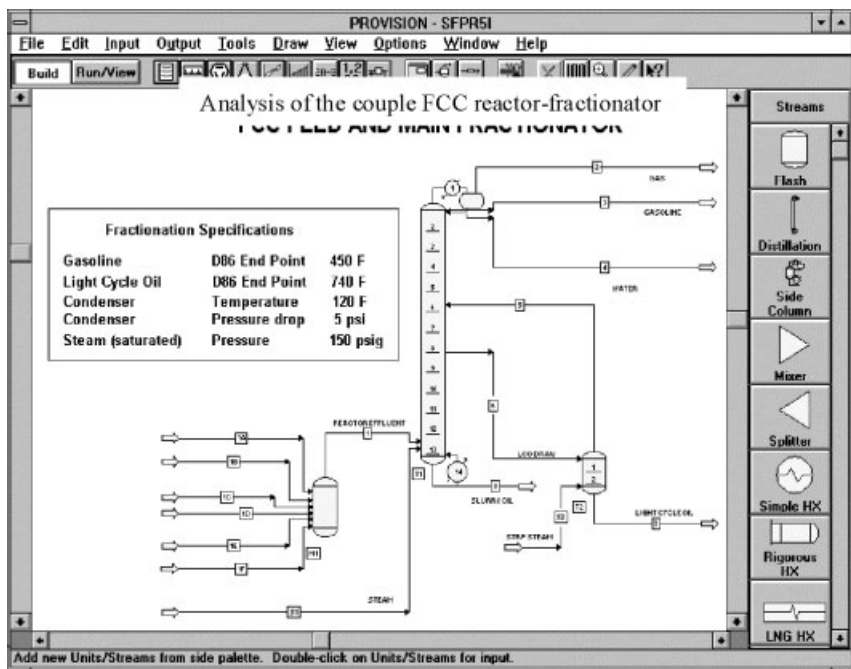


Figure 3.35 Presentation page of a block-oriented simulator for the analysis of a coupled FCC reactor-fractionator (Hysim™ 1995).

It is not difficult to observe that, in this example, we have the coupling of a specific reactor for petroleum fractionation together with a complex distillation column. If we intend to show the complexity of the process that will be simulated,

then it is important to say that more than 20 components can be found in the input of this installation in the reactor, separation column, condenser, reboiler and external flash device.

Despite the considerable progress made over the last decade, when steady-state flow-sheeting with modular process simulators became routinely employed by a large community of process engineers, there is considerable incentive to extend the range of model-based applications by improving the handling of models and by increasing the level of detail for representing the processes. Many studied cases of process engineering – not only in academia but especially in the research and development laboratories of the chemical industry – have shown the potential of employing non-standard models such as dynamic models, extremely detailed models of standard equipment, or models of non-standard equipment. The modular approach to modelling and simulation, though powerful and easily accessible to many engineers for the solution of standard flow-sheet problems, does not adequately support the solution of more complicated problems. This is largely due to the lack of pre-coded models for many unit operations at an adequate level of detail. In addition, most of the coded models neglect the mass or heat transfer, assuming the equilibrium state at interphases. Examples of models that are not available in present simulators, include multiphase reactors, membrane processes, polymerization reactors, biochemical reactors, hydrodynamic separators and the majority of units involving particulates. Therefore, costly and time-consuming model development for a particular unit is often required in some projects.

Equation-oriented languages largely contribute to the implementation of models, but they do not assist the user in developing the types of models that use engineering concepts. Indeed, equation-oriented languages are not useful in providing for the documentation of the modelling process during the lifecycle of a process or for the proper design and documentation of model libraries. In consequence, the reuse of previously validated models of a unit by a new group of users is then almost impossible.

The consistency and reliability of well designed model libraries is inevitably getting lost over time. Now, even though the market for these simulators is in full evolution, spectacular progress is not expected because the basic models of the units stay at mesoscale or macroscale.

Despite this last observation, for this type of simulation and modelling research, two main means of evolution remain: the first consists in enlarging the library with new and newly coded models for unit operations or apparatuses (such as the unit processes mentioned above: multiphase reactors, membrane processes, etc.); the second is specified by the sophistication of the models developed for the apparatus that characterizes the unit operations. With respect to this second means, we can develop a hierarchy dividing into three levels. The first level corresponds to connectionist models of equilibrium (frequently used in the past). The second level involves the models of transport phenomena with heat and mass transfer kinetics given by approximate solutions. And finally, in the third level, the real transport phenomena the flow, heat and mass transport are correctly described. In

this last case, oversimplifying hypotheses, such as non-resistive interfaces, are avoided

The *third phase* of the evolution for the modelling and simulation activities is represented by the current consumption of commercial software by scientific education. High level instruction languages such as MathCAD™, Matlab™, the CFD software, finite element softwares (for the integration of complex differential equation systems), high data volume graphic processors and softwares based on artificial intelligence represent some examples that show the important evolution of education and scientific research by modelling and simulation.

Considering the complexity and the diversity of the problems in chemical engineering research and design and taking into account the present evolution of modelling and simulation, we cannot claim that it will be possible to use universal chemical engineering simulators in the future.

The experimental researchers and the scientists that are only interested in in-depth modelling of physical phenomena are not attracted by complex simulators. The former seek models for data interpretation; the latter create models to propose solutions for a good knowledge of a concrete case. From other viewpoints, chemical engineering, because of its diversity, includes countless models. Most of them are quite interesting when they can add a lot more new situations based on particularization or modification to their starting cases. As far as the situations of this subject in chemical engineering are quite varied, it will be interesting to describe new modelling and simulation examples in the following sections. The examples shown below demonstrate firstly, how a model based on transport phenomena equations is developed and secondly, how we can extract important data for a process characterization by using a model simulation.

3.4.1

Problem of Heating in a Zone Refining Process

Among the methods of advanced purification of a crystallized or amorphous solid material, the zone refining methods occupy an important place. The principle of the method is based on the fact that an impurity from the processed material in a melting crystallization process, according to the distribution law, presents different concentrations in solid and liquid phases [3.45]. If the melting solid (liquid phase) is subjected to a movement along a stick, then the impurity will be concentrated in the position where the liquid phase is stopped. This process is also called refining. To make the solid melt and to move the melt, the solid is locally heated by means of a mobile heat inductor or a small mobile and cylindrical electrically heated oven. However, we can reach the same result by pulling the stick through a small heating source. From the heat transfer viewpoint, this example corresponds to a conductive non-steady state heating with an internal heating source (heat inductor) or with an external heating source (heating with an oven).

From the mathematical viewpoint, it is important to assume that a very rapid heat transfer occurs at the extremities of the stick, and that a rapid cooling system is activated when the heating source is stopped. In addition, as far as we only take

into account the melted region, we do not consider the coupling with the liquid–solid phase change.

Figure 3.36 shows the heating principle of the zone refining purification procedure and also introduces the geometric and material conditions that characterize the process. It also shows how the stick transfers heat to the contiguous medium. For a correct introduction to this problem, we assume that the production of heat by the inductor has Gaussian behaviour, so, for the heat generation rate, we can write Eq. (3.124) where the source amplitude (watt/m³) is A , $f(\tau)$ is a dimensionless function that keeps the maximum temperature for the inductor constant and k_1 and k_2 are the constants with L^{-1} dimension:

$$Q_g = Af(\tau)\exp\left(-\left(k_1(z - k_2w\tau)^2\right)\right) \quad (3.124)$$

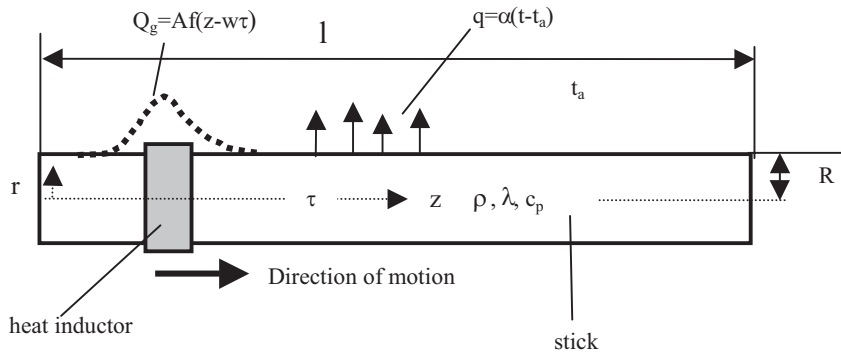


Figure 3.36 Heating scheme for a solid stick purified by a zone refining process.

From Fig. 3.36 we observe that the stick is characterized by its density ρ , thermal conductivity λ and sensible heating capacity c_p . The geometric dimensions of the stick are radius R and length l . The temperature distribution inside the stick results from relation (3.125) as a particularization of Eq. (3.6):

$$\rho c_p \frac{\partial t}{\partial \tau} = \lambda \left(\frac{\partial^2 t}{\partial r^2} + \frac{1}{r} \frac{\partial t}{\partial r} + \frac{\partial^2 t}{\partial z^2} \right) + Q_g \quad (3.125)$$

The univocity conditions that complete this general mathematical model can be written as follows:

- the initial distribution of the temperature into the stick:

$$\tau = 0 \quad -R \leq r \leq R \quad t = t_a \quad (3.126)$$

- the boundary thermal flux expression (type III conditions from the general class of boundary conditions):

$$\tau > 0 \quad r = -R \quad r = R \quad 0 < z \leq l. \quad -\lambda \frac{\partial t}{\partial r} = q = \alpha(t - t_a) \quad (3.127)$$

- the expression that gives the behaviour of the device of heat absorption placed at the stick extremity:

$$\tau > 0 \quad z = l \quad -\lambda \frac{\partial t}{\partial z} = k_{ab}(t_{ab} - t_{rab}) \quad (3.128)$$

For a correct perception of relation (3.128), we must notice that this is a heat sink that keeps its constant temperature due to a rapid heat exchange between the surface with a cooling medium maintained at constant (t_{rab}) temperature. The assembly of relations (3.124)–(3.126) represents in fact an abstract mathematical model for the above described heating case because the numerical value is given neither for the system geometry nor for the material properties. Apart from the temperature, all the other variables of the model can be transformed into a dimensionless form introducing the following dimensionless coordinates:

- the dimensionless time $T = \frac{\lambda \tau}{\rho c_p l^2}$ sometimes called Fourier number;
- the dimensionless radius coordinate $X = r/R$;
- the dimensionless axial coordinate $Z = z/l$;

With these transformations, the abstract model can now be described by assembling the following relations (3.129)–(3.133):

$$Q_g = Af \left(\frac{T \rho c_p R^2}{\lambda} \right) \exp \left(-k_1 Z * l - k_2 w \frac{T \rho c_p R^2}{\lambda} \right)^2 \quad (3.129)$$

$$T > 0 \quad X = -1 \quad X = 1 \quad 0 < Z \leq 1 \quad -\frac{\lambda}{R} \frac{\partial t}{\partial X} = q = \alpha(t - t_a) \quad (3.130)$$

$$T > 0 \quad Z = 1 \quad -\frac{\lambda}{l} \frac{\partial t}{\partial Z} = k_{ab}(t_{ab} - t_{rab}) \quad (3.131)$$

$$T > 0 \quad X = -1 \quad X = 1 \quad 0 < Z \leq 1 \quad -\frac{\lambda}{R} \frac{\partial t}{\partial X} = q = \alpha(t - t_a) \quad (3.132)$$

$$T > 0 \quad Z = 1 \quad -\frac{\lambda}{l} \frac{\partial t}{\partial Z} = k_{ab}(t_{ab} - t_{rab}) \quad (3.133)$$

Then, the heating model of the stick can simply be transposed by an adequate software for process simulation. Indeed, some conditions have to be chosen: the material properties (λ , ρ , c_p); the dimensionless stick geometry; the parameters of the heating source (A , k_1 , k_2 , w) and the external heat transfer parameter (α). The FlexPDE/2000™ simulator (PDE Solutions Inc. USA) based on the finite element method for integration of partial differential equations or systems has been used for the development of the simulation program. The simulator can give the results in various graphic forms. The source text of the program used to solve this model (Fig. 3.37) shows a very attractive macro language.

```

Title Heating in the zone refining
Coordinates: cylinder('Z','X')
select
cubic { Use Cubic Basis }
variables temp(range=0,1800)
definitions  $\lambda = 0.85$  {thermal conductivity}  $c_p = 1$  {heat capacity} long = 18
radius=1
 $\alpha = 0.4$  {free convection boundary coupling} Ta = 25 {ambient temperature}
A = 4500 {amplitude}
source = A*exp(-((z-1*t)/.5)**2)*(200/(t+199))
initial value
temp = Ta
equations
div( $\lambda$  *grad(temp)) + source =  $c_p$  *dt(temp)
boundaries region 1 start(0,0)
natural(temp) = 0 line to (long,0)
value(temp) = Ta line to (long,1)
natural(temp) = -  $\alpha$  *(temp - Ta) line to (0,1)
value(temp) = Ta line to finish
feature
start(0.01*long,0) line to (0.01*long,1)

time -0.5 to 19 by 0.01
monitors
for t = -0.5 by 0.5 to (long + 1)
elevation(temp) from (0,1) to (long,1) range=(0,1800) as "Surface Temp"
contour(temp)
plots
for t = -0.5 by 0.5 to (long + 1)
elevation(temp) from (0,0) to (long,0) range=(0,1800) as "Axis Temp"
histories
history(temp) at (0,0) (4,0) (8,0) (12,0) (16,0) (18,0)
end

```

Figure 3.37 FlexPDE™ text for the example 3.4.1.

The first simulations present the heating dynamics along the stick, i.e. the evolution of temperature with time for two points positioned at $X = 1$ (surface of the stick) and $X = 0$ (stick centre). If we note the temperature range from Figs. 3.38–3.41 as well as the values of the material properties we see that the simulated heating case corresponds to the zone refining of a material with a very high melting point such as an inorganic material (silicium). Figure 3.38, presents the time motion of the heating front along the stick. It is easy to observe how the temperature increases in each point of the stick due to heating. After the passage of the heating inductor along the stick, the temperature rapidly decreases due to the axial and radial heat transport. This local heating dynamics (heating followed by a good cooling resulting from a high temperature difference) can also be observed at the stick extremities. Consequently, all the temperature curves present an important elongation to the right part where the heat sink at constant temperature

t_a is placed, at the end of the stick. At the same time, Fig. 3.38 shows the importance of the heat flowing in the radial direction, from the centre to the external medium. Using Figs. 3.39 and 3.40, we can compute the radial and the axial temperature gradient with the time values from Fig. 3.38. For example for $T = 5$ and $l/R = 10$ (middle of the stick) the radial temperature gradient is $dt/dX = 330 \text{ drg/ul}$ ($ul = \text{units of length}$); this value is larger than the axial temperature gradient that, in this case, is $dt/dZ = 199 \text{ drg/ul}$.

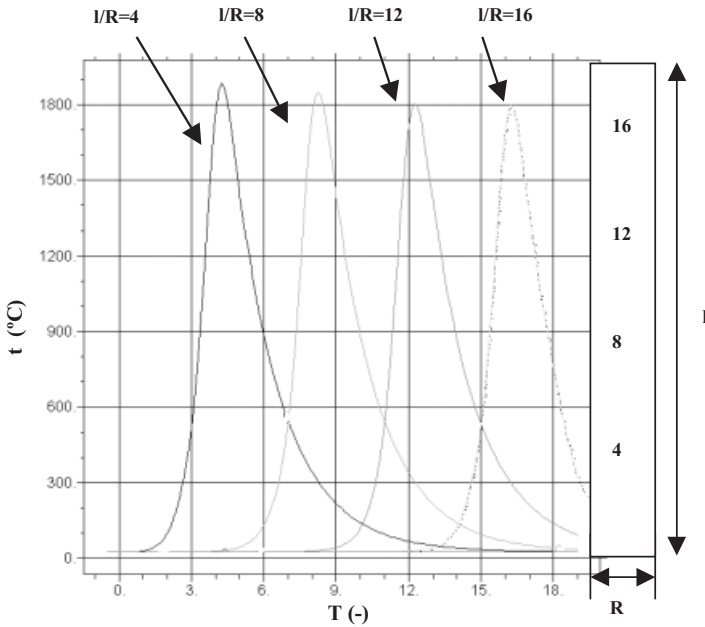


Figure 3.38 Evolution of the temperature for some points along the heated stick.

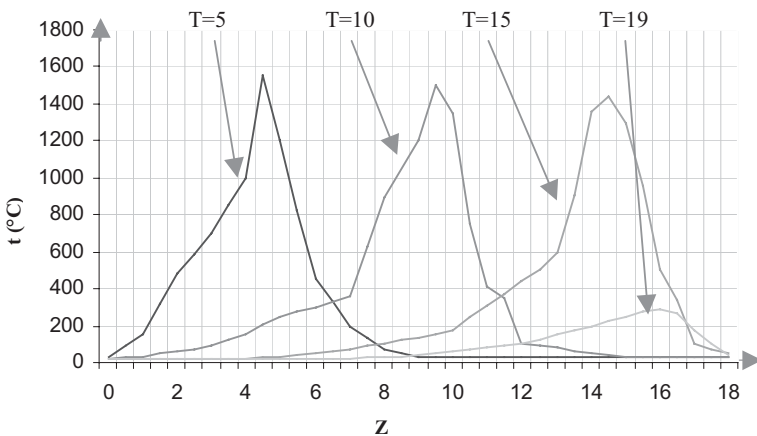


Figure 3.39 Evolution of the temperature of the surface of the stick along its length for various dimensionless times.

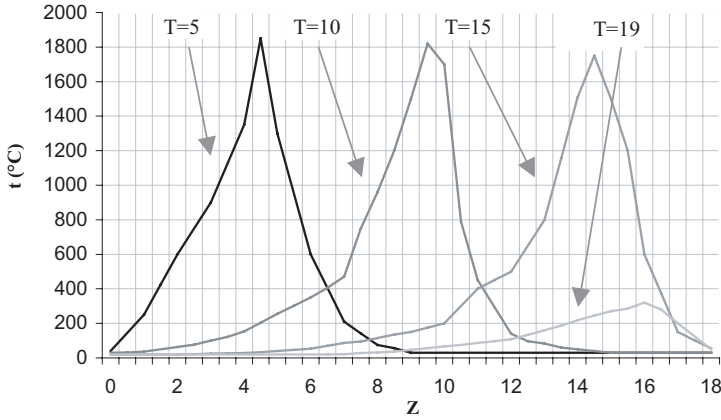


Figure 3.40 Evolution of the temperature at the centre of the stick and along its length and for various dimensionless times.

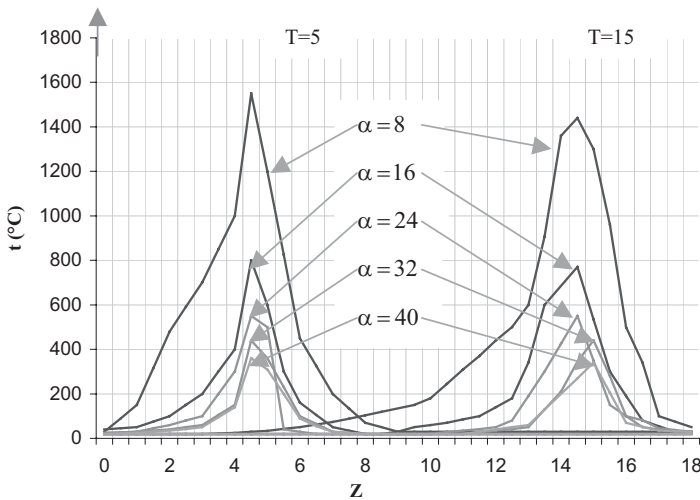


Figure 3.41 Effect of the external flow on the stick heat flow.

With respect to the data contained in Figs. 3.38–3.41, we can rapidly make a conversion to a concrete situation. For example for a stick with $\lambda = 2$ watt/(m deg), $\rho = 3000$ kg/m³, $c_p = 2000$ j/(kg deg) and with a radius $R = 0.01$ m, the dimensionless time $T = 5$ corresponds to a real time $\tau = 1500$ s. If the stick is 100 cm long, then, with an inductor motion speed of 10 dimensionless units for 1500 s (see the distances between the maximums of the temperature in Figs. 3.38–3.40) we obtain a value of 15000 s for the time corresponding to the motion of the inductor along the stick. This shows that the zone refining purification is not an efficient

method as far as time is concerned. Before closing these observations concerning heating with an inductor, we show that, in this case, the radial heat flow is permanently oriented from the stick to the adjacent medium. On the contrary, for the case of an electric oven heating, the direction of the heat flow is from the outside to the inside in the region of the stick covered by the oven.

The second simulation has been oriented to show the effect of an external flow around the stick on the thermal dynamics. It is known that the external flow around an entity, where a transport property is occurring, has a direct action on the coefficient of transfer of the property which characterizes the passing through the interface [3.3, 3.4, 3.45, 3.46]. The data obtained with the simulator when we change the values of the heat transfer coefficient from the stick to the external medium allows a quantitative estimation of the effect of this parameter. For this simulation, the temperature of the surface of the stick is considered as a dependent variable of the process. The heat source, the heat transfer coefficient α for the external fluid flow around the stick, the material properties and the stick geometry represent the independent variables of the process. Figure 3.41 shows the evolution of the stick heat flow for two values of the dimensionless time: $T = 5$ and $T = 15$. A spectacular reduction of the temperature of the stick surface occurs when the external flow becomes higher and the value of the heat transfer increases from $\alpha = 8 \text{ w}/(\text{m}^2\text{drg})$ to $\alpha = 40 \text{ w}/(\text{m}^2\text{drg})$. This phenomenon shows that an easy control of the stick-cooling rate is possible with the variation of α . Indeed, this fact can be very important for an actual process [3.45].

The third simulation example concerns the descriptive model of the cooling process of a hot stick that is maintained in a large volume of air. In the initial stages of the process, one of the stick's ends is maintained at high temperature for sufficient time for it to reach a steady state. The distribution of the temperature along the stick can then be calculated by relation (3.134). In a second step, the stick is placed in air and an unsteady cooling process starts. Concerning relation (3.134), we can notice that t_0 is the temperature of the heated end of the stick, and that all the other parameters have already been defined by the equations described above at the beginning of this section.

$$t = t_a + (t_0 - t_a) \exp\left(-\sqrt{\frac{2\alpha}{\lambda R}} z\right) \quad (3.134)$$

In this case, the simulator's text given in Fig. 3.37 has been modified, first considering $A = 0$, this statement is equivalent to the elimination of the source, and secondly by choosing the relation (3.134) as the initial value of the variable of the program named **temp**. The simulation results given in Figs. 3.42 and 3.43, show that a rapid cooling of the stick takes place, this phenomenon is mainly caused by the external conditions.

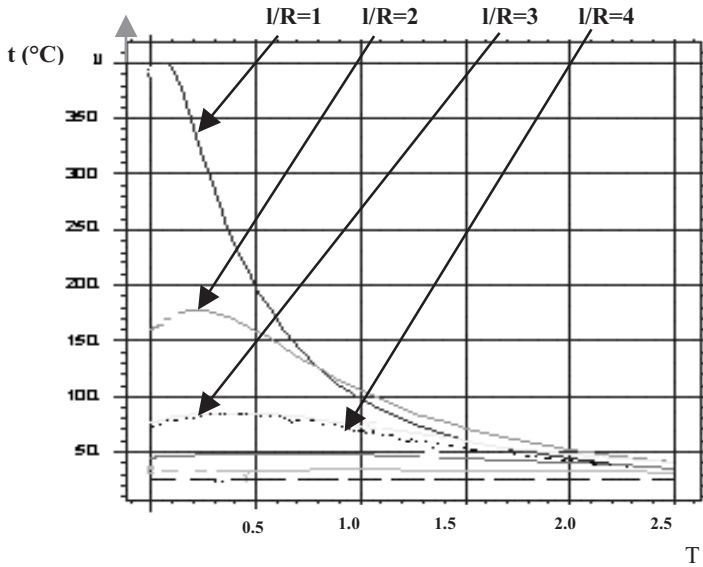


Figure 3.42 Cooling dynamics of the stick for high t_0 and small heat transfer coefficient ($\alpha = 8 \text{ w}/(\text{m}^2\text{drg})$).

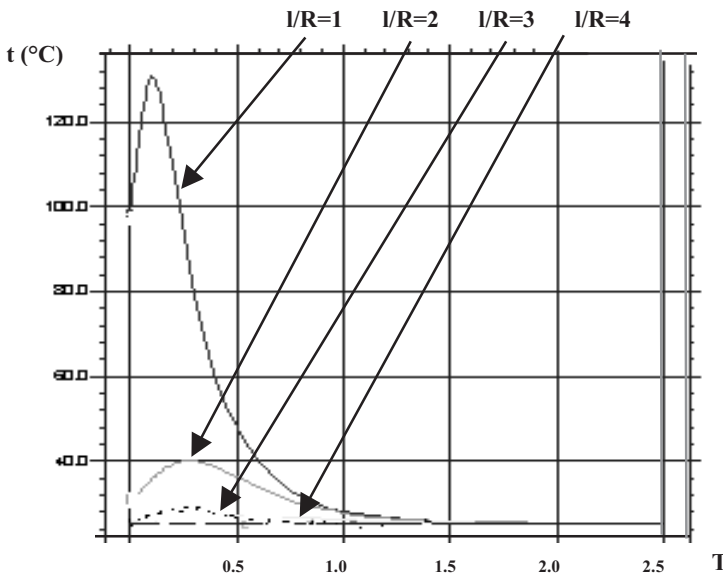


Figure 3.43 Cooling dynamics of the stick for slow t_0 and high heat transfer coefficient ($\alpha = 32 \text{ w}/(\text{m}^2\text{drg})$).

The zone refining process is extremely efficient for separating liquid or solid mixtures. In the old days, it was essentially applied in purifying germanium to be used in transistors. In multi-pass zone refining processes, the purification is carried out by slowly moving a series of closely spaced heaters along a relatively long solid ingot as shown in Fig. 3.36 or by restarting the heater movement when it reaches the end of the stick. The multi-pass zone refining process allows time saving because the following crystallization begins before the preceding one is completed. Many useful purifying operations can be carried out if the number and the size of the zones are properly selected. The distribution of impurities along an ingot depends on the value of the distribution coefficient, on the length of the molten zone, and on how many times the heaters move along the stick. Zone refining with a variable zone length is a topical scientific subject.

3.4.2

Heat Transfer in a Composite Medium

The description of heat transfer through a composite material can be a rather complicated task because this composite solid medium can contain various solids which are not uniformly dispersed and which have different thermal conductivity and sensible specific heat. Indeed, if we have a discrete setting of various solids in the total solid, the problems of heat transport become very complex when the number of solids and the number of agglomerations increase. These cases of totally or partly disordered composite media are not dealt with in this section. In an ordered solid composite medium, the heat can be generated or accumulated, captured or eliminated at the boundaries by a molecular-like mechanism. When the carriers pass from one zone of the solid to another, they change the frequency of discrete motion and the pathway length of each individual species because of the local properties. The heating or cooling problems of a block composed of two or more bricks (parallelepiped or other form) that exchanges energy with the adjacent medium represent the concrete case considered here. In the first modeling problem, we consider the case of a block of four bricks with different thermal conductivity, sensible specific heat and density. It is heated by a source with a Gaussian heat flow placed at the centre of the group of bricks. The group exchanges heat with the external medium at the upper and lower surface. At the surface level, the external medium is considered to be perfectly mixed and indeed, without any transfer resistance. No heat flow leaves the other block surfaces because they are completely isolated. The upper and lower contact surfaces of the bricks do not introduce any additional heat transfer resistance, so here the instantaneous heat flux equality is *a priori* accepted. The study of this model is attractive because: (i) the descriptive model given here can be explained by an interesting mathematical model; (ii) no significant problems are encountered if we carry out support modifications in order to find other important heat transfer cases; (iii) by analogy, we can obtain the data with respect to the characterization of some mass transfer cases occurring in a similar way.

For the general mathematical model construction, we consider the system of coordinates, the geometrical dimensions, the material properties and the initial temperature distribution for the block. Figure 3.44 gives a graphical introduction to the descriptive process model. We can now proceed with the particularization of the transport phenomena equations. Indeed, the concrete general mathematical process model contains:

- the partial differential equation that gives the temperature distribution in the solid block:

$$\rho c_p \frac{\partial t}{\partial \tau} = \lambda \left(\frac{\partial^2 t}{\partial x^2} + \frac{\partial^2 t}{\partial y^2} + \frac{\partial^2 t}{\partial z^2} \right) + Q_g \quad (3.135)$$

- the geometric and material conditions:

on the right region:

$$0 < x < l, \quad -L < z < 0, \quad -\frac{h}{2} < y < \frac{h}{2}, \quad \lambda = \lambda_1, \quad c_p = c_{p1}, \quad \rho = \rho_1 \quad (3.136)$$

$$0 < x < l, \quad 0 < z < L, \quad -\frac{h}{2} < y < \frac{h}{2}, \quad \lambda = \lambda_2, \quad c_p = c_{p2}, \quad \rho = \rho_2 \quad (3.137)$$

on the left region:

$$-l < x < 0, \quad -L < z < 0, \quad -\frac{h}{2} < y < \frac{h}{2}, \quad \lambda = \lambda_3, \quad c_p = c_{p3}, \quad \rho = \rho_3 \quad (3.138)$$

$$0 < x < l, \quad 0 < z < L, \quad -\frac{h}{2} < y < \frac{h}{2}, \quad \lambda = \lambda_4, \quad c_p = c_{p4}, \quad \rho = \rho_4 \quad (3.139)$$

- boundary conditions:

at the top surface:

$$\tau > 0, \quad z = L, \quad -l \leq x \leq l, \quad -\frac{h}{2} \leq y \leq \frac{h}{2}, \quad t = t_a \quad (3.140)$$

at the bottom surface:

$$\tau > 0, \quad z = -L, \quad -l \leq x \leq l, \quad -\frac{h}{2} \leq y \leq \frac{h}{2}, \quad t = t_a \quad (3.141)$$

for other surfaces:

$$\tau > 0, \quad x = l, \quad -\frac{h}{2} \leq y \leq \frac{h}{2}, \quad -L \leq z \leq L, \quad \frac{dt}{dx} = 0 \quad (3.142)$$

$$\tau > 0, \quad y = -\frac{h}{2}, \quad -l \leq x \leq l, \quad -L \leq z \leq L, \quad \frac{dt}{dy} = 0 \quad (3.143)$$

$$\tau > 0, \quad x = -1, \quad -\frac{h}{2} \leq y \leq \frac{h}{2}, \quad -L \leq z \leq L, \quad \frac{dt}{dx} = 0 \quad (3.144)$$

$$\tau > 0, \quad y = \frac{h}{2}, \quad -1 \leq x \leq 1, \quad -L \leq z \leq L, \quad \frac{dt}{dy} = 0 \quad (3.145)$$

- the heat flux continuity at the walls that separate the bricks:

$$\tau > 0, \quad x = 0, \quad -\frac{h}{2} \leq y \leq \frac{h}{2}, \quad -L \leq z \leq 0, \quad \lambda_1 \left(\frac{dt}{dx} \right)_{x=0+} = \lambda_3 \left(\frac{dt}{dx} \right)_{x=0-} \quad (3.146)$$

$$\tau > 0, \quad x = 0, \quad -\frac{h}{2} \leq y \leq \frac{h}{2}, \quad 0 \leq z \leq L, \quad \lambda_2 \left(\frac{dt}{dx} \right)_{x=0+} = \lambda_4 \left(\frac{dt}{dx} \right)_{x=0-} \quad (3.147)$$

$$\tau > 0, \quad z = 0, \quad 0 \leq x \leq 1, \quad -\frac{h}{2} \leq y \leq \frac{h}{2}, \quad \lambda_2 \left(\frac{dt}{dz} \right)_{z=0+} = \lambda_1 \left(\frac{dt}{dz} \right)_{z=0-} \quad (3.148)$$

$$\tau > 0, \quad z = 0, \quad -1 \leq x \leq 0, \quad -\frac{h}{2} \leq y \leq \frac{h}{2}, \quad \lambda_4 \left(\frac{dt}{dz} \right)_{z=0+} = \lambda_3 \left(\frac{dt}{dz} \right)_{z=0-} \quad (3.149)$$

- temperature conditions to start the heating (initial conditions of the problem):

$$\tau = 0, \quad -1 \leq x \leq 1, \quad -\frac{h}{2} \leq y \leq \frac{h}{2}, \quad -L \leq z \leq L, \quad t = t_a \quad (3.150)$$

- the relation that characterizes the local value of the rate of heat production (it is the case of a small power source as, for example, a small electrical heater placed in the centre of the block):

$$Q_g = A \exp(-k(x^2 + y^2 + z^2)) \quad (3.151)$$

Now we can transform the model relations into dimensionless forms. For this purpose, we use the dimensionless temperature as a measure of a local excess with respect to the adjacent medium $T_p = (t - t_a)/t_a$; the dimensionless time recognized as the Fourier number $\Gamma = \frac{\lambda_1 \tau}{\rho_1 c_{p1} l^2}$; the dimensionless geometric coordinates given by $X = x/l$, $Y = y/h$, $Z = z/L$ or as $X = x/l$, $Y = y/l$, $Z = z/l$. Table 3.12 contains the dimensionless state of the mathematical model of the process.

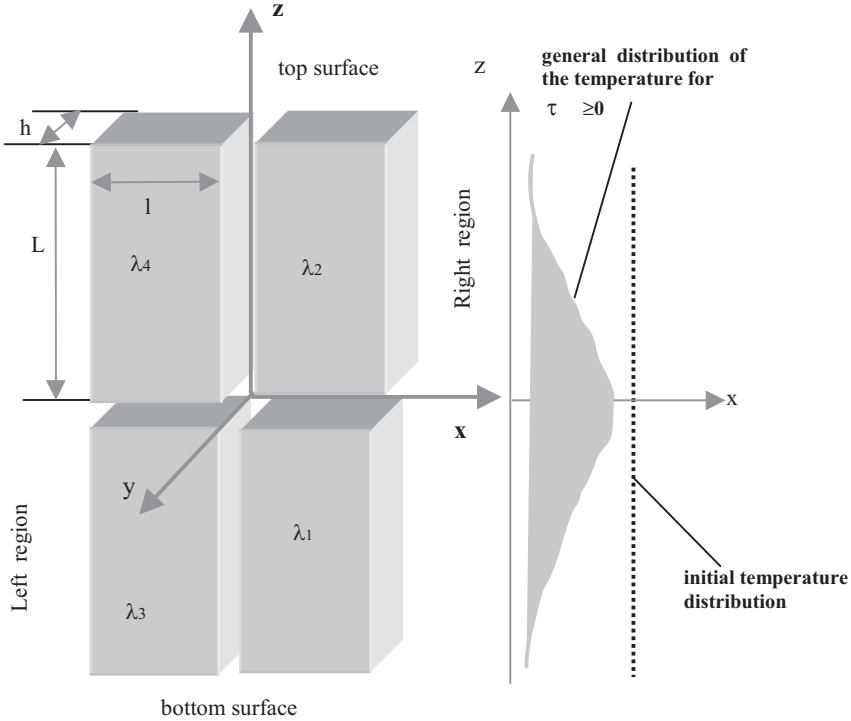


Figure 3.44 Description of the example of heating of four bricks.

Table 3.12 Dimensionless mathematical models for the case of the heating of a block of four bricks.

$$\frac{\partial T_p}{\partial \tau} = \left(\frac{\partial^2 T_p}{\partial X^2} + \frac{l^2}{h^2} \frac{\partial^2 T_p}{\partial Y^2} + \frac{l^2}{L^2} \frac{\partial^2 T_p}{\partial Z^2} \right) + Q_g'; \quad Q_g' = \frac{Q_g(4Llh)^{2/3}}{X_1 t a} \quad (3.135)$$

Materials conditions:

$$0 < X < 1, \quad -1 < Z < 0, \quad -\frac{1}{2} < Y < \frac{1}{2}, \quad \lambda = \lambda_1, \quad c_p = c_{p1}, \quad \rho = \rho_1 \quad (3.136)$$

$$0 < X < 1, \quad 0 < Z < 1, \quad -\frac{1}{2} < Y < \frac{1}{2}, \quad \lambda = \lambda_2, \quad c_p = c_{p2}, \quad \rho = \rho_2 \quad (3.137)$$

$$-1 < X < 0, \quad -1 < Z < 0, \quad -\frac{1}{2} < Y < \frac{1}{2}, \quad \lambda = \lambda_3, \quad c_p = c_{p3}, \quad \rho = \rho_3 \quad (3.138)$$

$$0 < X < 1, \quad 0 < Z < 1, \quad -\frac{1}{2} < Y < \frac{1}{2}, \quad \lambda = \lambda_4, \quad c_p = c_{p4}, \quad \rho = \rho_4 \quad (3.139)$$

Boundary conditions:

$$T > 0, \quad Z = 1, \quad -1 \leq X \leq 1, \quad -\frac{1}{2} \leq Y \leq \frac{1}{2}, \quad T_p = 0 \quad (3.140)$$

$$T > 0, \quad Z = -1, \quad -1 \leq X \leq 1, \quad -\frac{1}{2} \leq Y \leq \frac{1}{2}, \quad T_p = 0 \quad (3.141)$$

$$T > 0, \quad X = 1, \quad -\frac{1}{2} \leq Y \leq \frac{1}{2}, \quad -1 \leq Z \leq 1, \quad \frac{dT_p}{dX} = 0 \quad (3.142)$$

$$T > 0, \quad Y = -\frac{1}{2}, \quad -1 \leq X \leq 1, \quad -1 \leq Z \leq 1, \quad \frac{dT_p}{dY} = 0 \quad (3.143)$$

$$T > 0, \quad X = -1, \quad -\frac{1}{2} \leq Y \leq \frac{1}{2}, \quad -1 \leq Z \leq 1, \quad \frac{dT_p}{dX} = 0 \quad (3.144)$$

$$T > 0, \quad Y = \frac{1}{2}, \quad -1 \leq X \leq 1, \quad -1 \leq Z \leq 1, \quad \frac{dT_p}{dY} = 0 \quad (3.145)$$

$$T > 0, \quad X = 0, \quad -\frac{1}{2} \leq Y \leq \frac{1}{2}, \quad -1 \leq Z \leq 0, \quad \lambda_1 \left(\frac{dT_p}{dX} \right)_{x=0+} = \lambda_3 \left(\frac{dT_p}{dX} \right)_{x=0-} \quad (3.146)$$

$$T > 0, \quad X = 0, \quad -\frac{1}{2} \leq Y \leq \frac{1}{2}, \quad 0 \leq Z \leq 1, \quad \lambda_2 \left(\frac{dT_p}{dX} \right)_{x=0+} = \lambda_4 \left(\frac{dT_p}{dX} \right)_{x=0-} \quad (3.147)$$

$$T > 0, \quad Z = 0, \quad 0 \leq x \leq 1, \quad -\frac{1}{2} \leq Y \leq \frac{1}{2}, \quad \lambda_2 \left(\frac{dT_p}{dZ} \right)_{z=0+} = \lambda_1 \left(\frac{dT_p}{dZ} \right)_{z=0-} \quad (3.148)$$

$$T > 0, \quad Z = 0, \quad -1 \leq X \leq 0, \quad -\frac{1}{2} \leq Y \leq \frac{1}{2}, \quad \lambda_4 \left(\frac{dT_p}{dZ} \right)_{z=0+} = \lambda_3 \left(\frac{dT_p}{dZ} \right)_{z=0-} \quad (3.149)$$

$$T = 0, \quad -1 \leq X \leq 1, \quad -\frac{1}{2} \leq Y \leq \frac{1}{2}, \quad -1 \leq Z \leq 1, \quad T_p = 0 \quad (3.150)$$

$$Q_g = A \exp(-k(l^2X^2 + h^2Y^2 + L^2Z^2)) \quad (3.151)$$

In *the first simulation*, we consider a particular case of the heating dynamics of the four blocks when the heat is produced by a source at the centre of the blocks. In this example, we have different thermal conductivities for the material of each block. Figure 3.45 shows the simulation of a parallelepiped brick with its corresponding dimensionless length and width. The only difference between the dimensionless model shown in Table 3.12 and the model used in the simulator (Fig. 3.45) is the use of a partly dimensionless model in the simulator text. To show the complex dynamics of the temperature observed in Fig. 3.45, seven displaying points have been selected. These are: A – bottom right brick: A(1/2, -h/2, -L/2); B – bottom right brick: B(1/2, h/2, -L/2); C – bottom left brick: C(-1/2, h/2, -L/2); D – bottom left brick: D(-1/2, -h/2, -L/2); E – top right brick: E(1/2, -h/2, L/2); F – top right brick : F(1/2, h/2, L/2); G – top left brick: G(-1/2, h/2, L/2); H – centre of block: H(0, 0, 0).

```

title 'Simulator for the heating of a block of four bricks
select regrid=off { use fixed grid } ngrid=5
coordinates cartesian3
variables Tp
definitions long = 1 wide = 1  λ,cp,ρ      { - values supplied later }
              Q = 3.8*107*exp(-x2-y2-z2)      { Thermal source }
initial values Tp = 0.
equations
  div[λ *grad(Tp)] + Q = (ρcp) dt(Tp)      { the heat transport equation }
  extrusion z = -long,0,long      { divide Z into two layers }
boundaries
surface 1 value(Tp)=0 { bottom surface temp } surface 3 value(Tp)=0 { top surface temp }
Region 1      { define full domain boundary in base plane }
layer 1 λ=1  cp=2000 ρ=2000  { bottom right brick } layer 2  λ =0.1
cp=1800  ρ=1800  { top right brick }
  start(-wide,-wide)
  value(Tp) = 0      { fix all side temps }
  line to (wide,-wide) { walk outer boundary in base plane }
  to (wide,wide)
  to (-wide,wide)    to finish
Region 2      { overlay a second region in left half }
layer 1 λ=0.2  cp=1500 ρ=1200  { bottom left brick } layer 2  λ =0.4
cp=.1500  ρ=1500  { top left brick }
  start(-wide,-wide)
  line to (0,-wide)      { walk left half boundary in base plane }
  to (0,wide)
  to (-wide,wide)      to finish
time 0 to 3 by 0.01      { establish time range and initial time steep }
plots
  for t = endtime contour(Tp) on surface z=0 as "XY Temp" range=(0,6)
;contour(Tp) on surface x=0 as "YZ Temp" range=(0,6) ;contour(Tp) on surface y=0
as "XZ Temp" range=(0,6)
histories
  history(Tp) at (wide/2,-wide/2,-long/2) ;(wide/2,wide/2,-long/2) ; (-wide/2,wide/2,-
long/2) ; (-wide/2,-wide/2,-long/2) ; (wide/2,-wide/2,long/2);
(wide/2,wide/2,long/2) ; (-wide/2,wide/2,long/2) ; (0,0,0)      range=(0,6)
end

```

Figure 3.45 FlexPDE working text of the simulator for the heating of a block of four bricks.

Figure 3.46 presents the temperature distribution in the plane $y = 0$, which separates the left parts from the right parts of the bricks' assembly. The shape of the group of the isothermal curves shows a displacement towards the brick with the higher thermal conductivity. Using the values obtained from these isothermal curves, it is not difficult to establish that the exit heat flux for each brick from the bottom of the assembly (plane $Z = -1$) and for the top of the assembly (plane $Z = 1$) depends on its thermal conductivity and on the distribution of the isothermal curves. If we compare this figure to Fig. 3.47 we can observe that the data contained in Fig. 3.46 correspond to the situation of a steady state heat transfer.

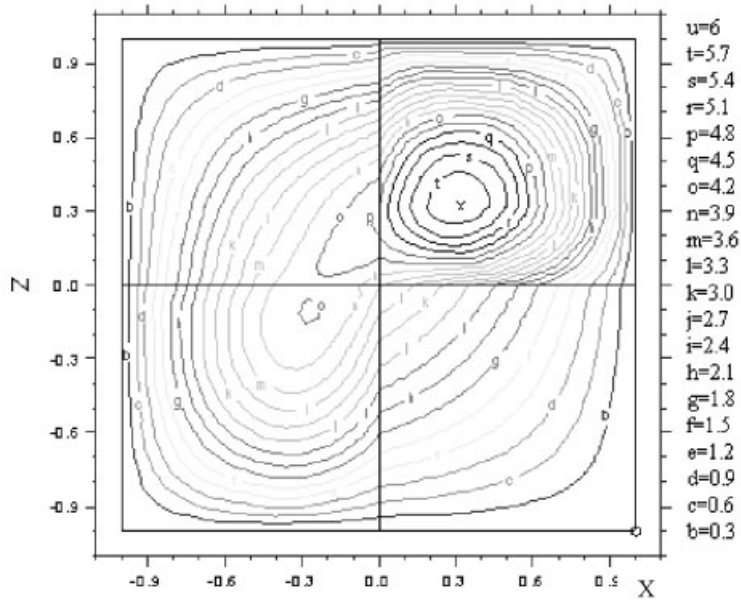


Figure 3.46 Temperature distribution at $T = 3$ for plane $y = 0$.

Figure 3.47 shows the evolution of the heating process of the composite block and how it attains a complex steady state structure with the surface zones covered by complicated isothermal curves (see also Fig. 3.46). Secondly, this figure shows how the brick with the higher thermal conductivity is at steady state and remains the hottest during the dynamic evolution. As explained above, this fact is also shown in Fig. 3.46 where all high isothermal curves are placed in the area of the brick with highest thermal conductivity. At the same time an interesting vicinity effect appears because we observe that the brick with the smallest conductivity does not present the lowest temperature in the centre (case of curve G compared with curves A and B). The comparison of curves A and B, where we have $\lambda = 0.2$, with curves C and D, where $\lambda = 0.4$, also sustains the observation of the existence of a vicinity effect. In Fig. 3.48, we can also observe the effect of the highest thermal conductivity of one block but not the vicinity effect previously revealed by Figs. 3.46 and 3.47. If we compare the curves of Fig. 3.47 with the curves of Fig. 3.48 we can appreciate that a rapid process evolution takes place between $T = 0$ and $T = 1$. Indeed, the heat transfer process starts very quickly but its evolution from a dynamic process to steady state is relatively slow.

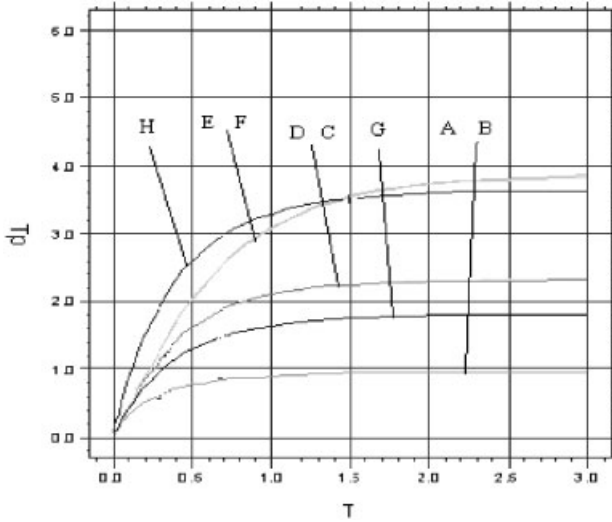


Figure 3.47 Temperature evolution inside the bricks that compose the heated block.

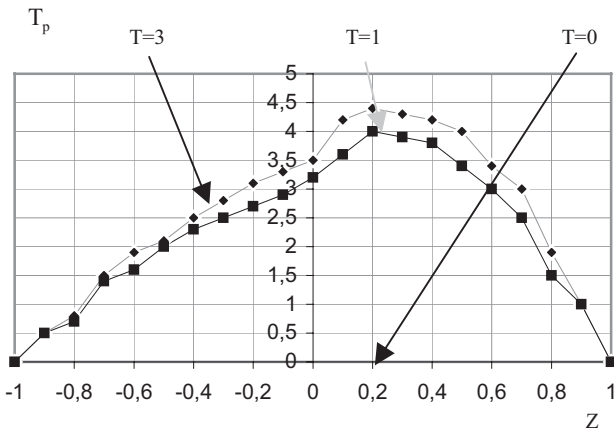


Figure 3.48 Temperature distribution along the Z axis for various dimensionless times.

The second simulation has been oriented to the analysis of the cooling process of the composite block. So, for the initial time, we have a block of four bricks heated to a constant temperature. All surfaces of the blocks except for $Z = -1$ and $Z = 1$, are isolated before placing the assembly of blocks in a cooling medium. We assume that we can use the boundary conditions of type I. To make the simulator respond to this new model with the written text shown in Fig. 3.45, we erase the generated heat ($Q = 0$) and we adequately change the initial temperature conditions. The examples given by Figs. 3.49–3.51 consider that the cooling of the com-

posite block begins when the dimensionless temperature is $T_p = 6$. Figure 3.49 shows that each brick presents its proper thermal dynamics. We can notice that the vicinity effects are similar to those already discussed in the previous example. However, here the cooling rate of each brick does not occur in accordance with the thermal conductivity but with the thermal diffusivity.

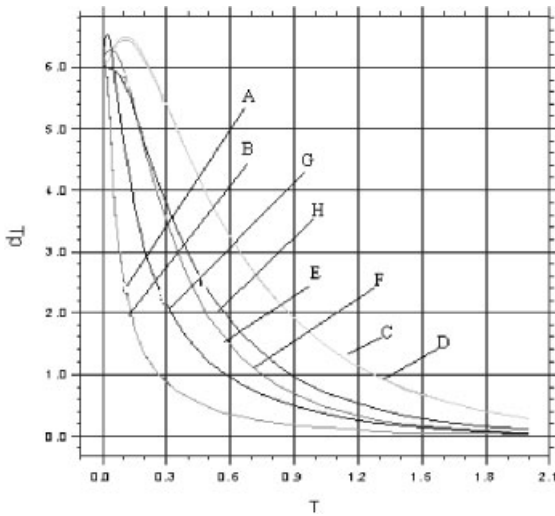


Figure 3.49 Cooling dynamics of a brick assembly for $L/l = 1$ and $V_a = 8.1^3$.

The curves E and F that refer to the brick with $\lambda/(\rho c_p) = 2.57 \times 10^{-7} \text{ m}^2/\text{s}$ show a higher cooling rate than curves A and B where we have $\lambda/(\rho c_p) = 1.1 \times 10^{-7} \text{ m}^2/\text{s}$. At the same time, curve G, where we have $\lambda/(\rho c_p) = 0.23 \times 10^{-7} \text{ m}^2/\text{s}$, shows a higher cooling rate than curves C, D, E, F. Table 3.13 contains data from some simulations where the block is considered to be composed of bricks which have the same thermal diffusivity. It clearly shows that each brick presents an identical temperature field. It is obvious that, for this simulation, the temperature at the centre of each brick and at the centre of the block have the role of the dependent variables of the process when the medium temperature, the cooling temperature at the beginning, the material diffusivity and the block geometrical dimensions are the inputs or independent variables of the process. In addition, we can say that, in spite of the type I boundary conditions for the bottom and top surfaces, the data shown in Table 3.13 allow one to appreciate that the block cooling process can be characterized by the integral relation: $T_{p\text{mean}} = T_{p0} \exp\left(-\frac{kA_t}{mc_p} \tau\right)$ where $T_{p\text{mean}}$ is the mean block temperature, k is the heat transfer coefficient with respect to the non-isolated surfaces, m represents the block mass and A_t is the value of the non-isolated surfaces.

Table 3.13 Evolution of the temperature at the centre of the block and at the centre of each brick.

Studied case: $\lambda_1/(\rho_1 c_{p1}) = \lambda_2/(\rho_2 c_{p2}) = \lambda_3/(\rho_3 c_{p3}) = \lambda_4/(\rho_4 c_{p4}) = 10^{-7} \text{ m}^2/\text{s}$.

T	0	0.25	0.5	0.75	1.0	1.25	1.50	1.75	2.0
T_p – block centre	6	5	2.0	0.8	0.4	0.15	0.05	0	0
T_p – each brick centre	6	2	0.8	0.3	0.08	0.04	0	0	0

If we significantly reduce the dimension of the Z axis, then we transform the three-dimensional cooling problem into an unsteady state and monodimensional problem. Figures 3.50 and 3.51 show the results of the simulations oriented to demonstrate this fact. We can notice that all curves present the same tendency as the analytical solution or Schmidt numerical solution of the monodimensional cooling problem:

$$\frac{\partial t}{\partial \tau} = \frac{\lambda}{\rho c_p} \frac{\partial^2 t}{\partial z^2}; \quad \frac{\lambda}{\rho c_p} = \sum_1^4 \frac{\lambda_i}{\rho_i c_{pi}}$$

$$\tau \geq 0, \quad z = -L \text{ and } z = l, \quad t = t_a; \quad \tau = 0, \quad -L < z < L, \quad t = t_0$$

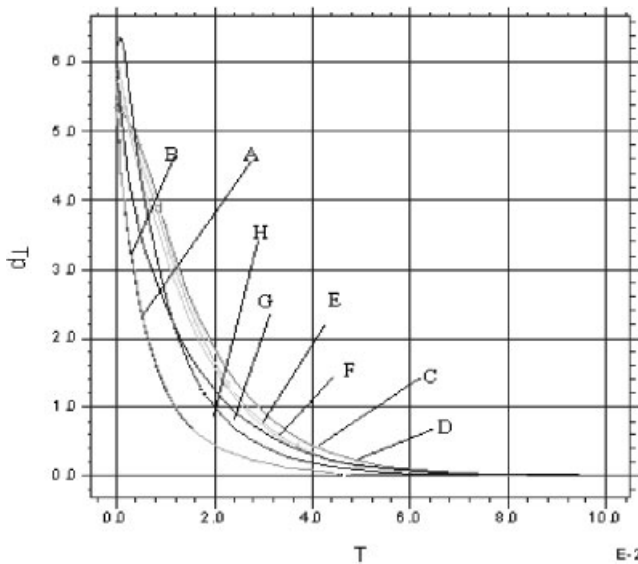


Figure 3.50 The cooling dynamics of the bricks assembly for $L/l = 0.1$.

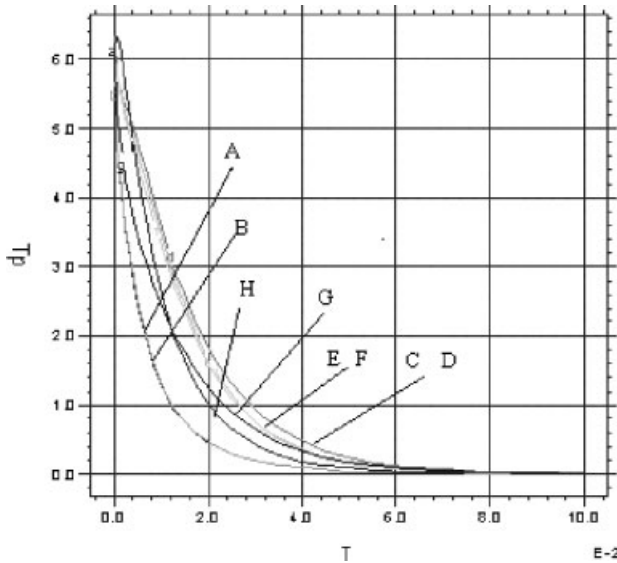


Figure 3.51 The cooling dynamics of the bricks assembly for $L/l = 0.01$.

The above-mentioned trend occurs in spite of the different conditions that characterize the calculation of each curve. As is known, the dimensionless time that characterizes cooling depends on the width of each brick. However, this dimensionless value has not changed in the simulations used for drawing Figs. 3.50 and 3.51. Consequently, these figures are characterized by the same dimensionless time axis division. In addition, the heat transfer surface used for the simulation also has the same value. Indeed, both figures are reported to use the same base of comparison.

In the *third simulation* example, we carried out an analysis of some of the aspects that characterize the case of the mass transfer of species through a membrane which is composed of two layers (the separative and the support layers) with the same thickness but with different diffusion coefficients of each entity or species. To answer this new problem the early model has been modified as follows: (i) the term corresponding to the source has been eliminated; (ii) different conditions for bottom and top surfaces have been used: for example, at the bottom surface, the dimensionless concentration of species is considered to present a unitary value while it is zero at the top surface; (iii) a new initial condition is used in accordance with this case of mass transport through a two-layer membrane; (iv) the values of the four thermal diffusion coefficients from the original model are replaced by the mass diffusion coefficients of each entity for both membrane layers; (v) the model is extended in order to respond correctly to the high value of the geometric parameter l/L .

It is clear that, for this problem, the normal trend is to use the monodimensional and unsteady state model, which is represented by the assembly of relations (3.152)–(3.156). It accepts a very simple numerical solution or an analytical solution made of one of the methods classically recommended such as the variable separation method:

$$\frac{\partial c}{\partial \tau} = D \frac{\partial^2 c}{\partial z^2} \quad (3.152)$$

$$\tau = 0, \quad -L \leq z \leq L, \quad c = 0 \quad (3.153)$$

$$\tau \geq 0, \quad z = -L, \quad c = c_0 \quad (3.154)$$

$$\tau \geq 0, \quad z = 0 \quad D_1 \left(\frac{dc}{dz} \right)_- = D_2 \left(\frac{dc}{dz} \right)_+ \quad (3.155)$$

$$\tau \geq 0, \quad z = L, \quad c = 0 \quad (3.156)$$

In addition, it is known that the transport of species through the membrane and its support are characterized by the coefficients of diffusion, which are experimentally determined with methods based on this model [3.47–3.51].

However, we cannot *a priori* use this model without the previous establishment of conditions which accept the transformation of the three-dimensional and unsteady state model into a one-dimensional model. These conditions can be studied using the simulations as a tool of comparison. At the same time, it is interesting to show the advantages of the dynamic (unsteady) methods for the estimation of the diffusion coefficient of the species through the porous membrane by comparison with the steady state methods.

Figures 3.52–3.54 show three cases of simulation of the process where the diffusion coefficients for the support and membrane take, respectively, the following values $D_1 = D_3 = D_{sp} = 10^{-8} \text{ m}^2/\text{s}$ $D_2 = D_4 = D_{mb} = 10^{-9} \text{ m}^2/\text{s}$. All simulated cases keep the total volume of the membrane assembly constant but differ from each other due to parameter l/L which takes the values: 10, 100, and 1000.

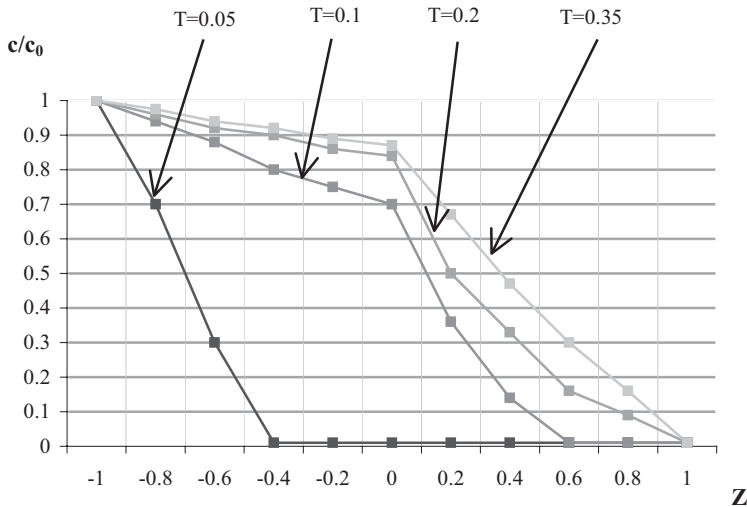


Figure 3.52 Dimensionless species concentration along the Z axis at various times (for $l/L = 10$).

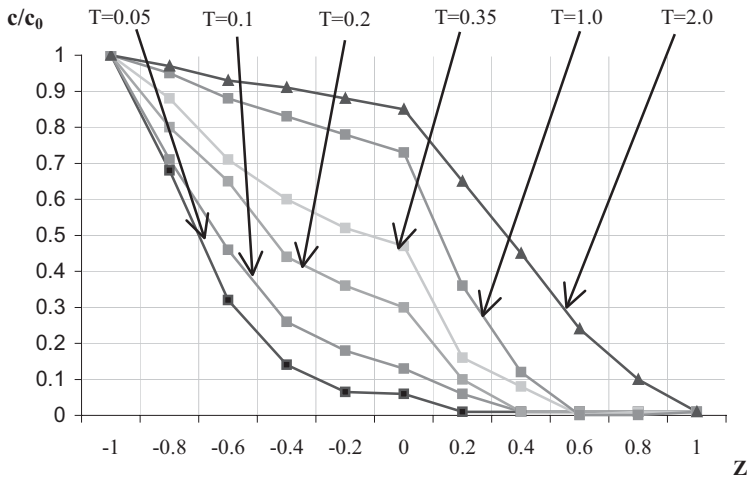


Figure 3.53 Dimensionless species concentration along the Z axis at various times (for $l/L=1000$).

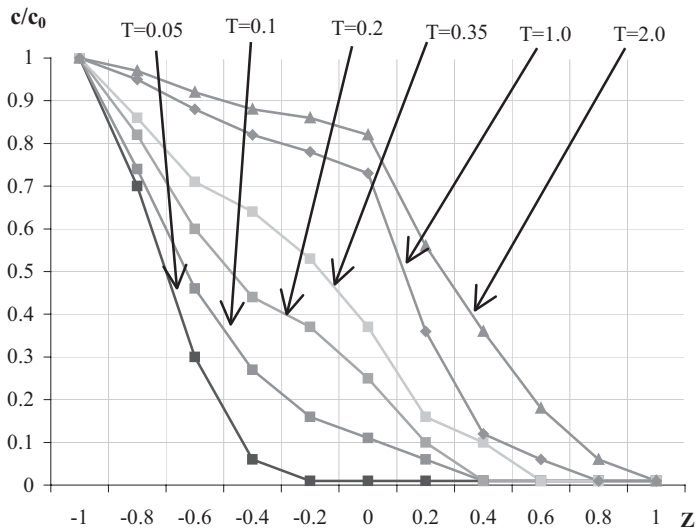


Figure 3.54 Dimensionless species concentration along the Z axis at various times (for $l/L=100$).

Figure 3.52 significantly differs from the next two figures, especially with respect to the evolution of C/C_0 with time. For this situation, where the value of the ratio length/thickness is not very high (10) we can accept that the diffusion occurs in all directions and also that it is very rapid in the membrane support. This last fact is responsible for this apparent fast evolution with time. For the other two situations, we can observe that the diffusion process tends to attain the stationary state when the concentration profile is $C = C_1 - (1 - C_1) * Z$ for

$-1 \leq Z \leq 0$ and $C = C_1 * (1 - Z)$ for $0 \leq Z \leq 1$ respectively. Here, the dimensionless species concentration for the steady state diffusion at the plane $Z = 0$ is given by C_1 . If we write the equality of the species flux for the support and for the membrane, we obtain:

$$\frac{1 - C_1}{C_1} = \frac{D_{mb} \delta_{sp}}{D_{sp} \delta_{mb}}$$

Unfortunately, we cannot measure the dimensionless concentration C_1 and, consequently, this relation cannot be used to determine D_{mb} , even if D_{sp} is known. At the same time, it is not simple to establish the end of the dynamic evolution and the beginning of the steady state diffusion. As an example, if we know the end of the unsteady state and the beginning of the steady state (as given in the simulations), the ratio $D_{mb} \delta_{sp} / D_{sp} \delta_{mb} = 0.1$ ($\delta_{mb} = \delta_{sp}$, $D_{mb} = 10^{-9} \text{ m}^2/\text{s}$, $D_{sp} = 10^{-8} \text{ m}^2/\text{s}$) for Figs. 3.52–3.54 then, for the steady state, $(1 - C_1)/C_1$ must be 0.1.

If we observe the value of $(1 - C_1)/C_1$ at $T = 2$ we have 0.135 for Fig. 3.52, 0.157 for Fig. 3.53 and 0.189 for Fig. 3.54; for all cases the persistency of the dynamic evolution is shown. Otherwise, if we insist on the development of the steady state method to determine the diffusion coefficient, then it is not difficult to observe that, from the experimental point of view, we must use the measurements of the flow rate of species (diffusion). Nevertheless, this type of experiment is not characterized by its reproducibility and simplicity.

Concerning the problem of the validity of the monodimensional and unsteady state model for the transport of an entity through the membrane, the simulations with $l/L > 100$ show that the transport in the Z direction is dominant. At the same time, Figs. 3.55 and 3.56, which give the state of the dimensionless concentration

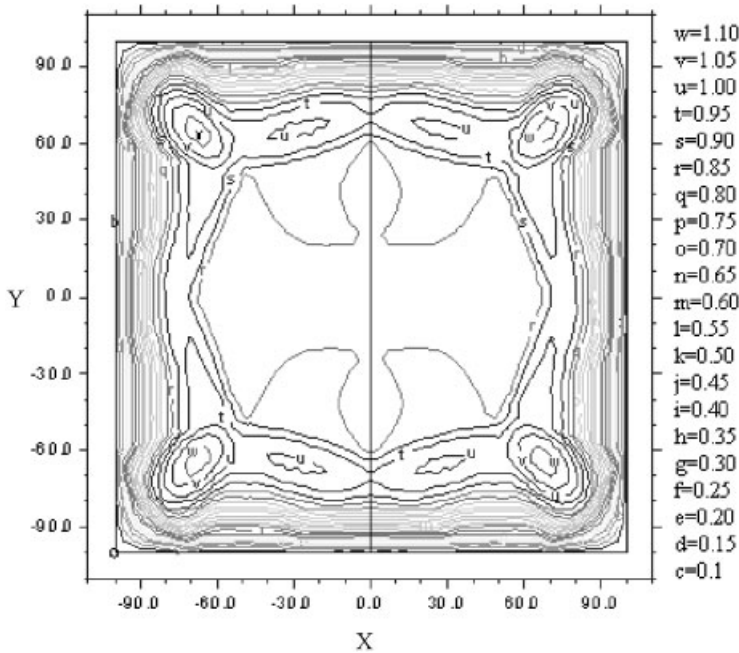


Figure 3.55 Dimensionless concentration for plane $Z = 0$ when $l/L = 1000$ and $T = 2$.

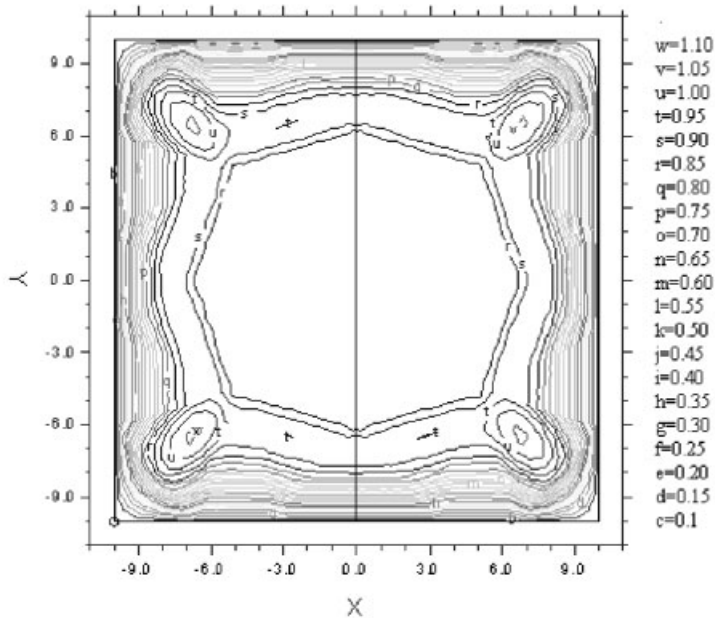


Figure 3.56 Dimensionless concentration for plane $Z = 0$ when $l/L = 100$ and $T = 2$.

of the species for plane $Z = 0$ (between the support and membrane) show that the X and Y concentration gradients are not absent in this case.

Because these gradients are not negligible, we cannot fully recommend, the monodimensional unsteady state model as a theoretical model that supports the use of dynamic methods for the characterization of the diffusion in a porous membrane. Even if over 60% of the membrane surface is covered by a constant dimensionless concentration of species, this event is not sufficient to allow the acceptance of the unsteady model. Nevertheless, looking closely at Figs. 3.55 and 3.56 we can notice that only 20% of the surface contains high concentration gradients. However, the boundary conditions chosen impose the absence of transport of the species throughout all surfaces except for $Z = -1$ and $Z = 1$. It is evident that these last observations sustain the validity of the monodimensional and unsteady state model. As a conclusion to this discussion, it is clear that the validity of the monodimensional and unsteady state model as a support for the dynamic methods to characterize the diffusion in a porous medium is not really affected. At the same time, these critical observations can be considered as a support of the various procedures that bring the necessary corrections to this model.

If both parts of the membrane (the support and the separative layers) can be characterized by values lower than 1 for the Knudsen number ($Kn = \lambda/2r_p$ where λ is the mean free path of species or molecules and r_p is the mean pore radius), then all the aspects mentioned here must be taken into consideration. To describe

the motion of a species in a porous structure, other models must be used when the Knudsen number value is higher than 1 or when the support is highly porous and the separative layer is dense.

One of the most convenient ways to investigate this process is to accept the monodimensional unsteady state model of transport inside the membrane and to measure the time lag characterizing the transitional process preceding the steady-state. Traditional time lag theory has been intensively used to study gas and vapour permeation through dense films. In most cases, the derived equations describing the time lag for diffusion through composite media accept the equilibrium assumption at interfaces. This assumption is valid when the mass transfer process at the interface is much faster than the transfer within the two adjacent phases. This model has also been used in describing transport through supported liquid membranes. In some cases, the interface resistance cannot be neglected, and can be described with chemical reaction or sorption–desorption rates at the surface.

3.4.3

Fast Chemical Reaction Accompanied by Heat and Mass Transfer

The problem of the modeling of a reactor where a homogeneous reaction (in the gas or liquid phase) takes place can be relatively simple to solve after selecting the type of reactor and its corresponding flow model. It is evident that, in accordance with the accepted flow model, the reactor model will contain the particularizations of the equation of the energy conservation and of the equations of the field of the species concentration. The source term of the equation of the concentration of one species is expressed by the kinetics reaction rate. Here we consider that the homogeneous reaction is carried out in a reactor where the hydrodynamics corresponds to a plug flow (PF) model and where the reaction $A + B \rightarrow C$ occurs in the presence of an inert component D. In accordance with the descriptive model of the reactor given in Fig. 3.57, the following relations and conditions show the associated mathematical model for a steady state operation and an elementary reactor's length dz :

- the balance equations of species A consumption:

$$w \frac{dX_A}{dz} = v_{rA} \quad (3.157)$$

- the links between local concentration of B, C, D and A:

$$y_B = y_{B0}(1 - X_A) \quad (3.158)$$

$$y_C = y_{C0}(1 + X_A) \quad (3.159)$$

$$y_A = y_{A0}(1 - X_A) \quad (3.160)$$

$$y_D = 1 - y_A - y_B - y_C \quad (3.161)$$

- the heat balance equation:

$$w \frac{dt}{dz} = \frac{\Delta H_{rA}}{\rho c_p} v_{rA} - \frac{4k}{\rho c_p d} (t - t_{ex}) \tag{3.162}$$

- the expression of the reaction kinetics:

$$v_{rA} = k_1 c_{A0}^m c_{B0}^n (1 - X_A)^{m+n} - k_2 c_{C0}^p (1 + X_A)^p \tag{3.163}$$

- the concentration and temperature conditions at the reactor input:

$$z = 0, X_A = 0, y_A = y_{A0}, y_B = y_{B0}, y_C = y_{C0}, t = t_0, t_{ex} = t_{ex0} \tag{3.164}$$

- the heat balance for the fluid that flows outside of the reactor:

$$\frac{dt_{ex}}{dz} = f(G_{ex}, \rho_{ex}, c_{pex}, k, d, t) \tag{3.165}$$

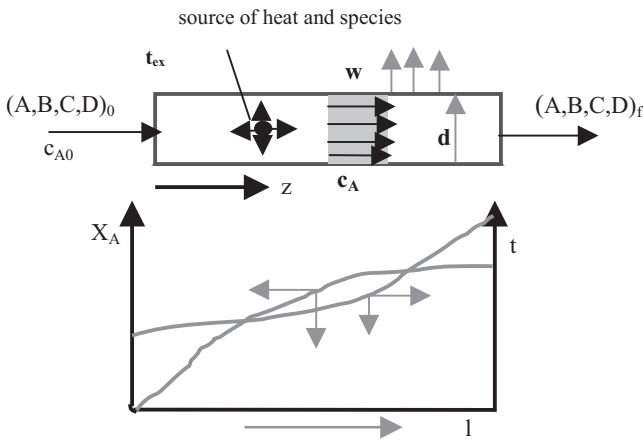


Figure 3.57 Scheme of a plug-flow reactor and homogeneous reaction.

In the PF homogeneous reactor, X_A is the conversion of species A into C, ($X_A = (c_A - c_{A0})/c_{A0}$, where c_A is the local molar concentration of A), y represents the molar fraction of species ($y_A = c_A/(c_A + c_B + c_C + c_D)$, etc.) and k_1, k_2, m, n, p characterize the kinetics as reaction constants with their partial reaction orders.

The unsteady state model will be completed by adding the unsteady evolution as $\partial X_A/\partial \tau$, $\partial t/\partial \tau$ and $\partial t_{ex}/\partial \tau$ respectively on the left part of the equations (3.155), (3.160) and (3.163). At the same time, the initial conditions must be adequately changed and new univocity conditions will be attached to this new problem.

The modeling procedure explained above is not valid for all types of homogeneous reactions, for example, a very fast exothermic reaction such as the combustion of gaseous or vaporized hydrocarbon with oxygen in air or the reaction of chloride and hydrogen in inert nitrogen, etc. We will develop an example of such reactions below:

- A gaseous mixture, which contains three components – a combustible, a comburent and an inert gas, is fed into a tubular reactor which has an efficient cooling in order to maintain the walls at constant temperature;
- The gaseous mixture comes into the reactor with uniform radial velocity (plug flow) and the gas velocity increases linearly with temperature inside the reactor. Indeed, we can consider the conversion as a function of r , $w\tau$ and τ ($X_A(r, w\tau, \tau)$) and, consequently, we can build the model taking r and τ into account;
- To start the reaction in the reactor input, we have a small surface with the function of a heat inductor where the temperature of the gaseous mixture increases very rapidly to attain the inductor temperature. Inside the reactor the inductor surface operates as a stripping heat surface;
- The process occurs symmetrically with respect to a plane that contains the z axis; at the same time, the temperature and the reactant conversion will present the maximum values in the centre of the reactor due to a high speed reaction. Therefore, we permanently have the right conditions for components and heat diffusion in the reactor.

Combustion reactions are known to occur through a free radical mechanism and from this viewpoint, their kinetics is complicated. At the same time, the coupling of the reaction kinetics with the flow dynamics, as well as the species and heat diffusion is very important for most real cases [3.52–3.55]. For simplification, we consider that the formal kinetics of this reaction is first order with respect to the limiting reactant and that its expression must show a strong dependence on temperature. Now, using the descriptive model (Fig. 3.58), we can build the general mathematical model of the process. Concerning our fast highly exothermic reaction, relation (3.166) often employs the quantitative description of the reactant consumption rate. Here c is the limitative species concentration and γ is a parameter related to the reaction activation energy:

$$v_r(c, \tau) = kc * \exp[\gamma(1/t_0 - 1/t)] = kc * \exp[\gamma/t_0(1 - 1/T_p)] \quad (3.166)$$

For small γ values, we obtain small or moderate reaction rates, whereas when γ increases, it corresponds to the start of the fast reaction or high temperatures, when the reaction rate can attain a dangerous level.

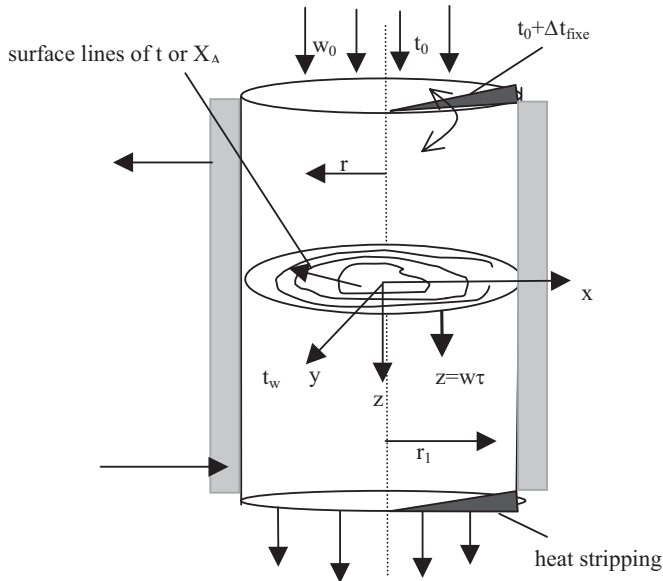


Figure 3.58 Description of a plug flow reactor with a constant wall temperature where a fast exothermic reaction occurs.

The mathematical model of the process is built only in x and y coordinates (or only in the r coordinate) because the z coordinate is self-defined using τ and w . Then, the general mathematical model contains the following equations and conditions:

- the equation of concentration field for the limitative reactant:

$$\frac{\partial c}{\partial \tau} = D_A \left(\frac{\partial^2 c}{\partial x^2} + \frac{\partial^2 c}{\partial y^2} \right) + v_r(c, t) \quad (3.167)$$

- the expression of temperature field inside the reaction mixture:

$$\frac{\partial t}{\partial \tau} = a_t \left(\frac{\partial^2 t}{\partial x^2} + \frac{\partial^2 t}{\partial y^2} \right) + v_r(c, t) \frac{\Delta H_r}{\rho c_p} \quad (3.168)$$

- the equations of the local gas velocity and plug flow reaction front position:

$$w = w_0 \frac{(271 + t)}{(271 + t_0)}; z = w\tau \quad (3.169)$$

- the respective initial conditions for the temperature and concentration domains:

$$\tau = 0, \quad 0 < x < r_1, \quad 0 < y < r_1, \quad c = 0, \quad t = t_0 \quad (3.170)$$

- the univocity conditions:

$$1. \text{ for the reactor input:} \\ \tau > 0, \quad 0 < x < r_1, \quad 0 < y < r_1, \quad x^2 + y^2 = r^2, \quad c = c_0, \quad t = t_0 \quad (3.171)$$

2. for the surface of thermal process control:

$$\begin{aligned} \tau = 0, \quad 0 < x < r_1, \quad 0 < \sqrt{(x^2 + y^2)} < r_1 \frac{\theta}{360}, \quad t = t_0 + \Delta t, \quad \frac{dc}{dr} = 0 \\ \tau > 0, \quad 0 < x < r_1, \quad 0 < \sqrt{(x^2 + y^2)} < r_1 \frac{\theta}{360}, \quad \frac{dt}{dr} = 0, \quad \frac{dc}{dr} = 0 \end{aligned} \quad (3.172)$$

3. for the reactor walls:

$$\tau > 0, \quad x = r_1, \quad y = r_1, \quad y_{r1} \in 360 - \theta, \quad \lambda \frac{dt}{dr} = -\alpha(t - t_w), \quad \frac{dc}{dr} = 0 \quad (3.173)$$

The set of Eqs. (3.166)–(3.173) represents the general mathematical model of the described fast exothermic reactions taking place in an externally cooled plug flow reactor. If we use the dimensionless expressions of time $T = D_A \tau / r_1^2$, coordinates $X = x/r_1, Y = y/r_1, Z = z/l, R = r/r_1$, temperature $T_p = t/t_0$ and conversion X_A as dimensionless concentration of the limitative reactant, then the process model can be described by the relations contained in Table 3.14.

Table 3.14 Dimensionless mathematical model for the heat and mass transfer in a plug flow reactor for a fast exothermic reaction.

$$\frac{\partial X_A}{\partial T} = \left(\frac{\partial^2 X_A}{\partial X^2} + \frac{\partial^2 X_A}{\partial Y^2} \right) + \beta_R (1 - X_A) \exp \left[\gamma \left(1 - \frac{1}{T_p} \right) \right] \quad (3.174)$$

$$\frac{\partial T_p}{\partial T} = \frac{Sc}{Pr} \left(\frac{\partial^2 T_p}{\partial X^2} + \frac{\partial^2 T_p}{\partial Y^2} \right) + \beta_T (1 - X_A) \exp \left[\gamma \left(1 - \frac{1}{T_p} \right) \right] \quad (3.175)$$

$$\frac{w}{w_0} = \frac{\alpha + T_p}{\alpha + 1}; \quad Z = Pe_d \left(\frac{r_1}{l} \right) T \quad (3.176)$$

$$T = 0, \quad 0 < Z < 1, \quad 0 < Y < 1, \quad 0 < X < 1, \quad X_A = 0, \quad T_p = 1 \quad (3.177)$$

$$T > 0, \quad 0 < X < 1, \quad 0 < Y < 1, \quad X^2 + Y^2 = R^2, \quad X_A = 1, \quad T_p = 1 \quad (3.178)$$

$$T > 0, \quad 0 < X < 1, \quad 0 < \sqrt{X^2 + Y^2} < \frac{\theta}{360}, \quad T_p = 1 + \frac{\Delta t}{t_0}, \quad \frac{dX_A}{dR} = 0 \quad (3.179)$$

$$T > 0, \quad 0 < X < 1, \quad 0 < \sqrt{X^2 + Y^2} < \frac{\theta}{360}, \quad T_p = 1 + \frac{\Delta t}{t_0}, \quad \frac{dX_A}{dR} = 0 \quad (3.180)$$

$$T > 0, \quad 0 < X < 1, \quad 0 < Y < 1, \quad Y_1 \in 360 - \theta, \quad \frac{dT_p}{dR} = Bi(T_p - T_w), \quad \frac{dX_A}{dR} = 0 \quad (3.181)$$

Specifications: $\beta_r = (kr_1^2)/D_A$ – Fourier number for the reaction,
 $Sc = v/D_A$ – Schmidt number $Pr = (c_p v \rho)/\lambda$ – Prandtl number,
 $Bi = (\alpha r_1)/\lambda$ – Biot number, $\beta_T = \beta_r (\Delta H_r c_0)/(\rho c_p t_0)$, ρ – density,
 v – kinematic viscosity, c_p – specific sensible heat,
 λ – thermal conductivity.

The *first simulation* program set is obtained after the model particularization using the numerical values of the parameters and the geometry and material properties as shown in Fig. 3.59. This program aims to show some characteristic aspects of this type of reactor with respect to the heat and reactant conversion dynamics using a graphic representation. In addition, the simulation allows one to know the evolution of the exit variables of the process (temperature and species concentration), when one or more of the input variables of the model are changed. For this concrete case and among these input variables, we can identify: (i) the input flow rate of reactants; (ii) the value of the limitative reactant concentration at the reactor feed; (iii) the value of the input temperature of the reactants; (iv) the temperature of the reactor walls; (v) the limitative reactant type, here introduced by the parameters that characterize the reaction kinetics.

```

Title 'PF reactor for fast exothermic reaction'
Select painted { make color-filled contour plots }
Variables Temp(range=0,5) XA(range=0,1)
definitions
  Lz = 1 r1=1 heat=0 gamma = 16 beta = 0.2 betat = 0.3
  BI = 1 T0 = 1 TW = 0.92 VRS = (1-XA)*exp(gamma-gamma/Temp)
  xev=0.96 yev=0.25 { some plot points }
initial value Temp=T0 XA=0
equations
  div(grad(Temp)) + heat + betat*VR = dt(Temp)
  div(grad(XA)) + beta*VRS = dt(XA)
boundaries
  region 1
  start (0,0) natural(Temp) = 0 natural(XA) = 0 line to (r1,0) { a mirror plane on X-axis }
  { "Strip Heater" at fixed temperature } value(Temp)=T0 + 0.2*uramp(t,t-0.05)
  { ramp the boundary temp, because discontinuity is costly to diffuse }
  natural(XA)=0 { no mass flow }
  arc(center=0,0) angle 5 { .. on outer arc }
  region 2
  natural(Temp)=BI*(TW-Temp) natural(XA)=0 { no mass flow }
  arc(center=0,0) angle 85 { ... on outer arc }
  natural(Temp) = 0 natural(XA) = 0 line to (0,0) finish {another mirror plane on Y- axis }
time 0 to 1
plots for cycle=10 { watch the fast events by cycle }
  contour(Temp) contour(XA) for t = 0.2 by 0.05 to 0.3 { show some surfaces during burn }
  surface(Temp) surface(C) as
histories history(Temp) at (0,0) (xev/2,yev/2) (xev,yev) (yev/2,xev/2) (yev,xev)
  history(C) at (0,0) (xev/2,yev/2) (xev,yev) (yev/2,xev/2) (yev,xev)
end

```

Figure 3.59 FlexPDE™ software for a fast exothermic reaction in a PF reactor.

The violent runaway of the reaction is clearly shown in Figs. 3.60 and 3.61, where the evolution of the reactant conversion and of the temperature is given for some points positioned in a fourth of the reactor section because of symmetry. As we can notice, time gives supplementary information about conversion with respect to the position in the z-axis of the reactor. From these figures, we can also

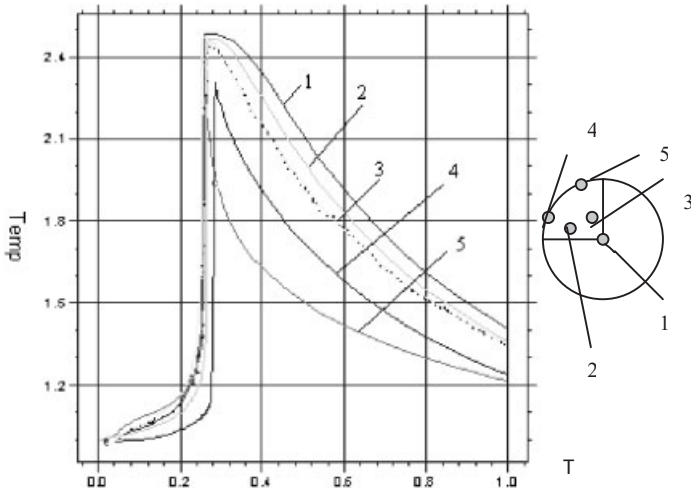


Figure 3.60 [block] caption. [block]

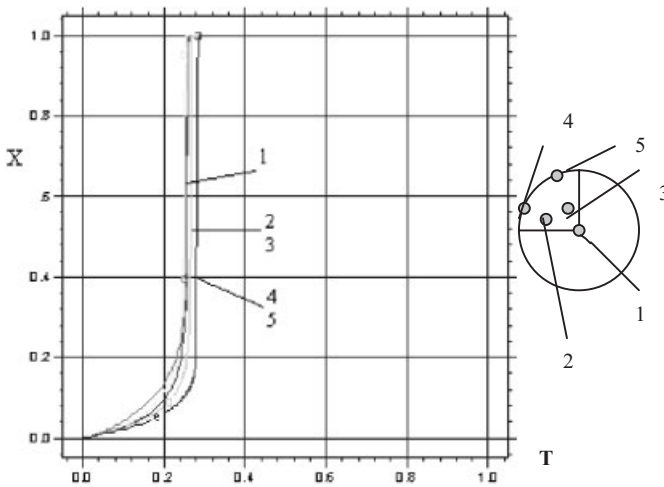


Figure 3.61 Evolution of the conversion of the reactant in the PF reactor when a fast exothermic reaction takes place.

observe that, after an induction period, when the reactant conversion reaches 0.15, the reaction becomes violent and in a very short time all the limiting reactant is consumed. The temperature evolution with time after the end of the reaction shown in Fig. 3.60 corresponds to the heat diffusion process. Indeed, the points positioned near the walls show a more rapid cooling than the points placed at the Z-axis of the reactor. With reference to the evolution through the Z-axis, the description of events is similar: after a short distance, when the conversion attains the above-mentioned value, the manifestation of the violent reaction that corre-

sponds to a small z distance begins; in the remaining length, the gas mixture continues flowing and gas cooling takes place.

It is not difficult to observe in Fig. 3.59 that we can still change some parameters in order to increase the reaction temperature: (i) by increasing the temperature of the reactants at the reactor input (we use a T_0 value higher than 1); (ii) by increasing the input concentration of the limiting reactant (we increase the value of beta in the simulation software); (iii) by increasing the wall temperature (T_w). In addition, we can consider an enhancement of the heat transfer through the walls by increasing the Biot number. Figures 3.62–3.64, which have been obtained with other start values for T_0 , T_w , Bi, c_0 , can be compared to Figs. 3.60 and 3.61. They aim to show the moments of reaction runaway more completely.

Figure 3.62 shows the temperature field of a quarter of the radial section of the reactor before the reaction firing. Combining the values of T_0 , T_w and Bi results in an effective cooling of the reactor near the walls during the initial instants of the reaction ($T = 0 - 0.05$). In Fig. 3.63 is shown the temperature field when the dimensionless time ranges between $T = 0.05$ and $T = 0.11$. Here, the reaction runaway starts and we can observe that an important temperature enhancement occurs at the reactor centre, at the same time the reactant conversion increases (Fig. 3.64). The evolution of the reaction firing and propagation characterize this process as a very fast process. We can appreciate in real time that the reaction is completed in 10 s. It is true that the consideration of isothermal walls can be criticized but it is important to notice that the wall temperature is not a determining factor in the process evolution when the right input temperature and the right input concentrations of reactants have been selected.

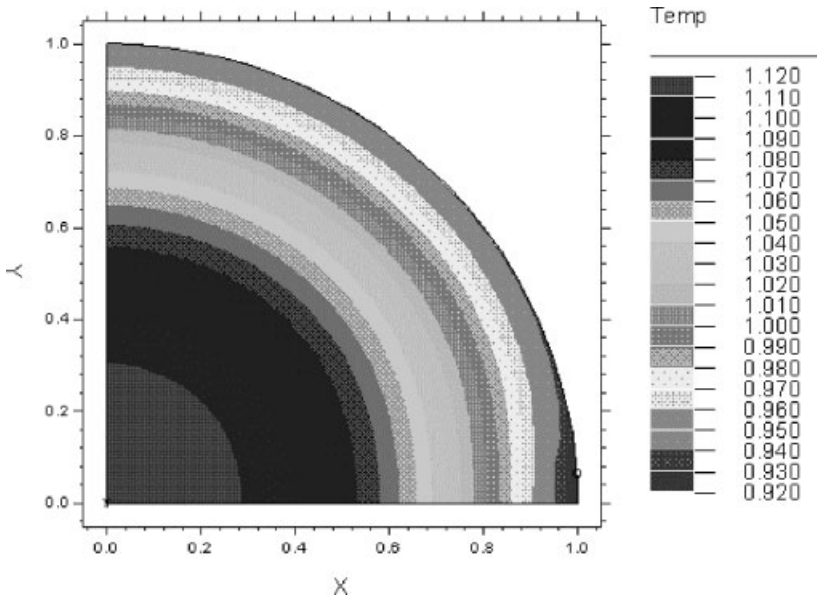


Figure 3.62 Temperature field before the reaction runaway for $T = 0.05$. ($T_0 = 1.05$, $T_w = 0.9$, $Bi = 10$, $c_0/c_{00} = 1.4$.)

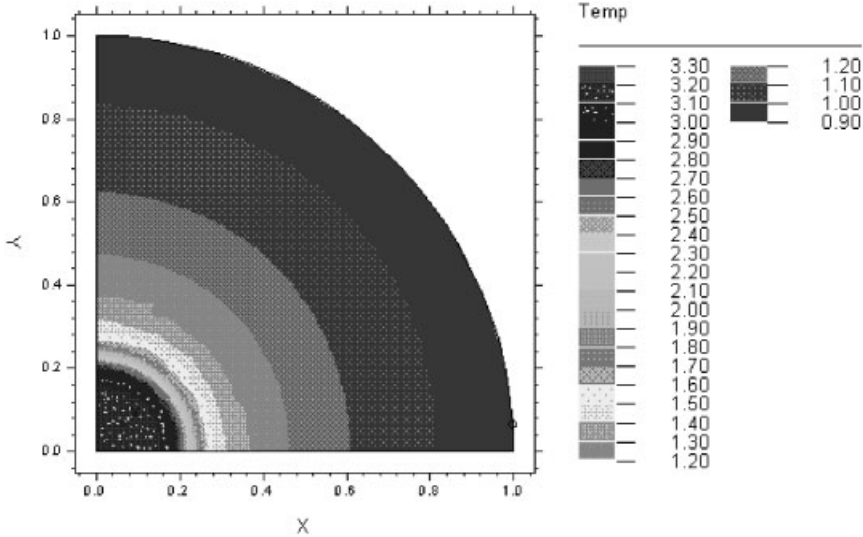


Figure 3.63 Temperature field for the time of reaction $T = 0.11$. ($T_0 = 1.05$, $T_w = 0.9$ $Bi = 10$, $c_0/c_{00} = 1.4$.)

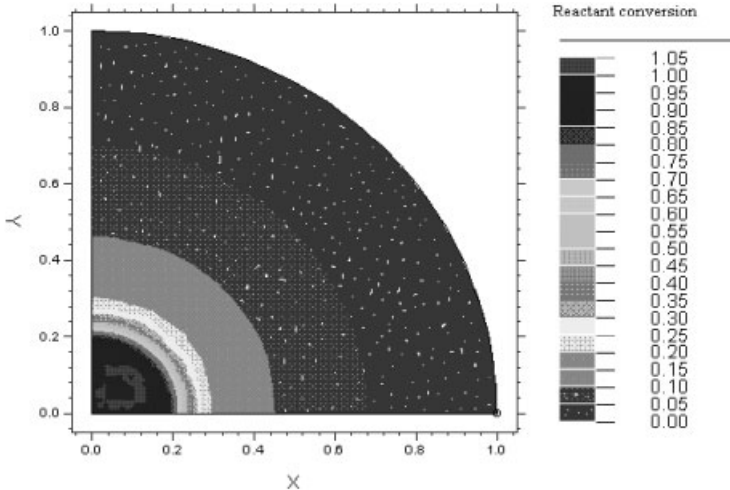


Figure 3.64 Conversion field for $T = 0.11$. ($T_0 = 1.05$, $T_w = 0.9$, $Bi = 10$, $c_0/c_{00} = 1.4$.)

With reference to the timing of the reaction firing, Table 3.15 presents the result of the simulations carried out with this purpose. The direction of the firing is already shown in this table. This can occur from the centre to the wall ($C > W$) or from the wall to the centre ($W > C$). Nevertheless, we will not investigate the technological problem involved with some of these input conditions now. We will mention this important fact: when the wall temperature is higher than that of the

input reactants, the reaction ignition virtually starts at the input of the reactor. However, in terms of simulation, this behaviour can be modulated with the reaction kinetics.

Table 3.15 Time of reaction firing when $Bi = 10$ and $c_0/c_{00} = 1$.

T_0	1	1.1	1.1	0.9	0.5	0.3	0.85	0.92	0.98	0.95
T_w	0.92	0.85	0.75	2	2	2	1.1	1	0.98	0.95
T Start	0.25	0.08	0.08	0.01	0.01	0.01	0.26	0.42	0.28	0.7
Finish	0.3	0.1	0.12	0.04	0.09	0.13	0.32	0.48	0.3	0.78
Sense	C > W	C > W	C > W	W > C	W > C	W > C	W > C	W = C	C > W	C > W

As far as controlling the process is concerned, it seems to be interesting to have similar values for T_0 and T_w . In this case, after the reaction ignition in the whole radial section of the reactor input, the fast reaction propagation occurs towards the reactor centre. Before closing the discussions about these first simulations, we have to notice that modifications of the model and the associated software allow the application of this example to many other cases. For example, when the wall temperature is higher than the reactor temperature, we can simulate the cases of endothermic homogeneous reactions such as hydrocarbon cracking. Such application needs two major software modifications: a negative β_t value and a more complete kinetics. It is important to specify that the developed model can simulate the firing reaction where the limiting reactant is uniformly distributed into the reactor input. For the case when we have a jet-feed of limitative reactant where a firing reaction occurs [3.55], a new model construction is recommended.

The second set of simulations is oriented towards the analysis of the simultaneous heat and mass transfer when two fluids are separated by a porous wall (membrane). The interest here is to couple the species transport through a wall associated with the heat transfer and to consider that the wall heat conduction is higher than the heat transported by the species motion. The process takes place through a cylindrical membrane and we assume the velocity to be quite slow in the inner compartment of the membrane. The process is described schematically in Fig. 3.65. The transformation of the above general model in order to correspond to this new description gives the following set of dimensionless equations:

- the dimensionless concentration field of transferred species:

$$\frac{\partial C_A}{\partial T} = \left(\frac{\partial^2 C_A}{\partial X^2} + \frac{\partial^2 C_A}{\partial Y^2} \right) \quad (3.182)$$

- the dimensionless evolution of the temperature:

$$\frac{\partial T_p}{\partial T} = \frac{Sc}{Pr} \left(\frac{\partial^2 T_p}{\partial X^2} + \frac{\partial^2 T_p}{\partial Y^2} \right) \quad (3.183)$$

- the movement expression for the z axis:

$$\frac{w}{w_0} = \beta \frac{\alpha + T_p}{\alpha + 1} \quad (3.184)$$

- the initial and univocity conditions:

$$T = 0, \quad 0 < Z < 1, \quad 0 < Y < 1, \quad 0 < X < 1, \quad C_A = 0, \quad T_p = 1 \quad (3.185)$$

$$T > 0, \quad 0 < X < 1, \quad 0 < Y < 1, \quad Z = 0, \quad C_A = 0, \quad T_p = 1 \quad (3.186)$$

$$T > 0, \quad X = 1, \quad Y = 1, \quad \frac{dT_p}{dR} = Bi(T_p - T_w). \quad (3.187)$$

$$T > 0, \quad X = 1, \quad Y = 1, \quad \frac{dC_A}{dR} = Bi_D \frac{1}{(1 + Bi_p)} (1 - C_A) \quad (3.188)$$

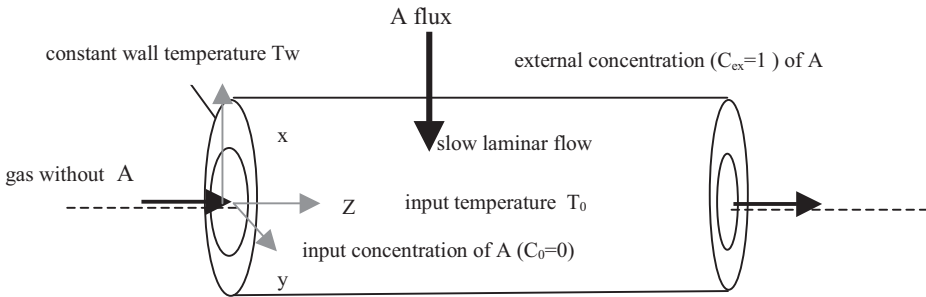


Figure 3.65 Explanatory scheme for heat and mass transport through a porous wall.

In the set of relations (3.182)–(3.188), β represents the coefficient for the velocity increase due to the species transport through the wall, Bi is the heat transfer Biot number ($Bi = (\alpha r_1)/\lambda$), Bi_D is the mass transfer Biot number for the gaseous phase ($Bi_D = (kr_1)/D_A$) and Bi_p is the Biot number for the porous wall ($Bi_p = (k\delta_w)/D_{Aw}$). Two new parameters δ_w and D_{Aw} , respectively, represent the wall thickness and the wall effective diffusion coefficient of species. The model described by the set of relations (3.182)–(3.188) can easily be modified to respond to the situation of a membrane reactor when a chemical reaction occurs inside the cylindrical space and when one of the reaction products can permeate through the wall. The example particularized here concerns the heat and mass transfer of a

gaseous fluid. Figures 3.66 and 3.67, respectively, present the dynamic evolution of the heat thermal field and the concentration of species A. As was explained in the previous example, the time parameter can be transformed into the z position using relation (3.184). It is interesting to observe that the steady state permeation of A is attained (the enhancement of the species concentration is linear) at dimensionless time $T = 0.2$ (which is relatively fast in real time). At $T = 1$ thermal equilibrium is reached and the heat transfer phenomenon disappears.

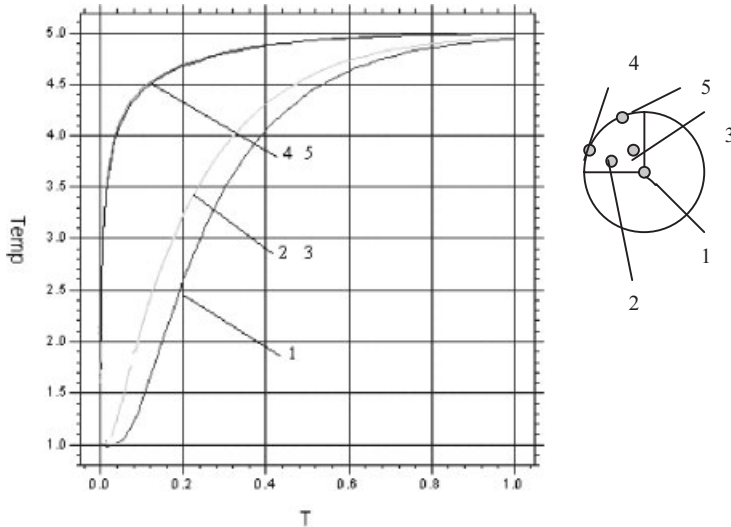


Figure 3.66 Temperature evolution inside the cylindrical membrane ($Bi = 10, Bi_D = 2, Bi_p = 100, T_w = 5$).

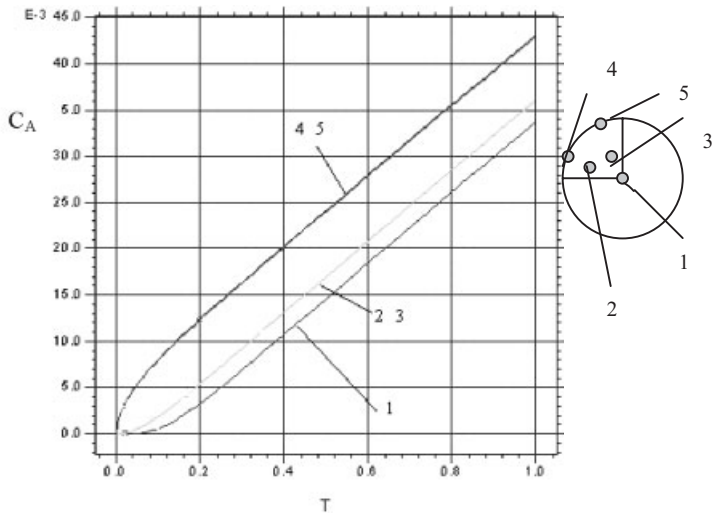


Figure 3.67 Evolution of concentration of A inside the cylindrical membrane ($Bi = 10, Bi_D = 2, Bi_p = 100, T_w = 5$).

In order to extract more data with respect to the gas composition in the cylindrical membrane, we carried out simulations taking a long-term gaseous permeation into account. Figure 3.68 shows this evolution for two different values of the membrane Biot number, which, in fact, is a measure of the membrane mass transfer resistance. We can observe that, over a long period, the dimensionless species concentration increases linearly, indicating that the permeate flux through the membrane wall has a constant value. This observation is in good agreement with the high value of the Biot number.

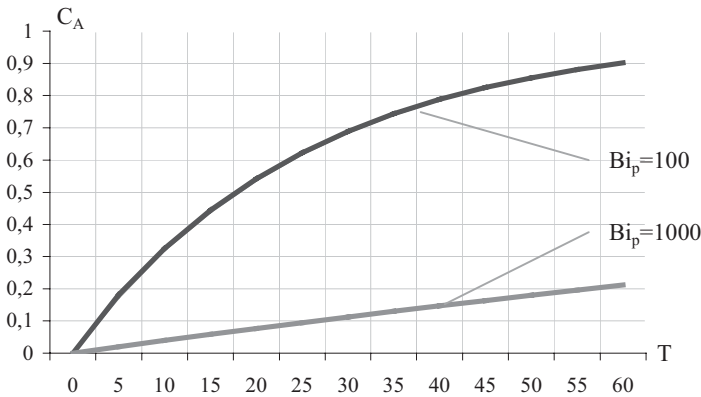


Figure 3.68 Evolution with time of the dimensionless concentration of species A.

If a light gas permeates through a 1 mm thick membrane, the Biot number corresponds to the highest value in Fig. 3.68. If we assume the pressure to be equal to 1 and normal temperature, then the gas flux will be 10^{-7} kmole/(m² s). With some light modifications, the software used for these simulations can be adapted to simulate the cases where the values of the Biot number of the membrane change with time. The Biot number evolution can occur in different situations when the membrane transport properties change, such as when the membrane is continuously clogged (e.g. in hydrocarbon dehydrogenation reactions in which coke is formed). The simulations presented here, as well as the observations exposed during the model presentation, show that it is not difficult to model and to simulate more complex cases such as membrane reactors. In such multifunctional chemical engineering devices, one or more reaction products or reactants can permeate through the membrane with different selectivity [3.56].

In membrane reactors, the reaction and separation processes take place simultaneously. This coupling of processes can result in the conversion enhancement of the thermodynamically-limited reactions because one or more of the product species is/are continuously removed. The performance of such reactors depends strongly on the membrane selectivity as well as on the general operating conditions which influence the membrane permeability.

3.5

Some Aspects of Parameters Identification in Mathematical Modelling

The notion of model parameters defines one or more numerical values that are contained as symbolic notations in the mathematical model of a process. These numerical values cannot be obtained without any experimental research. In reality, the most important part of experimental research is dedicated to the identification of the models' parameters. Generally, all the experimental works, laboratory methods and published papers beginning with the words “*determination of.....*” are in fact particular problems of identification of parameters. The chemical and biochemical sciences use various and countless models that introduce various types of parameters into their description. We can single out the real parameters that have a physical dimension so as to accept a dimensional formula. Indeed, they are related with a process state or with material properties that characterize the process. They differ from abstract parameters, which can have a dimensional formula but are an artificial creation. The parameters characterize the investigated process and not the mathematical model in which they appear as a consequence. At the same time, they can be considered as a special class of input variables of the process. Indeed, when we start with a problem of parameter identification, then we *a priori* accept a mathematical model, which contains these parameters for the process evolution. The problem of identifying parameters is formulated schematically in Fig. 3.69.

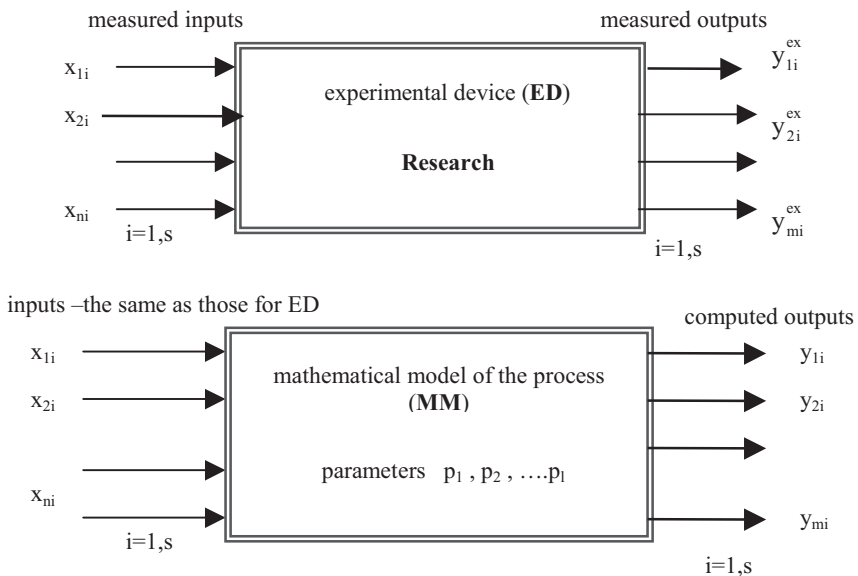


Figure 3.69 Introduction to a problem of identifying the parameters of a process.

We can notice that, when a total number of “s” experimental measures have been made for the outputs, the result of the experimental investigation of the process is given by the vector:

$$Y_i^{\text{ex}} = \begin{bmatrix} y_{1i}^{\text{ex}} \\ y_{2i}^{\text{ex}} \\ \vdots \\ y_{mi}^{\text{ex}} \end{bmatrix}, \quad i = 1, s$$

The vector Y_i^{ex} is obtained for s coupled values of the input process variables, so we can consider the vector inputs as follows:

$$X_i = \begin{bmatrix} x_{1i} \\ x_{2i} \\ \vdots \\ x_{ni} \end{bmatrix}, \quad i = 1, s$$

At the same time, the mathematical model of the process (MM) can produce – for the established values of the vector locations of the input process – the following values of the output vector:

$$Y_i = \begin{bmatrix} y_{1i} \\ y_{2i} \\ \vdots \\ y_{ni} \end{bmatrix}, \quad i = 1, s$$

If the values of the vector of parameters $P = [p_1, p_2, \dots, p_l]$ are known and if we obtain analogous results for the measured and MM outputs for the same input variables, then we can consider that the set of parameter values of model p_1, p_2, \dots, p_l are good enough.

The theory and the practice of parameter identification concern the assembly of procedures and methods showing the estimation of the values of p_1, p_2, \dots, p_l with the objective of having similar values for vectors Y_i^{ex} and Y_i . Generally, the parameters of a process are linked with various types of dependences called *constraints*. Constraints show that each parameter presents a region where a minimal and a maximal value is imposed and can be classified according to equality, inequality and inclusion constraints. Inclusion constraints are frequently transformed into inequality constraints because the latter have the quality of being easily introduced into the overall identification problem.

The formulation of the mathematical problem of parameter identification for an actual case needs the use of the following general particularizations given below:

1. *One relation or an assembly of relations* that contains the condition necessary to impose the absence of important differences between the computed outputs and experimental outputs. This relation or assembly of relations frequently contains the requirement of a minimal dispersion (variance) between computed and experimental process outputs. So we need to minimize the function:

$$\Phi(p_1, p_2, \dots, p_l) = \sum_{k=1}^m \sum_{i=1}^s (y_{ki} - y_{ki}^{\text{ex}})^2 \quad (3.189)$$

In the case of process exit coded by k , this equation can also be written as follows:

$$\Phi(p_1, p_2, \dots, p_l) = \sum_{k=1}^m \sum_{i=1}^s [(F_k(p_1, p_2, \dots, p_l, x_{1i}, x_{2i}, \dots, x_{ni}) - y_{ki}^{\text{ex}})^2] = \min \quad (3.190)$$

where $F_k(p_1, p_2, \dots, p_l, x_{1i}, x_{2i}, \dots, x_{ni})$, $k = 1, m$ give the computed y_{ki} values of the model. If a minimal dispersion between the computed and experimental results is necessary for each process output, then we must minimize the following assembly of functions:

$$\Phi_k(p_1, p_2, \dots, p_l) = \sum_{i=1}^s [F_k(p_1, p_2, \dots, p_l, x_{1i}, x_{2i}, \dots, x_{ni}) - y_{ki}^{\text{ex}}]^2 = \min ; k = 1, 2, \dots, m \quad (3.191)$$

In addition to the formulation that minimizes the dispersion described above, other mathematical expressions have been suggested with the purpose of obtaining the values of the parameters by requiring the model to reproduce the experimental data.

2. *An assembly of relations* that contains the introduction of expressions for equality type constraints; this assembly links some or all of the parameters of the model. From the mathematical viewpoint we can write these relations as follows:

$$H_j(p_1, p_2, \dots, p_l) = 0, \dots, j = 1, \dots, l \quad (3.192)$$

We observe here that we have “ l ” independent relations for “ l ” number of parameters. However, it is not strictly necessary to have the same number of parameters and relations that characterizes the equality type inter-parameter links.

3. *An assembly of relations* that contains the inequality type constraints which are considered for all parameters of an incomplete group of parameters or for only one parameter. We write these relations as follows:

$$G_j(p_1, p_2, \dots, p_l) \succ 0, \dots, j = 1, \dots, l \quad (3.193)$$

$$L_j(p_1, p_2, \dots, p_l) \prec 0, \dots, j = 1, \dots, l \quad (3.194)$$

It is important to notice that the equality and inequality type constraints described above can be absent in a problem of parameter identification.

The methods for identifying the parameters of a model can be classified in terms of the complexity of the mathematical model and constraints accepted for its parameters.

All the methods used for the identification of parameters are in fact the particularizations of the general methods to determine an extreme function. This func-

tion can be simple or complicated and can be given by one or more algebraic equations or can be introduced by an assembly of relations that contains differential equations or partial differential equations. The classification for these methods is given in Table 3.16.

Table 3.16 Classification of the methods for identifying the parameters of a model.

n	Type of method	Method name	Required conditions	Examples
1	Analytical methods	Pure analytical method	<ol style="list-style-type: none"> 1. Deterministic mathematical model given by analytical functions that are differentiable with respect to each parameter 2. Without constraints 	The latest small squares method
		Lagrange coefficients method	<ol style="list-style-type: none"> 1. Deterministic mathematical model given by analytical functions that are differentiable respect to each parameter 2. With constraints of equality type 	
		Variational methods	<ol style="list-style-type: none"> 1. Deterministic mathematical model given by analytical or numerical functions that are differentiable respect to each parameter 2. With or without constraints 	
2	Mathematical programming methods	Method of geometrical programming	<ol style="list-style-type: none"> 1. Deterministic mathematical model given as: $\Phi(p_1 \dots p_l) = \sum_{j=1}^1 C_j P_j(p_1 \dots p_l)$ where $P_j(p_1 \dots p_l) = \sum_{i=1}^1 P_i^{a_{ij}}$ 2. Without constraints. 	
		Methods of dynamic programming	<ol style="list-style-type: none"> 1. Mathematical model that describe a process with sequential states 2. With or without constraints 	
		Methods of linear programming	<ol style="list-style-type: none"> 1. Deterministic mathematical model given as: $\Phi(p_1 \dots p_l) = \alpha_1 p_1 + \alpha_2 p_2 + \dots \alpha_l p_l$ 2. With inequality type constraints 	The simplex method
3	The gradient methods	Various methods	<ol style="list-style-type: none"> 1. Deterministic process mathematical model especially given by differential equations 2. With or without inequality type constraints 	The very high slope method

n	Type of method	Method name	Required conditions	Examples
4	The combined methods	Various variants	<ol style="list-style-type: none"> 1. Process mathematical models with distributed inputs 2. Capacity to be associated with a Kalman filter 3. Without inequality type constraints 	The maximum likelihood method

It is important to point out that to identify the parameters of the model, the experimental research made with physical laboratory models (apparatus) has previously established the experimental working methods that allow the identification of the actual process parameters. These experimental methods tend to be promoted as standardized methods and this reduces the dimension of the problem that is formulated for identifying the parameters of the model to the situations where $\Phi(p_1, p_2, \dots, p_l)$ contains one, two or a maximum of three parameters to be estimated simultaneously.

3.5.1

The Analytical Method for Identifying the Parameters of a Model

This type of method includes the classical methods, which are based on the observation that the minimal value of function $\Phi(p_1, p_2, \dots, p_l)$ is quite near zero. Indeed, we can derive the conditions of a minimal value of $\Phi(p_1, p_2, \dots, p_l)$ which can be written as a system of algebraic equations (3.195) where the unknowns are parameters p_1, p_2, \dots, p_l .

$$\begin{cases} \frac{\partial \Phi(p_1, p_2, \dots, p_l)}{\partial p_1} = 0 \\ \frac{\partial \Phi(p_1, p_2, \dots, p_l)}{\partial p_2} = 0 \\ \frac{\partial \Phi(p_1, p_2, \dots, p_l)}{\partial p_l} = 0 \end{cases} \quad (3.195)$$

The applicability of this method is limited by the form of function $\Phi(p_1, p_2, \dots, p_l)$ that must present an analytical expression with respect to each parameter (p_1, p_2, \dots, p_l) . At the same time, the dimension and the nonlinearity of system (3.195) can also be considered as the limitative factors of this method. Various concrete formulations of system (3.195) can be obtained for the mathematical model of an actual process. For example, if, in Fig. 3.69, we consider that we have only one output where y_i^{ex} and y_i $i = 1, s$ are, respectively, the measured and the computed output values of the process and if we accept that the mathematical model of the process is given by Eqs. (3.196), then the function which must be minimized is given by relation (3.197):

$$y = p_0 + p_1 f_1(x_1, x_2, \dots, x_n) + p_2 f_2(x_1, x_2, \dots, x_n) + \dots + p_L f_L(x_1, x_2, \dots, x_n) \quad (3.196)$$

$$\Phi(p_1, p_2, \dots, p_L) = \sum_{i=1}^s \left([p_0 + p_1 f_1(x_{1i}, x_{2i}, \dots, x_{ni}) + \dots + p_L f_L(x_{1i}, x_{2i}, \dots, x_{ni})] - y_i^{\text{ex}} \right)^2 = \min \quad (3.197)$$

For this case the system (3.195) leads to the following algebraic system:

$$\left\{ \begin{array}{l} sp_0 + p_1 \sum_{i=1}^s f_1(x_{1i}, x_{2i}, \dots, x_{ni}) + p_2 \sum_{i=1}^s f_2(x_{1i}, x_{2i}, \dots, x_{ni}) + \dots + p_L \sum_{i=1}^s f_L(x_{1i}, x_{2i}, \dots, x_{ni}) = \sum_{i=1}^s y_i^{\text{ex}} \\ p_0 \sum_{i=1}^s f_1(x_{1i}, x_{2i}, \dots, x_{ni}) + p_1 \sum_{i=1}^s [f_1(x_{1i}, x_{2i}, \dots, x_{ni})]^2 + p_2 \sum_{i=1}^s f_2(x_{1i}, x_{2i}, \dots, x_{ni}) f_1(x_{1i}, x_{2i}, \dots, x_{ni}) + \dots \\ p_L \sum_{i \gg 1}^s f_L(x_{1i}, x_{2i}, \dots, x_{ni}) f_1(x_{1i}, x_{2i}, \dots, x_{ni}) = \sum_{i=1}^s y_i^{\text{ex}} f_1(x_{1i}, x_{2i}, \dots, x_{ni}) \\ p_0 \sum_{i=1}^s f_2(x_{1i}, x_{2i}, \dots, x_{ni}) + p_1 \sum_{i=1}^s f_1(x_{1i}, x_{2i}, \dots, x_{ni}) f_2(x_{1i}, x_{2i}, \dots, x_{ni}) + p_2 \sum_{i=1}^s [f_2(x_{1i}, x_{2i}, \dots, x_{ni})]^2 + \dots \\ p_L \sum_{i \gg 1}^s f_L(x_{1i}, x_{2i}, \dots, x_{ni}) f_1(x_{1i}, x_{2i}, \dots, x_{ni}) = \sum_{i=1}^s y_i^{\text{ex}} f_1(x_{1i}, x_{2i}, \dots, x_{ni}) \\ p_0 \sum_{i=1}^s f_L(x_{1i}, x_{2i}, \dots, x_{ni}) + p_1 \sum_{i=1}^s f_1(x_{1i}, x_{2i}, \dots, x_{ni}) f_L(x_{1i}, x_{2i}, \dots, x_{ni}) + p_2 \sum_{i=1}^s f_2(x_{1i}, x_{2i}, \dots, x_{ni}) f_L(\dots) + \dots \\ p_L \sum_{i \gg 1}^s [f_L(x_{1i}, x_{2i}, \dots, x_{ni})]^2 = \sum_{i=1}^s y_i^{\text{ex}} f_L(x_{1i}, x_{2i}, \dots, x_{ni}) \end{array} \right. \quad (3.198)$$

The solution of this system allows the estimation of the numerical values of parameters p_1, p_2, \dots, p_L . This system is in fact the expression of the least squares method. This method is used for the development and solution of example 3.5.1.1.

3.5.1.1 The Pore Radius and Tortuosity of a Porous Membrane for Gas Permeation

Gaseous permeation can be used for the characterization of porous membranes using an apparatus working with the technique of fixed volume–variable pressure as shown in Fig. 3.70. The technique, which was initially developed for dense polymer membranes, is based on the recording of the pressure evolution with time of a downstream compartment, which is separated from an upstream compartment filled with a pure gas by a flat membrane. Before starting the experiments, both compartments are put under very low pressure and, at the initial time of the measurements, a relatively high pressured pure gas is introduced into the upstream compartment [3.59].

The pressure evolution of the downstream compartment versus time is recorded in a curve which generally has a typical “s” shape which presents an initial small nonlinear increase and later becomes time linearly dependent. At the end of the experiment, when the gradient becomes negligible, the curve presents a nonlinear decrease [3.60].

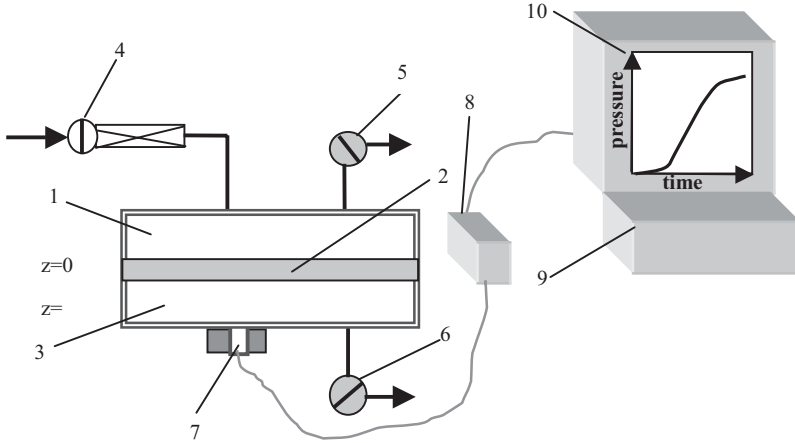


Figure 3.70 Scheme of a gas permeation apparatus. 1 – upstream compartment, 2 – membrane, 3 – downstream compartment (V_{inf}), 4 – pure gas entrance valve, 5 and 6 – vacuum valves, 7 – pressure transducer (P_{inf}), 8 – data acquisition system, 9 – computer, 10 – curve pressure vs. time.

Once the descriptive model has been realized, we need to make the mathematical model of the process, which can be used to identify the mean pore radius of the membrane pores and the associated tortuosity. Before starting with the establishment of the model, we consider that the elementary processes allowing the gas flow through the membrane are a combination of Knudsen diffusion with convective flow. If we only take into account the linear part of the curve of the pressure increase with time then we can write:

$$p_1 = \alpha_1 + \beta\tau \tag{3.199}$$

Indeed, the gas flow rate that permeates through the membrane is:

$$G_M = V_{inf} \frac{dc}{d\tau} = \frac{V_{inf}}{RT} \frac{dp_{inf}}{d\tau} = \frac{V_{inf}}{RT} \beta \tag{3.200}$$

and then we obtain for the measured gas flux:

$$N_A = \frac{G_M}{\epsilon S m} = \frac{V_{inf}}{RT \epsilon S m} \beta \tag{3.201}$$

the slope β of the pressure–time dependence is estimated with the variation of p_i with τ_i , and, consequently, we can transform the equation above as follows:

$$N_{Ai}^{ex} = \frac{V_{inf}}{RT \epsilon S m} \frac{p_{i+1} - p_i}{\tau_{i+1} - \tau_i} \tag{3.202}$$

As explained above, we consider that the gas transport is carried out by the Knudsen and hydrodynamic flow through the porous media, then the theoretical expression for the gas flux is given by the following relation:

$$N_A = - \left(\frac{2}{3} r\psi \sqrt{\frac{8RT}{\pi M}} + r^2\psi \frac{p}{8\eta} \right) \frac{dp}{RTdx} \quad (3.203)$$

Because N_A is constant, we can separate out the variables of the relation (3.203), then the integral relation (3.205) concerning the gas flux through the membrane is obtained after integrating the whole thickness of the membrane:

$$N_A \int_0^\delta dx = \int_{p_1}^{p_2} \left(\frac{2}{3} r\psi \sqrt{\frac{8RT}{\pi M}} + r^2\psi \frac{p}{8\eta} \right) dp \quad (3.204)$$

$$N_A = \frac{4\sqrt{2}}{3\delta} \frac{r\psi}{\sqrt{RT\pi M}} (p_2 - p_1) + \frac{r^2\psi}{16\eta\delta} (p_2^2 - p_1^2) \quad (3.205)$$

Relation (3.205) can be written in the form (3.206) where it shows the expression for the model of instantaneous gas flux through the membrane:

$$N_{Ai} = \frac{4\sqrt{2}}{3\delta} \frac{r\psi}{\sqrt{RT\pi M}} (p_{2i} - p_{1i}) + \frac{r^2\psi}{16\eta\delta} (p_{2i}^2 - p_{1i}^2) \quad (3.206)$$

If p_{1i} increases linearly with time; then p_{2i} can be calculated by $p_{2i} = p_0 - \beta_i \tau_i$ in Eq. (3.206). Here, bottom and top compartments have been considered to have the same volume. It is not difficult to observe that the parameters requiring identification are $r\psi$ and $r^2\psi$ where r is the mean pore radius and ψ the tortuosity. In this case, in accordance with relation (3.189), the function for the minimization will be written as follows:

$$\Phi(r\psi, r^2\psi) = \sum_{i=1}^s \left[\frac{4\sqrt{2}}{3\delta} \frac{r\psi}{\sqrt{RT\pi M}} (p_{2i} - p_{1i}) + \frac{r^2\psi}{16\eta\delta} (p_{2i}^2 - p_{1i}^2) - \frac{V \inf}{RT\epsilon Sm} \frac{p_{1i+1} - p_{1i}}{\tau_{i+1} - \tau_i} \right]^2$$

By introducing the notations $A = \frac{4\sqrt{2}}{3\delta} \frac{r\psi}{\sqrt{RT\pi M}}$, $B = \frac{r^2\psi}{16\eta\delta}$, $\alpha = \frac{V \inf}{RT\epsilon Sm}$ and by computing the conditions that impose the minimal value of the function

$\Phi(r\psi, r^2\psi)$, we obtain equations system (3.207) where N represents the number of experiments considered for the parameter identification.

$$\begin{cases} A \sum_{i=1}^N (p_{2i} - p_{1i})^2 + B \sum_{i=1}^N (p_{2i}^2 - p_{1i}^2)(p_{2i} - p_{1i}) = \alpha \sum_{i=1}^N \left(\frac{p_{1i+1} - p_{1i}}{\tau_{i+1} - \tau_i} \right) (p_{2i} - p_{1i}) \\ A \sum_{i=1}^N (p_{2i} - p_{1i})(p_{2i}^2 - p_{1i}^2) + B \sum_{i=1}^N (p_{2i}^2 - p_{1i}^2)^2 = \alpha \sum_{i=1}^N \left(\frac{p_{1i+1} - p_{1i}}{\tau_{i+1} - \tau_i} \right) (p_{2i}^2 - p_{1i}^2) \end{cases} \quad (3.207)$$

The solution to equation system (3.207) will allow calculation of the values of $r\psi$ and $r^2\psi$, which are obtained after the estimation of A and B .

In our actual example, the first step for this calculation is the determination of $r\psi$ and $r^2\psi$ by using data from Tables 3.17 and 3.18. These data have been obtained with an experimental device with $V_{inf} = V_{sup} = 7 * 10^{-5} \text{ m}^3$ $\delta = 4 * 10^{-3} \text{ m}$ and for the following gases: He ($M = 2 \text{ kg/kmol}$, $\eta = 10^{-5} \text{ kg/ (m s)}$) and N_2 ($M = 28 \text{ kg/kmol}$, $\eta = 1.5 * 10^{-5} \text{ kg/ (m s)}$). The starting pressure at the upstream compartment is $p_0 = 2 * 10^5 \text{ N/m}^2$ and $1.5 * 10^3 \text{ N/m}^2$ for the downstream compartment.

Table 3.17 Pressure evolution in the downstream compartment for He permeation.

C.n	1	2	3	4	5	6
τ (s)	10	20	50	70	90	110
p_1 (N/m ²)	10^4	$2.5 * 10^4$	$4 * 10^4$	$5.52 * 10^4$	$7 * 10^4$	$8.41 * 10^4$

Table 3.18 Pressure evolution in the downstream compartment for N_2 permeation.

C.n	1	2	3	4	5	6
τ (s)	40	80	120	160	200	240
p_1 (N/m ²)	$2.06 * 10^4$	$3.41 * 10^4$	$4.72 * 10^4$	$6.06 * 10^4$	$7.41 * 10^4$	$8.7 * 10^4$

The algorithm for the experimental data processing follows the steps:

1. We introduce the fixed data of the problem:
 $V_{inf}, V_{sup}, \delta, S_m, \epsilon, M, \eta, p_0, R; T; N;$
2. We give the evolution of p_{1i} versus $\tau_i, i = 1, N;$
3. We compute the mean slope of the p_{1i} versus τ_i dependence:

$$\beta = \frac{p_{1N-1} - p_{12}}{\tau_{N-1} - \tau_2};$$

4. We establish the corresponding p_{2i} value for each τ_i :
 $p_{2i} = p_0 - \beta_i \tau_i, i = 1, N;$
5. We compute: $\alpha = V_{inf}/(RT\epsilon S_m);$
6. We obtain the values of the following sums:

$$S_1 = \sum_{i=1}^N (p_{2i} - p_{1i})^2, \quad S_2 = \sum_{i=1}^N (p_{2i}^2 - p_{1i}^2)(p_{2i} - p_{1i}),$$

$$S_3 = \alpha \sum_{i=1}^N \left(\frac{p_{1i+1} - p_{1i}}{\tau_{i+1} - \tau_i} \right) (p_{2i} - p_{1i}), \quad S_4 = \sum_{i=1}^N (p_{2i}^2 - p_{1i}^2)^2,$$

$$S_5 = \alpha \sum_{i=1}^N \left(\frac{p_{i+1} - p_{1i}}{\tau_{i+1} - \tau_1} \right) (p_{2i}^2 - p_{1i}^2);$$

7. We solve system (3.207) for A and B which is written as follows:

$$\begin{cases} AS_1 + BS_2 = S_3 \\ AS_2 + BS_4 = S_5 \end{cases} \quad (3.208)$$

8. We compute $r\psi$ and $r^2\psi$ by using the computed A and B.

Figure 3.71 contains the MathCAD™ working text of this problem in the case of N_2 permeation. The values obtained for $r\psi = 1.2 \cdot 10^{-10}$ m and $r^2\psi = 0.85 \cdot 10^{-20}$ m² are almost the same as those calculated for He permeation.

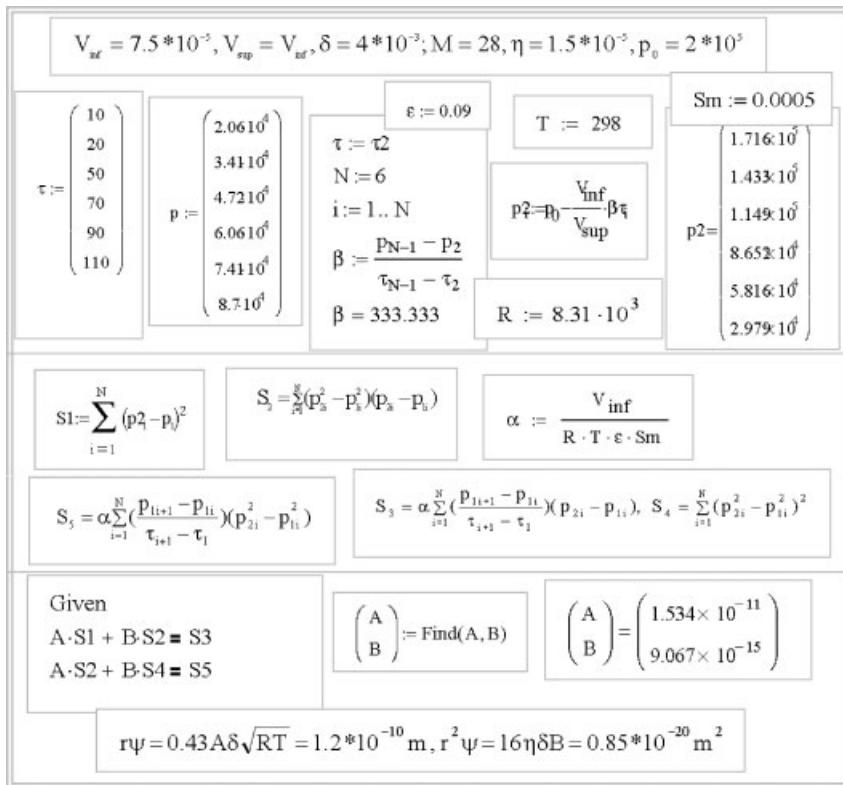


Figure 3.71 Software working text for example 3.6.1.1.

3.5.2

The Method of Lagrange Multipliers

This high confidence method is used when one or more equality constraints are imposed on the parameters of the process [3.61]. So, if our problem is to obtain the minimal value of function $\Phi(p_1, p_2, \dots, p_L)$ and the parameters' requirement to verify the constraints $f_i(p_1, p_2, \dots, p_L)$, $i = 1, g$ simultaneously, then the solution is obtained from the formulation of the following auxiliary function:

$$L(p_1, p_2, \dots, p_L, \lambda_1, \dots, \lambda_g) = \Phi(p_1, p_2, \dots, p_L) + \sum_{i=1}^g \lambda_i f_i(p_1, p_2, \dots, p_L) \quad (3.209)$$

Function $L(p_1, p_2, \dots, p_L, \lambda_1, \dots, \lambda_g)$ supports the same minimization as $\Phi(p_1, p_2, \dots, p_L)$ but here, the number of parameters is increased with $\lambda_1, \lambda_2, \dots, \lambda_g$ which are called the Lagrange multipliers. Then, the equation system that must be solved here is written as:

$$\begin{cases} \frac{\partial L(p_1, p_2, \dots, p_L, \lambda_1, \dots, \lambda_g)}{\partial p_k} = 0 & , \quad k = 1, L \\ \frac{\partial L(p_1, p_2, \dots, p_L, \lambda_1, \dots, \lambda_g)}{\partial \lambda_i} = 0 & , \quad i = 1, g \end{cases} \quad (3.210)$$

From Eq. (3.210) we can obtain one or more set(s) of values for p_1, p_2, \dots, p_L which give for function $\Phi(p_1, p_2, \dots, p_L)$ one or more extreme values. If we have various extremes for this function, we choose the set of parameters which gives a physical meaning of the problem. With respect to the Lagrange method, we can observe that each equality type constraint introduces its parameter in the building of $L(p_1, p_2, \dots, p_L, \lambda_1, \dots, \lambda_g)$. Indeed, this method is strictly recommended when we have equality type constraints.

3.5.2.1 One Geometrical Problem

A chemical engineer who is designing a drug factory has to solve a problem which concerns the building of a spherical reservoir over a conical support as shown in Fig. 3.72. For this construction, the total volume must not exceed 5 m^3 . At the same time, the relation between the sphere diameter and the cone height is imposed in accordance with the golden section principle ($D_s = I/5$).

The building process must be carried out minimizing the operations such as surface finishing, colouring, etc. After a few days, the engineer concludes that it is not possible to build such a structure, even though, the motivation for the response remains unknown. In order to know the reasons that motivated the engineer's decision we will use the parameters identification method of Lagrange multipliers. To do so, we have to minimize the function that represents the surface of the building:

$$F(D, G, I) = \pi DG + \pi DI/2 + \pi(I/5)^2 \quad (3.211)$$

with the constraint that imposes a fixed building volume :

$$C(D, G, I) = \pi G(D/2)^2 + \pi(I/3)(D/2)^2 + \pi/6(I/5)^3 - V \tag{3.212}$$

The associated Lagrange function $L(G, I, D, \lambda) = F(G, H, D) + \lambda C(G, H, I)$ gives the following equation system:

$$\begin{cases} G + 0.5 I + 0.5\lambda G D + 0.166\lambda I D = 0 \\ 0.5D + 0.08I + 0.0833\lambda D^2 + 0.004\lambda I^2 = 0 \\ 0.25\lambda D = -1 \\ 0.25GD^2 + 0.0833ID^2 + 0.001333 I^3 = V/\pi \end{cases} \tag{3.213}$$

Considering that the fixed volume is $V = 5 \text{ m}^3$, the solution to this system results in the following values for the heights and diameter: $G = -1.45 \text{ m}$, $I = 8.8 \text{ m}$ and $D = 1.43 \text{ m}$. We can notice here that the value of G is not realistic.

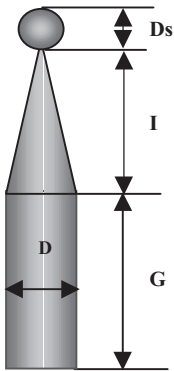


Figure 3.72 Scheme of example 3.6.2.1.

3.5.3

The Use of Gradient Methods for the Identification of Parameters

Among the methods used to identify the parameters of a process, the gradient methods play an important role because of their excellent adaptation to software making. These methods are generally quite efficient for solving problems that require the establishment of extreme positions for the assemblies of linear or non-linear functions. This statement is especially true when the functions of assemblies are given through differential or partial differential equations. This is the major reason why these methods are widely used. They are based on the establishment of the values of momentary parameters that produce the highest variation of the minimized or maximized function. From the geometrical viewpoint, this fact is equivalent to a displacement of the function along its gradient towards the extreme position. It is known that the gradient in a point of the surface of response has an orthogonal state with respect to the surface. The different gradi-

ent methods are classified depending on: (i) the procedure for the localization of the calculation point; (ii) the length of the step that characterizes the motion of the calculation point; (iii) the number of tests along the established direction; (iv) the criteria used to stop the calculation; (v) the global method simplicity.

The most important aspect of these methods, which follow the localization of an extreme for a given function, is represented by the identification of the most rapid variation of the function for each calculation point on the direction. For this problem of parameter identification, the function is given by the expression $\Phi(p_1, p_2, \dots, p_L)$. The graphic representation of Fig. 3.73 shows the function–gradient relation when the vector gradient expression is written as in relation (3.214).

$$\vec{\text{grad}}\Phi = \frac{\partial\Phi}{\partial p_1}\vec{i}_1 + \frac{\partial\Phi}{\partial p_2}\vec{i}_2 + \dots + \frac{\partial\Phi}{\partial p_L}\vec{i}_L = \text{vect}\left(\frac{\partial\Phi}{\partial p_1}, \frac{\partial\Phi}{\partial p_2}, \dots, \frac{\partial\Phi}{\partial p_L}\right) \tag{3.214}$$

Here $\vec{i}_1, \vec{i}_2, \dots, \vec{i}_L$ are the axis vectors expressed in unitary coordinates.

From the theoretical viewpoint, the scalar value of the partial derivate $\partial\Phi/\partial p_i$ is the vector gradient projection to the axis p_i . Indeed, it can be described with their module and the spatial angle between the vector of the gradient and the axis p_i as in relation (3.215):

$$\text{grad}\Phi = \sqrt{\sum_{i=1}^L \left(\frac{\partial\Phi}{\partial p_i}\right)^2} \cos(\vec{\text{grad}}\Phi, \vec{i}_i) \tag{3.215}$$

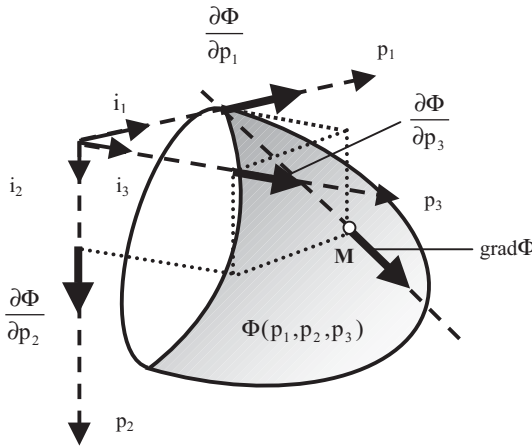


Figure 3.73 Function $\Phi(p_1, p_2, p_3)$, the M point gradient and its axis projections.

Concerning the problem of the direction of the advancement, it is important to select the length of the step of progression. It is evident that this selection first depends on the relations characterizing the response surface. When the processes are described with a complex model, this surface can only be given in a numerical form. A small length of the advancing step imposes a long and difficult computation. When the advancing step is big, it is possible to cross over the wanted

extreme. These problems can be avoided using a variable length step; at the beginning, we use a big length step and, when an extreme neighbourhood is detected, the length of the step is progressively decreased. The step dimension Δp_i , $i = 1, \dots, L$ must verify first the condition that all calculation points are placed onto the gradient line beginning at the starting point and, secondly, if the constraints are active, the step dimension must respect them. The length of the step for the variable (parameter) p_i is computed using the partial derivatives of the problem function with respect to the current calculation point:

$$\Delta p_i = \frac{k \frac{\partial \Phi}{\partial p_i}}{\sqrt{\sum_{i=1}^L \left(\frac{\partial \Phi}{\partial p_i} \right)^2}} \quad (3.216)$$

Here k is a constant value, which is the same for the displacement of all variables (parameters). It is not difficult to appreciate that the value of k is very important for the step length.

Concerning the requirement to have an orthogonal gradient to the surface response of the process, we can notice that it first imposes the base point; if, for one of these 'L' directions, the length of the step is too big, then the vector that starts from the base point should not respect the orthogonal condition between the surface of the response and the new point where we will stop the motion. The selection of an adequate step length presumes that the derivatives of the function related to the new point stay close to the derivatives of the base point.

Despite the differences that exist between various gradient methods, the algorithm to determine the extreme point for a given function remains identical with respect to some general common guidelines [3.62, 3.63]:

1. we choose a base point;
2. starting from this point we establish the direction of the development;
3. we find the step length to prepare the motion along the gradient line;
4. we establish the position of the new point and consider whether it is a current point or must be transformed into a new base point;
5. we compare the value of the function for the new point and for the new base point with the value of the function of the former base point; the value of the new function is normally lower;
6. we select the new development direction for the new base point and the computation gives the area of the minimum function value; here small motion steps are recommended.

3.5.3.1 Identification of the Parameters of a Model by the Steepest Slope Method

The steepest slope method is a particular class of gradient method. This method will be illustrated with an example of the minimization of a function with two parameters with an explicit graphic interpretation. Figure 3.74 gives an excellent introduction to the steepest slope method (SSM) by showing some curves with constant Φ . They are placed around the minimum function and near the first base point. The motion progresses along the gradient line which is localized for each selected point. The development of this method starts at the first base point $M_0(p_1^0, p_2^0)$ beginning the exploration of the steepest slope by computation. We increase p_1^0 by δp_1^0 and establish the value of $\Phi(p_1^0 + \delta p_1^0, p_2^0)$. Now we repeat the computation by increasing p_2^0 by δp_2^0 and then $\Phi(p_1^0, p_2^0 + \delta p_2^0)$ is obtained. With $\Phi(p_1^0 + \delta p_1^0, p_2^0)$ and $\Phi(p_1^0, p_2^0 + \delta p_2^0)$ we can estimate the values of the two partial derivatives:

$$\left(\frac{\partial \Phi}{\partial p_1}\right)_0 = \frac{\Phi(p_1^0 + \delta p_1^0, p_2^0) - \Phi(p_1^0, p_2^0)}{\delta p_1^0} \tag{3.217}$$

$$\left(\frac{\partial \Phi}{\partial p_2}\right)_0 = \frac{\Phi(p_1^0, p_2^0 + \delta p_2^0) - \Phi(p_1^0, p_2^0)}{\delta p_2^0} \tag{3.218}$$

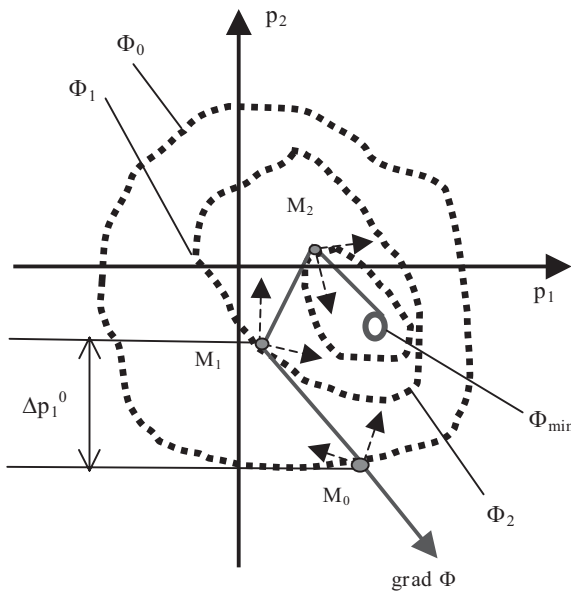


Figure 3.74 Scheme for the SSM graphic introduction.

These derivatives allow the selection of the length of the step displacement or, in other words, they control the computation of each parameter modification. Δp_1^0 and Δp_2^0 are recognized when we finish the exploring computation so when we have established the vector $\text{grad}\Phi$. The values of Δp_1^0 and Δp_2^0 are proportional to

the module of the vector $\vec{\text{grad}}\Phi$ but they are in the opposite direction. If the modifications of the values of these parameters can be determined using the partial derivatives shown in relation (3.219), then we can assert that the observations advanced previously were correct.

$$\Delta p_1^0 = -\alpha \left(\frac{\partial \Phi}{\partial p_1} \right)_0 \quad \Delta p_2^0 = -\alpha \left(\frac{\partial \Phi}{\partial p_2} \right)_0 \quad (3.219)$$

For a more general case, we can write the relation (3.219) in the form shown in Eq. (3.220), α is a constant in both relations:

$$\Delta p_i^0 = -\alpha \left(\frac{\partial \Phi}{\partial p_i} \right)_0 \quad i = 1, L \quad (3.220)$$

If, after each calculation step, we compute the net change ($\Delta\Phi$) of function Φ and it is negative, then we are progressing and we can continue (look at the line which join the points M_0 and M_1 in Fig. 3.74). If $\Delta\Phi > 0$, then the displacement has to be stopped and we begin a new exploration considering the last point position until we can establish a new good direction (such as M_1M_2 in Fig. 3.74). Step by step the computation tends to approach the minimum value of the investigated function. This fact is observed by the decrease in the values of the current advancing factor ε_n .

$$\varepsilon_n = \text{abs} \left(\frac{\partial \Phi}{\partial p_1} \right)_n + \text{abs} \left(\frac{\partial \Phi}{\partial p_2} \right)_n \quad (3.221)$$

In addition to SSM, other methods like the total gradient method (TGM) present the capacity to localize the minimal value of function $\Phi(p_1, p_2, \dots, p_L)$. The TGM operates like an SSM but it establishes the direction of the gradient at each calculation point; at the same time, it progressively decreases the length of the step. If we have one or more constraints in the SSM formulation, then these will be represented in Fig. 3.74 by lines or curves, which cannot be affected or crossed by the gradient line. In the case of a two-parameter problem these constraints can result in a closed surface that includes the minimum function value. For this situation, it is important for the first base point to be inside the constraint surface. Otherwise we cannot move the calculation point to the minimum value of the function due to what the displacement along the constraint becomes imposed so a free gradient line is not detected. In other words, this situation determines an infinite displacement around the constraint surface.

We can extend the observations given here for a two-parameter problem to cases with more parameters. As an example, when the problem has three parameters, then, the problem of closed constraint surface becomes the problem of closed constraint volume.

Fortunately, the problems where one or more parameters are identified towards experimental research, we do not have those constraints; consequently these precautions with respect to the base point selection and with respect to the length of displacement are not important.

Some important considerations have to be taken into account in order to efficiently use the SSM and all other gradient methods with rapid displacement towards a minimum function value [3.64]: (i) the good selection of the base point; (ii) the modification of the parameters' dimension from one step to another; (iii) the complexity of the process surface response; (iv) the number of constraints imposed on the parameters. In some cases we can couple the minimization of the function with the constraint relations in a more complex function, which will be analyzed again. In this case, the problem is similar to the Lagrange problem but it is much more complex.

3.5.3.2 Identifying the Parameters of an Unsteady State Perfectly Mixed Reactor

We carried out a decomposition reaction in the experimental device shown in Fig. 3.75. The reaction is endothermic and takes place in a permanently perfectly mixed (PM) reactor. As shown in Fig. 3.75, reactant A is fed at the reactor input in a liquid flow at constant concentration value. The heat necessary for the endothermic decomposition is supplied by an oil bath, which is electrically heated in order to maintain a constant temperature (t_e). The reactor operates at constant volume because input and output flows are similar.

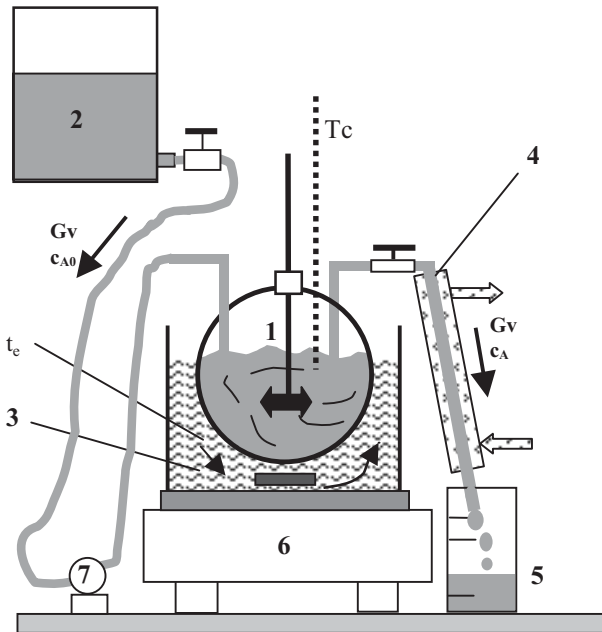


Figure 3.75 Laboratory scale plant with a continuous PM reactor.
1 – reactor, 2 – reservoir, 3 – oil bath, 4 – syphon and cooling device,
5 – collector, 6 – electrical heating device, 7 – pump.

The following input process variables are given or have been measured:

- the input and output flow rate are: $Gv = 10^{-6} \text{ m}^3/\text{s}$
- the value of the reaction enthalpy: $\Delta H_r = 60\,000 \text{ kJ/kg}$ of A species;
- the activation energy of the reaction: $E = 1\,400\,000 \text{ J/kmole}$ of A species;
- the temperature of the feed flow: $t_0 = 140 \text{ }^\circ\text{C}$;
- the initial temperature of the liquid in the reactor: $t_{00} = 200 \text{ }^\circ\text{C}$;
- the concentration of species A in the reactor feed: $c_{A0} = 50 \text{ kg/m}^3$;
- the initial concentration of species A in the reactor: $c_{A00} = 0 \text{ kg/m}^3$;
- the sensible heat capacity of the mass of liquid reacting: $c_p = 3000 \text{ J/(kg }^\circ\text{C)}$;
- the density of the liquid media: $\rho = 800 \text{ kg/m}^3$;
- the value of the heat transfer area between the oil bath and the reactor's vessel: $A_t = 0.03 \text{ m}^2$

When the oil bath reaches the set point of constant temperature, the experiment begins by starting the pump and activating the sample collecting device at the reactor's exit. During the experiments, the temperature of the liquid reacting mixture is continuously recorded. We measure the concentration of species A for each collected sample. The result of one set of experiments is given in Table 3.19. In this example, the reaction constant k_0 , the reaction order n and the heat transfer coefficient from oil to liquid mass reaction k are poorly estimated and then their values are calculated from the obtained experimental data.

Table 3.19 Evolution of the temperature and concentration of A with time at the exit flow of the reactor.

τ (s)	150	300	600	1500
c_A (kg/m ³)	3.4	4.3	4.7	4.95
t (°C)	185	135	80	64

To make the calculation for the identification of parameters k_0 , n , k by using the highest slope method (MHSM), we must determine the function that will be minimized and the mathematical model of the process which correlates these parameters with the computed values of c_A and t . Because we have the dependences $c_A - \tau$ and $t - \tau$ we can consider for the minimization the functions below written as:

$$\Phi_1(k_0, n, k) = \sum_{j=1}^4 \left(c_A(k_0, n, k, \tau_j) - c_A^{\text{exp}}(\tau_j) \right)^2 \quad (3.222)$$

$$\Phi_2(k_0, n, k) = \sum_{j=1}^4 \left(t(k_0, n, k, \tau_j) - t^{\text{exp}}(\tau_j) \right)^2 \quad (3.223)$$

The relations defining functions $\Phi_1(k_0, n, k)$ and $\Phi_2(k_0, n, k)$ contain the values of $c_A(k_0, n, k, \tau_j)$ and $t(k_0, n, k, \tau_j)$, which are obtained here from the mathematical model of the reactor. The MHSM supply the values of k_0, n, k for the mathematical model.

The process is described by the mathematical model of a nonisothermal, unsteady state, continuous and perfectly mixed reactor. It is defined by the below differential equations:

$$\frac{dc_A}{d\tau} = \frac{Gv}{V}(c_{A0} - c_A) - k_0 \exp\left(-\frac{E}{RT}\right) c_A^n \quad (3.224)$$

$$\frac{dt}{d\tau} = \frac{Gv}{V}(t_0 - t) - \frac{kA}{V\rho c_p}(t - t_r) + \frac{k_0 \exp\left(-\frac{E}{RT}\right)}{\rho c_p} c_A^n (-\Delta H_r) \quad (3.225)$$

$$\tau = 0 \quad c_A = c_{A00} \quad t = t_{00} \quad (3.226)$$

The solution to the problem of identifying parameters frequently needs the integration of the mathematical model of the process. The software used for this purpose is shown in Fig. 3.76. The starting point of MHSM is M_0 ; it has the corresponding coordinates $M_0 = M_0(k_0^0 = 0.03, n^0 = 0.5, k^0 = 250)$ in the k_0, n, k axis system. If it is not possible to operate MHSM while simultaneously minimizing functions $\Phi_1(k_0, n, k)$ and $\Phi_2(k_0, n, k)$, we have to introduce a unique and dimensionless minimizing function.

```

Title Unsteady state continuous PM reactor
Select ngrid=1 variables ca(range=0,50) tt(range=20,400)
definitions
Gv=10**(-6) V=10**(-3) ca0=50 k0=unknown (will be established by MHSM)
E=1400000 deltaH=60000 k= unknown (will be established by MHSM)
A=0.03 ro=880 cp=3000 n= unknown (will be established by MHSM)
t00=200 tr=340 R=8310 t0=140 c00=0
initial values ca = c00 tt=t00
equations
dt(ca) = Gv*(ca0-ca)/V-k0*exp(-E/(R*(tt+273)))*(ca**n) { The ODE }
dt(tt)=Gv*(t0-tt)/V-k*A*(tt-tr)/(V*ro*cp)+k0*exp(-E/(R*(tt+273)))*(ca**n)*(-deltaH*1000)/ro/cp
boundaries region 1 { define a fictitious spatial domain }
start (0,0) line to (1,0) to (1,1) to (0,1) to finish
time 0 to 2000 { define the time range }
histories { Plot the solution: } history(ca) at (0.5,0.5) history(tt) at (0.5,0.5)
end

```

Figure 3.76 Numerical FlexPDE™ state of the mathematical model of the process (CPM reactor).

The example presented in Table 3.20 shows that the numerical transposition of a concrete example with the MHSM is not a straightforward problem. We can also

notice that to start the MHSM, the selection of the first base point must be the result of a primary selection process. Here, we can intuitively suggest the values of the parameters and, using the mathematical model of the process, we can find the proposal that shows a likeness and proximity between the computed and the experimentally measured values for the dependent process variables. The accepted proposal will be considered as the base point for the MHSM:

1. To identify the problems in which the process presents various exits, the use of a function for the minimization of each exit frequently attains contradictory situations when, for example, we must increase the value of a parameter in one function whereas the same parameter must be decreased in a second function. Nevertheless, if we can suggest a global function with rational participation of each partial function we can easily go on.
2. For the case when the dimensionless state of a global function is preferred for the computation, then we can operate with dimensionless process variables and with a dimensionless mathematical model of the process. However, we can also operate with dimensional variables but with partly dimensionless functions.

Table 3.20 The MHSM particularization developed to solve application 3.6.3.2.

STARTING POINT: $M_0(k_0^0 = 0.03, n^0 = 0.5, k^0 = 250)$

The computed values for dependences $c_A - \tau$ and $t - \tau$

τ (s)	150	300	600	1500
c_A (kg/m ³)	3.0	4.2	5.2	6.2
t (°C)	165	120	70	35

Φ_1 and Φ_2 values:

$$\Phi_1(k_0^0 = 0.03, n^0 = 0.5, k^0 = 250) = (3 - 3.4)**2 + (4.2 - 4.3)**2 + (5.2 - 4.5)**2 + (6.2 - 4.95)**2 = 2.2225 ;$$

$$\Phi_2(k_0^0 = 0.03, n^0 = 0.5, k^0 = 250) = (165 - 185)**2 + (120 - 135)**2 + (70 - 80)**2 + (35 - 60)**2 = 1350$$

$$E_1/k_0: k_0^{01} = 1.1 * k_0^0 = 0.033; M_0^{01}(k_0^0 = 0.033, n^0 = 0.5, k^0 = 250)$$

The computed values for dependences $c_A - \tau$ and $t - \tau$ (first exploration)

τ (s)	150	300	600	1500
c_A (kg/m ³)	2.8	3.8	4.6	5.6
t (°C)	160	110	62	26

Φ_1 and Φ_2 values:

$$\Phi_1(k_0^{01} = 0.033, n^0 = 0.5, k^0 = 250) = 1.045 ; (\Phi_2(k_0^{01} = 0.033, n^0 = 0.5, k^0 = 250) = 2685$$

Φ_1 decrease but Φ_2 increase and so increasing k_0 is not recommended

$$E_2//n: n^{01} = 1.1n^0 = 0.55; M_0^{02}(k_0^0 = 0.03, n^{01} = 0.55, k^0 = 250)$$

The computed values for dependences $c_A - \tau$ and $t - \tau$ (second exploration)

τ (s)	150	300	600	1500
c_A (kg/m ³)	3.	4	4.8	5.6
t (°C)	165	115	62	30

Φ_1 and Φ_2 values:

$$\Phi_1(k_0^0 = 0.03, n^{01} = 0.55, k^0 = 250) = 0.685$$

$$\Phi_2(k_0^0 = 0.03, n^{01} = 0.55, k^0 = 250) = 2024$$

Φ_1 decrease but Φ_2 increase and so increasing n is not recommended

$$E_3//k: k^{01} = 1.1k^0 = 275; M_0^{03}(k_0^0 = 0.03, n^{01} = 0.5, k^0 = 275)$$

The computed values for dependences $c_A - \tau$ and $t - \tau$ (third exploration)

τ (s)	150	300	600	1500
c_A (kg/m ³)	3.	4.2	5.2	6.0
t (°C)	172	128	77	50

Φ_1 and Φ_2 values:

$$\Phi_1(k_0^0 = 0.03, n^0 = 0.5, k^{01} = 275) = 1.525 ;$$

$$\Phi_2(k_0^0 = 0.03, n^0 = 0.5, k^{01} = 275) = 327.$$

Φ_1 increase and Φ_2 decrease and so increasing k is not recommended

$$E_4//k_0: k_0^{02} = 0.9 * k_0^0 = 0.027; M_0^{04}(k_0^{02} = 0.027, n^0 = 0.5, k^0 = 250)$$

The computed values for dependences $c_A - \tau$ and $t - \tau$ (fourth exploration)

τ (s)	150	300	600	1500
c_A (kg/m ³)	3.1	4.7	6.1	7.15
t (°C)	176	125	75	40

Φ_1 and Φ_2 values:

$$\Phi_1(k_0^{02} = 0.027, n^0 = 0.5, k^0 = 250) = 7.12$$

$$\Phi_2(k_0^{02} = 0.027, n^0 = 0.5, k^0 = 250) = 606$$

Φ_1 increase and Φ_2 decrease and so decreasing k is not recommended

$$E_5//n: n^{02} = 0.9 * n_0 = 0.45; M_0^{05}(k_0^0 = 0.03, n^{02} = 0.5, k^0 = 250)$$

The computed values for dependences $c_A - \tau$ and $t - \tau$ (fifth exploration)

τ (s)	150	300	600	1500
c_A (kg/m ³)	3.	4.5	5.9	7.1
t (°C)	170	120	72	40

Φ_1 and Φ_2 values:

$$\Phi_1(k_0^0 = 0.03, n^{02} = 0.45, k^0 = 250) = 6.25$$

$$(\Phi_2(k_0^0 = 0.03, n^{02} = 0.45, k^0 = 250)) = 914$$

Φ_1 increase and Φ_2 decrease and so decreasing n is not recommended

All exploring essays have produced contradictory conclusions. So we decide to unify Φ_1 and Φ_2 as a dimensionless function

$$\Phi(k_0, n, k) = \Phi_1(k_0, n, k)/c_{A0}^2 + \Phi_2(k_0, n, k)/(t(\tau) - t_{00})^2$$

The values of dimensionless function for exploration cases

	base	Increasing k_0	Increasing n	Increasing K	Reduction k_0	Reduction n
Φ_1	0.000889	0.00418	0.000274	0.00061	0.002800	0.002505
Φ_2	0.01167	0/01588	0.01750	0.002828	0.005240	0.007907
Φ	0.012559	0.01588	0.01774	0.003438	0.00804	0/0104
Decision :		reject	reject	Accepted	accepted	accepted

The computation of the partial derivatives :

$$\left(\frac{\partial\Phi}{\partial k_0}\right)_0 = \frac{\Phi_{k_0}^0 - \Phi_0^0}{\Delta k_0} = \frac{0.00804 - 0.012559}{(0.027 - 0.03)/0.03} = 0.04519$$

$$\left(\frac{\partial\Phi}{\partial n}\right)_0 = \frac{\Phi_n^0 - \Phi_0^0}{\Delta n} = \frac{0.0104 - 0.012559}{(0.45 - 0.5)/0.5} = 0.02159$$

$$\left(\frac{\partial\Phi}{\partial k}\right)_0 = \frac{\Phi_k^0 - \Phi_0^0}{\Delta k} = \frac{0.003438 - 0.012559}{(275 - 250)/250} = -0.09079.$$

Point advancing : $i_{k_0} = 0.498$; $i_n = 0.0219/0.09079 = 0.238$; $i_k = -1$.

Increase k by 3 units: $k^{(1)} = 250 + 3 = 253$ w/(m²grd).

$dn = i_k * (dk/k) / i_n * n = -1(3/250/0.238)*0.5 = -0.025$; $n^{(1)} = 0.5 - (-0.025) = 0.525$;

$dk_0 = -1(3/250/0.498)*0.03 = -0.00072$; $k_0^{(1)} = 0.03 - (-0.00072) = 0.0307$

The computed values for dependences $c_A - \tau$ and $t - \tau$ for $M_1(0.0307, 0.525, 253)$

τ (s)	150	300	600	1500
c_A (kg/m ³)	3.0	4	4.85	5.6
t (°C)	185	115	65	30

Φ value: $\Phi_1^1 = 0.0003009$; $\Phi_2^1 = 0.011712$; $\Phi^{(1)} = 0.0120129$; $\Phi^{(1)} < \Phi^{(0)}$. New point M_2 coordinates: $k_0^{(2)} = 0.0307 + 0.0007 = 0.0314$, $n^{(2)} = 0.525 + 0.25 = 0.55$, $k^{(2)} = 253 + 3 = 256$.

The computed values for dependences $c_A - \tau$ and $t - \tau$ for $M_2(0.0314, 0.55, 256)$

τ (s)	150	300	600	1500
c_A (kg/m ³)	2.8	3.7	4.5	5.2
t (°C)	160	110	60	32

Φ value: $\Phi_1^{(2)} = 0.000329$; $\Phi_2^{(2)} = 0.021055$; $\Phi^{(2)} = 0.02189$; $\Phi^{(2)} \succ \Phi^{(1)}$.

New exploring start

Decreasing k_0 : $k_0^1 = 0.9k_0^0 = 0.9 \cdot 0.03146 = 0.02826$

The computed values for dependences $c_A - \tau$ and $t - \tau$ for $M_2^{(1)}$ (0.0286, 0.55, 256)

τ (s)	150	300	600	1500
c_A (kg/m ³)	3.1	4.2	5.2	5.95
t (°C)	165	120	65	38

Φ value: $\Phi_{1k_0}^{(2)} = 0.00054$; $\Phi_{2k_0}^{(2)} = 0.011539$; $\Phi_{k_0}^{(2)} = 0.012079$; Correct advancing direction.

Increasing n : $n^1 = 0.55 + 0.05 = 0.6$

The computed values for dependences $c_A - \tau$ and $t - \tau$ for $M_2^{(2)}$ (0.0314, 0.6, 256)

τ (s)	150	300	600	1500
c_A (kg/m ³)	2.8	3.55	4.2	4.7
t (°C)	168	108	59	29

Φ value: $\Phi_{1n}^{(2)} = 0.000485$; $\Phi_{2n}^{(2)} = 0.02093$; $\Phi_n^{(2)} = 0.0211315$; Correct advancing direction.

Increasing k : $k^1 = 256 + 24 = 280$

The computed values for dependences $c_A - \tau$ and $t - \tau$ for $M_2^{(3)}$ (0.0314, 0.6, 280)

τ (s)	150	300	600	1500
c_A (kg/m ³)	2.95	3.7	4.4	4.95
t (°C)	166	120	75	50

Φ value: $\Phi_{1k}^{(2)} = 0.000261$; $\Phi_{2n}^{(2)} = 0.00615$; $\Phi_k^{(2)} = 0.00641315$; Correct advancing direction.

The computation of the partial derivatives: $\left(\frac{\partial\Phi}{\partial k_0}\right)_2 = \frac{\Phi_{k_0}^{(2)} - \Phi_0^{(2)}}{\Delta k_0} = 0.09612$

$$\left(\frac{\partial\Phi}{\partial n}\right)_0 = \frac{\Phi_n^{(2)} - \Phi_0^{(2)}}{\Delta n} = 0.006325; \left(\frac{\partial\Phi}{\partial k}\right)_0 = \frac{\Phi_k^{(2)} - \Phi_0^{(2)}}{\Delta k} = -0.16510.$$

Point advancing: $i_{k_0} = 0.58$; $i_n = -0.38$; $i_k = -1$.

Increase k by 3 units: $k^{(3)} = 256 + 3 = 259$

$dn = i_k \cdot (dk/k) / i_n \cdot n = -1(3/256)/(-0.38) \cdot 0.5 = 0.16$; $n^{(3)} = 0.55 + 0.16 = 0.71$

$dk_0 = -1(3/256/0.58) \cdot 0.0314 = -0.006$; $k_0^{(3)} = 0.0314 + (-0.006) = 0.0254$

The computed values for dependences $c_A - \tau$ and $t - \tau$ for M_3 (0.0254, 0.71, 259)

τ (s)	150	300	600	1500
c_A (kg/m ³)	3.05	3.84	4.5	4.95
t (°C)	170	115	61	32

Φ value: $\Phi_1^{(3)} = 0.00024$; $\Phi_2^{(3)} = 0.011712$; $\Phi^{(3)} = 0.0153$; $\Phi^{(1)} \prec \Phi^{(0)}$. New point M_4

$k_0^{(4)} = 0.0254 - 0.006 = 0.0194$, $n^{(4)} = 0.71 + 0.16 = 0.87$, $k^{(4)} = 259 + 3 = 262$

The computed values for dependences $c_A - \tau$ and $t - \tau$ for M_4 (0.0194, 0.87, 262)

τ (s)	150	300	600	1500
c_A (kg/m ³)	3.1	4.1	4.6	4.95
t (°C)	180	120	62	32

Φ value: $\Phi_1^{(3)} = 0.00056$; $\Phi_2^{(3)} = 0.0077$; $\Phi^{(3)} = 0.00776$; $\Phi^{(1)} < \Phi^{(0)}$. New point M_5
 $k_0^{(5)} = 0.0194 - 0.006 = 0.0134$, $n^{(5)} = 0.87 + 0.16 = 1.03$, $k^{(5)} = 265 + 3 = 268$

Running the algorithm allows the estimation of the most favourable parameters which are:
 $k_0 = 0.0106$, $n = 0.97$, $k = 301$ w/(m² deg)

3.5.4

The Gauss–Newton Gradient Technique

The process of parameter identification using the Gauss–Newton gradient technique is especially meant for the cases where we have a complex mathematical model of a process that imposes an attentive numerical processing.

For a process with a complex mathematical model, where the exits can be described by partial differential equations, we have the general form below:

$$Y(z, \tau, P) = F\left(Y, z, \tau, \frac{\partial Y}{\partial z}, \frac{\partial^2 Y}{\partial z^2}, \frac{\partial Y}{\partial \tau}, P\right) \tag{3.227}$$

where $Y(z, \tau)$ and $F(z, \tau)$ are the columns of N-dimensional vectors (Y – responses vector, F – functions vector) while z and τ show the space and time where and when the process takes place. The unknown parameters are contained in the M-dimensional vector P . In addition, the model must be completed with the univocity conditions expressed by the following vectors:

- the vector of initials conditions:

$$Y(z, 0) = Y_0(z) \tag{3.228}$$

- the vectors of the limitative conditions for $z = 0$ and $z = z_f$:

$$G\left(Y_{z=0}, 0, \tau, \frac{\partial Y}{\partial z} /_{z=0}, \frac{\partial^2 Y}{\partial z^2} /_{z=0}, P\right) = 0 \tag{3.229}$$

$$H\left(Y_{z=z_f}, 0, \tau, \frac{\partial Y}{\partial z} /_{z=z_f}, \frac{\partial^2 Y}{\partial z^2} /_{z=z_f}, P\right) = 0 \tag{3.230}$$

The identification of the unknown M parameters requires supplementary conditions, which are obtained with experimental research. They are given in the column vector $Y_{\text{exp}}(z, \tau)$. This column has the same dimension as $Y(z, \tau)$. As is known, the identification of the parameters requires minimization of the dispersion vector that contains the square of the differences between the observed and computed exits of the process:

$$\Phi(P) = \sum_{r=1}^R \sum_{s=1}^S [Y_{\text{exp}}(z_s, \tau_r) - Y(z_s, \tau_r, P)]^2 \tag{3.231}$$

In the relation (3.231) s represents the number of experimental points located on the z_s coordinate while r characterizes the time position when a measure is executed. The base of the development of the Newton–Gauss gradient technique resides in the Taylor expansion $Y(z, \tau, P)$ near the starting vector of parameters P_0 :

$$Y(z, \tau, P) = Y(z, \tau, P_0) + (P - P_0) \left[\frac{\partial(Y(z, \tau, P_0))}{\partial P} \right]^T + \dots \tag{3.232}$$

If we replace relation (3.232) in Eq. (3.231) we have:

$$\Phi(P) = \sum_{r=1}^R \sum_{s=1}^S \left[Y_{\text{exp}}(z_s, \tau_r) - Y(z_s, \tau_r, P_0) - (P - P_0) \left[\frac{\partial(Y(z_s, \tau_r, P_0))}{\partial P} \right]^T \right]^2 \tag{3.233}$$

The dispersions vector attains its minimal value with respect to vector P when its derivate has a zero value with respect to this vector; it is written as follows:

$$\frac{\partial\Phi(P)}{\partial P} = \sum_{r=1}^R \sum_{s=1}^S 2 \left[Y_{\text{exp}}(z_s, \tau_r) - Y(z_s, \tau_r, P_0) - (P - P_0) \left[\frac{\partial(Y(z_s, \tau_r, P_0))}{\partial P} \right]^T \right] = 0 \tag{3.234}$$

The relation (2.334) can be also written as:

$$\sum_{r=1}^R \sum_{s=1}^S Y_{\text{exp}}(z_s, \tau_r) - \sum_{r=1}^R \sum_{s=1}^S Y(z_s, \tau_r, P_0) - (P - P_0) \sum_{r=1}^R \sum_{s=1}^S \left[\frac{\partial(Y(z_s, \tau_r, P_0))}{\partial P} \right]^T = 0 \tag{3.235}$$

and, in addition, for non-repeated measures it can be particularized as:

$$Y_{\text{exp}}(z_s, \tau_r) - Y(z_s, \tau_r, P_0) - (P - P_0) \left[\frac{\partial(Y(z_s, \tau_r, P_0))}{\partial P} \right]^T = 0 \tag{3.236}$$

After the separation of vector P , the last relation can be written in a state that announces the iterative process of Gauss–Newton:

$$P = P_0 + [Y_{\text{exp}}(z_s, \tau_r) - Y(z_s, \tau_r, P_0)] \left[\left[\frac{\partial(Y(z_s, \tau_r, P_0))}{\partial P} \right]^T \left[\frac{\partial(Y(z_s, \tau_r, P_0))}{\partial P} \right] \right]^{-1} \tag{3.237}$$

The most important form of relation (3.237) is given by its transposition as an iterative Gauss–Newton procedure:

$$P_{i+1} = P_i + m_i [Y_{\text{exp}}(z_s, \tau_r) - Y(z_s, \tau_r, P_i)] \left[\left[\frac{\partial(Y(z_s, \tau_r, P_i))}{\partial P} \right]^T \left[\frac{\partial(Y(z_s, \tau_r, P_i))}{\partial P} \right] \right]^{-1} \tag{3.238}$$

where m_i represents a multiplier which is selected in order to respect the movement of vector $\Phi(P)$ towards the minimum direction. This condition is written as $\Phi(P_{i+1}) \leq \Phi(P_i)$. In accordance with the established relations, the computation adjusts the selected starting vector P_0 , by an iterative procedure. The computation can be finished when the convergence condition is attained. It requires a vector of accepted errors:

$$|P_{i+1} - P_i| \leq E_r \tag{3.239}$$

When the vector of accepted errors contains dimensionless values with respect to each parameter, we have a special case where these values can all be equalled, with a small ε . With this condition we can write the relation (3.239) as follows:

$$\varepsilon \geq \sum_{j=1}^M \left| (P_{ij+1} - P_{ij}) / P_{ij} \right| \tag{3.240}$$

Here p_{ij} gives the value of the parameter having the number i for the iteration with the number j . The parameter m_i of the relation (3.238) can be estimated using a variation of the Gauss–Newton gradient technique. The old procedure for the estimation of m_i starts from the acceptance of the vector of parameters being limited between a minimal and maximal *a priori* accepted value: $P_{\min} < P < P_{\max}$. Here we can introduce a vector of dimensionless parameters $P_{nd} = (P - P_{\min}) / (P_{\max} - P_{\min})$, which is ranged between zero and one for the minimal and the maximal values, respectively. With these limit values, we can compute the values of the dimensionless function for $P_{nd} = 0, 0.5, 1$ as $\Phi(0), \Phi(0.5)$ and $\Phi(1)$ and then they can be used for the estimation of m_i :

$$m_i = \begin{cases} 1 & \text{when } \Phi(1) < \Phi(0) \\ 0.5 & \text{when } \Phi(1) > \Phi(0) \text{ but } \Phi(0.5) < \Phi(0) \\ m_i = \frac{|3\Phi(0) - 2\Phi(0.5) + \Phi(1)|}{|4\Phi(0) - 8\Phi(0.5) + 4\Phi(1)|} & \end{cases} \tag{3.241}$$

It is important to notice that the modern methods of Gauss–Newton gradient operate with variable m_i values, which are obtained for each calculation step by using a more or less complicated particular procedure.

It is easily observable that, for the case of identification of only one parameter, relation (3.238) becomes the famous Newton method for solving a transcendent equation of type $\Phi(p) = 0$. Indeed, this particularization gives the following chain of iteration:

$$P_{j+1} = P_j - \frac{y(z_s, \tau_r, P_j) - y_{\text{exp}}(z_s, \tau_r)}{\left[\frac{dy(z_s, \tau_r, P_j)}{dp} \right]^2} \tag{3.242}$$

In this particular case of only one-parameter identification, the identification method by research is in competition with the Gauss–Newton method. However,

the choice of one particular method depends on different conditions. For instance, when the mathematical model of the process presents a simple form it is limited to an algebraic or a simple differential equation, the Newton method will then be preferred because it is the most rapid method to identify the parameters. All other methods available for solving transcendent equations can be used to identify a single parameter. These methods, along with the Newton method, become difficult to operate when we have many different experimental results because we will have many s and r in the relation (3.242). In these cases, a particularization of the relation (3.235) can be a good solution.

3.5.4.1 The Identification of Thermal Parameters for the Case of the Cooling of a Cylindrical Body

The problem analysed here considers the case of a cylinder made of an unknown material. Its dimensions are $R = 0.02$ m and $H = 0.3$ m, and it is maintained in an oven at a constant temperature of 250°C . After a long time, it is taken out of the oven and kept in air at 20°C , where the cooling process starts. A reservoir of boiling water is placed on the top of the cylinder as shown in Fig. 3.77:

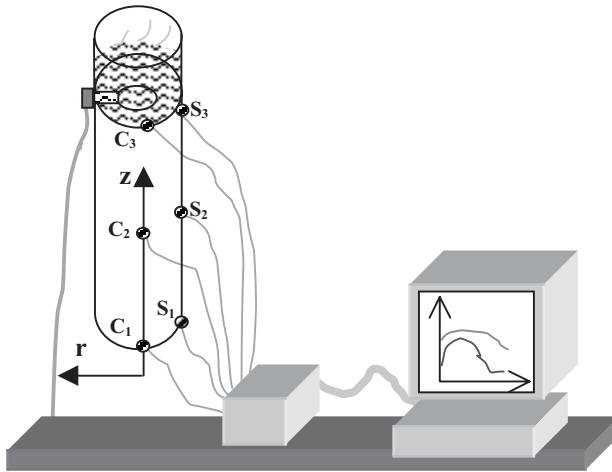


Figure 3.77 The recording of the exit variables for the cooling of a cylindrical body.

During the cooling process, the temperature at points $C_1(0.05, 0)$, $S_1(0.05, 0.02)$, $C_2(0.15, 0)$, $S_2(0.15, 0.02)$, $C_3(0.25, 0)$ et $S_3(0.25, 0.02)$ is measured and recorded. The points marked C are placed in the centre of the cylinder along its axis and the points marked S are placed at the surface. The specific sensible heat of the material of the cylinder is $c = c_p = 870$ j/ (kg deg). The evolution of the temperature at points S and C is given in Figs. 3.78 and 3.79. The heat exchange between the cylinder and the adjacent air is characterized by the evolution of the measured temperature. The heat transfer coefficient from the cylinder to the air and the

thermal conductivity of the material must be determined. If we consider the Gauss–Newton gradient technique, the vector that contains the measured exits is written as shown in relation (3.243). The vector of the computed exits of the process has a similar expression but here the list of arguments of the vector of variables will be completed with the parameters λ (thermal material conductivity) and α (heat transfer coefficient from cylinder to air).

$$Y_{\text{exp}}(z_s, \tau_r) = \begin{bmatrix} t_c(z_s, \tau_r) \\ t_{\text{sf}}(z_s, \tau_r) \end{bmatrix} \tag{3.243}$$

To begin the identification of the parameters with the Gauss–Newton method, the mathematical model of the process must be available. This model allows computation of the values of the temperature at the centre and the surface of the cylinder. At the same time, to estimate the starting vector of parameters (P_0), the method needs a first evaluation of the thermal conductivity λ_0 and of the heat transfer coefficient α_0 .

The mathematical model of the process is given by the assembly of relations (3.244)–(3.248) that represent the particularization of the transport phenomena to the descriptive model introduced by Fig. 3.77. It is not difficult to observe that this model is a case of a three-dimensional unsteady heat conduction (τ, r, z) cylinder.

$$\frac{\partial t}{\partial \tau} = \frac{\lambda}{\rho c_p} \left(\frac{\partial^2 t}{\partial r^2} + \frac{2}{r} \frac{\partial t}{\partial r} + \frac{\partial^2 t}{\partial z^2} \right) \tag{3.244}$$

$$\tau = 0, \quad 0 \leq z \leq H, \quad 0 \leq r \leq R, \quad t = t_0 \tag{3.245}$$

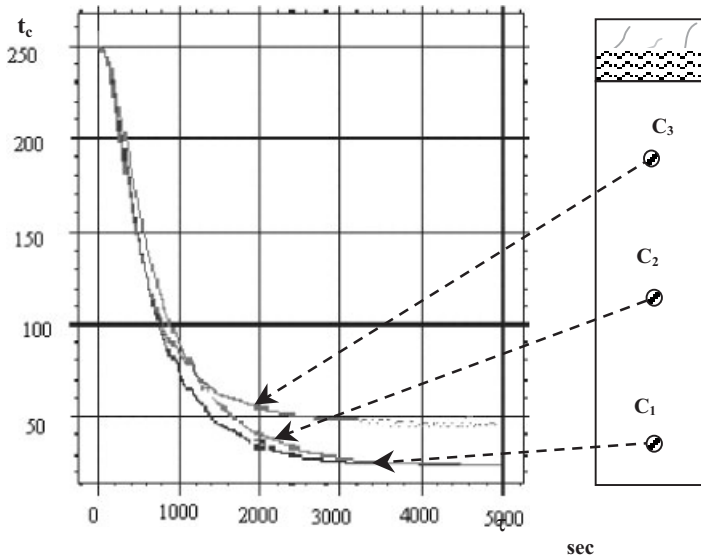


Figure 3.78 Evolution of the measured temperature at points C_1, C_2 and C_3 .

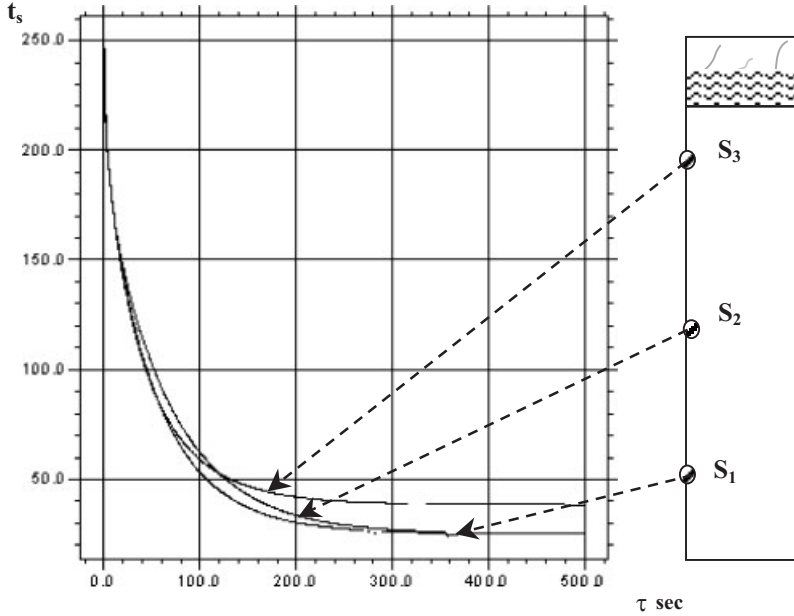


Figure 3.79 The evolution of the measured temperature at points S_1 , S_2 and S_3 .

$$\tau > 0, \quad 0 < z \leq H, \quad r = R, \quad \lambda \frac{dt}{dr} = \alpha(t - t_e) \quad (3.246)$$

$$\tau > 0, \quad z = H, \quad 0 < r < R, \quad t = t_F \quad (3.247)$$

$$\tau > 0, \quad z = 0, \quad 0 < r < R, \quad \lambda \frac{dt}{dr} = \alpha(t - t_e) \quad (3.248)$$

The numerical values of all material properties (except thermal conductivity), geometric data and all initial and boundary conditions required by the process have been established by the mathematical model. These values are $\rho = 6100 \text{ kg/m}^3$, $c_p = 870 \text{ J/(kg deg)}$, $R = 0.02 \text{ m}$, $H = 0.3 \text{ m}$, $t_0 = 250 \text{ }^\circ\text{C}$ and $t_F = 100 \text{ }^\circ\text{C}$.

The relation (3.249) used for the iterative calculation allowing the identification of the unknown parameters is given here below. It is a particularization of the general Gauss–Newton algorithm (3.238):

$$\left| \frac{\lambda}{\alpha} \right|_{i+1,j} = \left| \frac{\lambda}{\alpha} \right|_{i,j} + m_i \left[\begin{array}{cc} \left(\frac{\partial t_s}{\partial \lambda} \right)_{i,j} & \left(\frac{\partial t_s}{\partial \alpha} \right)_{i,j} \\ \left(\frac{\partial t_s}{\partial \lambda} \right)_{i,j} & \left(\frac{\partial t_s}{\partial \alpha} \right)_{i,j} \end{array} \right] \cdot \left[\begin{array}{cc} \left(\frac{\partial t_s}{\partial \lambda} \right)_{i,j} & \left(\frac{\partial t_s}{\partial \alpha} \right)_{i,j} \\ \left(\frac{\partial t_s}{\partial \lambda} \right)_{i,j} & \left(\frac{\partial t_s}{\partial \alpha} \right)_{i,j} \end{array} \right]^{-1} \left| \begin{array}{c} t_{c,exp,j} - t_{c,calc,i,j} \\ t_{s,exp,j} - t_{s,calc,i,j} \end{array} \right| \quad (3.249)$$

The computation obtained with this particularization is given in Fig. 3.80. In this example we consider that the experimental data of the first group (C_1, S_1) is the starting point.

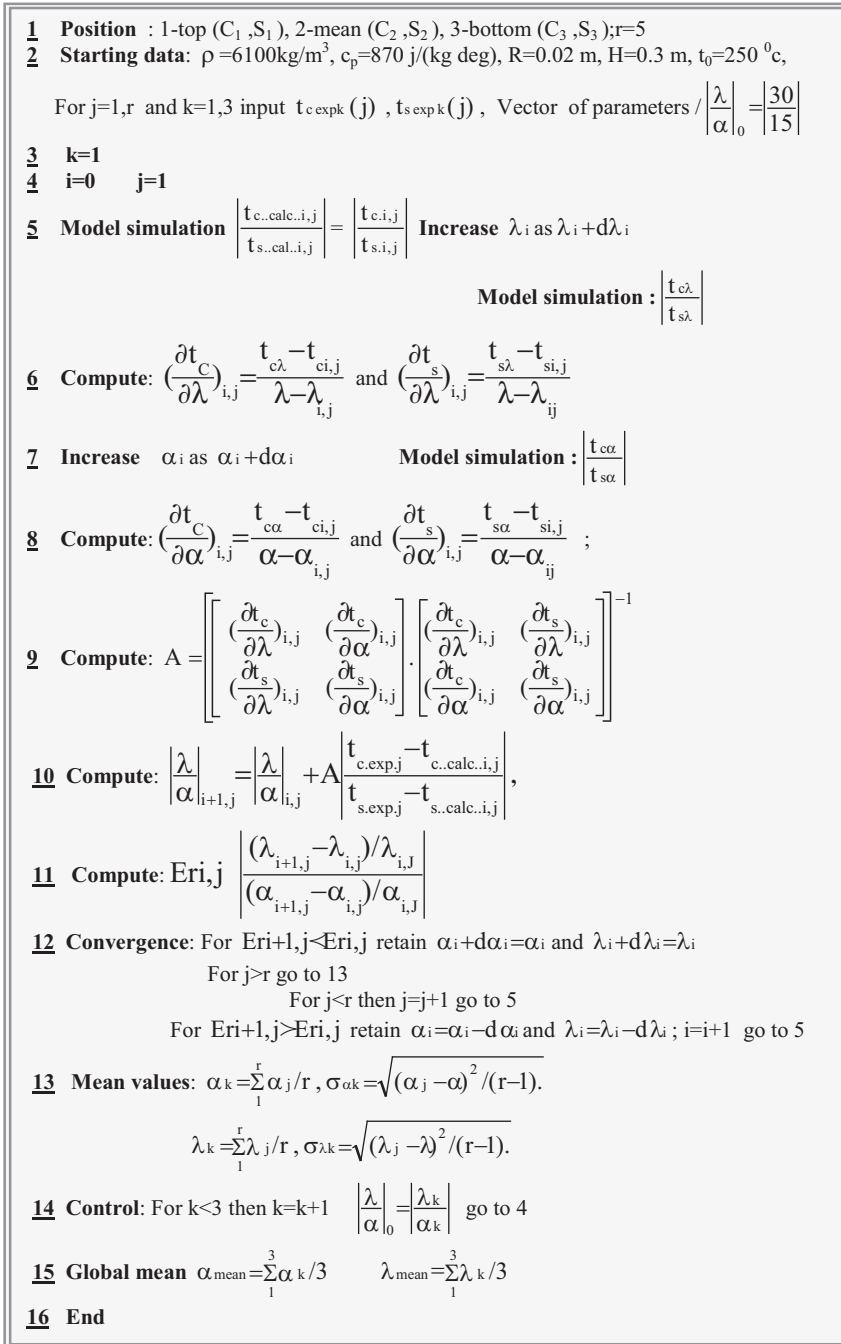


Figure 3.80 The particularization of the Gauss–Newton algorithm for the application.

We can observe that it is important to have a simulator of the model of the process ((3.244)–(3.248)) in order to estimate the value of the vector $\begin{bmatrix} t_{ci,j} \\ t_{si,j} \end{bmatrix}$. The simulator allows the computation of the matrix of derivatives $\begin{bmatrix} \left(\frac{\partial t_c}{\partial \lambda}\right)_{i,j} & \left(\frac{\partial t_c}{\partial \alpha}\right)_{i,j} \\ \left(\frac{\partial t_s}{\partial \lambda}\right)_{i,j} & \left(\frac{\partial t_s}{\partial \alpha}\right)_{i,j} \end{bmatrix}$, used in the iteration processes, as shown in the numerical example given here.

The model simulator of the process is based on the description given in Fig. 3.77; it considers the transformations recommended earlier as well as an adaptation to the model conditions ((3.43)–(3.46)). In the following example the $FRC(\lambda, \alpha)$ gives the values of $t_{ci,j}$ and $t_{si,j}$ respectively.

The positions of the points are: C_1, S_1 ; time = 1000 s/ $t_{c \text{ exp}} = 69$, $t_{s \text{ exp}} = 52$ / P_0 : $\lambda = 30$, $\alpha = 15$ / $FRC(30,15)$, $t_{c \text{ calc}} = 65$, $t_{s \text{ calc}} = 39$ / $\lambda + d\lambda = 35$ / $FRC(35,15)$ $t_{c\lambda} = 81$, $t_{s\lambda} = 57$, $dt_c/d\lambda = (81-65)/5 = 3.2$, $dt_s/d\lambda = (57-39)/5 = 3.6$ / $\alpha + d\alpha = 20$ / $FRC(30,20)$ $t_{c\alpha} = 49$, $t_{s\alpha} = 32$, $dt_c/d\alpha = (49-65)/5 = -3.2$, $dt_s/d\alpha = (32-39)/5 = -1.4$ / $B =$

$$\begin{aligned} & \begin{vmatrix} 3.2 & 3.6 \\ -3.2 & -1.4 \end{vmatrix} * \begin{vmatrix} 3.2 & -3.2 \\ 3.6 & -1.4 \end{vmatrix} = \begin{vmatrix} 12.24 & 16 \\ 16 & 4.9 \end{vmatrix}, \det B = -73, A = (1/\det B)*\min(B) \\ & = \begin{vmatrix} -0.2 & -0.21 \\ -0.21 & -0.16 \end{vmatrix}; \left| \frac{\lambda}{\alpha} \right| = \left| \frac{30}{15} \right| + \begin{vmatrix} -0.2 & -0.21 \\ -0.21 & -0.16 \end{vmatrix} * \left| \frac{69-65}{52-39} \right| = \left| \frac{30-1.64}{15-4.81} \right| = \\ & \left| \frac{28.46}{10.19} \right| / E = \left| \frac{0.055}{0.32} \right| / \text{Go on with } FRC(28.46,10.19) \ t_{c \text{ calc}} = 75, \ t_{s \text{ calc}} = 38 / \lambda + d\lambda = \\ & 33.16 / FRC(33.16,10.19) \ t_{c\lambda} = 77, \ t_{s\lambda} = 43, \ dt_c/d\lambda = (77-75)/5 = 0.4, \ dt_s/d\lambda = (43 \\ & - 38)/5 = 1/\alpha + d\alpha = 15.16 / FRC(28.46,15.16) \ t_{c\alpha} = 65, \ t_{s\alpha} = 32, \ dt_c/d\alpha = (65-75)/5 \\ & = -0.2, \ dt_s/d\alpha = (32-38)/5 = -1.2 / B = \begin{vmatrix} 0.4\dots 1 \\ -2\dots -1.2 \end{vmatrix} * \begin{vmatrix} 0.4\dots -2 \\ 1\dots -1.2 \end{vmatrix} = \begin{vmatrix} 4.16\dots 2.8 \\ 2.8\dots 2.41 \end{vmatrix}, \\ & \det B = -2.16, \ A = (1/\det B)*\min(B) = \left| \frac{1.9\dots 1.28}{1.28\dots 1.09} \right| / \left| \frac{\lambda}{\alpha} \right| = \left| \frac{28.46}{10.19} \right| - 0.5 * \\ & \left| \frac{1.9\dots 1.28}{1.28\dots 1.09} \right| * \left| \frac{69-65}{52-39} \right| = \left| \frac{28.46+8.5}{10+15.4} \right| = \left| \frac{36.96}{25.4} \right| / E = \left| \frac{0.32}{1.5} \right| / \end{aligned}$$

We used here a too large displacement of λ and α for the construction of the matrices (relation (3.242)). However, the real computation uses a small displacement of the parameters. This explains the differences between both values of the vectors of errors as well as the evolution of the vector of the parameters along both iterations. The software of the mathematical model of the process is given by $FRC(\lambda, \alpha)$. In this specific computation, we introduced definite values of λ and α for the calculation of the corresponding temperatures ($t_{c \text{ calc}}$, $t_{s \text{ calc}}$, $t_{c\lambda}$, $t_{s\lambda}$ etc) for points C_1 and S_1 respectively.

The final result of identification allows the estimation of $\alpha = 9.7 \pm 0.88$ w/(m² deg) and $\lambda = 49.8 \pm 2.35$ w/(m deg). Considering the value of λ , we can appreciate that the cylinder is certainly made of a type of steel, whereas the value of α shows that the occurring heat transfer is the natural convection between the cylinder and the adjacent air. This last observation is in good agreement with the descriptive model of the process given at the beginning of this section.

3.5.4.2 Complex Models with One Unknown Parameter

The identification of the parameters of a process can be examined from two completely different viewpoints. The former is given by laboratory researchers, who consider the identification of parameters together with a deep experimental analysis; it is then frequently difficult to criticize the experimental working methods, the quality and quantity of the experimental data. The latter is given by researchers specialized in mathematical modelling and simulation. These researchers consider that the mathematical aspects in the identification of parameters are prevailing. Nevertheless, this last consideration has some limits because, in all cases, a similar number of parameters and independent experimental data are necessary for a correct identification.

It is important to notice that, from both viewpoints, as well as in all working procedures, experimental data are required and that, at the same time, mathematical models are absolutely needed for data processing. Generally, when the mathematical model of a process is relatively complex, a good accuracy and an important volume of experimental data are simultaneously required. Therefore, in these cases the quality of the determination of parameters is the most important factor to ensure model relevance. The strategy adopted in these cases is very simple: for all the parameters of the process that accept an indirect identification, the research procedure of identification is carried out separately from the real process; whereas for the very specific process parameters that are difficult to identify indirectly, experiments are carried out with the actual process.

When we have N measures for the exit variables in a process, the technical problem of identification of the unknown parameter resides in solving the equation $\Phi(p) = 0$. From the theoretical viewpoint, all the methods recommended for the solution of the transcendent equation can be used to determine parameter p . The majority of these methods are of iterative type and require an expression or an evaluation of the $\Phi(p)$ derivate. When we evaluate the derivate numerically, as in the case of a complex process model, then important deviations can be introduced into the iteration chain. Indeed, the deviation propagation usually results in an increasing and non-realistic value of the parameter. This problem can be avoided by solving the equation $\Phi(p) = 0$ by integral methods such as the method of minimal function value (MFV). When $\Phi(p)$ values are only obtained in the area of influence of parameter p , the MFV method is reduced to a dialogue with the mathematical model of the process and then the smallest $\Phi(p)$ value gives the best value for the parameter.

The following example details how the MFV method is used to identify the diffusion coefficient of species with respect to their motion in a particle of activated carbon.

Diffusion of Species Inside a Particle of Activated Carbon

Among the inexhaustible plant resources for the production of activated carbon, we have the nutshell, which can be transformed by pyrolysis and activation with overheated water vapour. In this example, activated carbon has been used to retain some hydrocarbon traces from water using a batch reactor. The interest here is to

characterize the diffusion of the chemical species that are adsorbed on the activated carbon and its dependence on the operating conditions.

Experiment. Nutshells, granulated to a maximum 6 mm diameter, were used as raw material. The reaction was carried out in a pyrolysis reactor heated with an electrical resistance and the temperature evolution inside the bed of solid was measured with a thermocouple. The integral expression of the pyrolysis dynamics was determined by the loss of weight with respect to the initial quantity of nutshells loaded into the reactor. The experimental data are presented in Fig. 3.81. The final weight loss corresponds to the removal of some non-oxygenated compounds, (which burned with a blue flame, color indicating the absence of oxygen) from the raw material. 100 g of pyrolysed material, divided into three parts, was prepared for each batch loaded into the reactor. One third, which followed a different activation treatment, was used for comparison with the other samples. The activation was performed by flowing the overheated steam through the fixed bed of pyrolysed material. Two different activation treatments, which differ in the overheated steam temperature and flow were used. The nine different activated carbons prepared are reported in Table 3.21. They were identified depending on the operating conditions as: S1, S2, S3, S1A1, S1A2, S2A1, S2A2, and S3A1 and S3A2.

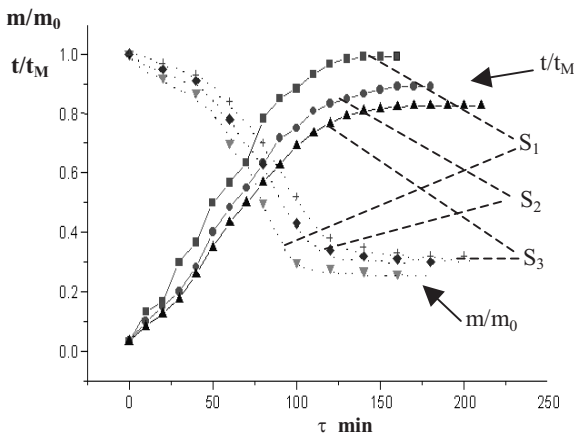


Figure 3.81 Dynamics of the weight loss and of the increase in the temperature for the nutshell pyrolysis (dimensionless).

The samples called S were used without any activation whereas the samples called SxAy were used after activation.

Characterization of the activated carbon by adsorption: nearly saturated water with benzene and activated carbon were introduced into a batch reactor with a 0.06 and 0.14 ratio of solid/liquid phases. In each experiment, the evolution of the concentration of benzene in water was determined spectrophotometrically and by potassium permanganate titration. Tables 3.22 and 3.23 as well as Figs. 3.82–3.84 show

the dynamics of the concentration of the organic compound in the water for the different types of activated carbon. The mass balance of species allows one to know the mean benzene concentration adsorbed by the activated carbon particles for each experiment and in each time interval.

Table 3.21 Activation conditions for the pyrolysed material.

No.	Time (min)	A1		A2	
		t (°C)	Steam flow (kg/s)	t (°C)	Steam flow (kg/s)
1	0	300	$0.83 \cdot 10^{-4}$	300	$0.83 \cdot 10^{-4}$
2	20	700	$1.25 \cdot 10^{-4}$	600	$1.25 \cdot 10^{-4}$
3	40	700	$1.25 \cdot 10^{-4}$	600	$1.25 \cdot 10^{-4}$
4	60	700	$2.83 \cdot 10^{-4}$	600	$2.83 \cdot 10^{-4}$
5	80	700	$2.83 \cdot 10^{-4}$	600	$2.83 \cdot 10^{-4}$
6	100	700	$0.83 \cdot 10^{-4}$	600	$0.83 \cdot 10^{-4}$

Table 3.22 Evolution of the concentration of benzene in water for a solid/liquid ratio of $s/l = 0.06$.

No.	Time (min)	c/c ₀								
		S1	S2	S3	S1A1	S1A2	S2A1	S2A2	S3A1	S3A2
1	0	1	1	1	1	1	1	1	1	1
2	10	0.81	0.86	0.91	0.8	0.76	0.85	0.77	0.89	0.83
3	25	0.73	0.80	0.86	0.7	0.66	0.77	0.69	0.82	0.75
4	50	0.59	0.71	0.75	0.53	0.51	0.62	0.54	0.74	0.63
5	80	0.56	0.59	0.62	0.50	0.49	0.58	0.51	0.61	0.59
6	120	0.55	0.57	0.59	0.49	0.48	0.55	0.50	0.59	0.57
7	160	0.54	0.56	0.57	0.49	0.48	0.54	0.50	0.57	0.54
8	210	0.53	0.55	0.56	0.49	0.48	0.53	0.50	0.55	0.54
9	260	0.53	0.55	0.56			0.53		0.55	0.54
10	360		0.55	0.56						

Table 3.23 Evolution of the concentration of benzene in water for an $s/l = 0.14$ solid/liquid ratio.

No.	Time (min)	c/c_0									
		S1	S2	S3	S1A1	S1A2	S2A1	S2A2	S3A1	S3A2	
1	0	1	1	1	1	1	1	1	1	1	
2	10	0.75	0.82	0.84	0.7	0.68	0.79	0.77	0.83	0.85	
3	25	0.69	0.73	0.74	0.50	0.48	0.66	0.49	0.71	0.75	
4	50	0.57	0.62	0.64	0.41	0.38	0.55	0.40	0.59	0.65	
5	80	0.49	0.59	0.61	0.32	0.30	0.46	0.32	0.51	0.56	
6	120	0.39	0.50	0.52	0.27	0.25	0.38	0.27	0.45	0.47	
7	160	0.34	0.41	0.43	0.25	0.23	0.32	0.24	0.39	0.39	
8	210	0.30	0.34	0.36	0.25	0.23	0.29	0.23	0.34	0.32	

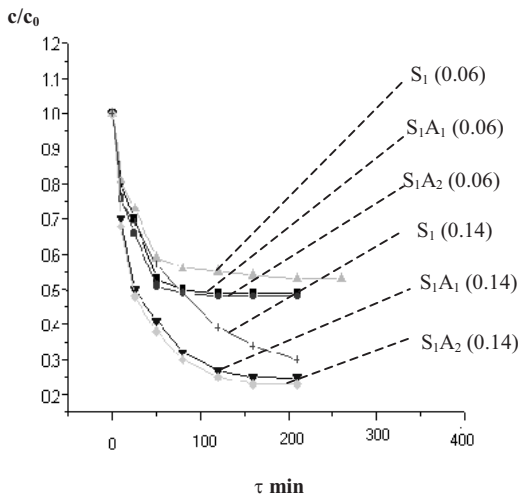


Figure 3.82 Evolution of the benzene concentration in water for the adsorption with activated carbon S_1 , S_1A_1 and S_1A_2 .

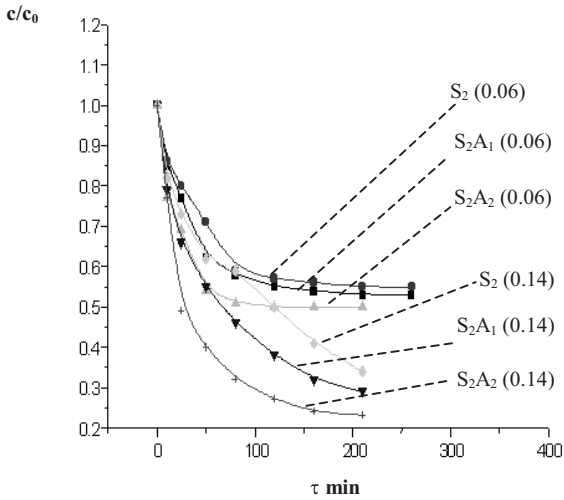


Figure 3.83 Dynamics of the benzene adsorption for the S_2 , S_2A_1 and S_2A_2 activated carbon.

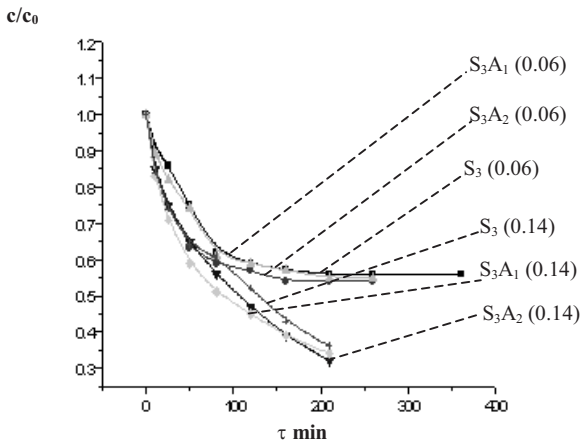


Figure 3.84 Dynamics of the benzene adsorption for the S_3 , S_3A_1 and S_3A_2 activated carbon.

From these representations we can notice that: (i) *the 600 °C pyrolysis* results in an activated carbon with the best adsorption speed; (ii) *the activation* increases the speed of adsorption of the organic compound, probably as a consequence of the increase in the effective diffusion coefficient and not as a result of the opening of new pores (in which case the final equilibrium concentrations for S_1 , S_2 , S_3 , S_1A_1 , S_1A_2 , S_2A_1 , S_2A_2 , S_3A_1 , S_3A_2 should be different); (iii) *the use of more intense steam activation conditions* (higher temperature) leads to a small increase in the speed of adsorption of the organic compound.

We can consider that the measured values of the concentration at the end of the experience at constant temperature represent the equilibrium concentrations. These data are given in Tables 3.22 and 3.23. The equilibrium constant is determined according to its definition by the following relation:

$$k_d = \frac{\frac{m_1 c_{ech}}{m_s}}{c_0 - c_{ech}} = \frac{r \cdot c_{ech}}{c_0 - c_{ech}} = \frac{r}{\frac{c_0}{c_{ech}} - 1} \tag{3.250}$$

Table 3.24 shows the computed data for k_d , for both solid/liquid ratios and the mean values if we consider the hypothesis of a linear equilibrium isotherm.

Table 3.24 Adsorption equilibrium constants for all activated carbon species at 25 °C.

	S1	S2	S3	S1A1	S1A2	S2A1	S2A2	S3A1	S3A2
$k_d(0.06)$	0.0677	0.0733	0.0764	0.0576	0.0676	0.0677	0.0600	0.0733	0.070
$k_d(0.14)$	0.0600	0.0721	0.0787	0.0466	0.0418	0.0572	0.0418	0.0721	0.066
$k_d(\text{mean})$	0.0639	0.0727	0.0775	0.0521	0.0547	0.0625	0.0509	0.0727	0.068

From this table, the weak dependence between the distribution constant, the pyrolysis and activation conditions can be noticed.

Identification of the effective diffusion coefficient with the mathematical model of batch adsorption. The model assumes that the carbon particles are spherical and porous (ϵ_p - voids fraction). Using c (kg A/m³ fluid inside the pores) and q (kg A/kg adsorbent) to express the concentration of the transferable species through the pores and through the particle respectively, we can write the following expression for transport flux:

$$J_{A,r} = - \left[D_{ef} \frac{\partial c}{\partial r} + \rho_p D_s \frac{\partial q}{\partial r} \right] \tag{3.251}$$

where D_{ef} represents the effective diffusion coefficient through the pores, D_s is the surface diffusion coefficient and ρ_p is the particle density. When the adsorption flow of species has been defined, it is necessary to give the net speed of adsorption using a general expression such as: $v_{ad} = G(c, q)$.

The unit for the net speed of adsorption is kmoles or kg of A by unit of solid weight and by unit of time. For example, for the net speed of adsorption, the Langmuir model gives:

$$G(c, q) = k_a(q_\infty - q) - k_{ds} \cdot q \tag{3.252}$$

Here q is the maximal concentration of the adsorbed species into the solid, k_a is the rate of adsorption; k_{ds} is the rate of desorption. The ratio $k_d = k_a/k_{ds}$ is usually called the equilibrium constant. With the considerations given above, we can now write the expression for the concentration fields c and q :

$$\varepsilon_p \frac{\partial c}{\partial \tau} = \frac{1}{r^2} \frac{\partial}{\partial r} \left(r^2 D_{ef} \frac{\partial c}{\partial r} \right) - \rho_p G(c, q) \quad (3.253)$$

$$\frac{\partial q}{\partial \tau} = \frac{1}{r^2} \frac{\partial}{\partial r} \left(r^2 D_s \frac{\partial q}{\partial r} \right) + G(c, q) \quad (3.254)$$

For a full definition of the model of transport through the particle, it is necessary to set up the univocity conditions for the above equations:

- the concentration fields c and q inside of the particle at the start of the process:

$$\tau = 0, \quad 0 < r < R, \quad c = q = 0 \quad (3.255)$$

- the absence of transport of the species into the centre of the particle:

$$\tau > 0, \quad r = 0, \quad \frac{\partial c}{\partial r} = \frac{\partial q}{\partial r} = 0 \quad (3.256)$$

- the equality of the convection and conduction flux at the surface of the particle:

$$\tau > 0, \quad r = R, \quad k(c_l - c_R) = D_{ef} \frac{\partial c}{\partial r} \Big|_R + \rho_p D_s \frac{\partial q}{\partial r} \Big|_R \quad (3.257)$$

For the adsorbed species on the external surface of the particle, the next condition has to be fulfilled:

$$\tau > 0, \quad r = R, \quad \frac{\partial q}{\partial r} \Big|_{r=R} = G(c_R, q_R) \quad (3.258)$$

The next equation presents the balance of the adsorbable species for the fluid outside the particle:

$$V \frac{\partial c_l}{\partial \tau} = - \left(\frac{m_p}{\rho_p} \right) \frac{3}{R} \left[D_{ef} \frac{\partial c}{\partial \tau} + \rho_p D_s \frac{\partial q}{\partial \tau} \right]_R \quad (3.259)$$

Here m_p is the total mass of the particles with radius R placed in the contactor with a useful volume V . In some cases, the surface diffusion is considered the slowest process because organic components such as hydrocarbons are generally strongly adsorbed on activated carbon [3.65, 3.66]. Indeed, we can consider here that, at the surface of the particle, the adsorption equilibrium is achieved faster than the surface diffusion process. In these conditions the batch model equations are:

$$\frac{\partial q}{\partial \tau} = \frac{1}{r^2} \frac{\partial}{\partial r} \left(r^2 \overline{D_s} \frac{\partial q}{\partial r} \right) \quad (3.260)$$

$$r = R, k_1(c_1 - c_R) = \rho_p \overline{D}_s \frac{\partial q}{\partial r} \quad (3.261)$$

$$r = R, G(c, q) = 0, r = 0, \frac{\partial q}{\partial r} = 0 \quad (3.262)$$

$$V \frac{dc_1}{d\tau} = \frac{3}{R} \left(\frac{m_p}{\rho_p} \right) \rho_p \overline{D}_s \frac{\partial q}{\partial r} \Big|_R \quad (3.263)$$

$$\tau = 0, c_1 = c_{1,0}, q = 0 \quad (3.264)$$

where \overline{D}_s is the effective coefficient of the surface diffusion. The minimization of the squares of the differences between the experimental and the theoretical values of the transferable species allows the identification of \overline{D}_s . The calculation is made following the next steps:

1. Suggest a value for \overline{D}_s ;
2. Propose $c_R < c_1$;
3. Determine q_R from Eq. (3.262);
4. Numerical integration of Eq. (3.261) and determination of $q(r, \tau)$, $0 < r < R$;
5. Calculation of $\frac{\partial q}{\partial r} \Big|_R$ and verification of the condition given by the relation (3.261). If it is not verified go back to 2;
6. Determine $c_1(\tau) = c_{1,th}$ from Eq. (3.263);
7. Calculate $\left(c_{1,exp} - c_{1,th} \right)_i^2$;
8. Increase τ to cover the entire period of the experiment and go to step 2;
9. Calculate $\sigma(D_s) = \frac{1}{n-1} \sqrt{\sum_{i=1}^n \left(c_{1,exp} - c_{1,th} \right)_i^2}$;
10. Propose a new value for \overline{D}_s and go to step 2;
11. Identify the minimum value of the dispersion, $\sigma(D_s)$, in order to obtain the best value of the effective coefficient of the surface diffusion.

Figure 3.85 and Table 3.25 show the identified values of the effective diffusion coefficient for all adsorption experiments. The activation technique applied can be shown to allow the enhancement of \overline{D}_s , so the speed of the transport process will be higher. Table 3.25 also contains the values of \overline{D}_s identified by the Newton-Gauss method.

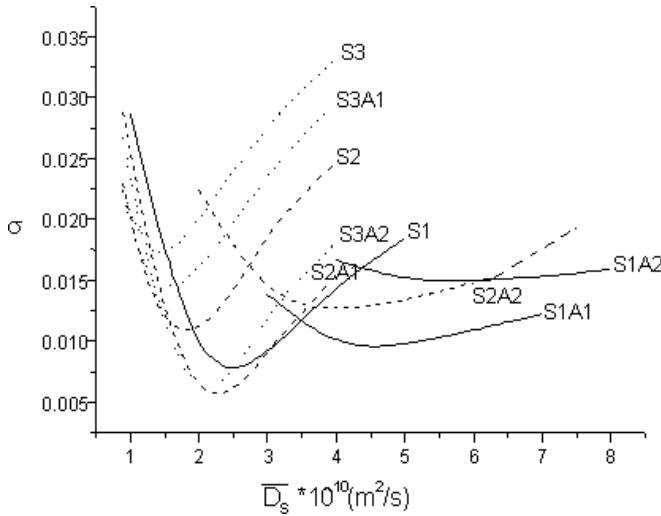


Figure 3.85 The state of the dispersion between the experimental and the theoretical values of c/c_0 versus $\bar{D}_s \cdot 10^{10} \text{ m}^2/\text{s}$.

Table 3.25 Identified \bar{D}_s values for all activated carbons (first line – from Fig. 3.85, second line – by Newton–Gauss method.

	S1	S2	S3	S1A1	S1A2	S2A1	S2A2	S3A1	S3A2
σ	0.009	0.011	0.020	0.001	0.015	0.006	0.013	0.016	0.0065
$\bar{D}_s \cdot 10^{10} \text{ m}^2/\text{s}$	3	2	2	5	6	2	4	2	2
$\bar{D}_s \cdot 10^{10} \text{ m}^2/\text{s}$	3.12 ± 0.42	2.09 ± 0.31	1.92 ± 0.27	5.57 ± 0.62	6.15 ± 0.76	2.11 ± 0.29	3.88 ± 0.25	1.98 ± 0.11	2.06 ± 0.19

The increase in the activation time (A_2 regime) results in the best values of \bar{D}_s with respect to all other cases. It can be observed that the best speed of adsorption is reached with an activated carbon produced by the first type of pyrolysis treatment (S1 samples), whereas no improvement is observed in the adsorption properties, when the activated carbon has been produced by a process in which the raw material (S3) presented the lowest loss of mass.

In conclusion, we can assert that the pyrolysis and activation process applied for the manufacture of activated carbons from nutshells resulted in good quality adsorbents. We have demonstrated the influence of both processes on the speed of the benzene adsorption from water solutions. The hypothesis that the effective surface diffusion is the slowest step of the global process was used and the estimation of the effective diffusion coefficient resulted in values ranging between 2 and $6 \times 10^{-10} \text{ m}^2/\text{s}$.

3.5.5

Identification of the Parameters of a Model by the Maximum Likelihood Method

The maximum likelihood method (MLM) is used effectively to identify the unknown parameters of mathematical models when the parameters are distributed. If we consider Fig. 3.1, the actions of the normal distributed perturbations on the process cannot be neglected. Indeed, all process exits will be distributed with individual parameters that depend on the distribution functions associated to the perturbations.

In order to show the effect of the distributed perturbations on the model exits, we begin the analysis by writing the mathematical model of the process as:

$$X = f(X, U, V, \tau) \quad (3.258)$$

where X is the state vector (internal characterization of the process), U the control vector (for all or for the most important inputs of the process) and V is defined as the disturbance (perturbation) vector of the process. In all cases, all the experimental measurements have been affected by the errors which are distributed normally; the process contains one or more variables with probability distributed actions, etc. The formal measurements of vectors depend on the vectors themselves and on their state, they will be given by:

$$Y = g(X, U, V, \tau) \quad (3.259)$$

They are composed of the numerical values contained in the following sequence:

$$Y_N = \langle y_1, y_2, \dots, y_N \rangle \quad (3.260)$$

This sequence shows the instant values of the exit of the process conditioned by the vector parameter $P = P(p_1, p_2, \dots, p_L)$. Indeed, Y_N/P is the exit random vector conditioned by the vector parameter P . In this case $p(Y_N/P)$, which is the probability density of this variable, must be a maximum when the parameter vector P is quite near or superposed on the exact or theoretical vector P . Therefore, the maximum likelihood method (MLM) estimates the unknown parameter vector P as \hat{P} , which maximizes the likelihood function given by:

$$L = \ln[p(Y_N/P)] \quad (3.261)$$

Now we can consider that the prediction error (measurement errors) given for the k exit is shown by:

$$\varepsilon_k = (y_k - \bar{y}_k) \quad (3.262)$$

where \bar{y}_k is the expected mean value. When the mean value is "white" or zero $E(\varepsilon_k) = 0$, (E operator to calculate the mean value). It can be shown that the max-

imization of L from relation (3.261) is equivalent to the minimizations of the L_{MDL} given by:

$$L_{MDL} = \frac{1}{2N} \sum_{k=1}^N [\varepsilon_k^T R_k^{-1} \varepsilon_k + \ln(\det(R_k))] \tag{3.263}$$

Here, R_k is the prediction error covariance matrix (it will be chosen from the start of the minimization) and N represents the number of the experiments carried out. The Kalman filter approach [3.66, 3.67] must be used in different situations: (i) in the estimation of the ε_k vector when \bar{y}_k is unknown in Eq. (3.262), (ii) in the correction of the model state when it is possible to compensate some inaccuracies due to the model deficiencies and experimental plant disturbances [3.68]. In this latter case, if the model state is not corrected, considerable errors in parameter estimation can arise, even if the model structure is very close to the *correct* one. The extended Kalman Filter approach is also necessary [3.69, 3.70] when the mathematical models of the process show a nonlinear state.

The principle of the MLM is shown in Fig. 3.86. It is important to specify that the minimization of the MLM can be carried out by various techniques. The MLM algorithm works as follows:

1. It makes an initial choice of the estimated vector parameter (indeed, for $i = 0$ it chooses \hat{P}_0).
2. It uses the Kalman filter and performs a simulation with $\hat{P} = \hat{P}_i$ and then it computes $L_{MDL} = L_{MDLi}$.
3. It uses a minimization technique to update a new estimation of vector parameter: $\hat{P}_{i+1} = \hat{P}_i + \Delta\hat{P}_i$.
4. It verifies whether convergence has happened: if not, it goes back to point 2 and adds $i = i + 1$.

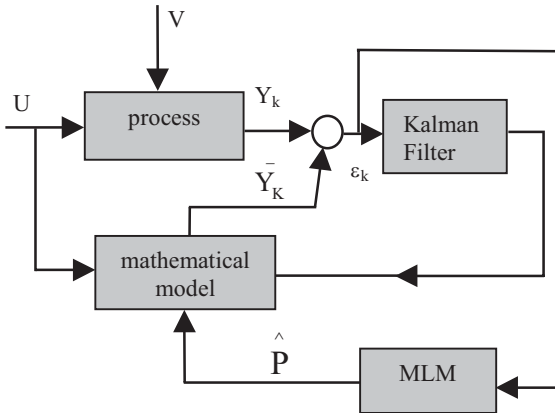


Figure 3.86 Structure of the MLM method.

When a model state is described by nonlinear equations, the extended Kalman filter has been applied using the well-known Kalman filter equations for the linearization of equations. If the state vector is enlarged with the parameter vector P_k (P_k is used because it corresponds to the discrete version of the state model) and if it is considered to be constant or varying slowly, then it is possible to transform the problem of parameters estimation into a problem of state estimation. The $P_{k+1} = P_k + n_k$ with n_k white noise correction represents the model suggested for P . It will introduce $\bar{X}_k = \begin{bmatrix} X_k \\ P_k \end{bmatrix}$ in the augmented state vector. Then, the discrete version of the state model will be written as:

$$\bar{X}_{k+1} = \bar{X}_k + \Delta\tau * F(\bar{X}_k, U_k, V_k) \tag{3.264}$$

The structure of the augmented (extended) Kalman filter is shown in Fig. 3.87, which also presents the schematic methodology for obtaining the exit-computed vector \bar{Y}_k . It can be observed that coupling the process with computation procedures allows parameter identification and control of the process.

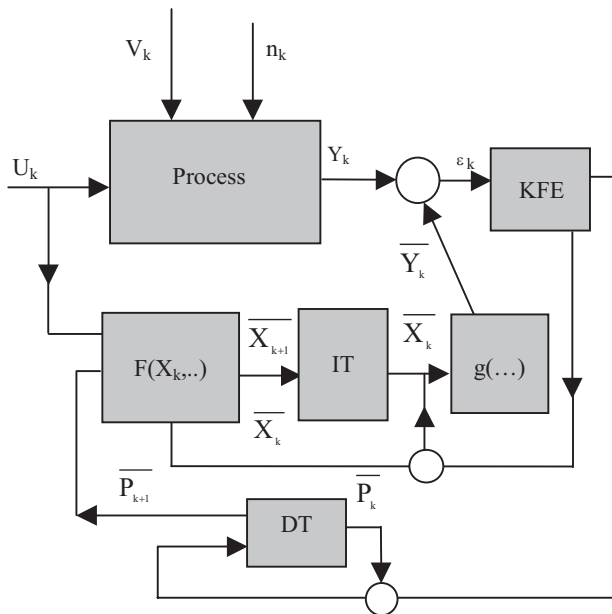


Figure 3.87 The extended Kalman filter method.

The vector \bar{Y}_k can be calculated either with the normal Kalman Filter (KF) which gives \bar{X}_k for the discrete equation state ($F(\bar{X}_k, U_k, V_k)$) or with the extended Kalman filter (KFE) which gives \bar{P}_{k+1} in the calculation system. For this estimation, it is also necessary to obtain the state of the system \bar{X}_k from the next state \bar{X}_{k+1} . This estimation is made by block IT (inversion translator); another IT block gives

the \hat{P}_{k+1} used for state system estimation with \hat{P}_k from KFE. Both methods need the Kalman filter to be started. Indeed, an introduction of the Kalman filter equations is required in order to correctly appreciate how the MLM and KFE methods operate.

3.5.5.1 The Kalman Filter Equations

This method is frequently used for filtering, smoothing and identifying parameters in the case of a dynamic time process. It has been developed taking into account the following conditions: (i) acceptance of the gaussian distribution of the disturbances and exits of the variables of the process; (ii) there is a local linear dependence between the exit vector and the state vector in the mathematical model of the process.

The Kalman filter problem. Considering the relations (3.258) and (3.259) we can write the following discrete-time system:

$$\begin{cases} X_{k+1} = F_k X_k + G_k W_k \\ Y_k = H_k X_k + V_k \end{cases} \quad (3.265)$$

where the input disturbance vector W_k is $N(0, Q_k)$, the exit disturbance vector V_k is $N(0, R_k)$ and the initial input vector X_0 is $N(m_0, S_0)$. In the expression $N(\alpha, \beta)$, α represents the mean value and β is the dispersion or covariance with respect to the mean value.

The dimensions of the state vector X_k and of the observation vector (exit vector) are N and M respectively. This short introduction is completed by assuming that R_k is positive ($R_k > 0$).

The problem considered here is the estimation of the state vector X_k (which contains the unknown parameters) from the observations of the vectors $Y_k = [y_0, y_1, \dots, y_k]$. Because the collection of variables $Y_k = (y_0, y_1, \dots, y_k)$ is jointly gaussian, we can estimate X_k by maximizing the likelihood of conditional probability distributions $p(X_k/Y_k)$, which are given by the values of conditional variables. Moreover, we can also search the estimate \hat{X}_k , which minimizes the mean square error $\epsilon_k = X_k - \hat{X}_k$. In both cases (maximum likelihood or least squares), the optimal estimate for the jointly gaussian variables is the conditional mean and the error in the estimate is the conventional covariance.

In what follows, we will develop the conditional mean and covariance for the couple X_k and Y_k . This is followed by a description of the Kalman filter and a rapid and practical method for a recursive or iterative calculation of the conditional mean and covariance for the random variable vector X_k/Y_k .

In many different softwares such as SCILAB[®], computational programs are available for calculating: (i) the steady-state Kalman filter which can be used when the matrices of the systems in (3.265) do not vary with time; (ii) the unsteady-state Kalman filter which can be used when the matrices of the systems in (3.265) vary with time; (iii) the square-root Kalman filter for time or non-time-varying matrices of the systems when high numerical accuracy is required.

Mean and covariance for conditional gaussian random vector. The minimum mean square estimate of a gaussian random vector when we only have observations of some of its elements is the conditional mean of the remaining elements. The error covariance of this estimate is the conditional covariance. Consequently, if Z is a random gaussian vector composed of sub-vectors x and y , then we may write:

$$Z = \begin{bmatrix} x \\ y \end{bmatrix} \text{ is } N\left(\begin{bmatrix} m_x \\ m_y \end{bmatrix}, \begin{bmatrix} C_x & C_{xy} \\ C_{yx} & C_y \end{bmatrix}\right) \quad (3.266)$$

where m_x and m_y are the mean of x and y , C_x is the covariance of x with itself, C_{xy} is the covariance of x with y , etc. It is known that the marginal and conditional distributions of a gaussian random vector are also gaussian. Indeed, the distribution of x for a given y has a probability density $p(x/y)$ of normal type:

$$p(x/y) = N(m_{x/y}, C_{x/y}) \quad (3.267)$$

In this case the conditional mean ($m_{x/y}$) and the conditional covariance ($C_{x/y}$) may be calculated as follows:

$$m_{x/y} = m_x + C_{x/y} C_y^{-1} (y - m_y) \quad (3.268)$$

$$C_{x/y} = C_x - C_{xy} C_y^{-1} C_{yx} \quad (3.269)$$

These two relations are the basis for other important developments of the Kalman filter equations. Concerning the problem considered above, the calculation of the minimum mean square error can be carried out either:

1. By considering the individual observations on the concentrated vector Y_k . Because X_k and Y_k are both gaussian, then Eqs. (3.268) and (3.269) represent the vector used to obtain the conditional mean and covariance of X_k for a given Y_k . However, when the dimension of the vector is too large, problems with matrix multiplication and inversion can appear.
or
2. By developing a special recursive update for the estimation of x_k from X_k based on the linear system (3.265) and a special property derived from Eqs. (3.268) and (3.269). More precisely, if the best estimate of x_k based on the observations Y_k is given (denote this estimate $\hat{x}_{k/k}$) with a new observation y_{k+1} , it is shown how to obtain the best estimate $\hat{x}_{k+1/k+1}$ and its error covariance matrix $CE_{k+1/k+1}$.

Linear systems over a gaussian random vector. If x or X is a gaussian vector with mean value m_x and covariance C_x (the minimum square error estimate for x is \hat{x} and $\hat{x} = m_x$) which is considered to be in a formal linear system completed with a zero-mean gaussian vector (v is $N(0, R)$) then we have:

$$y = Hx + v \quad (3.270)$$

The mean and covariance of y are calculated, by their definition, as follows:

$$m_y = E|y| = E|Hx + v| = Hm_x \quad (3.271)$$

$$C_y = E|y - m_y| * |y - m_y|^T = E|H(x - m_x) + v| * |H(x - m_x) + v|^T = HC_xH^T + R \quad (3.272)$$

Consequently, the minimum mean square error estimate for y is $\hat{y} = Hm_x$ and the associated covariance of this is $C_y = HC_xH^T + R$.

Recursive estimation of gaussian random vectors. We consider here a gaussian random vector composed of three sub-vectors x, y and z :

$$\begin{bmatrix} x \\ y \\ z \end{bmatrix} \text{ is } N \left(\begin{bmatrix} m_x \\ m_y \\ m_z \end{bmatrix}, \begin{bmatrix} C_x & C_{xy} & C_{xz} \\ C_{yx} & C_y & C_{yz} \\ C_{zx} & C_{zy} & C_z \end{bmatrix} \right)$$

From Eqs. (3.268) and (3.269) the minimum mean square estimate of x for a given y is:

$$\hat{x}(y) = m_x + C_{xy}C_y^{-1}(y - m_y) \quad (3.273)$$

and the associated error covariance can be computed as follows:

$$C_x(y) = C_x - C_{xy}C_y^{-1}C_{yx} \quad (3.274)$$

It is important to note that $E[\hat{x}(y)] = m_x$

Now if z is also observed, then the minimum mean square error estimate of x for a given y and z is:

$$\hat{x}(y, z) = m_x + [C_{xy} \quad C_{xz}] * \begin{bmatrix} C_y & C_{yz} \\ C_{zy} & C_z \end{bmatrix}^{-1} \begin{bmatrix} y - m_y \\ z - m_z \end{bmatrix} \quad (3.275)$$

and the error covariance:

$$C_x(y, z) = C_x - [C_{xy} \quad C_{xz}] * \begin{bmatrix} C_y & C_{yz} \\ C_{zy} & C_z \end{bmatrix}^{-1} \begin{bmatrix} C_{yx} \\ C_{zx} \end{bmatrix} \quad (3.276)$$

When y and z stay independent then $C_{yz} = C_{zy} = 0$, and the relation (3.275) can be simplified as follows:

$$\hat{x}(y, z) = m_x + C_{xy}C_y^{-1}(y - m_y) + C_{xz}C_z^{-1}(z - m_z) = \hat{x}(y) + C_{xz}C_z^{-1}(z - m_z) \quad (3.277)$$

The use of Eq. (3.277) needs a recursive method to calculate $\hat{\mathbf{x}}(y, z)$ for a given $\hat{\mathbf{x}}(y)$ and z . The problem is that Eq. (3.275) depends on y and z , which are independent vectors. Fortunately, changing variables makes it possible to change the estimation procedure for Eq. (3.275) and then Eq. (3.277) can be modified considering the random vector ν defined by:

$$\nu = z - \hat{z}(y) = z - [m_z + C_{xy}C_y^{-1}(y - m_y)] = (z - m_z) - C_{xy}C_y^{-1}(y - m_y) \quad (3.278)$$

Here $\hat{z}(y)$ is the minimum mean square estimate of z for a given observation of y and this is used in Rel. (3.278) by means of Rel. (3.268). This new random vector, ν , has several interesting properties, which are important for the development of the Kalman filter equations:

1. Because m_ν is zero, ν , is a zero-mean random value:

$$m_\nu = E[(z - m_z) - C_{xy}C_y^{-1}(y - m_y)] = 0.$$

2. Since

$$C_{\nu y} = E[\nu(y m_y)^T] = E[(z - m_z)(y - m_y)^T - C_{xy}C_y^{-1}(y - m_y) \times (y - m_y)^T] = C_{zy} - C_{zy}C_yC_y^{-1} = 0$$

we consider that ν and y are independent .

3. Because $C_{\nu x(y)}$ is given by relation

$$C_{\nu x(y)} = E[\nu(m_x + C_{xy}C_y^{-1}(y - m_y))^T] = E[\nu(y - m_y)^T C_y^{-1} C_{yx}] = 0,$$

and considering the previous property (2.), we obtain that ν is independent with respect to y and $\hat{\mathbf{x}}(y)$.

Now, if we replace z by ν in Eq. (3.275), we can rewrite the result as follows:

$$\begin{aligned} \hat{\mathbf{x}}(y, z) &= \hat{\mathbf{x}}(y, \nu) = m_x + [C_{xy} \quad C_{x\nu}] * \begin{bmatrix} C_y & 0 \\ 0 & C_\nu \end{bmatrix}^{-1} \begin{bmatrix} y - m_y \\ \nu \end{bmatrix} \\ &= m_x + C_{xy}C_y^{-1}(y - m_y) + C_{x\nu}C_\nu^{-1}\nu = \hat{\mathbf{x}}(y) + C_{x\nu}C_\nu^{-1}\hat{\nu} \end{aligned} \quad (3.279)$$

It is easy to observe that from Eq. (3.274) we can obtain:

$$C_{x\nu} = E[(x - m_x)(z - m_z - C_{xy}C_y^{-1}(y - m_y)) = C_{xz} - C_{xy}C_y^{-1}C_{yz} \quad (3.280)$$

and the variable correlation for ν is then:

$$\begin{aligned} C_\nu &= E[(z - m_z - C_{xy}C_y^{-1}(y - m_y))(z - m_z - C_{xy}C_y^{-1}(y - m_y))^T] \\ &= C_z - C_{zy}C_y^{-1}C_{yz} \end{aligned} \quad (3.281)$$

It may be noticed that the equality of $\hat{\mathbf{x}}(y, z)$ and $\hat{\mathbf{x}}(y, \nu)$ is the result of the conservation of all information while the variables in Eq. (3.278) are being replaced. Indeed, we are simply adding a constant vector to z , and this vector makes ν and y independent of each other. The error covariance here noted as $CC_x(y, \nu)$ associated with Eq.(3.277) is:

$$\begin{aligned}
 CC_x(y, v) &= C_x - [C_{xy} \quad C_{xv}] * \begin{bmatrix} C_y & 0 \\ 0 & C_v \end{bmatrix}^{-1} * \begin{bmatrix} C_{yx} \\ C_{vx} \end{bmatrix} \\
 &= C_x - C_{xy} C_y^{-1} C_{yx} - C_{xv} C_v^{-1} C_{vx} = C_x(y) - C_{xv} C_v^{-1} C_{vx}
 \end{aligned} \tag{3.281}$$

The Kalman Filter Equations are here obtained from the formulation of the Kalman filter with the purpose of finding a recursive estimation procedure for the solution of a problem (estimation of state vector). Before detailing the procedure, we have to introduce other new notations. The minimum square estimate of \hat{x}_k for the given observations $Y_1 = [y_0, y_1, \dots, y_1]$ is defined by $\hat{x}_{k|}$. Furthermore $CC_{k/l}$ represents the error covariance associated with $\hat{x}_{k/l}$.

With these notations, we can now explain the estimation of $\hat{x}_{k/k}$ from the estimate $\hat{x}_{k/k-1}$ and the new observation y_k . From Eqs. (3.279) and (3.281) we obtain:

$$\hat{x}_{k/k} = \hat{x}_{k/k-1} + C_{xkvk} C_{vk}^{-1} v_k \tag{3.282}$$

$$CC_{k/k} = CC_{k/k-1} - C_{xkvk} C_{vk}^{-1} C_{vkvk} \tag{3.283}$$

If v_k is extracted from Eqs. (3.265), (3.270) and (3.271) then we have:

$$v_k = y_k - H_k \hat{x}_{k/k-1} \tag{3.284}$$

The covariance matrices from Eqs. (3.282) and (3.283) may be calculated using the definition of some established relations. The following relations are then obtained:

$$\begin{aligned}
 C_{vk} &= E \left[(y_k - H_k \hat{x}_{k/k-1})(y_k - H_k \hat{x}_{k/k-1})^T \right] \\
 &= E \left[[(H_k(x_k - \hat{x}_{k/k-1}) + v_k)][(H_k(x_k - \hat{x}_{k/k-1}) + v_k)]^T \right] \\
 &= H_k CC_{k/k-1} H_k^T + R_k
 \end{aligned} \tag{3.285}$$

$$\begin{aligned}
 C_{xkvk} &= E \left[(x_k - E(x_k)) v_k^T \right] = E \left[(x_k - E(x_k) + E(x_k) - \hat{x}_{k/k-1}) v_k^T \right] \\
 &= E \left[(x_k - \hat{x}_{k/k-1}) v_k^T \right] = E \left[(x_k - \hat{x}_{k/k-1})(y_k - H_k \hat{x}_{k/k-1})^T \right] \\
 &= E \left[(x_k - \hat{x}_{k/k-1})(x_k - \hat{x}_{k/k-1})^T H_k^T \right] = CC_{k/k-1} H_k^T
 \end{aligned} \tag{3.286}$$

Substituting Eqs. (3.286), (3.285) and (3.284) into Eqs.(3.283) and (3.282) we have:

$$\hat{x}_{k/k} = \hat{x}_{k/k-1} + K g_k (y_k - H_k \hat{x}_{k/k-1}) \tag{3.287}$$

$$CC_{k/k} = CC_{k/k-1} - K g_k H_k CC_{k/k-1} \tag{3.288}$$

where the Kalman gain of the filter is given by $Kg_k = CC_{k/k-1}H_k^T [H_kCC_{k/k-1}H_k^T + R_k]^{-1}$. It is important to observe the subtraction of $R_k > 0$ considered in the definition of the disturbance vector. If $R_k > 0$, Kg_k always exists. However, if we accept that R_k is not necessarily positive, we can have problems making the inverse matrix necessary to calculate Kg_k .

Using Eqs. (3.271), (3.272) and (3.265) to complete Eqs. (3.287) and (3.288), we can establish the next two auxiliary equations:

$$\hat{x}_{k+1/k} = F_k \hat{x}_{k/k}, \quad CC_{k+1/k} = F_k CC_{k/k} F_k^T + G_k Q_k G_k^T \quad (3.289)$$

Combining relations (3.287), (3.288) and (3.289) results in a set of recursive equations, which are called the *Kalman filter equations*:

$$\hat{x}_{k+1/k} = F_k \hat{x}_{k/k-1} + F_k Kg_k (y_k - H_k \hat{x}_{k/k-1}) \quad (3.290)$$

$$CC_{k+1/k} = F_k CC_{k/k-1} F_k^T - F_k Kg_k H_k CC_{k/k-1} F_k^T + G_k Q_k G_k^T \quad (3.291)$$

To be operational, the Kalman filter equations must be completed with the starting conditions $\hat{x}_{0/-1}$ and $CC_{0/-1}$, which correspond to $k = 0$ in relations (3.290) and (3.291). These conditions are obtained from the statistical starting of the initial state vector:

$$\hat{x}_{0/-1} = m_0 \quad CC_{0/-1} = s_0 \quad (3.292)$$

The optimized values for the unknown model state parameters are obtained by coupling the Kalman filter equations with the mathematical models of the process that give matrices F_k , H_k and G_k . The coupling above has to be completed step by step: we must first use an initial estimator vector for the process state (which is the starting point in the previous method) and then consider a judicious error covariance matrix and experimental data. Depending on the problem formulation stated by Eq. (3.265) there are situations where the Kalman procedure does not give satisfactory results. Indeed, in some cases, the Kalman filter can provide state estimates which diverge from the actual evolution of the vector. However, generally, this divergence is not the result of a fault of the Kalman filter, but, rather, is due to the process model provided by the user. In such cases, the user may re-examine the model formulation in order to give a better version of the model used for the estimation problem. From the mathematical viewpoint, the Kalman filter is only valid for time invariant formulations of the model in Eq. (3.265). This assertion implies that the studied system must be controllable and observable. These two conditions allow the matrix of error covariance $CC_{k/k-1}$ to converge towards a finite and positive constant matrix. Consequently, the error in the estimate $\hat{x}_{k/k-1}$ is bounded as $k \rightarrow \infty$ because of the $CC_{k/k-1}$ bounding.

Another consequence of the steady state analysis of the Kalman filter is that we can use the steady state Kalman gain instead of the time varying Kalman gain. The advantage of such an approach is that considerable computational savings are possible because we do not need to recalculate the Kalman gain for each new observation.

3.5.5.2 Example of the Use of the Kalman Filter

The example analyzed here is one of the simplest problems because it is two-dimensional with respect to the vectors state. The example illustrates the Kalman tracking for a system model, which is controllable and observable. To this aim, we use the following system model and prior statistics:

- the process state vector:

$$\mathbf{x}_{k+1} = \begin{bmatrix} 1.1 & 0.1 \\ 0 & 0.8 \end{bmatrix} \mathbf{x}_k + \begin{bmatrix} 1 & 0 \\ 0 & 1 \end{bmatrix} \mathbf{w}_k$$

- the measurement vector:

$$\mathbf{y}_k = \begin{bmatrix} 1 & 0 \\ 0 & 1 \end{bmatrix} \mathbf{x}_k + \mathbf{v}_k$$

- prior statistics:

$$\begin{aligned} E(\mathbf{w}_k \mathbf{w}_k^T) &= \begin{bmatrix} 0.03 & 0.01 \\ 0.01 & 0.03 \end{bmatrix}; E(\mathbf{v}_k \mathbf{v}_k^T) = \begin{bmatrix} 2 & 0 \\ 0 & 2 \end{bmatrix}; E(\mathbf{x}_0) = \begin{bmatrix} 10 \\ 10 \end{bmatrix}; \\ E[(\mathbf{x} - \mathbf{m}_0)(\mathbf{x} - \mathbf{m}_0)^T] &= \begin{bmatrix} 2 & 0 \\ 0 & 2 \end{bmatrix} \end{aligned}$$

For actual cases, the model of the process is given *a priori* and the process state vector can be built according to the rule presented here for the case of the Gauss–Newton method. The dispersion due to the normal disturbances of the process input or the dispersion that characterizes the errors of the exit measurements must be appreciated and proposed, as shown in our case. In this example, it is not difficult to observe that the model presents two exit variables: y_1 (that decreases with the state parameters) and y_2 (that increases with the state parameters). The observations of the process (measured data of y_1 and y_2) have been generated using the system formulation and values for \mathbf{x}_k from a random number generator that add the random multiplication of its dispersion to the mean value. Ten observations have been generated by using adequate software and have been exploited as input for the Kalman filter. The result of these observations and the estimations carried out by the Kalman procedure are illustrated in Fig. 3.88. In this figure, we can observe the actual state path and the Kalman estimation of the state path as solid and dashed lines respectively. The actual locations of the state and estimated values are indicated as white and black circles. The ellipses in the figure are centred near the positions of the actual state path and their borders represent the two standard deviations of the estimation error calculated from the matrices of error covariance. The numerical values of the standard deviations are also given in the figure.

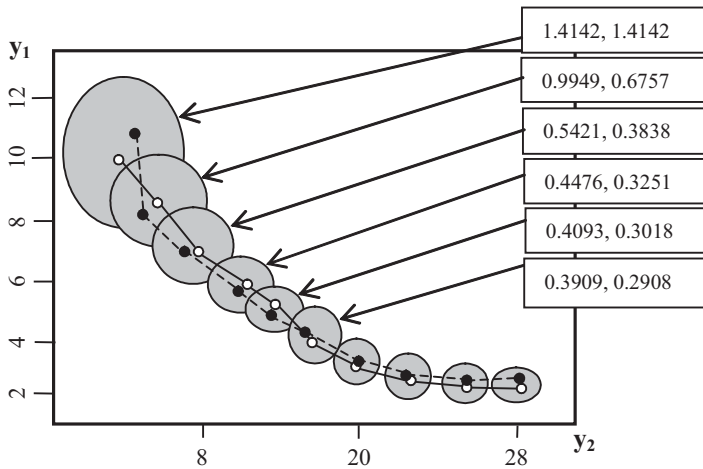


Figure 3.88 Numerical example of the Kalman filter tracking.

3.6

Some Conclusions

All theoretical aspects, engineering observations and commentaries and actual examples presented in this chapter illustrate some basic or particular aspects of the modelling and simulation of processes based on transfer phenomena in the field of chemical engineering

The essential features of the presented aspects can be described as follows:

1. Mathematical models are developed for teaching, for engineering calculations and for finding solutions to the technical problems of design using rigorous procedures where the core resides in the particularization of the transport phenomena equations to the actual case modelled. The main purpose of modelling is to provide engineers and practitioners with prediction parameters of direct practical interest, i.e. the value of concentrations and temperature, shear rates, heat and mass transfer rates, as functions of the operating conditions including equipment geometry and dimensions, the properties of the media and the process features.
2. Mathematical models have been developed by considering classical flow models. At the same time, the capacity of computational fluid dynamics to be coupled with heat and mass transfer processes and with a reaction has been considered.
3. Every mathematical model is a simplified mirror image of a real phenomenon. To sustain the modeling assumptions, all

exemplified models are characterized by experimental or simulated data. This characterization also shows the strongly cognitive capacity of the developed models.

4. Modelling usually includes several consecutive steps of calculations; therefore, to make the method practical, the software simplification of the main equations has to be accepted with respect to the practical application. In many cases, we can reduce the simulation complications without impairing the reliability of the obtained results.
5. Model-based estimation techniques applied to identify or simply estimate parameters are presented as mathematical formulations and are sustained by practical applications.

References

- 3.1 R. B. Bird, W. E. Steward, E. N. Lightfoot, *Transport Phenomena*, John Wiley, New York, 1960.
- 3.2 V.A. Levich, *Physico-Chemical Hydrodynamics*, McGraw-Hill, New York, 1962.
- 3.3 A. Foust, *Principles of Unit Operations*, John Wiley, New York, 1966.
- 3.4 V.A. Luikov, *Heat and Mass Transfer*, Mir Publishers, Moscow, 1980.
- 3.5 E. A. Bratu, *Processes and Apparatus for Chemical Industry, Vol. 1*, Technical Book, Bucharest, 1969.
- 3.6 J. C. Slatery, *Momentum, Energy and Mass transfer in Continua*, McGraw-Hill, New York, 1972.
- 3.7 V. V. Veverka, F. Madron, *Material and Energy balancing in the Process Industries*, Elsevier, Amsterdam, 1997.
- 3.8 H. Schlichting, *Boundary Layer Theory*, 7th Edn., McGraw-Hill, New York, 1979.
- 3.9 R. G. E. Franks, *Modeling and Simulation in Chemical Engineering*, Wiley-Interscience, New York, 1972.
- 3.10 J. N. Kapur, *Mathematical Modeling*, John Wiley, New York, 1988.
- 3.11 S. Kotake, K. Hijikata, *Numerical Simulation of Heat Transfer and Fluid Flow on a Personal Computer*, Elsevier Science, North-Holland, Amsterdam, 1999.
- 3.12 B. Volesky, J. Votruba, *Modeling and Optimization of Fermentation Processes*, Elsevier Science, North-Holland, Amsterdam, 1999.
- 3.13 W. L. Luyben, *Process Modeling, Simulation and Control for Chemical Engineering*, 4th Edn., McGraw-Hill, New York, 1990.
- 3.14 A. Hinchliffe, *Chemical Modeling: From Atoms to liquids*, Wiley-VCH, Weinheim, 1999.
- 3.15 C. Truesdell, *Rational Thermodynamics*, McGraw-Hill, New York, 1969.
- 3.16 Th. L. Bott, E. Ehrfeld, *Chem. Eng. J.* **2000**, 80, 163, 245.
- 3.17 G. Barralla, M. Mattea, V. Gekas, *Sep. Pur. Technol.* **2001**, 22–23, 1–3, 489.
- 3.18 M. Hamachi, M. Cabassud, A. Davin, M. Peucho, *Chem. Eng. Process.* **1999**, 38, 3, 200.
- 3.19 W. B. Richard, N. S. Hartham, I. J. Calco, *Sep. Pur. Technol.* **2001**, 24, 162, 297.
- 3.20 L. Yonghum, M. M. Clarke, *J. Membr. Sci.* **1998**, 149, 2, 181.
- 3.21 V. Nassachi, *Chem. Eng. Sci.* **1998**, 53, 6, 1253.
- 3.22 T. Dobre, J. Sanchez, V. S. Dinu, G. Iavorschi, Modeling and Simulation of a Tangential Filter Unit, *Proc. of the 12th International Romanian Chemistry and Chemical Engineering Conference*, S5, P29, 2001.
- 3.23 O. Levenspiel, *Chemical Reaction Engineering*, Wiley, New York, 1999.
- 3.24 C. T. Dickenson, *Filters and Filtration Handbook*, 4th Edn., Elsevier, North-Holland, Amsterdam, 1999.

- 3.25 A. J. Reynolds, *Turbulent Flows in Engineering*, Wiley, New York, 1974.
- 3.26 D. W. Deckwer, *Bubble Column Reactors*, John Wiley, New York, 1991.
- 3.27 G. Hebrand, D. Bastoul, M. Roustan, P. M. Comte, C. Beck, *Chem. Eng. J.* **1999**, *72*, 109.
- 3.28 S. Najarian, J. B. Bellhouse, *Chem. Eng. J.* **1999**, *75*, 105.
- 3.29 D. W. Deckwer, *Bubble Column Reactors*, John Wiley, New York, 1991.
- 3.30 J. H. Ferziger, M. Peric, *Computational Method for Fluid Dynamics*, Springer-Verlag, Berlin, 1996.
- 3.31 V. Novozhilov, *Prog. Energ. Combust. Sci.* **2001**, *27*, 611.
- 3.32 R. Krisna, M. J. Van Baten, *Nature*, **1999**, *398*, 208.
- 3.33 R. Krisna, M. I. Urseanu, M. J. Van Baten, J. Ellenberger, *Int. Commun. Heat. Mass Transfer* **1999**, *26*, 781.
- 3.34 A. H. Boerner, U. R. Qi, *Int. J. Multiphase Flow* **1997**, *23*, 523.
- 3.35 J. K. Marschall, L. Mlezko, *Chem. Eng. Sci.* **1999**, *54*, 2085.
- 3.36 J. Dong, D. Gidaspow, *AIChE J.* **1990**, *36*, 523.
- 3.37 M. G. B. Van Wachem, C. J. Schouten, R. Krisna, M. C. Van der Bleek, *Comput. Chem. Eng.* **1998**, *22*, 299.
- 3.38 M. G. B. Van Wachem, C. J. Schouten, R. Krisna, M. C. Van der Bleek, *Chem. Eng. Sci.* **1999**, *54*, 2141.
- 3.39 A. Lapin, A. Lubert, *Chem. Eng. Sci.* **1994**, *49*, 3661.
- 3.40 J. T. Lin, J. Reese, T. Hong, S. L. Fan, *AIChE J.* **1996**, *42*, 301.
- 3.41 A. Sokolichin, G. Eingenberger, *Chem. Eng. Sci.* **1994**, *49*, 5375.
- 3.42 A. Sokolichin, G. Eingenberger, *Chem. Eng. Sci.* **1997**, *52*, 611.
- 3.43 S. S. Thakre, B. J. Joshi, *Chem. Eng. Sci.* **1999**, *54*, 5055.
- 3.44 B. Mehta, T. K. Chang, K. Nandakumar, *Chem. Eng. Res. Des. Trans.* **1998**, *7*, 843.
- 3.45 M. J. Van Baten, R. Krisna, *Chem. Eng. J.* **2000**, *77*, 143.
- 3.46 C. Reid, *Zone Refining*, McGraw-Hill, New York, 1956.
- 3.47 J. Welty, E. Ch. Wicks, E. R. Wilson, L. G. Rorrer, *Fundamentals of Momentum Heat and Mass Transfer*, Wiley, New York, 2000.
- 3.48 H. K. Keneth, R. T. Stein, *Math. Biosci.* **1967**, *1*, 412.
- 3.49 H. L. Frisch, *J. Phys. Chem.* **1959**, *63*, 1249.
- 3.50 R. Ash, M. R. Barrer, T. H. Chio, *J. Phys. Eng. Sci. Instrum.* **1978**, *11*, 262.
- 3.51 J. Sanchez, L. Gijiu, V. Hynek, O. Muntean, A. Julbe, *Sep. Pur. Technol.* **2001**, *7*, 116.
- 3.52 H. P. Nelson, M. S. Auerbach, *Chem. Eng. J.* **1999**, *74*, 43.
- 3.53 K. Kuo, *Principle of Combustion*, John Wiley, New York, 1986.
- 3.54 S. Candel, J. P. Martin, Coherent Flame Modeling of Chemical Reactions in Turbulent Mixing Layer, in *Complex Chemical Reaction Systems*, J. Warnatz, W. Joger (Eds.), Springer-Verlag, Berlin, 1987.
- 3.55 P. H. Thomas, The Growth of Fire-Ignition to Full Involvements, in *Combustion Fundamentals of Fire*, G. Cox (Ed.), Academic Press, London, 1995.
- 3.56 A. Cavaliere, R. Ragucci, *Prog. Energ. Combust. Sci.* **2001**, *27*, 547.
- 3.57 J. G. Sanchez Marcano, T. T. Tsotsis, *Catalytic Membranes and Membrane Reactors*, Wiley-VCH, Weinheim, 2002.
- 3.58 M. Niedzwiecki, *Identification of Time-Varying Processes*, Wiley, New York, 2000.
- 3.59 G. Maria, E. Heinze, *J. Loss. Prev. Process. Ind.* **1998**, *11*, 187.
- 3.60 J. C. Nash, M. Walker-Smith, *Nonlinear Parameter Estimation: An Integrated System in Basic*, Marcel Dekker, New York, 1987.
- 3.61 W. S. Rutherford, D. D. Do, *Chem. Eng. J.* **1999**, *74*, 155.
- 3.62 V. V. Kafarov, *Cybernetic Methods for Technologic Chemistry*, Himia, 1969.
- 3.63 R. Fletcher, *Practical Method of Optimization*, 2nd Edn., Wiley, New York, 2000.
- 3.64 E. K. Atkinson, *Introduction to Numerical Analysis*, Wiley, New York, 2000.
- 3.65 G. Bastin, D. Dochain, *On Line Estimation and Adaptive Control of Bioreactors*, Elsevier, North-Holland, Amsterdam, 1999.
- 3.66 I. Riekert, *AIChE J.* **1985**, *14*, 19.
- 3.67 M. Suzuki, K. Kwazoe, *J. Chem. Eng. Jpn.* **1975**, *8*, 379.
- 3.68 M. R. Onsiovic, L. S. Cruz, *Chem. Eng. Sci.* **2000**, *55*, 20, 4667.

- 3.69 S. G. Mohinder, P. A. Angus, *Kalman Filtering: Theory and Practice Using MATLAB*, 2th Edn., Wiley-VCH, Weinheim, 2001.
- 3.70 S. Saelid, N. A. Jensen, T. Lindstad, L. Kolbeisen, Modeling, Identification and Control of a Fluidized Bed Reactor, in *Identification and System Parameters Estimation-Proceedings of 5th IFAC Symposium*, Iserman R. (Ed.), Darmstadt, 1979.
- 3.71 X. Wu, H. K. Bellgardt, *J. Biotechnol.* **1998**, *62*, 11.

